



CHARACTERISING IgA1 SOLUTION STRUCTURES IN IgA NEPHROPATHY

Thesis submitted for the degree of Master of Philosophy
at the University of Leicester

Owen Learoy Vennard
Department of Infection, Immunity and Inflammation
University of Leicester

2014

Abstract

Characterising IgA1 Solution Structures in IgA Nephropathy Owen Vennard

IgA nephropathy (IgAN) remains the commonest pattern of primary glomerulonephritis seen worldwide and results in the development of end-stage renal failure in over 30% of affected individuals. It is characterised by IgA1 containing immune complex formation and deposition within the mesangium; the reasons for which are unknown. IgAN is associated with aberrant serum *O*-glycoforms, characterised by over representation of IgA1 molecules displaying undergalactosylation. While a number of studies have postulated a pathogenic role for the IgA1 hinge region *O*-glycans in IgAN, none have investigated the impact of altered glycosylation on its three-dimensional shape.

A combination of small-angle X-ray scattering (SAXS), and analytical ultracentrifugation (AUC) experiments were used to determine whether the monomeric IgA1 (mIgA1) conformational shape was altered in IgAN. Serum IgA1 from a healthy subject and three patients with IgAN with differing IgA1 galactosylation were isolated using jacalin affinity chromatography. Monomeric IgA1 species were isolated by FPLC. Relative hinge region *O*-galactosylation was determined using a standardised *helix aspersa* agglutinin (HAA) lectin assay.

The Guinier X-ray radius of gyration (R_G) for the healthy control, and the IgAN mIgA1 samples with both elevated and reduced galactosylation were 6.10–6.30 nm. This agreed well with that previously reported for mIgA1 and indicated that under the experimental conditions mIgA1 did not adopt a significantly altered conformation. The AUC sedimentation coefficients for all samples were 6.2 S, in agreement with this. The distance distribution curve $P(r)$ gave an overall length (L) of 21 nm for the healthy mIgA1 control and 22–25 nm for IgAN-associated mIgA1. Purified IgAN-associated IgA1 monomers with the reduced *O*-galactosylation thus displayed an increased molecular length L , indicating a more extended arrangement in comparison to the healthy mIgA1 control. Elevated *O*-galactosylation however did not alter the length of mIgA1. The formation of dimer species was observed by AUC for all samples.

Although the initial data analyses do not suggest major conformation change, these results provide a promising insight into the potential for altered *O*-galactosylation in IgA1 to promote self-aggregation, and unravelling of its hinge region which may expose neoantigenic epitopes for autoantibodies and alter IgA-receptor and IgA-extracellular matrix interactions.

Acknowledgements

This last year has for a number of reasons, perhaps been the most difficult and challenging years of my life. There are a number of people without whom this thesis might not have been written, for which I am greatly indebted.

In particular I would like to take this opportunity to say thank you to Dr Karen Molyneux for being the most extraordinarily supportive, motivating and inspirational supervisor throughout my project. Her unrelenting enthusiasm, sense of humour and encouragement throughout has been directly, and indirectly instrumental in the production of this thesis. Thank you most of all for being there for me.

I also would like to thank Dr Jonathan Barratt for giving me the opportunity to undertake this research project and providing me with his continued support and assistance.

I am grateful to Professor Stephen Perkins for his guidance, advice and kind support throughout this project. My thanks also go to Jayesh Gor and all members of Professor Perkins' group for their invaluable help both at UCL, London and in France.

My sincere thanks goes to all members of the Renal Group, particularly Trisha Higgins, Jez Brown (my right hand man), Dr Iza Pawluczyk, Dr Alice Smith, Dr Ravi Chana, Dr Alan Bevington, Dr Joanna Boyd and Dr Chee K. Cheung. You have all been so welcoming and have made my time in the laboratory extremely enjoyable.

May I also say thank you to Dr Roger James for your encouragement in submitting this MPhil.

Finally, I would like to thank my family and Anisha Thanki for their support, patience and encouragement. I wish Anisha the best of luck in her doctoral studies!

I must also acknowledge the University Hospitals of Leicester NHS Trust and Kidney Research UK for providing funding for this research.

Merci à tous!

Oral and Poster Presentations

3rd European Congress of Immunology 2012, Glasgow, UK (*Poster presentation*)

2nd East Midlands Research Showcase 2012, Loughborough, UK (*Poster presentation*)

6th University of Leicester Postgraduate Festival of Research 2012, Leicester, UK (*Poster presentation; Leicester Mercury 1st prize*)

3rd East Midlands Research Showcase 2013, Loughborough, UK (*Oral presentation; 2rd prize*)

Table of Contents

Abstract.....	i
Acknowledgements.....	ii
Oral and Poster Presentations	iii
Table of Contents.....	iv
Figures and Tables	vi
Abbreviations.....	ix
Introduction.....	1
1.1 Antibody classes and biological activities	2
1.1.2 Immunoglobulin G	2
1.1.3 Immunoglobulin M.....	2
1.1.4 Immunoglobulin D	2
1.1.5 Immunoglobulin E.....	3
1.2 Immunoglobulin A.....	5
1.2.1 Biochemistry of monomeric IgA.....	9
1.2.2 <i>N</i> - and <i>O</i> -linked carbohydrates.....	9
1.3 IgA nephropathy.....	17
1.3.1 Pathogenesis	18
1.3.2 Macromolecular characteristics of IgA in IgAN	20
1.3.4 Clinical features.....	23
1.3.5 Diagnosis and treatment	23
1.3.6 Clinical associations with IgA and IgAN.....	26
1.4 Methods used to determine immunoglobulin structure.....	28
1.4.1 Electron microscopy	29
1.4.2 Nuclear magnetic resonance.....	31
1.4.3 X-ray crystallography	31
1.4.2 Analytical ultracentrifugation	32
1.4.2.1 Sedimentation velocity	32
1.4.2.2 Sedimentation equilibrium	36

1.4.2.2 Combining AUC and solution scattering	40
1.4.3 Solution scattering experiments	40
1.4.3.1 Neutron scattering	42
1.4.3.2 X-ray scattering	42
1.4.3.3 Application to other proteins	47
1.4.4.1 Guinier analysis	49
1.4.4.2 R_G and R_{XS} analysis.....	49
1.4.4.3 Distance distribution function analysis	50
Materials and Methods.....	52
2.1 Sample selection and purification of IgA1.....	53
2.1.1 Jacalin affinity chromatography	53
2.1.2 Size-exclusion chromatography	54
2.1.3 Enzyme-linked immunosorbent assay.....	55
2.1.4 Enzyme-linked <i>Helix aspersa</i> lectin binding	56
2.1.5 Sodium dodecyl sulfate polyacrylamide gel electrophoresis (SDS-PAGE) and immunoblotting	57
2.2 Analytical ultracentrifugation.....	59
2.3 X-ray scattering	61
Results.....	63
3.1 Purification and hinge glycosylation of IgA1	64
3.1.2 Fast performance liquid chromatography	66
3.1.3 SDS-PAGE.....	72
3.2 Analytical ultracentrifugation	75
3.3 Small-angle X-ray scattering.....	85
Discussion.....	95
4.1 Discussion	96
Appendix I	101
Appendix II.....	104
Appendix III.....	201
Bibliography	208

Figures and Tables

Chapter One - Introduction

Table 1.01 – Summary of the major properties of human immunoglobulins IgG, IgM, IgA, IgD and IgE.

Table 1.02 – A comparison of the concentrations of IgA and IgG in various human secretions.

Table 1.03 – Major differences between X-ray and neutron scattering experiments.

Figure 1.01 – Schematic diagram of the immunoglobulin fold domains for human IgA1 and IgA2.

Figure 1.02 – Human monomeric IgA1 amino acid sequence.

Figure 1.03 – Various O-linked glycoforms of IgA1 hinge region.

Figure 1.04 – Schematic diagram of the domain structure of dimeric IgA1.

Figure 1.05 – Schematic diagram of the structure and synthesis of secretory IgA.

Figure 1.06 – Renal pathology in IgA nephropathy from biopsy.

Figure 1.07 – Henoch–Schönlein purpura of the legs in a 4-year old child.

Figure 1.08 – Electron micrographs of human IgA selected from total IgA.

Fig 1.09 – Principles of sedimentation of a molecule and the analytical ultracentrifuge during a sedimentation velocity experiment.

Figure 1.10 – Detection methods for solution aggregation.

Figure 1.11 – Example analyses of sedimentation velocity experiments using SEDFIT software.

Figure 1.12 – The effect of macromolecular elongation on the radius of gyration (R_G) and sedimentation coefficient ($s_{20,w}^0$).

Figure 1.13 – Schematic diagram of solution scattering experiments.

Figure 1.14 – Solution scattering curve, illustrating the Guinier region, which provides information corresponding to the overall shape of the molecule.

Figure 1.15 – Previously determined solution structures for IgA1 and IgA2m(1).

Figure 1.16 – The pair-distribution function in SAXS experiments

Equation 1.1 – The Svedberg equation, used to describe the behavioural characteristics of a macromolecule during centrifugation.

Chapter Two – Materials & Methods

Table 2.01 – Concentration series used for mIgA1 AUC-SV experiments.

Table 2.02 – Concentration series used for mIgA1 SAXS experiments.

Table 2.03 – Exoglycosidase enzyme digestion of IgA1.

Figure 2.01 – Simplified flow scheme of IgA1 deglycosylation.

Chapter Three - Results

Table 3.01 – IgAN patient sample selection using HAA lectin binding.

Figure 3.01 – Elution profile for standardised molecular weight markers ran on Superdex 200 pg column (mAU normalised).

Figure 3.02 – Calibration curve for Superdex 200 pg column

Figure 3.03 – Typical gel filtration elution profile for jacalin-affinity purified IgA1 (mAU normalised).

Figure 3.04 – Overlaid gel filtration elution profiles of IgA1 samples 1-4 (mAU normalised).

Figure 3.05 – Overlaid gel filtration elution profiles of monomeric IgA1 samples 1-4 (mAU normalised).

Figure 3.06 – Gel filtration of HMW polymeric IgA1 fraction (mAU normalised).

Figure 3.07– 6% SDS-PAGE Western blot of total IgA1 FPLC fractions (F20-F30).

Figure 3.08 – G-250 Coomassie blue stained 4-12% SDS-PAGE of purified monomeric IgA1 samples 1-4.

Figure 3.09 – G-250 Coomassie blue stained SDS-PAGE of pooled HMW IgA1.

Figure 3.10 – Sedimentation velocity of control sample 1.

Figure 3.11 – Sedimentation velocity IgAN patient sample 2.

Figure 3.12 – Sedimentation velocity of IgAN patient sample 3.

Figure 3.13 – Sedimentation velocity of IgAN patient sample 4.

Figure 3.14 – Concentration-dependence plots for AUC-SV monomer and dimer peaks.

Figure 3.15 – SAXS Guinier fits X-ray Guinier analyses for mIgA.

Figure 3.16 – RXS-1 plots mIgA1 patient and control samples 1.

Figure 3.17 – RXS plot for X-ray Guinier analyses for mIgA1.

Figure 3.18 – Guinier X-ray R_G , R_{XS1} and R_{XS2} comparison

Figure 3.19 – X-ray distance distribution functions $P(r)$ for mIgA1, samples 1-4.

Figure 3.20 – Distance distribution M1 and M2 maxima lengths for mIgA1 samples 1-4.

Abbreviations

AUC	Analytical ultracentrifugation
ARB	Angiotensin receptor blockers
BP	Blood pressure
BSA	Bovine serum albumin
CHO	Carbohydrate
CKD	Chronic kidney disease
dIgA	Dimeric IgA
ECL	Electrochemiluminescence
ELISA	Enzyme-linked immunosorbent assay
EM	Electron microscopy
ESRD	End-stage renal disease
ESRF	European Synchrotron Radiation Facility
Fab	Fragment antigen binding
Fc	Fragment crystallisation
FPLC	Fast performance liquid chromatography
GA	β -1,3 galactosidase
Gal	Galactose
GalNAc	<i>N</i> -acetylgalactosamine
GNA	α - <i>N</i> -acetylgalactosaminidase
HAA	<i>Helix aspera</i> agglutinin
HMW	High molecular weight
HRP	Horseradish peroxide
HSP	Henoch–Schönlein purpura

IC	Immune complex
Ig	Immunoglobulin
IgA	Immunoglobulin A
IgAN	IgA nephropathy
J-chain	Joining chain
kDa	Kilodalton
LMW	Low molecular weight
M	Mole
MALDI - MS	Matrix-assisted laser desorption/ionization mass spectrometry
mIgA	Monomeric IgA
mAU	mili Absorbance Unit
MWCO	Molecular weight cut-off
NA	Neuraminidase
NeuNAc	<i>N</i> -acetylneuraminic acid
NMR	Nuclear magnetic resonance
OPD	1, 2-phenylenediamine dihydrochloride
PBS	Phosphate buffered saline
PDB	Protein Data Bank
pIgA	Polymeric IgA
pIgR	Polymeric immunoglobulin receptor
PTM	Post-translational modification
RMSD	Root-mean-square deviation
r.p.m	Revolutions per minute
SANS	Small-angle neutron scattering
SAS	Small-angle scattering
SAXS	Small-angle X-ray scattering
SC	Secretory component

SDS	Sodium dodecyl sulphate
SIgA	Secretory IgA
SE	Sedimentation equilibrium
SEC	Size exclusion chromatography
SV	Sedimentation velocity
TBST	Tris buffered saline with Tween 20
TEMED	N,N,N',N'-tetramethylethylenediamine
UV	Ultraviolet
v/v	volume/volume
w/v	weight/volume

Chapter One

Introduction

1.1 Antibody classes and biological activities

Antibodies are important effector molecules of the humoral immune system, providing highly evolved adaptive immune protection to supplement innate responses. A number of antibodies, at various concentrations and classes exist in human serum; all comprising a common generic structure (Table 1.01).

1.1.2 Immunoglobulin G

Immunoglobulin G (IgG) is the most abundant antibody class present in human serum, present at approximately 12.3 mg/ml, which constitutes around 80% of the total serum antibody content. It is monomeric with a molecular mass of ~ 150 kDa. It consists of two γ heavy chains bound to two κ or λ light chains. The heavy chain of IgG has three constant domains, C_H1, C_H2 and C_H3 (Murphy 2011).

1.1.3 Immunoglobulin M

Immunoglobulin M (IgM) is the first antibody class to be expressed on immature B cells and also the first antibody class secreted in a primary immune response. IgM accounts for approximately 5-10% of total serum immunoglobulins, and is at a serum concentration of ~1.5 mg/ml. Pentameric IgM has a molecular mass of around 970 kDa and is membrane-bound (Nikolayenko et al. 2005). The heavy chain of IgM contains an additional constant domain to the generic antibody structure that is designated C_H4.

1.1.4 Immunoglobulin D

Immunoglobulin D (IgD) is monomeric with a molecular mass of ~180 kDa and a serum concentration of ~30 μ g/ml. IgD represents about 0.25% of total serum immunoglobulins. IgD has three constant heavy chain domains and the longest hinge region of all antibody

classes, with 64-residues connecting the Fab and Fc regions (Nikolayenko et al. 2005). Secreted IgD has been shown to be more sensitive to proteolytic enzymes than IgM, and this may in part be due to its long and relatively exposed hinge region.

1.1.5 Immunoglobulin E

Immunoglobulin E (IgE) is monomeric with a molecular mass of 188 kDa and it is present in very low concentrations in serum at $\sim 0.3 \mu\text{g/ml}$ (Murphy 2011). The heavy chain of IgE contains an extra constant domain compared to the generic antibody structure that is designated C_{H4} .

Properties	Immunoglobulin isotypes						
	IgG1-4	IgM	IgA1	IgA2	SIgA	IgD	IgE
Heavy chain	γ_{1-4}	μ	α_1	α_2	α_1/α_2	δ	ϵ
Light chain	κ, λ	κ, λ	κ, λ	κ, λ	κ, λ	κ, λ	κ, λ
Other chains	-	J-chain	J-chain, Secretory component			-	-
Quantity of four-chained units	1	5	1,2,3	1,2,4	2	1	1
Molecular mass (kDa)	146, 146, 170 & 146 respectively	970	160	160	385	184	188
Average concentration in sera (mg/ml)	9, 3, 1 & 0.5 respectively	1.5	3.0	0.5	0.05	0.03	0.00005
Half-life (days)	21, 20, 7 & 21 respectively	10	6	6	6	3	2
Proportion of total serum immunoglobulins (%)	50, 17, 5 & 3 respectively	10	16	2	Trace	<1	Trace
Carbohydrate content (%)	2-3	12	7-11	7-11	7-11	9-14	12
Complement activation by alternative pathway	+	-	+	+	-	-	+
	(IgG ₄ only)						

Table 1.01 – Summary of the major properties of human immunoglobulins IgG, IgM, IgA, IgD and IgE. Table adapted from Nikolayenko et al. 2005.

1.2 Immunoglobulin A

Originally identified and described in 1959 (Heremans, Heremans, & Schultze, 1959) immunoglobulin A (IgA) (Figure 1.01) presents as a highly heterogeneous and also the most abundant immunoglobulin present in a wide variety of human secretions (Table 1.02). Daily production of IgA has been estimated to exceed that all other immunoglobulin classes at 65 mg/kg (Kerr, 1990).

Human IgA comprises of two identical light chains (κ or λ) and two identical heavy chains ($\alpha 1$ or $\alpha 2$) giving rise to two isotypes, IgA1 and IgA2 (Figure 1.01). There are at least two well characterised allotypic variants of IgA2, termed IgA2m(1) and IgA2m(2). The amino acid sequences of IgA1 and IgA2 differ in that IgA1 has a 23 amino acid hinge region located between the Fab and the Fc regions which is lacking in IgA2 (Figure 1.01) (Section 1.2.1).

The molecular shape of the IgA1 and IgA2 is unique amongst other immunoglobulins with IgA distinctly lacking the classic "Y-shape" antibody structure seen in other immunoglobulins such as IgG (Almogren & Kerr, 2008; Boehm, Woof, Kerr, & Perkins, 1999; Bonner, Almogren, Furtado, Kerr, & Perkins, 2009) and instead adopting a 'T' shaped structure (Figure 1.15).

The *O*-glycosylated hinge in IgA1 results in an increased Fab-Fc distance and greater molecular rigidity (Boehm et al, 1999). This provides IgA1 with a T-shaped structure in solution. The structure of IgA2 however lacks this hinge region is therefore more compact (Almogren & Kerr, 2008)

IgA is considered a poor activator of complement in comparison to IgG and IgM. IgA does not activate complement by the classical pathway and does not bind C1q, however some studies have shown it to play a role in the activation of the alternative pathway of complement by mannose-binding lectin (MBL) (Roos et al. 2001; Endo 1998; Oortwijn et al. 2008).

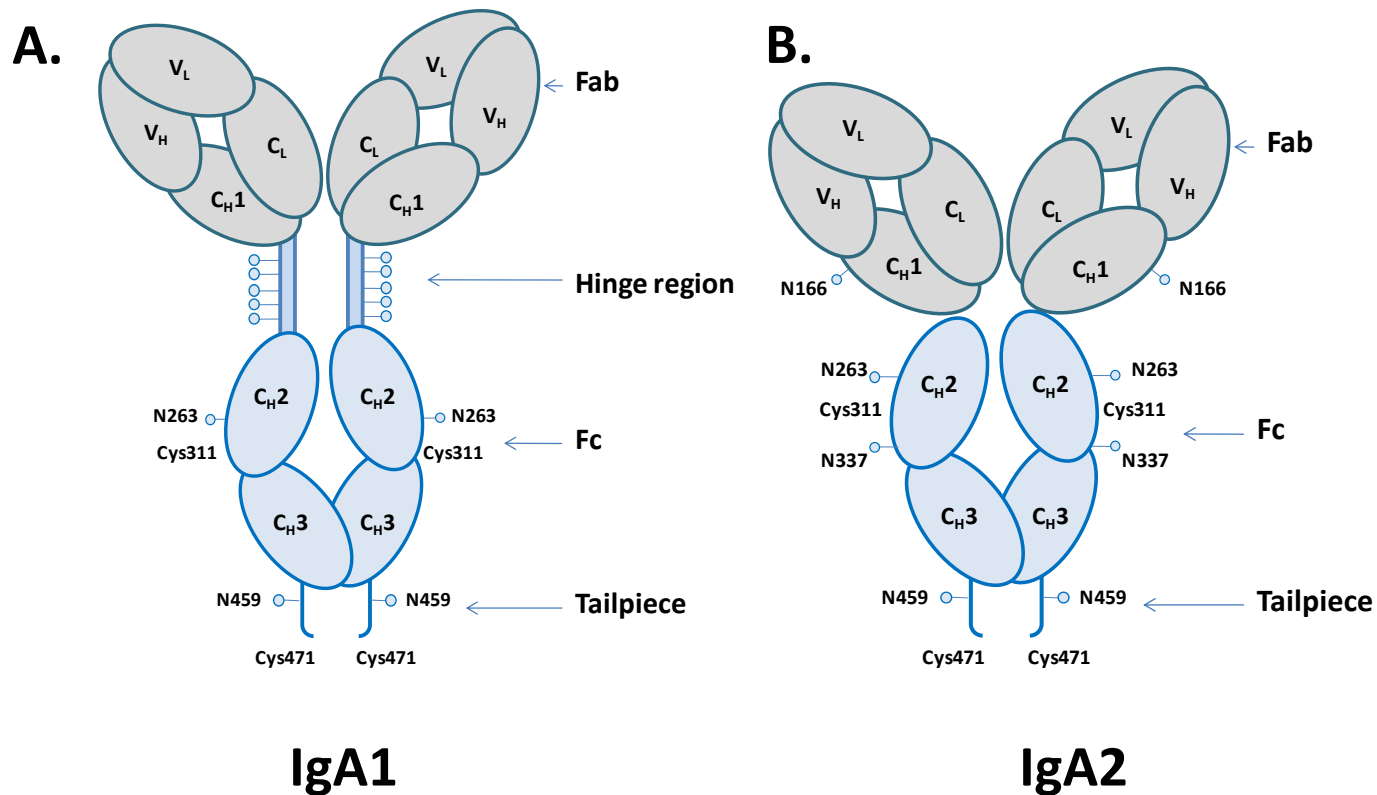


Figure 1.01 - Schematic diagram of the immunoglobulin fold domains for human IgA1 and IgA2. (A) In IgA1 the four-domain Fab fragments (V_L, C_L and C_{H1}) are linked to the four-domain Fc domain (C_{H2}-C_{H3}) by a structurally distinct serine and threonine rich 23 residue hinge region. The hinge linker of IgA1 confers it flexibility to effectively bind antigens (Boehm et al., 1999). This region is highly heterogeneous and contains up to 10 sites of *O*-glycosylation based upon a core *N*-Acetylgalactosamine (GalNAc) glycan. Subsequent sugars, specifically galactose (Gal) and sialic acid (NeuNAc) may be added via glycosyltransferases. The IgA2 allotype (B) (IgA2m(1) shown here) amino acid sequence differs significantly in its shorter hinge with no sites for glycosylation (Y. S. Liu & Putnam, 1979; Torano & Putnam, 1978). This has been shown to reduce both the antibody's flexibility and its susceptibility to bacterial proteases (Furtado et al., 2004; Plaut, Wistar, & Capra, 1974)

Fluid	IgG (mg/ml)	IgA (mg/ml)	pIgA (%)	Ratio IgA1/IgA2
Serum	12.3	3.28	13	89:11
Colostrum	0.1	12.34	96	65:35
Saliva	0.05	0.30	96	63:37
Jejunal	0.34	0.28	95	70:30
Colonic	0.86	0.83	n.d.	35:65
Hepatic bile	0.18	0.11	65	74:26
Nasal	0.06	0.26	n.d.	95:5
Bronchial	0.02	n.d.	82	67:33

Table 1.02 – A comparison of the concentrations of IgA and IgG in various human secretions.

This table shows the varying concentrations of both IgA and IgG immunoglobulins present in human secretions. The final column highlights the ratio of IgA1 to IgA2 isotypes across these secretions; demonstrating the increased presence of IgA1. (n.d. denotes not detectable) (Table adapted from (Kerr, 1990)).

1.2.1 Biochemistry of monomeric IgA

Human IgA is a highly heterogeneous molecule comprised of two heavy ($\alpha 1$ or $\alpha 2$) and two light chains (κ or λ). There are therefore two isotypes of IgA, IgA1 and IgA2 respectively. Structurally the major difference between these isotypes is the arrangement of inter-chain disulphide bridges. In humans, serum IgA is predominantly present as a monomer species (mIgA) with a molecular weight of around 160 kDa (M A Kerr 1990). Higher molecular weight dimeric and polymeric forms (three or more monomers) may also be found with a weight of around 345 kDa and >345 respectively. These molecules are covalently linked through an 18 kDa cysteine rich joining chain (J-chain) (Johansen et al. 2000; A. Bonner et al. 2008).

The monomeric form of all IgA subclasses and allotypes contain 12 domains, including six constant heavy domains (C_{H1} , C_{H2} and C_{H3}), two variable heavy domains (V_H), two constant light domains (C_L) and two variable light domains (V_L) (M A Kerr 1990) (Figure 1.01)

The C terminus of the Fc fragment heavy chain is flanked by two 18 amino acid residue tailpieces. The tailpiece and Cys471 play an important role in dimerisation (Atkin, Pleass, Owens, & Woof, 1996), removal and mutation of Cys471 serves to have a role in the prevention of the formation of dimeric isotypes of IgA1.

1.2.2 *N*- and *O*-linked carbohydrates

Antibodies are glycoproteins, and the glycosylation has substantial effects on the antibody structure and function. IgA1 is unique amongst serum proteins in its possession of both *N*-linked and *O*-linked glycosylation sites. Some of the *N*-linked glycosylation sites (N263 and N459) are conserved in both IgA1 and IgA2 subclasses.

The presence of *O*-linked glycans are rarely found in other serum proteins, the exceptions being IgD, C1 esterase inhibitor (C1Inh), chorionic gonadotrophins, plasminogen, fetuin, and cytokines such as IL-2 and IL-6 (Hortin & Trimpe 1990; Allen et al. 1995).

The hinge region of IgA1 is 23 residues in length with a capacity for five *O*-linked oligosaccharides across a 13 residue region rich in Pro, Ser and Thr amino acids. The hinge region is located directly between the C_{H1} and C_{H2} domains of each heavy chain, giving rise to a total of 10 glycosylation sites (Figure 1.01 and Figure 1.03). Glycosylation is added as a post-translational modification (PTM) through enzyme specific glycotransferases to the core protein in the Golgi apparatus. The addition of the galactose (Gal) sugar derivatives via a 1, 3 galactosamine addition to core N-acetylgalactosamine (GalNAc) may further be supplemented by the addition of sialic acid (NeuNAc).

The various permutations of glycosylation in the hinge region result in vast diversity and huge heterogeneity in the composition of individual IgA1 glycoforms. There therefore exists a complex assortment of glycosylation profiles in any one individual's IgA1 (Figure 1.03).

The hinge peptide contains nine potential *O*-glycosylation sites, corresponding to 18 sites per IgA1 molecule, however only a maximum of five sites are occupied in a sequence. Amino acid sequence analysis of IgA1 identified that *O*-glycans are mainly located at Thr228, Ser230, Ser232, Thr225 and Thr235 (Mattu, 1998).

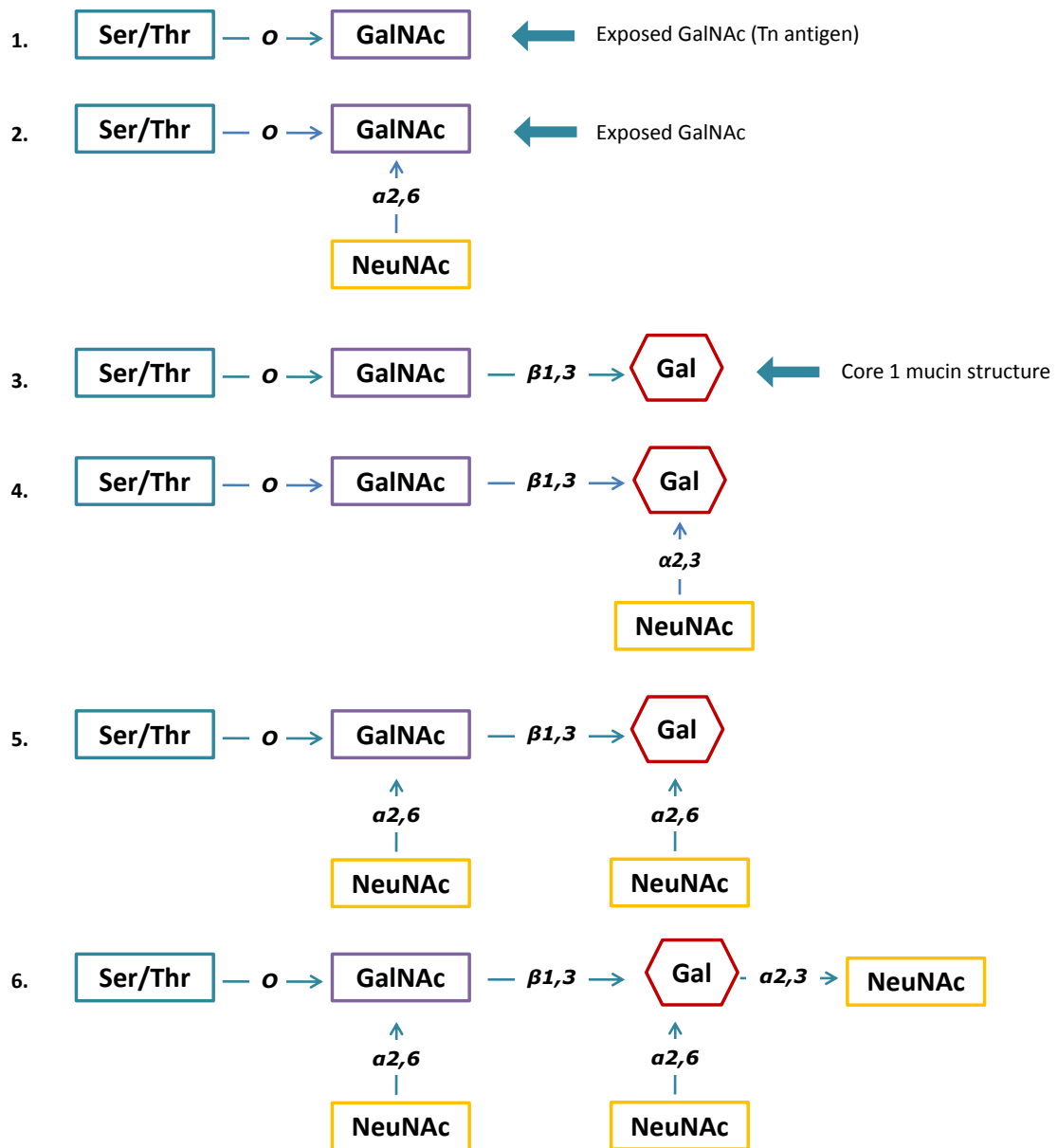


Figure 1.03 – Various O-linked glycoforms of IgA1 hinge region. Each serine (Ser) or threonine (Thr) residue forming the amino acid backbone to of the IgA1 hinge region can have an $\alpha 1$ O-linked N-acetylgalactosamine (GalNAc) sugar residue (J Barratt & Feehally, 2005; Takahashi et al., 2006). This GalNAc core may be terminal (1), or may be further extended with Sialic acid (NeuNAc) via a $\alpha 2, 3$ linkages (2). Terminal Gal may also be substituted to the GalNAc core through $\beta 2, 3$ linkages (3). Finally a final permutation of these glycoforms is the addition of NeuNAc to either a terminal Gal residue through $\alpha 2, 3$ linkage (4) or both Gal and GalNAc (5).

1.2.2 Dimeric IgA

Dimeric IgA (dIgA) (Figure 1.04) is formed of two monomers through the binding of tailpiece Cys471 to Cys15 and Cys68 of the joining chain (J-chain). This J-chain is a 137 residue, 18 kDa glycoprotein covalently linked with the monomers. All isotypes of IgA; IgA1, IgA2m(1) and IgA2m(2) are capable of dimerisation. dIgA present in the lamina propria forms the precursor to secretory IgA prior to transcytosis across an epithelia cell layer into the mucous membranes.

Early structural studies using electron microscopy of IgA have depicted the two monomers connected via their Fc regions forming a double Y-shape structure (Figure 1.08). Higher molecular weight J-chain containing molecular forms of IgA1, such as trimers and tetramers are also found in serum arranged around a single J-chain polypeptide.

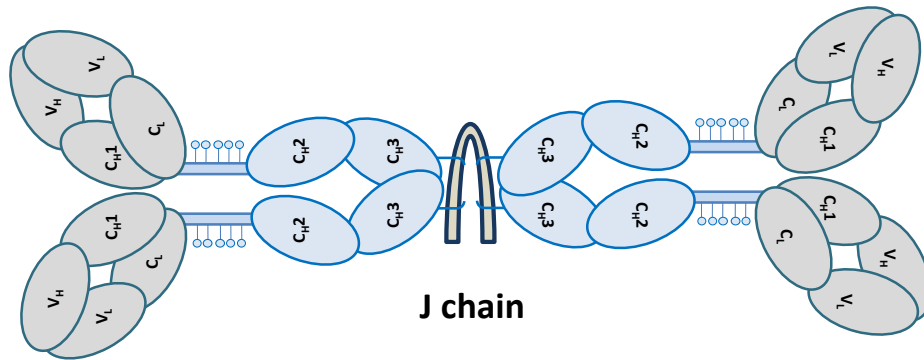


Figure 1.04 – Schematic diagram of the domain structure of dimeric IgA1. Shown here is the dimerisation of two IgA1 monomers covalently linked by a joining chain (J-chain). The J chain is an 18 kDa 137 amino acid residue polypeptide which permits the dimerisation of monomers. The 18 amino acid residue tailpieces of IgA has been shown to be essential in the correct formation of the dimer (Johansen, Braathen, & Brandtzaeg, 2000; Richard, Atkin, & Woof, n.d.). Solution structure determination of myeloma dIgA (PDB code: 2QTJ) has previously been reported (Bonner, Furtado, Almogren, Kerr, & Perkins, 2008) revealing dIgA to have a near-planar solution structure. This work was initiated through the use of the solution structure of mIgA1 (PDB code: 1IGA;) (Boehm et al., 1999).

1.2.3. Secretory IgA

The human mucosal surfaces, at $>400 \text{ m}^2$ present an extremely large surface area to the external environment, and as such are continually exposed to a variety of antigens and pathogens (Lamm 1997; MacDonald 2003).

The IgA molecule in external secretions has several features that distinguish it from its serum counterpart, principally the addition of the five domain glycoprotein secretory component (SC). Dimeric IgA (although higher oligomeric forms can be implicated) is produced at mucosal surfaces on the lamina propria where it binds to the extracellular domain of the polymeric Ig receptor (pIgR). The complex is subsequently transcytosed with SC formed by the cleavage to part of the pIgR; the formed dIgA-SC complex is termed secretory IgA (sIgA) (425 kDa) and is transcytosed across the cell into the lumen (A. Bonner et al. 2008; Mostov 1994) (Figure 1.05). Secretory IgA is the predominant immunoglobulin in secretory fluids of the body (Boehm et al. 1999; M A Kerr 1990; Oortwijn et al. 2008; Jenny M Woof & Mestecky 2005).

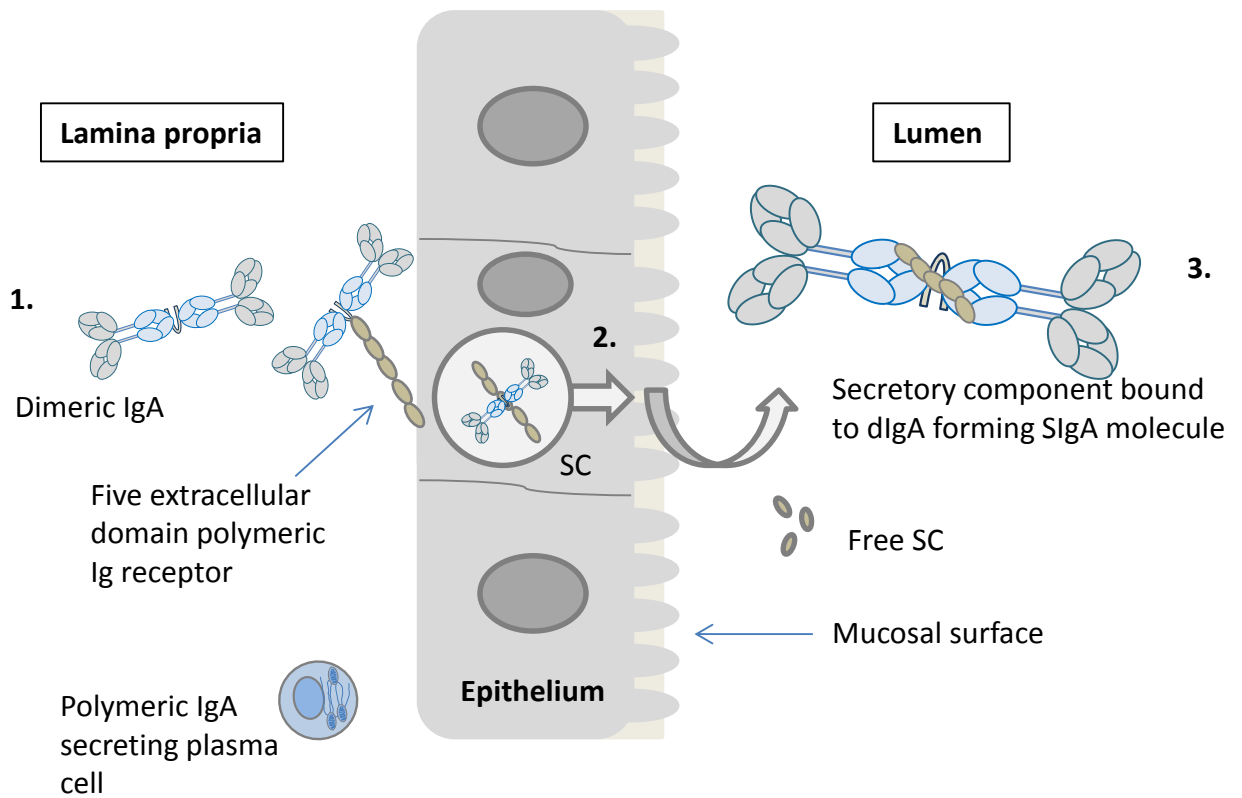


Figure 1.05 – Schematic diagram of the structure and synthesis of secretory IgA. At mucosal sites, polymeric IgA (predominantly in the dimeric (dIgA) form) is produced by IgA secreting cells at the lamina propria of epithelial cells (1). The dimeric IgA molecules become bound to the five domain transmembrane protein - polymeric immunoglobulin receptor (pIgR) (Brandtzaeg, 2007; Kerr, 1990). The pIgR is expressed extracellularly. Once bound, the dIgA-pIgR complex is subsequently internalised into the epithelial cell via receptor-mediated endocytosis (2), whereby proteolytic cleavage of the pIgR results in secretory component (SC). The release of secretory IgA (SIgA) into mucosa on the luminal side follows (3). The transcytosis of pIgR without IgA leads to the release of free SC into the lumen. SIgA may be of either isotype of IgA (IgA1 shown) (Bonner et al., 2008).

1.3 IgA nephropathy

Originally described over 40 years ago in 1968 by Berger and Hinglais, IgA nephropathy (IgAN) has since become recognised as an important cause of progressive end-stage renal disease (ESRD) worldwide. Initially termed Berger's disease, IgAN is characterised by the predominant deposition of IgA in glomerular mesangium. In accompaniment to abnormal IgA deposition, extracellular matrix expansion and mesangial cell hypercellularity are also constituent features of the disease which frequently affects young adults (J Barratt & Feehally, 2005; Cattran et al., 2009; D'Amico, 2000).

Today, IgAN is the leading cause of chronic kidney disease (CKD) through primary glomerulonephritis worldwide (J Barratt & Feehally, 2005) where renal biopsy is performed. Over the many years since its discovery, it is generally understood to be a complex, multifactorial disease with an as yet unclear etiologic cause. With highly variable clinical and pathologic outcomes, ranging from asymptomatic haematuria to varying rates of progressive renal failure, up to a third of patients diagnosed with IgAN progress to ESRD within 20 years.

The disease can occur in patients of any age, though is more prevalent in those between 16-35 years old and uncommon in those under 10 years old. IgAN affects males:females with a reported ratio between 6:1 and 2:1.

Epidemiologically, IgAN has a worldwide distribution with varying rates of incidence being reported. The cause of this variation however is likely due to the differing screening programmes that exist. Legal routine urinary screening of school children in Japan, among

others for example are evidently more likely to identify and further investigate haematuria and proteinuria- which incidentally may be due to IgAN.

With a growing global incidence of CKD, IgAN is an important and increasing source of patient morbidity and mortality with wide ranging socioeconomic implications (Alebiosu & Ayodele, 2005; White, Cass, Atkins, & Chadban, 2005).

1.3.1 Pathogenesis

IgAN is a glomerular disease initiated through the deposition and accumulation of IgA. Deposited IgA is occasionally accompanied by complement component C3 and IgG. The degree of mesangial cell hyperproliferation and inflammatory glomerular injury are variable in IgAN, with the renal outcome spectrum for patients resting between an asymptomatic, subclinical state of disease to one of acute kidney disease accompanied by crescentic glomerulonephritis (Barratt & Feehally, 2005; Coppo & Amore, 2004). Most patients however present chronically. The initiating and characteristic hallmark of this is invariably the accumulation of glomerular IgA. The precise mechanisms of deposition however remain unknown.

The exploration into the initiation of spontaneous mesangial deposition of IgA using mouse models, in particular the ddY strain has proven useful in the establishment of an IgAN model (Barratt, Smith, Molyneux, & Feehally, 2007; H. Suzuki et al., 2005; Tomino, 2008). These studies although valuable as models of IgA deposition (but not glomerular injury) fall short in their transferability to humans and clarity regarding the precise mechanisms involved in IgAN.

Despite a number of genome wide linkage studies, it remains uncertain as to the exact genetic nature of IgAN. However a familial incidence of increased serum IgA has been noted in unaffected IgAN patient family members (Schena et al., 1993)

It has been proposed that a number of potential mechanisms are involved in the complete pathogenesis of IgA1, including mesangial propensity to deposition, altered production or handling of systemic IgA and physiochemical changes to the molecule (Barratt et al., 2007). It may be possible that these mechanisms either alone, or together may co-segregate into differing phenotypes of observed IgAN.

1.3.2 Macromolecular characteristics of IgA in IgAN

Circulating and deposited IgA1 eluted from the glomeruli of patients with IgAN has shown the IgA to possess a number of macromolecular characteristics implicated in the promotion of IgA deposition and disease activity. These characteristics are principally related to IgA isotype, concentration, molecular charge, light chain usage and altered hinge glycosylation. Together these attributes, in combination or co-segregated, constitute a theoretical 'pathogenic IgA' molecule.

Mesangial deposited IgA is present uniquely as IgA1, manifesting principally in higher molecular weight polymeric forms (pIgA) and immune-complexes. IgAN patients have higher circulating concentrations of IgA1; however an elevated serum IgA1 concentration alone is not sufficient for glomerular deposition. HIV and in particular IgA myeloma patients may have extremely high circulating IgA with no deposition (Barratt & Feehally, 2005; Monteiro et al., 1993). Polymeric forms of IgA1 have been shown to exhibit stronger binding and stimulatory effects on mesangial cells, in addition to possessing a greater degree of undergalactosylation in comparison to its monomeric IgA1 counterpart (Oortwijn et al., 2006).

Studies investigating the distribution of light chain usage in IgAN patients and control groups have identified an increased λ light chain predomination of glomerular eluted and serum IgA1, with an increased pathogenicity for pIgA1 (Lai, Chui, Lewis, Poon, & Lam, 1994; Lai, To, Li, & Leung, 1996; Leung, Tang, Lam, Chan, & Lai, 2001; Suen, Lewis, & Lai, 1997). The higher proportion of λ light chains gives rise to an elevated anionic charge (Harada, Hobby, Courteau, Knight, & Williams, 1989; Leung et al., 2001).

Despite the varying macromolecular picture of pathogenic IgA1 in IgAN, consensus agrees that the defect appears to lie intrinsically with the IgA1 molecule itself (Lai, 2006).

1.3.3 O-linked glycosylation in IgAN

Defects in IgA1 hinge region O-glycosylation have been the most widely studied and consistently implicated observation in IgAN (Allen, Bailey, Barratt, Buck, & Feehally, 1999; J Barratt & Feehally, 2005; Beerman, Novak, Wyatt, Julian, & Gharavi, 2007; Hiki et al., 1998, 2001). HAA lectin binding is an indirect technique which captures the entire IgA molecule on an ELISA principle. The technique does not possess the discriminatory power to resolve the exact locations or structures of the hypogalactosylated hinge region. It does however enable the overall proportion of glycosylation to be assessed in a population. Glycoforms of IgA1 present as a heterogeneous mixture within an individual, with varying occupancy and conformations of GalNAc, galactose and sialic acid content (Hiki et al., 1998, 2001). Aberrant glycosylation of circulating and glomerular deposited IgA1 in IgAN however presents with a reduction in terminal galactose and/or sialic acid, resulting in an increased exposure of core GalNAc residues (Figure 1.03)

Aberrantly glycosylated IgA1 molecules undergo self-aggregation *in vitro* forming high molecular weight (HMW) immune complexes (Gomes et al., 2010; Novak et al., 2007; Novak, Julian, Tomana, & Mestecky, 2008). Moreover an auto-immune mechanism for IgA1 deposition brought about through the formation of circulating undergalactosylated, over-exposed IgA1 core GalNAc residues generates novel antigenic determinants that can be recognized by naturally occurring IgG and other IgA1 antibodies (Novak et al., 2011). This leads to the formation of circulating immune complexes.

The co-deposition of IgG however is not always identified in the renal mesangium of patients, and furthermore is not necessary for disease activity or diagnosis of IgAN (J Barratt & Feehally, 2005; D'Amico, 2000).

The unique *O*-glycosylation, specific localisation of the hinge (bridged between the binding and effector fragments of the immunoglobulin) and its fundamental role in providing flexibility in antigen binding are peculiar to IgA1 and integral to its function. The global effect of the altered glycosylation upon viable IgA1 structure and functions remains unknown.

1.3.4 Clinical features

The clinical presenting features of IgAN are variable but most commonly include the onset of visible haematuria, a symptom described by patients as ‘cola’ coloured urine, and both asymptomatic microscopic haematuria and proteinuria detected by routine urinalysis. IgAN is principally diagnosed via renal biopsy with positive IgA antisera immunofluorescence staining (Figure 1.06; C). This pattern is often also accompanied by mesangial hypercellularity (Figure 1.06; A-B).

Interestingly, inadvertent renal allograft transplants from patients with undiagnosed IgAN into renal recipients suffering from ESRD not caused by IgAN have shown complete remission of on-going glomerulonephritis and mesangial IgA deposition (Frohnert, Donadio, Velosa, Holley, & Sterioff, 1997; Ji et al., 2004; Sanfilippo, Croker, & Bollinger, 1982; K. Suzuki et al., 2003). This further supports an extrarenal, inherent abnormality of the IgA1 molecule.

1.3.5 Diagnosis and treatment

Aside from generic clinical features such as microscopic haematuria and proteinuria and developing renal insufficiency, there is no unifying archetypal presentation for patient diagnosis of IgAN (Barratt & Feehally, 2005). The ‘gold standard’ of diagnosis for IgAN therefore remains to be the presence of IgA in the glomerular mesangium detected by renal biopsy (Boyd et al., 2012) (Figure 1.6 A-C). To date an effective treatment for IgAN remains elusive with treatment regimens focussing principally on the amelioration of the symptoms of renal insufficiency (Barratt & Feehally, 2006).

The recent Oxford Classification of IgA Nephropathy published in 2009 has sought to consolidate and address the varying clinicopathological findings and outcomes observed in the disease, aiding physicians in identifying features suggestive of poor prognosis (Cattran et al., 2009). A large cohort of international patient data was reviewed by a consensus group of the International IgA Nephropathy Network and the Renal Pathology Society to develop a classification for the large number of pathologic variables seen. The classification defines biopsy features that are predictive of progression, independent of any clinical prognostic factors. These factors are graded resulting in a 'MEST' score. Histopathologically this is comprised of mesangial hypercellularity (M), endocapillary hypercellularity (E), segmental glomerulosclerosis (S) and tubular atrophy/interstitial fibrosis (T). Alone and in conjunction, these factors were all shown to possess value in assessing IgAN prognosis.

Currently treatment therapies that may serve to prevent or limit mesangial IgA deposition do not exist, therefore treatment strategies aim to limit the extent of kidney damage akin to all patients with chronic renal disease. Effective control of blood pressure (BP) by maintaining a target BP of <135/75 mmHg is critical, alongside cardiovascular risk reduction.

In patients with proteinuria (>1g/24 hrs) renin angiotensin system (RAS) blockade can be highly beneficial. This may be achieved through the administration of ACE inhibitors and/or angiotensin receptor blockers (ARBs).

There is no conclusive evidence for the use of immunosuppressive agents in IgAN. The use of treatments such as fish oil, anti-coagulants and anti-platelet agents have also been

reported, however they have no proven benefit. It remains therefore, that most effective treatment in patients with ESRD is transplantation. The risk of disease recurrence post-transplantation is 13-60%. This treatment method is however, not without its own risks and considerations.

Ultimately however, a better understanding of the root cause of IgA1 deposition, and an early, complete removal of mesangial deposited IgA1 at this stage would serve to be the most effective treatment option (Tanaka, Seki, Someya, Nagata, & Fujita, 2011).

1.3.6 Clinical associations with IgA and IgAN

Alongside primary IgAN there exist a number of other diseases associated with glomerular deposits of IgA, the most evident case being that of Henoch–Schönlein purpura nephritis (HSPN). Henoch–Schönlein nephritis HSP, unlike IgAN, is not glomerular specific, but a systemic small-vessel vasculitis, with deposition of IgA containing immune complexes. This presents as a characteristic purpuric rash, normally seen in children but also adults (Jonathan Barratt et al., 2007; Feehally & Floege, 2010).

The renal pathogenesis is indistinguishable from that of IgAN and a differential diagnosis is principally made through extra-renal manifestations (Cattran et al., 2009; Feehally & Floege, 2010) (Figure 1.07). Aberrant glycosylation of IgA1 in HSP has also been identified (Novak et al., 2007; Yu, Chiang, & Yang, 2012).

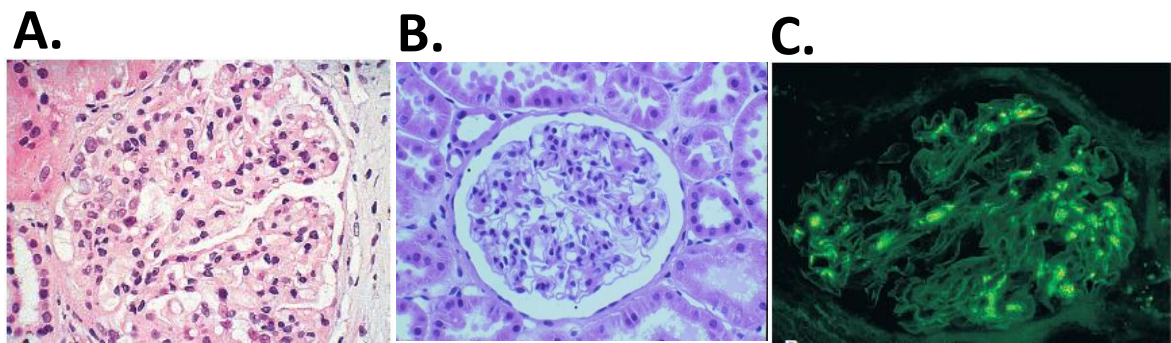


Figure 1.06 – Renal pathology in IgA nephropathy from biopsy. (A) Light microscopic haematoxylin-eosin stain of a glomerulus, illustrating the loss of glomerular morphology and mesangial cell proliferation. The alteration to glomerular architecture results in progressive decline in function culminating in renal failure. (B) Light micrograph of glomerulus demonstrating mesangial hypercellularity. (C) Indirect immunofluorescence microscopy of glomerulus using fluorescein isothiocyanate (FITC) labelled anti-IgA demonstrating the presence of IgA. Co-deposition of IgG, IgM and complement factor C3 in the glomerulus may also be seen; however neither is needed for the diagnosis of IgAN. Images adapted from (Feehally & Floege, 2010).



Figure 1.07 – Henoch-Schönlein purpura of the legs in a 4-year old child. The deposition of aberrantly glycosylated IgA1 is a shared characteristic between HSP and IgAN; rendering HSP pathologically indistinguishable from IgAN. Clinically, extrarenal features (those not relating to renal function) such as a palpable purpuric rash of the lower limbs, and the early age of disease onset in HSP are some factors which clinically distinguish them. (Image taken from Dermatology Image Atlas - dermatlas.med.jhmi.edu - ID: 1353783694)

1.4 Methods used to determine immunoglobulin structure

The three-dimensional structural determination of a protein enables an evaluation of its conformation and function, often facilitating direct relation to physical function *in vivo*. This has important consequences for the study of complex, multi-domain proteins such as antibodies in a state of both health and disease.

Antibodies are large, flexible and occasionally polymeric structures or complexes. In the particular case of IgA1 they are complicated further by containing highly heterogeneous glycosylated regions in its hinge regions. This has the effect of rendering certain high-resolution techniques such as nuclear magnetic resonance (NMR) or X-ray crystallography very difficult to apply to these molecules. These structure determination methods have the advantage of resolving protein structure information at an atomic coordinate level (0.1-0.3 nm). This is of increased benefit when producing molecular models.

In such a situation, the approach of using solution scattering and analytical ultracentrifugation combined with constrained modelling, allows the structural and hydrodynamic examination of antibodies in near-physiological conditions. These provide structural information to a medium resolution level (1-2 nm) (Mertens & Svergun, 2010; Neylon, 2008; Stephen J Perkins & Bonner, 2008).

1.4.1 Electron microscopy

Electron microscopy (EM) has a greater magnification and resolving power to that of light microscopy, yet the high level of radiation produced can potentially damage the biological sample.

Providing low resolution structural details, and a low signal to noise ratio means that the information obtained by EM from many macromolecules must be combined and averaged. In a typical solution, protein molecules are not ordered but may exist in several conformations or views. This is particularly true for antibodies such as IgA1, where the hinge regions and tailpieces increase molecular flexibility, permitting increased antigenic reach.

It is often necessary to process the protein samples to successfully visualise the protein structure using EM. Protein fixation and staining techniques can damage or distort the protein structure, altering its three dimensional arrangement from that in native physiological conditions. In addition protein samples are visualised *in vacuo*.

Determinations of the site of interaction between proteins or the structures of multiple proteins within a complex are difficult to determine by EM and this is exemplified by the two EM structures for IgA. These studies have illustrated the end-to-end 'Y' shapes of IgA in the dimer (Dourmashkin, Virella, & Parkhouse, 1971; Munn, Feinstein, & Munro, 1971) (Figure 1.08 A & B).

A.



B.

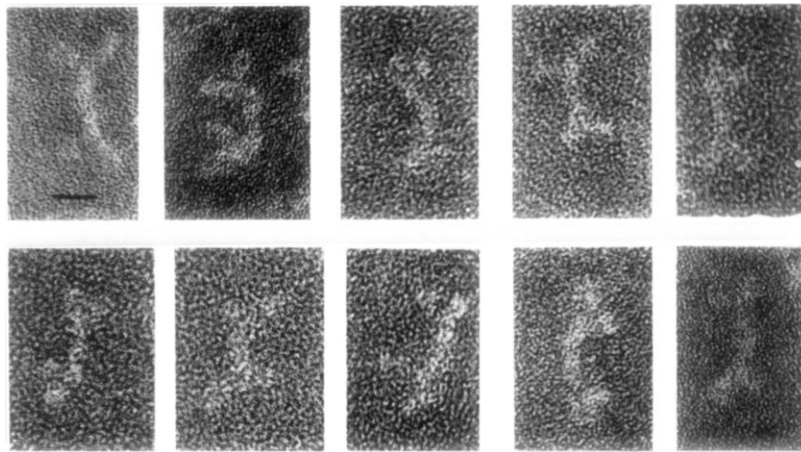


Figure 1.08 - Electron micrographs of human IgA selected from total IgA. Early studies using EM looking at the structure of IgA revealed the appearance and flexibility of both mouse (not shown) and human IgA. (A) and (B) Dimeric human IgA myeloma, identifying the ‘double Y’ immunoglobulin appearance (four Fab regions connected via J-chain linker at Fc regions) of dimeric IgA (Dourmashkin et al., 1971; Munn et al., 1971). The slight variations in structure of the IgA in the EM micrographs can be attributed to the artefacts of the protein fixation and staining methods utilised, and the high level of radiation.

1.4.2 Nuclear magnetic resonance

Nuclear magnetic resonance (NMR) is a high-resolution biophysical technique which provides information relating to the position of atoms of proteins in a solution state. This is done by exploiting the specific magnetic properties of certain nuclei.

The large molecular masses of antibodies (~ 150 kDa; Table 1.2) renders them much larger than the maximum molecular mass normally used for NMR, which is around 30-40 kDa (S J Perkins et al., 2008; Widmer & Jahnke, 2004). The large size means that a structural determination of intact IgA1 is unlikely with conventional NMR alone due to signal overlap and is therefore unsuitable. Information from NMR may however be used to complement X-ray crystallography and small angle scattering studies (Widmer & Jahnke, 2004).

1.4.3 X-ray crystallography

As with NMR, X-ray crystallography is high-resolution structural technique (0.1 nm). Provided crystals can be grown, during crystallography experiments the electrons of a protein fixed in a crystal lattice are exposed to a monochromatic, collimated X-ray beam. The acquisition of diffraction data and electron density maps permits the resolution of individual atoms; it is to this in which a structure is normally fitted.

Although X-ray crystallography has the advantage of providing detailed information regarding the organisation of fixed proteins, or protein fragments, it fails in capturing the dynamic native-like conformation of flexible multi-domain proteins in solution. Scattering experiments therefore provide the best means for obtaining an overall structure of the protein, albeit at lower resolutions.

1.4.2 Analytical ultracentrifugation

Analytical ultracentrifugation (AUC) provides information on the solution behaviour of macromolecules over a wide range of concentrations and in a large number of different solvents. It provides a number of advantages to the study of solution proteins; principally it is a non-destructive, rapid, and simple technique.

Although the same instrument is used, there exist two types of AUC analysis - sedimentation velocity (AUC-SV) (Section 1.4.2.1) and sedimentation equilibrium (AUC-SE) (Section 1.4.2.2). These both provide differing information in relation to a protein (Ralston, 1993). Measurement of sample monodispersity (presence of a single protein) by AUC-SV experiments are superior to gel matrix methods (such as size exclusion chromatography) as there is no non-specific binding to the resin, e.g. large aggregates and all of the original sample is recoverable. It is therefore a particularly powerful technique in the determination of homogeneity of protein preparations and allows further biophysical analysis with sensitive techniques such as solution scattering. The sedimentation coefficient generated from these experiments serves as an independent parameter of macromolecular elongation (Figure 1.09).

1.4.2.1 Sedimentation velocity

AUC sedimentation velocity (AUC-SV) experiments represent a dynamic technique, permitting the study of macromolecular structures in solution by spectroscopically following their sedimentation behaviour on subjection to high centrifugal force (Ralston, 1993) (Figure 1.09).

The fundamental principle of AUC-SV is governed by the observation of the movement of solute away from the meniscus (narrower end of sector-shape cell, Figure 1.09; B) toward the bottom of the cell. On commencement of an AUC-SV experiment the protein sample is initially present within the cell at a uniform solution throughout. During centrifugation, the particles move along a gravitational force lines resulting in the meniscus being cleared of solutes, and a moving boundary forming between the solvent depleted of solutes and the solvent of finite concentration (Figure 1.11 A). Each macromolecule presents as having a different mobility under a gravitational field and this principle is exploited to separate the species with a different sedimentation coefficient.

The sedimentation coefficient (S) is a measure of the rate at which a particle sediments and corresponds to the elongation, shape and molecular weight of a macromolecule (Equation 1.1). Higher values indicate less compact, heavier structures. Therefore the more extended a molecule is, the slower it will sediment and the larger its S value will become. A more compact molecular structure will however sediment faster than an equally weighted molecule, due to the generation of less friction. The S value is also an independent parameter of the radius of gyration (R_G), with more extended structures demonstrating increased Guinier R_G values (Figure 1.12). AUC-SV experiments are usually reported to normalised standard conditions of water at 20°C ($s_{20,w}^0$).

$$S = \frac{v}{w^2 r} = \frac{M(1 - \bar{v}\rho_{sol})}{N_{AV}F}$$

Where;

v = velocity of particle

w = angular velocity

r = distance from centre of rotation

M = molecular weight

\bar{v} = partial specific volume

ρ_{sol} = density of solvent

N_{AV} = Avogadro's number

F = frictional coefficient

Eq. 1.1 – The Svedberg equation, used to describe the behavioural characteristics of a macromolecule during centrifugation. The Svedberg coefficient is derived from the Svedberg equation and describes the movement of a particle in terms of molecular weight and frictional coefficient.

AUC-SV, especially when coupled with scattering experiments can also be used to study the homogeneity of a solution. The hallmarks of a homogenous solution are a single sharp symmetrical sedimenting boundary throughout the duration of the AUC-SV experiment. (Figure 1.11 B) Impurities may present as additional peaks, shoulders on the main peak or asymmetry of the main peak. SV can also be used to detect changes in conformation as the sedimentation rates of compact or disorganised molecules will be different.

For AUC-SV experiments, a minimum of 400 μ l of sample is required. When loading into the cells, it is necessary to load more of reference buffer (the buffer in which the molecule is suspended) to give the appropriate absorbance/interference pattern (Figure 1.09 B). Interference optics can be used in the range 0.5 – 5 mg/ml and absorbance optics at concentrations greater than 0.1 mg/ml (Ralston, 1993).

The buffer density and viscosity are required for sedimentation coefficient determination. The buffer density and viscosity may be determined experimentally using a viscometer for example or calculated theoretically using the programme SEDNTERP (Laue et al., 1992). In general, an increase in temperature results in a decrease in density.

The unique partial specific volume for a molecule is calculated from both the amino acid and carbohydrate content of the molecule. Some consideration and assumption of the large carbohydrate hinge region of IgA1 was required and trial experimentation using SEDNTERP showed that total/partial removal of carbohydrate did not alter the partial specific volume for the IgA1 molecule.

1.4.2.2 Sedimentation equilibrium

Analytical ultracentrifuge sedimentation equilibrium (AUC-SE) experiments require much lower centrifugal forces than those of AUC-SV experiments. In AUC-SE, a centrifugal force is applied so that the opposing diffusion of the macromolecule is equal to that of the sedimentation. Thus in contrast to AUC-SV experiments, where macromolecules are forced to the base of a cell, solute molecules are held in equilibrium between sedimentation and opposing diffusion. This results in a net movement of zero for the macromolecule.

The AUC-SE sample column is 2 mm in length (much shorter than that in AUC-SV) to allow equilibrium to be reached in between 10 – 36 hours, depending on the protein shape and rotor speed.

Whereas AUC-SV is concerned with obtaining information related to macromolecular shape, equilibrium experiments are important in determining macromolecular weight and stoichiometry.

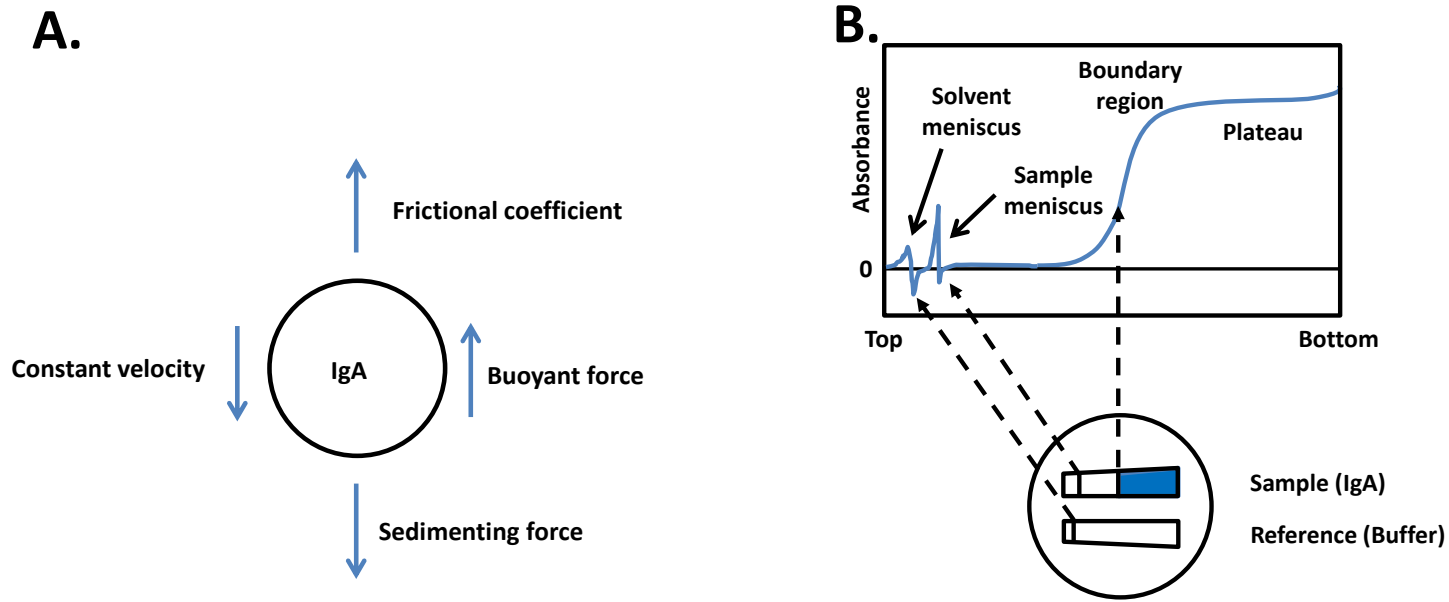


Fig 1.09 – Principles of sedimentation of a molecule and the analytical ultracentrifuge during a sedimentation velocity experiment.

(A) Sedimentation of large molecules in solution will occur if the solution is left to stand, due to the effects of gravity. The rate at which a molecule sediments can be increased by the application of centrifugal force. During sedimentation a molecule experiences a number of forces; principally the sedimenting force and the frictional coefficient, derived from the rotor speed and solvent resistance exerted on the molecule. Molecules which differ in density, shape or size can be separated because they sediment at different rates in a centrifugal field. (B) Sample and reference solutions are placed in sector-shaped cells and undergo sedimentation. The protein is present at a uniform concentration throughout the cell. As the protein sediments towards the bottom of the cell over time, a moving boundary of protein depleted solvent is formed. The boundary region is detected spectroscopically using absorbance and interference optics. (Figures adapted from (Ralston, 1993)) The use of $c(s)$ distribution plots in computational software programs such as SEDFIT model process all the scans and identify the sedimenting species present. This is useful in providing information relating to the monodispersity of a sample preparation (S J Perkins et al., 2008; Schuck, 2000)

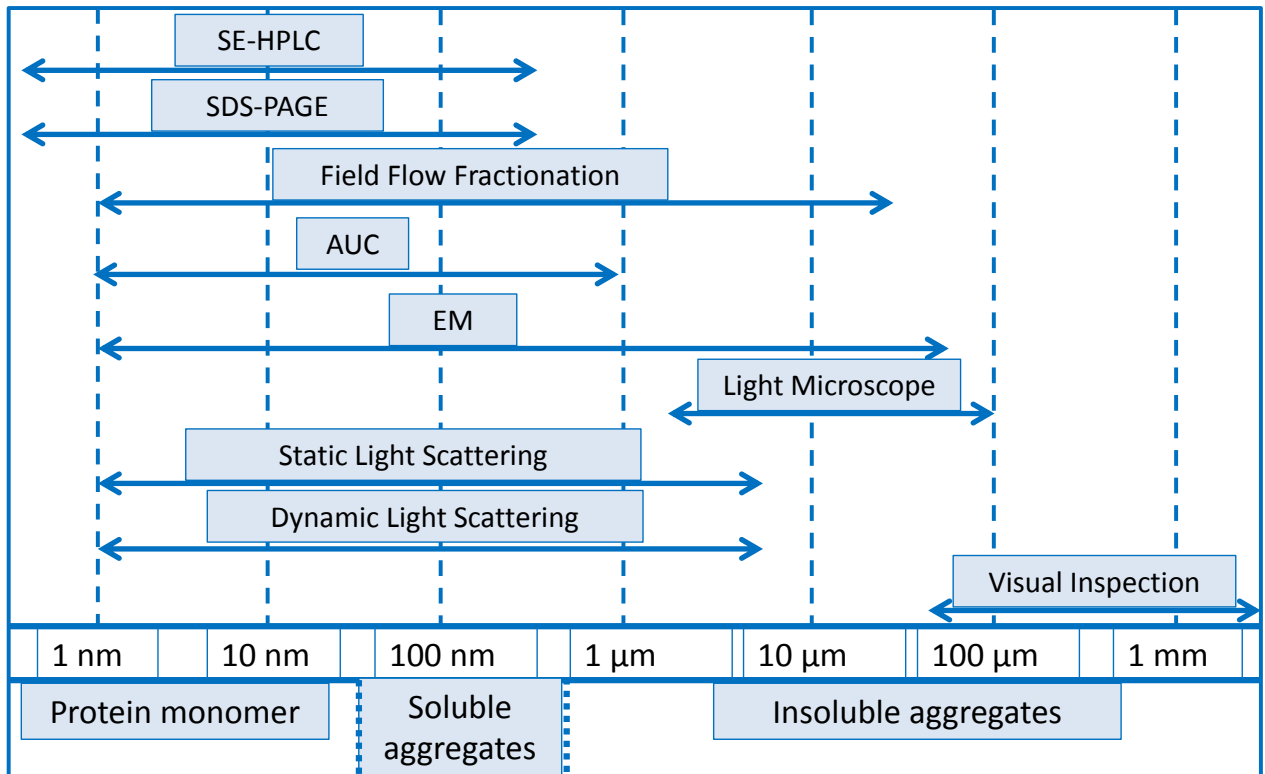


Figure 1.10 - Detection methods for solution aggregation. Obtaining a monodisperse, aggregate and fragment-free protein solution for structural determination is clearly of paramount importance. Small amounts of solution aggregation (as low as 1-2%) can significantly affect techniques like solution scattering, compromising results enough to render them unusable. Aggregation and polydispersity can be seen on Guinier R_G plots, usually presenting as non-linearity of plots for the latter. With the potential for trace aggregates to compromise results, it is clearly of paramount importance to ensure aggregate-free, monodisperse mIgA1. Analytical ultracentrifugation in particular has many advantages over SEC, and serves as vital techniques in the identification of aggregates species, which can vary considerably in size (J. Liu, Andya, & Shire, 2006). This figure illustrates various techniques and their size sensitivity, utilised in the detection of aggregates in solution. (Adapted from (Mahler, Friess, Grauschopf, & Kiese, 2009))

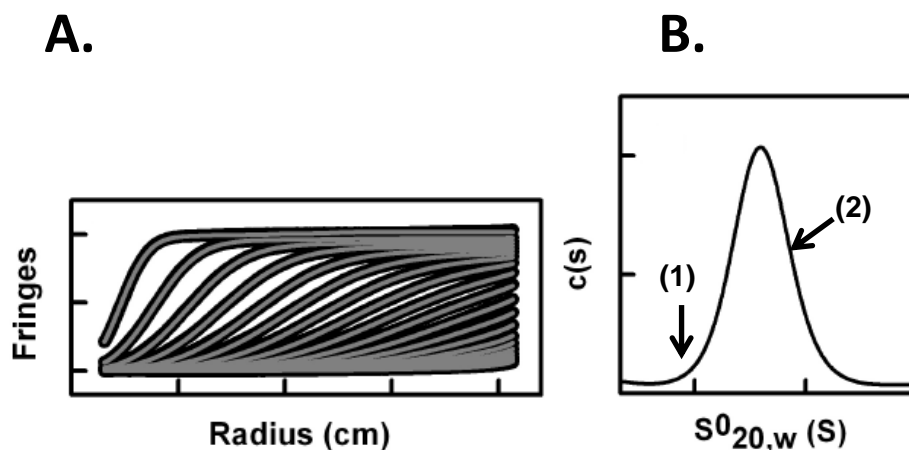


Figure 1.11 - Example analyses of sedimentation velocity experiments using SEDFIT software. (A) The formation and movement of boundary regions during a sedimentation velocity experiment (AUC-SV). (B) The $c(s)$ distribution plot, reflecting the populations of different sedimenting species. Aggregates and small fragments can often be very difficult to visualise with other techniques such as size-exclusion chromatography and SDS-PAGE. Impurities and polydisperse solutions may present with additional peaks around the main peak of interest (1) or shoulders on the main peak itself (2).

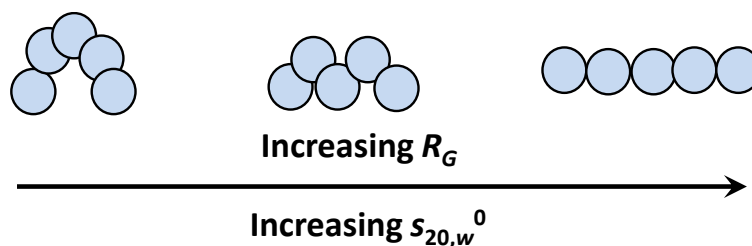


Figure 1.12 - The effect of macromolecular elongation on the radius of gyration (R_G) and sedimentation coefficient ($s_{20,w}^0$). As a molecule becomes more elongated (towards the right of figure), there is a detectable effect upon the radius of gyration (R_G). As an independent, complementary parameter of elongation, the sedimentation coefficient ($s_{20,w}^0$) also demonstrates increase with Guinier R_G when a molecule becomes more extended.

1.4.2.2 Combining AUC and solution scattering

Analytical ultracentrifugation data monitors the extent of macromolecular elongation through the sedimentation coefficient. The radius of gyration, obtained through Guinier analysis (R_G) of scattering curves is also a measure of macromolecular elongation. AUC-SV experiments, in addition to information relating to monodispersity provide an independent structural parameter for a molecule (Figure 1.12). This is beneficial when modelling scattering data, which can further be constrained by the S value of a particular protein.

1.4.3 Solution scattering experiments

Small angle solution scattering (SAS) is a method which offers low-resolution structural information (2-4nm) concerning macromolecules in a native solution state without some of the complications seen in other structural techniques such as X-ray crystallography and NMR. In contrast to X-ray crystallography, SAS is a solution technique which can offer insights into the flexibility and the solution structure of macromolecules under a variety of concentrations and conditions. Both X-ray and neutron solution scattering (SAXS and SANS) experiments are carried out in a similar manner, differing principally in their atomic interactions and the information they reveal (Table 1.03).

In contrast to SAXS, SANS has a more straightforward sample preparation, requires less material and the duration of the experiment is shorter. With SAS the requirement for a given molecule to form crystals is not an issue.

Homology modelling - the combination of both low resolution data from SAS experiments with known atomic resolution data obtained from crystal structures, on either part of the molecule or similar domains from other proteins, provide an overall molecular model of the protein in solution to a medium resolution (1-2 nm). This approach does not generate a unique structure, but instead a range of structures which can be ranked on their homology to the experimental data. This is a good method with which to study the structure of IgA1 in IgAN as crystallisation of the intact antibody is not possible, whereas crystal structures of the Fab and Fc fragments of IgG have been obtained.

The major strengths of solution scattering are that it provides multi-parameter structural information on proteins, in the absence of a crystal structure; which are analysed in near-physiological conditions. These include the molecular mass, radius of gyration, hydrated volumes and the maximum macromolecular diameter (S J Perkins et al., 2008; Petoukhov & Svergun, 2007).

Furthermore, this data serves as an ideal complementary method for high-resolution models identifying any significant oligomeric or conformational differences between the solution and crystal structure) or where they cannot be applied. (Nan, Gor, & Perkins, 2008; Stephen J Perkins & Bonner, 2008). Diffraction of X-rays and neutrons is described by Bragg's Law;

$$\lambda = 2d \sin \theta,$$

where 2θ corresponds to the scattering angle and d is the diffraction spacing.

High flux beam sources such as the European synchrotron research facility (ESRF) and the Institut Laue-Langevin (ILL), Grenoble have served to vastly improve the quality and efficiency in which solution scattering experiments can be performed.

1.4.3.1 Neutron scattering

In SANS experiments, a sample is irradiated with a monochromatic, collimated beam of neutrons. These neutrons are deflected by atomic nuclei. The absence of radiation damage and possibility of contrast variation by selective deuteration ($\text{H}_2\text{O}/^2\text{H}_2\text{O}$) makes SANS an extremely useful complementary tool to SAXS. Unlike light or SAXS experiments however where scattering is proportional to the number of electrons present in a protein, in SANS experiments the neutron-nuclei interactions vary irregularly – between isotopes of elements. The most significant of these is seen with the scattering angles of hydrogen (^1H), which has a negative scattering length (-0.374 fm) and deuterium (^2H), which has a positive scattering length ($+0.667 \text{ fm}$) in line with other organic elements (Perkins, et al., 1998; Perkins, 1988; Petoukhov & Svergun, 2007). This scattering characteristic permits the use of selected deuteration of a protein.

In neutron experiments the hydration shell, that is solvent water molecules closely associated with the protein by way of hydrogen bonding, are not visible and almost undetectable. While in X-ray scattering experiments this hydration shell is visible (Petoukhov & Svergun, 2006).

1.4.3.2 X-ray scattering

During SAXS experiments, samples are irradiated with a monochromatic, collimated beam of X-rays. Diffraction of these X-rays from the electrons present in the molecule result in a

scattering pattern. This is for all molecules randomly orientated within a solution (Figure 1.13).

The use of X-rays results in radiation damage to the protein during data collection, and can cause spontaneous aggregation of the molecule impairing the accuracy of the collected data. Continuous sample checks need to be made to ensure that this has not occurred (Figure 1.14). Radiation damage caused by X-rays is minimised by limiting exposure times to 10 seconds and continuously moving the sample. Concentration series are also prepared to show that there are no concentration dependent effects on the scattering curve.

X-rays are also absorbed by high-salt buffers, so it is important to consider the buffer in which the protein is formulated. Water molecules that are hydrogen bonded to the molecule have an electron density higher than that of the bulk water, meaning that it is the hydrated dimensions of the molecule which are detected. In X-ray experiments the hydration shell for a protein is visible (Petoukhov & Svergun, 2007). Table 1.03 illustrates the major differences between the two methods.

Small angle X-ray scattering (SAXS)	Small angle neutron scattering (SANS)
X-rays interact with electrons	Neutrons interact with nuclei
Scattering proportional to number of electrons	Scattering not proportional to atom size. Both light and heavy elements are equally visible
Contrast variation experiments not possible	Contrast variation possible due to differing scattering length densities of hydrogen and deuterium
Monolayer of water molecules bonded to protein surface reveal hydrated dimensions of macromolecules– hydration shell	Bound water molecules not visible in heavy water, reveals unhydrated dimensions of macromolecules - no hydration shell
Radiation induced damage, technique enables checks for radiation damage	No radiation induced damage, however sample may aggregate in a non-specific manner due to heavy water buffers
0.1-0.2 second beam exposure times	1-2 hour beam exposure times
Smaller sample size and concentration required for analysis (~100 μ l, > 0.3 mg/ml)	Larger sample size and concentration required for analysis (~500 μ l ,>2 mg/ml)
Sample non recoverable after irradiation	Sample may be recovered and reused for additional studies (AUC, FPLC etc.)

Table 1.03 – Major differences between X-ray and neutron scattering experiments. The interaction with matter by both X-rays and neutrons during scattering experiments is fundamentally different, providing a variety of differing but mutually applicable information on the solution state of a macromolecule.

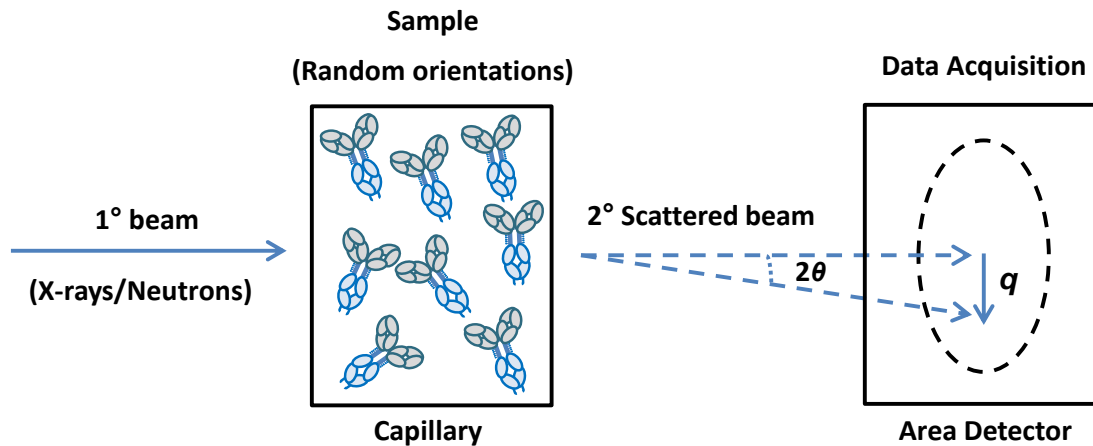


Figure 1.13 – Schematic diagram of solution scattering experiments. A collimated, monochromatic primary beam of X-rays or neutrons is applied to a sample, resulting in diffraction from electrons or atomic nuclei respectively. The accumulation of diffraction produces a scattering pattern obtained by an area detector. This represents the raw data acquisition stage. The radial average of the scattering pattern, around the position of the primary beam gives rise to the scattering curve $I(Q)$ in reciprocal space (See also Fig 1.1.4) (Perkins et al, 2009). The primary beam would damage the area detector, and is therefore masked by a beam stop. The application of a Fourier transformation of this gives rise to real space information for the protein in the form of a $P(r)$ curve.

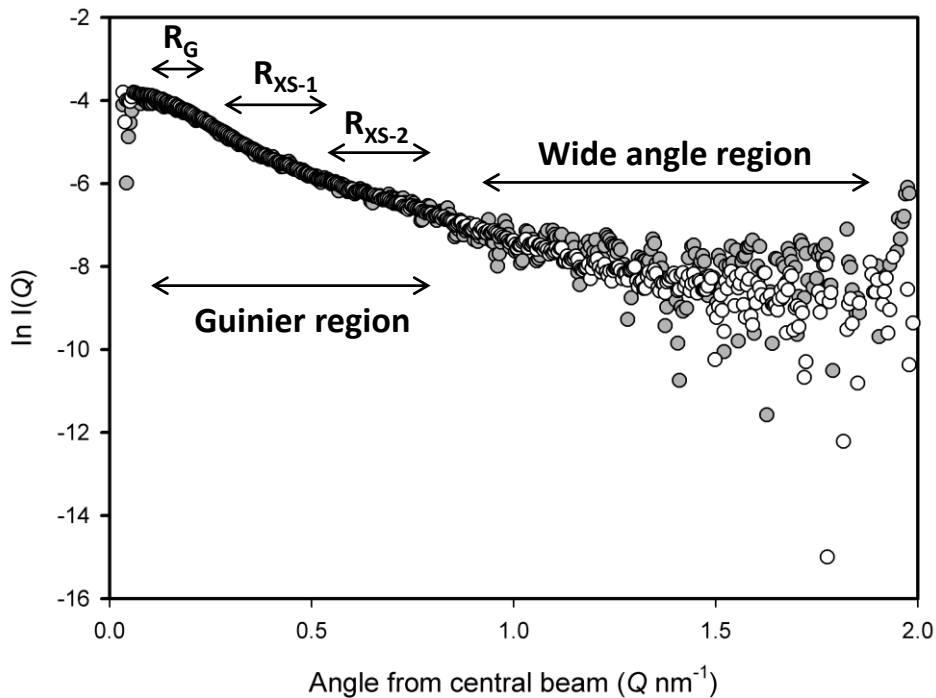


Figure 1.14 – Solution scattering curve, illustrating the Guinier region, which provides information corresponding to the overall shape of the molecule. The scattering curve shown here is an overlay of both a single frame (white) and the merged average of 10 time frames (grey) scattering data for mIgA1. This illustrates no radiation damage during sample irradiation. The curve is truncated at low Q due to the presence of the beam stop on the area detector. The linearity of the Guinier plots such as this also shows a measure of the monodispersity of the solution (the presence of only one type of species).

1.4.3.3 Application to other proteins

Solution scattering experiments, including the application of AUC have successfully been employed with a number of other immunoglobulins such as IgM and IgD and complement protein C3. These experiments provide an appreciation of function, receptor binding and protein organisation, examples include the identification of a near-planar solution structure of dimeric IgA1 (PDB code 2QTJ) and the major oligomeric forms of rat mannose-binding lectin (Bonner et al., 2008; Miller, Phillips, Gor, Wallis, & Perkins, 2012). The solution structure of pentameric IgM (PDB code 2RCJ) has also been determined using solution scattering experiments (Perkins et al. 1991).

These experiments when coupled with constrained molecular modelling techniques have enabled a unique view of the protein's structure in its native solution state, providing information that is directly relevant to biological function. This is particularly relevant to IgA1 in further clarifying its specific role in the mucosa tissue, interaction with multiple antigens and identifying the adopted 'T' shape structure of the Fab for increased antigenic reach (Figure 1.15).

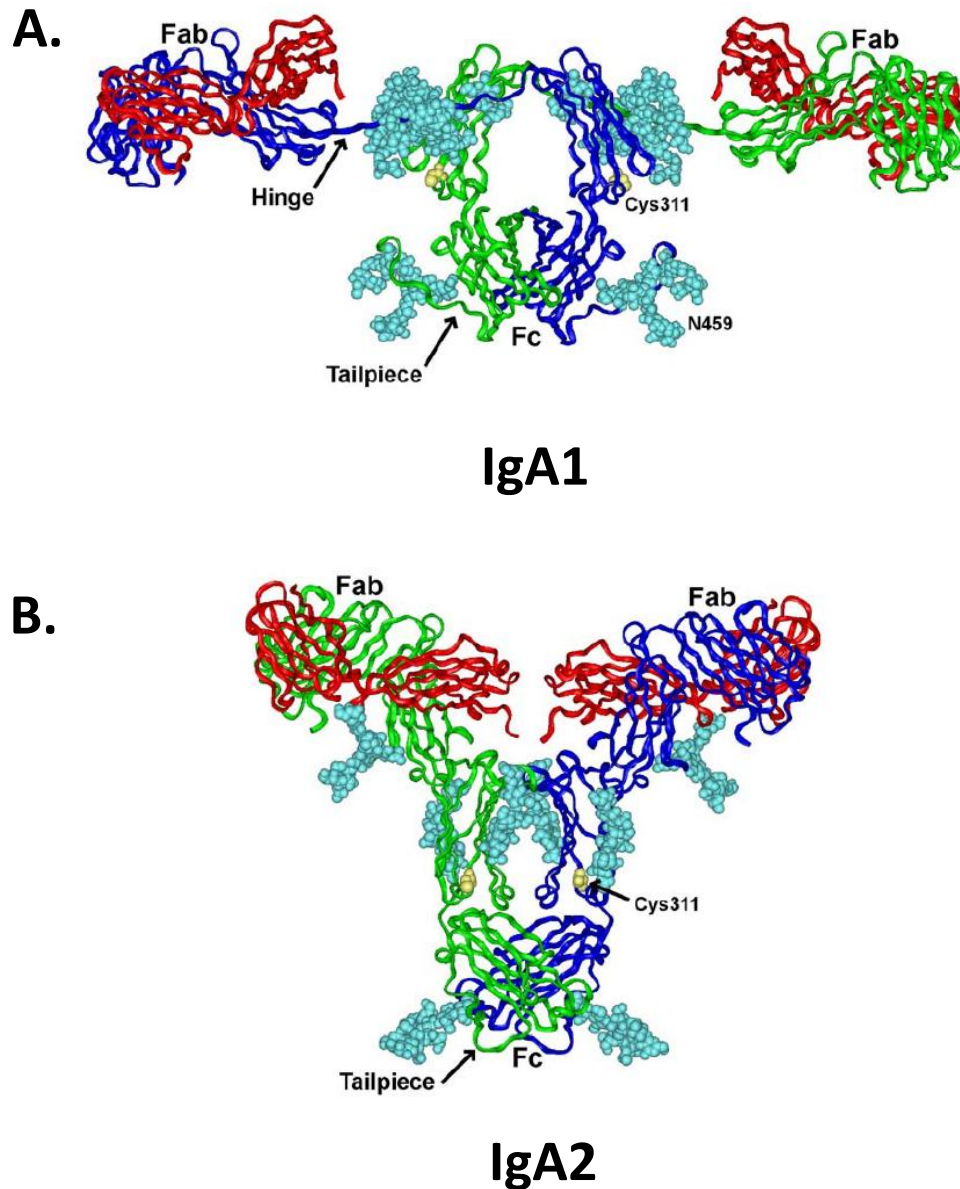


Figure 1.15 – Previously determined solution structures for IgA1 and IgA2m(1). The use of SAS experiments has previously been applied to (A) IgA1 (PDB 1IGA; Boehm et al., 1999) and (B) IgA2m(1) (PDB 1R70; Furtado et al., 2004), and these are shown as ribbon diagrams. The Fab, Fc and tailpiece of both antibodies are indicated. These diagrams illustrate the major structural differences between the best-fit solution structures for both subclasses, in particular the ‘T’ shape of IgA1. The antibody heavy chains (blue and green) and light chains (red), N-linked and O-linked carbohydrates (cyan) are also shown.

1.4.4 Data interpretation

The interpretation of scattering data collected by the area detector in both SANS and SAXS experiments are recorded on facility computers, ready for analysis. The extraction of low resolution structural information relating to a protein is obtained through Guinier and distance distribution analysis using the GNOM program (Svergun, 1991).

1.4.4.1 Guinier analysis

Information on molecular weight, radius of gyration (R_G), monodispersity and three-dimensional structural information can be obtained through Guinier analysis. At low resolution, the scattering can be described by the Guinier approximation. The difference between the primary X-ray beam and the scattered X-ray beam gives rise to a Q value. The most common approximation to use is the Guinier approximation for estimating the radius of gyration (R_G). The R_G describes the square root of the average squared distance of each scattered X-ray from the particle centre, relative to a molecules centre of gravity, or an axis or a given axis. Other methods also exist, including the Debye approximation, which are useful for the measurement of elongated proteins

1.4.4.2 R_G and R_{XS} analysis

In a given solute-solvent contrast, the radius of gyration R_G is a measure of the elongation of the glycoprotein assuming that the internal inhomogeneity of scattering densities within the glycoprotein has no effect (Perkins, 2008). Guinier analyses at low Q give the R_G and the forward scattering at zero angle $I(0)$. The R_G and R_{XS} analyses lead to the triaxial dimensions of the macromolecule if the structure can be represented as an elliptical cylinder

The lowest resolution portion of the SAXS curve $I(Q)$ is dictated by the R_G of the molecule. This is the square root of the average squared distance of each scatterer from the particle centre. The calculation of molecular weight is possible from the $I(0)$ parameter when Q equals zero. The linearity of any given Guinier plot shows a measure of the monodispersity of the solution, and serves as a vital check in ascertaining whether there has been any protein-protein aggregation due prolonged storage or agitation for example.

1.4.4.3 Distance distribution function analysis

The distance distribution function is a useful analysis which describes the paired-set of all distances between points (electrons in SAXS) within a macromolecular object such as IgA1. This is ascertained through indirect Fourier transformation of the scattering $I(Q)$ curve from reciprocal space, the pair-distance distribution function $P(r)$ of the molecule represents the population of distances (r) between volume elements in a solution in real space.

The $P(r)$ analyses are performed using the GNOM program (Svergun, 1991). Peaks in $P(r)$ plots indicate the most commonly occurring distances in the molecule, and are assigned maxima 1 (M1) and maxima 2 (M2) in the case of IgA1. Changes in these values can indicate internal conformational changes. This offers an alternative calculation of R_G and $I(0)$ which is based on the full range of the scattering curve, and also gives the maximum length dimension of the molecule, denoted as L .

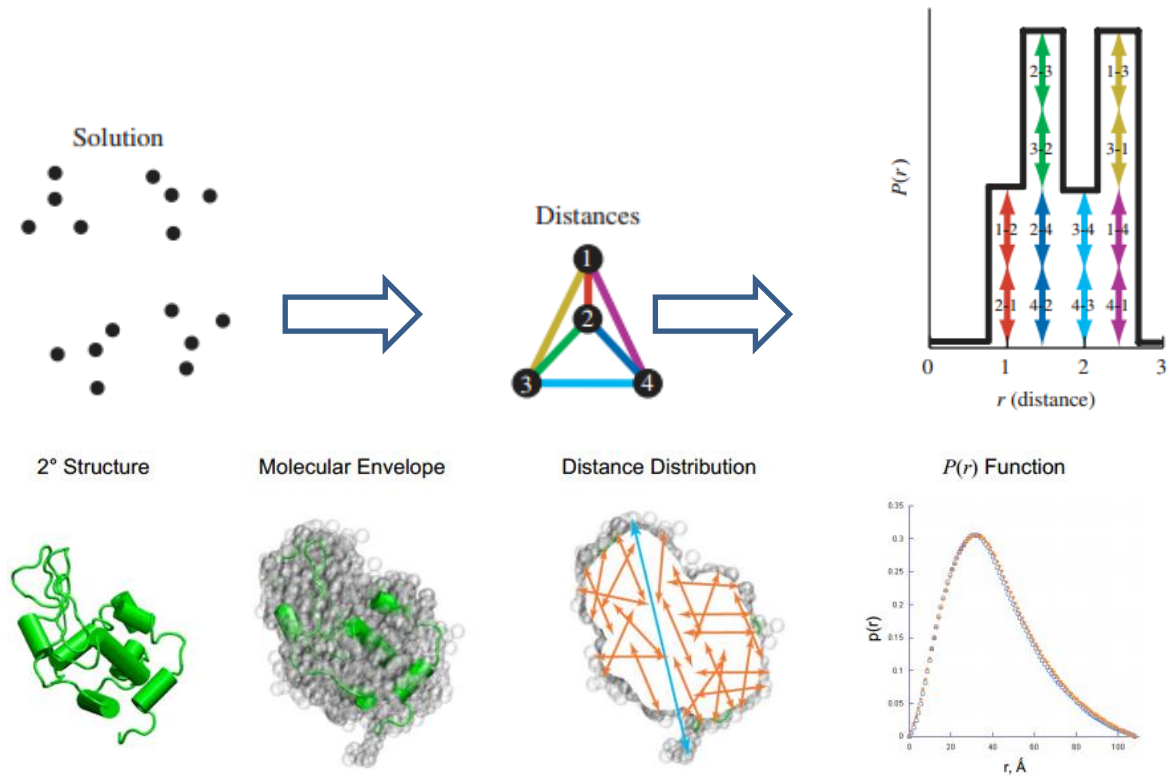


Figure 1.16 – The pair-distribution function in SAXS experiments. The $P(r)$ function provides a histogram of the paired set of all interatomic distances between scattering points within a molecule. This function enables small conformation changes in the relative positions of structural elements to be visualised. This figure illustrates the scattering points within the molecule (1-4; top panel) and their distance frequencies. The bottom panel demonstrates production of the $P(r)$ curve from the secondary structure of the protein.

Chapter Two

Materials and Methods

Unless stated otherwise, all reagents were purchased from Sigma-Aldrich, UK.

2.1 Sample selection and purification of IgA1

For the work presented in this thesis, serum was obtained with informed consent from 3 patients with biopsy-proven IgAN attending the Nephrology Clinic at Leicester General Hospital (LGH) and 1 healthy control subject. Two patients had progressive IgAN and had progressed to end-stage renal failure; one patient had non-progressive IgAN, the benign form of the disease. All patient and control personal data was anonymised.

2.1.1 Jacalin affinity chromatography

Serum IgA1 was purified by affinity chromatography using the lectin jacalin cross-linked with agarose (Vector Laboratories, USA) according to the previously described method (Allen et al. 1999). Briefly, high molecular weight proteins were precipitated from 10 ml of serum using an equal volume of 45% ammonium sulfate solution in PBS. After discarding the supernatant the precipitate was fully redissolved in 0.175 M Tris-HCl buffer, pH 7.5. The solution was mixed with a 50% suspension of packed jacalin-bound agarose. This mixture was stirred gently for at least 2 hours at room temperature to facilitate binding of the IgA1. The jacalin-bound proteins were centrifuged at 13,000 rpm for 10 minutes and the supernatant; containing any unbound protein was stored. The jacalin-agarose beads were then washed extensively with 4 washes in Tris-HCl buffer to remove any unbound protein from the saturated agarose beads. The IgA1 was subsequently eluted by addition of 1 M galactose in Tris-HCl for at least 2 hours at room temperature.

The eluted IgA1 in galactose buffer was clarified using a 0.2 µm syringe filter and dialysed overnight at 4°C against PBS using Spectra/Por 2 dialysis tubing (Spectrum Labs, UK) of

an appropriate molecular weight cut-off (8-10 kDa). This was performed with a minimum of two buffer changes. Purified IgA1 samples were then either used immediately or stored by freezing at -20°C until further analysis. Freeze-thawing was limited to a single occasion. This ensured improved sample integrity and also minimised aggregation induced through freeze-thaw cycles, which would result in reduced sample recovery.

2.1.2 Size-exclusion chromatography

Monomeric IgA was isolated from total IgA1 by fast performance liquid chromatography (FPLC). Total IgA1 was loaded on a Superdex 200 pg column (Amersham Biosciences, Sweden) and run under the control of an ÄKTA Prime system at a constant flow rate of 0.5 ml/min in phosphate buffer saline (137 mM NaCl, 10 mM phosphate, 2.7 mM potassium chloride, and pH 7.4). Fractions volumes of 2 ml were collected. All samples and buffers were initially clarified by filtering through a 0.2 µm filter prior to loading.

Fractions containing low molecular weight (LMW) mIgA1 and higher molecular weight (HMW), fractions 28-30 and 31-34 respectively, were pooled and concentrated with centrifugal filter devices (Millipore, USA) with a 50,000 Da molecular weight cut-off. Samples were subsequently frozen at -20°C until further analysis.

Immediately prior to all structural experiments, mIgA1 samples were run on a Superose 6 column (Amersham Biosciences) under the control of an ÄKTA Prime system at a constant flow rate of 0.5 ml/min in PBS. This 'polishing' step was performed in order to remove non-specific aggregates induced through storage/freezing. Sample purity and integrity was checked using reducing and non-reducing SDS-PAGE before and after data collection.

2.1.3 Enzyme-linked immunosorbent assay

IgA1 determination were performed using a sandwich enzyme-linked immunosorbent assay (ELISA). Here, IgA1 was captured onto 96-well microtitre immunoplates (Nunc, Life Technologies) using anti-human IgA antibodies (Dako, Denmark).

Polyclonal rabbit anti-human α -heavy chains (DAKO, Denmark) at 10 μ g/mL in 0.05M carbonate/bicarbonate, pH 9.6 was applied at 100 μ l/well to 96 well immunoplates (Nunc Immunoplate, Life Technologies). The plates were incubated at 4°C for at least 24 hours prior to use.

The plates were washed four times with wash buffer (PBS, 0.3 M NaCl, 0.1% Tween 20, pH 7.2) and unbound sites blocked using 2% BSA in PBS for 1 hour at room temperature. Diluted IgA1 samples isolated from patients and controls were added in duplicate alongside an immunoglobulin standard solution obtained from the Binding Site, UK. Plates were incubated at room temperature overnight at 4°C. After this, the plate was washed four times with wash buffer and the IgA was then detected by addition of anti-human IgA horseradish peroxidase (HRP) conjugate (Dako, UK) for 90 minutes at room temperature. The plate was finally washed four times before the addition of 1, 2-phenylenediamine dihydrochloride (OPD) and hydrogen peroxide substrate. After several minutes of colour development on the plate, 1 M sulphuric acid was added to stop the reaction. The colour reaction was quantitated using an ELISA plate reader (Titertek Multiscan) set with a 492 nm UV filter. Sample concentrations were elucidated from the standard curve. Samples values falling outside the slope of the standard curve were excluded.

2.1.4 Enzyme-linked *Helix aspersa* lectin binding

An IgA1 specific enzyme-linked *Helix aspersa* (HAA) lectin binding assay, with specificity to ungalactosylated GalNAc was used to determine relative hinge region galactosylation. HA lectin binding studies investigate the *O*-glycans in situ on the whole native IgA1 molecule, enabling rapid, qualitative characterisation of the hinge profile (Allen et al. 1995; J Barratt et al. 2007; Gomes et al. 2010). This method has even been suggested for potential use in genetic screening studies for IgAN (Kiryluk et al. 2010).

Briefly anti-human IgA1 capture antibodies were bound to 96 well immunoplates, washed and blocked with 2% BSA in an identical way to that described in Section 2.1.3. Serum samples at 1/100 dilution in PBS were applied to the immunoplates in duplicate and incubated overnight at 4°C in order to capture IgA1 molecules. An in-house standard curve of serum with varying galactosylation profiles was also added in duplicate. After washing, biotinylated HAA lectin diluted at 1/500 in PBS was applied to the plate. The plate was incubated at room temperature for 2 hours before washing and the addition of peroxidase-conjugated avidin (Vector Labs) diluted 1/2000 in PBS. The lectin binding was measured using the substrate 1, 2-phenylenediamine dihydrochloride (OPD) and hydrogen peroxide as described previously.

Results were expressed as arbitrary units from the standard curve of serum IgA1 galactosylation. A high HAA lectin binding value (>30 AU) was taken to represent increased exposed GalNAc. This corresponds to reduced hinge galactosylation.

2.1.5 Sodium dodecyl sulfate polyacrylamide gel electrophoresis (SDS-PAGE) and immunoblotting

The eluted fractions were analysed by SDS-PAGE on 6% acrylamide Tris-glycine resolving gels to identify high and low molecular weight IgA1 species. All casting and running gels were ran according to Laemmli using a BioRad Miniprotean II electrophoresis system.

Samples were reduced by boiling for 3 minutes in an equal volume of reducing buffer (0.5 M Tris-HCl pH 6.8, 10% SDS, 0.4% β -mercaptoethanol, 0.05% bromophenol blue). Unreduced samples were prepared in a non-reducing buffer (the same as the reducing buffer with the β -mercaptoethanol omitted). Samples were electrophoresed at 35 mA/gel until the dye front reached the bottom of the gel and the molecular weight standard shown adequate separation.

Gels were stained continually using a 0.2% solution of Coomassie Brilliant Blue R250 (GE Healthcare, UK) for 1 hour with gentle agitation on a rocker. This was followed by destaining until protein bands were visualised.

For immunoblotting, the separated proteins were transferred from the gel to a nitrocellulose membrane (Millipore, USA) by electrophoresis in aqueous 25 mM Tris- HCl, 190 mM glycine containing 10% methanol at 4°C for 1 hour at 100 V. The membrane was subsequently blocked in 5% non-fat dried milk powder (Marvel, UK) in 0.05% TBST buffer for at least 1 hour under gentle agitation prior to probing. Horseradish peroxidase (HRP) conjugated goat anti-human IgA1 (Dako, Denmark) was then applied at a dilution of 1:2000 in 5% non-fat dried milk powder (Marvel, UK) in Tris buffered saline with 0.05%

Tween 20 (TBST) overnight with gentle agitation. The membrane was then washed exhaustively using 0.05% TBST buffer. Probed bands were visualised after addition of enhanced chemiluminescence (ECL) substrate (Thermo Scientific, UK). Protein molecular weights were estimated from their mobilities relative to a molecular weight standard (GE Healthcare, UK).

2.2 Analytical ultracentrifugation

Analytical ultracentrifugation data was obtained for all four mIgA1 samples using one of either of two Beckman XL-I instruments fitted with AnTi50 and AnTi60 rotors run at speeds of 20,000, 30,000. The protein concentrations were varied for each sample to provide a concentration series (Table 2.01).

Sedimentation velocity experiments were carried out at 20°C with an AnTi50 rotor speed of 30,000 rpm and 40,000 r.p.m in two sector cells with column heights of 12 mm. All AUC experiments were performed in the presence of 137 mM NaCl PBS.

Data obtained was analysed using the software SEDFIT (version 12.5) (Schuck 1998; Schuck 2000) based on the continuous $c(s)$ distribution model. This model processes all the scans and identifies the sedimenting species present. A total of 200 scans were used to fit the distribution. The final analysis was performed by visually floating the detected meniscus, and baseline of the sedimenting program using SEDFIT.

The buffer density was calculated to be 1.00543 g/ml for PBS and 1.11238 g/ml from their compositions using SEDNTERP (Laue et al., 1992), and the viscosity was taken as 0.01002 cp. The partial specific volume for IgA1 was calculated to be 0.724 ml/g from its composition (Boehm et al. 1999; A. Bonner et al. 2008; Stephen J. Perkins 1986).

Sample	AUC-SV concentration (mg/ml)					
Healthy Control 1	2.52	1.51	0.9	0.54	0.32	0.19
IgAN Patient 2	3.22	1.93	1.15	0.69	0.41	-
IgAN Patient 3	1.86	1.11	0.66	0.39	0.23	-
IgAN Patient 4	1.89	1.13	0.68	0.41	-	-

Table 2.01 – Concentration series used for mIgA1 AUC-SV experiments. In order to determine concentration dependence, a number of concentrations were prepared for AUC.

2.3 X-ray scattering

X-ray scattering data was obtained on the Beamline ID02 at the European Synchrotron Radiation Facility (ESRF), Grenoble. The wavelength was 0.0995 nm with the beam being supplied in four bunch mode. The ring energy was 6.0 GeV. All data was collected at a sample temperature of 20°C with a sample-detector distance of 3 metres.

A concentration series for IgA1 monomer samples were prepared in PBS (137 mM NaCl, 10 mM phosphate, 2.7 mM potassium chloride, and pH 7.4) (Table 2.02). A concentration series, with at least four concentrations was used to measure the protein to ensure consistent results and that no concentration-dependence occurred. For each of the samples a minimum of four sets of ten time frames were taken with exposure times of 0.1 sec, and 0.2 sec, per frame.

In order to analyse the data, buffer subtraction was carried out, followed by visual inspection of the wide-angle scattering curves for each of the time frames in the ten time frames taken. This was to check for the absence of radiation damage. Time frames illustrating radiation damage were eliminated from the data analysis. The average of the ten time frames was then used for the Guinier analysis for a better signal to noise ratio.

Sample	SAXS Concentration (mg/ml)				
Healthy Control 1	0.25	0.51	0.76	1.02	-
IgAN Patient 2	0.33	0.49	0.66	0.99	1.33
IgAN Patient 3	0.24	0.36	0.48	0.72	0.97
IgAN Patient 4	0.31	0.47	0.63	0.94	1.26

Table 2.02 – Concentration series used for mIgA1 SAXS experiments. In order to determine concentration dependence, a number of concentrations were prepared for SAX experiments.

Chapter Three

Results

3.1 Purification and hinge glycosylation of IgA1

Total IgA1 and mIgA1 was purified from serum samples obtained with informed consent from 3 patients with biopsy-proven IgAN attending the Nephrology Clinic at Leicester General Hospital (LGH). Serum had been collected and stored in the Leicester IgAN serum bank for up to 25 years, enabling appropriate selection of patients by disease outcome. Two patients had progressive IgAN, which is defined as those patients who progress to end-stage renal failure within a 20 year period. One patient had non-progressive IgAN, the benign form of the disease; serum creatinine had remained stable for up to 10 years. Serum from one healthy subject with no known kidney disease served as control IgA1 for structural experiments.

Quantification of hinge region glycosylation was performed using a modified ELISA principle using HAA lectins to identify hinge region terminal *N*-acetylgalactosamine entities. Samples were loaded onto a 96-well plate in duplicate and the experiment repeated at least twice. This was performed using whole serum, Jacalin-affinity purified IgA1 and mIgA1 (Table 3.01). The relative hinge region galactosylation of the IgA1 samples was then interpreted as ‘normal’, ‘undergalactosylated’ and elevated ‘galactosylation’.

Sample/Subject	Disease progression	HAA (serum)	HAA (iso. IgA)	O-linked GalNAc Interpretation
Healthy (Control 1)	N/A	22	21	‘Normal’
IgAN Patient (Sample 2)	Progressive	32	31	Undergalactosylated
IgAN Patient (Sample 3)	Non-Progressive	13	12	Elevated galactosylation
IgAN Patient (Sample 4)	Progressive	33	33	Undergalactosylated

Table 3.01 – IgAN patient sample selection using HAA lectin binding. Serum samples selected from an IgAN serum bank for isolation of mIgA1, respective HAA binding and IgAN disease progression.

3.1.2 Fast performance liquid chromatography

Assessment of adequacy of protein purification and correct molecular weight separation of serum isolated IgA1 species was performed using FPLC. All samples were run utilising an ATKA prime system at either 1 ml/min (Superdex 200 pg) or 0.5 ml/min (Superose 6) in PBS buffer. Following optimisation, 2 mg/ml samples were clarified by 0.2 µm filtration and loaded. All buffers were clarified and degassed.

Under identical conditions to IgA1 separation, Superdex 200 pg column performance was ascertained using gel filtration molecular weight marker containing proteins of 12,000 – 2000,000 Da (Sigma, MWGF200). The elution profile molecular weight markers (Figure 3.01) demonstrate good resolution with separate, well-defined peaks for each eluted protein. Although a decreased flow rate of 0.5 ml/min did improve observed resolution slightly, 1 ml/min was determined optimal due to faster separation speeds. Increased flow rates caused deterioration in protein resolution.

Plotting the relationship between elution volume (V_e/V_o) and molecular size was performed in order to produce a linear calibration curve. The V_e represents the elution volume for a molecule (volume of solvent collected between sample injection and sample elution) and V_o represents the elution volume of a large, entirely excluded molecule (blue dextran). The calibration curve for the Superdex 200 pg column (Figure 3.02) demonstrated ideal separation; both above and below that required for IgA1, and was in agreement with that specified in the column technical bulletin.

Typical separation of Jacalin purified IgA1 on the Superdex 200 pg column resulted in an elution profile measured in mili absorbance units (mAU). For the healthy control sample, this demonstrated three distinct, sequential peaks which relate to polymeric/IgA-IC (~40 ml), dimeric (~50 ml) and monomeric IgA1 (~60 ml) respectively (Figure 3.03). Low molecular weight protein, likely degraded IgA1 consisting of free κ/λ light and α -heavy chains was eluted with a higher retention.

Figure 3.04 illustrates the elution profiles for the separated control and IgAN patient samples, which are overlaid for clarity. Although adequate separation was observed, the IgAN patients did however show an alternative molecular weight composition to that seen for healthy and freshly prepared serum (Figure 3.03). Patient 3 and patient 4 in particular (Figure 3.04 (3)(4)) reproducibly had increased levels of pIgA1 and dIgA1 and with patient 3 there appeared to be suppression/reduction in mIgA1. This may be disease attributable, where increased circulating pIgA1 and IgA-IC species are frequently observed in IgAN patients. The serum had also been frozen for long periods of time in the IgAN serum bank, and possibly exposed to numerous freeze-thaw cycles, therefore the higher complex formation of IgA1 may be attributable in part to this. All patient samples had a slightly increased proportion of degraded IgA1.

In order to determine monodispersity, following separation of total IgA1, fractions containing isolated mIgA1 from all samples were concentrated and ran immediately prior to structural experiments with a Superose 6 column (Figure 3.05). Due to storage and agitation, formation of aggregate and degraded protein can be seen (Figure 3.05 (1) and (2) respectively), and these were removed (arrows indicated). Short-term storage did not

prevent the formation of these aggregating species, necessitating a further gel filtration step. All mIgA1 samples demonstrated a single, symmetrical peak.

Pooled and concentrated pIgA1 was gel filtrated at 0.5 ml/min using Superdex 200 pg column to illustrate the HMW heterogeneity and the lack of a single peak (Figure 3.06). These HMW proteins include complexes of IgA1-fibronectin, IgA1-albumin and other higher polymerisation states of IgA1. Separation of these complexes was extremely difficult and unrealistic due to their large size, low concentration, heterogeneity and increased potential for aggregation.

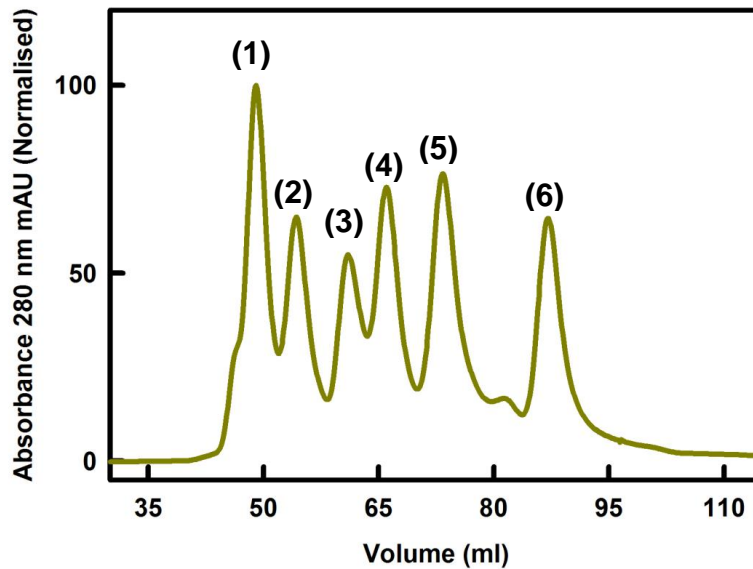


Figure 3.01 – Elution profile for standardised molecular weight markers ran on Superdex 200 pg column (mAU normalised). Peaks correspond to: (1), Blue dextran (2,000 kDa), (2), β -amylase from sweet potato (200 kDa), (3), Alcohol dehydrogenase from yeast (150 kDa), (4), Bovine serum albumin (66 kDa), (5), Carbonic anhydrase from bovine erythrocytes (29 kDa), (6), Cytochrome c (12.4 kDa).

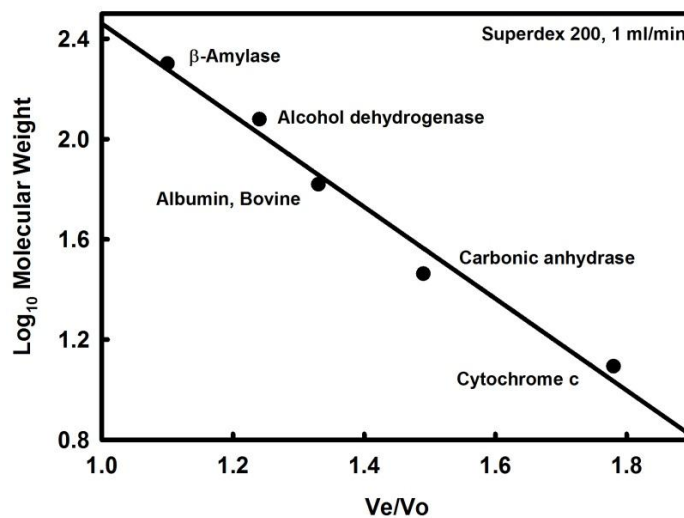


Figure 3.02 – Calibration curve for Superdex 200 pg column. Calibration curve obtained using a Superdex 200 pg column ran at 1 ml/min with reconstituted molecular weight standard proteins of 12,000 – 2000,000 Da in PBS buffer.

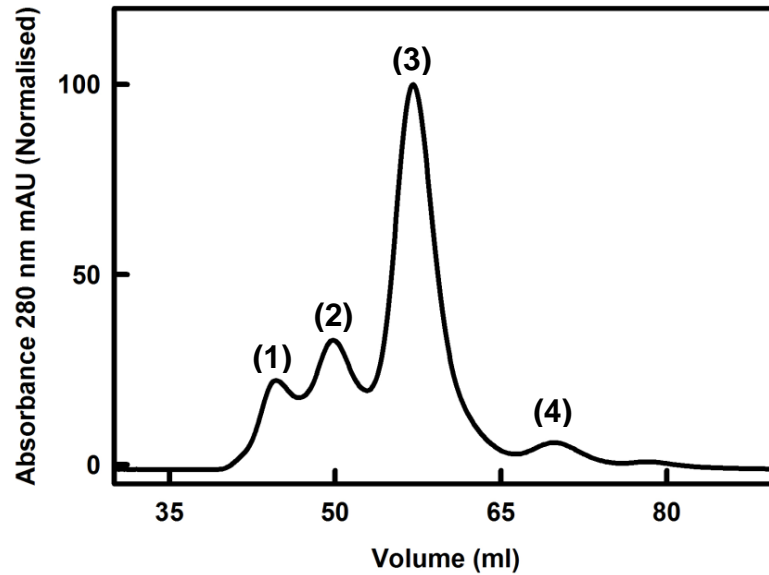


Figure 3.03 – Typical gel filtration elution profile for jacalin-affinity purified IgA1 (mAU normalised). Jacalin isolated IgA1 from human serum subjected to gel filtration on a Superdex 200 pg column at 1 ml/min. Peaks correspond to (1) HMW polymeric IgA1, (2) dimeric IgA1, (3) monomeric IgA1 and (4) degraded IgA1 (likely free light/heavy chains).

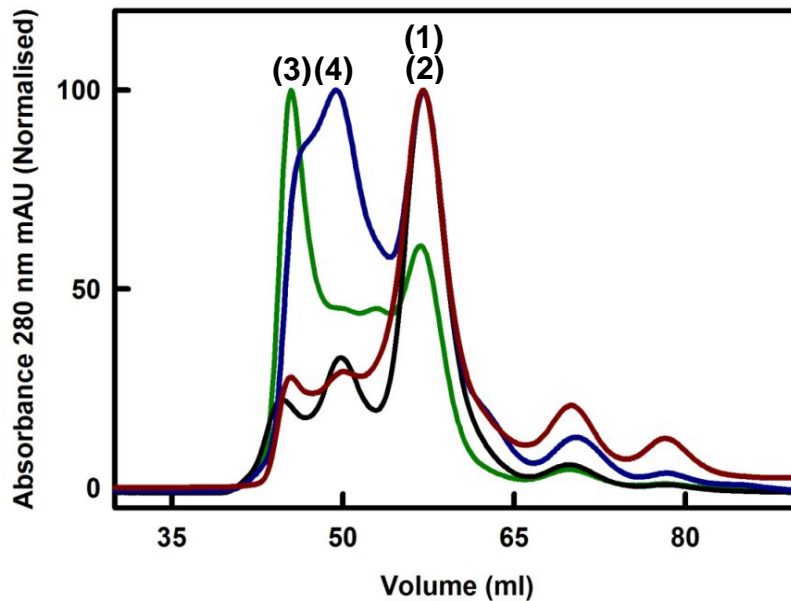


Figure 3.04 – Overlaid gel filtration elution profiles of IgA1 samples 1-4 (mAU normalised). Jacalin purified IgA1 was isolated from serum and subjected to gel filtration on a Superdex 200 pg column. Healthy control sample 1 (black), sample 2 (red), sample 3 (green) and sample 4 (blue).

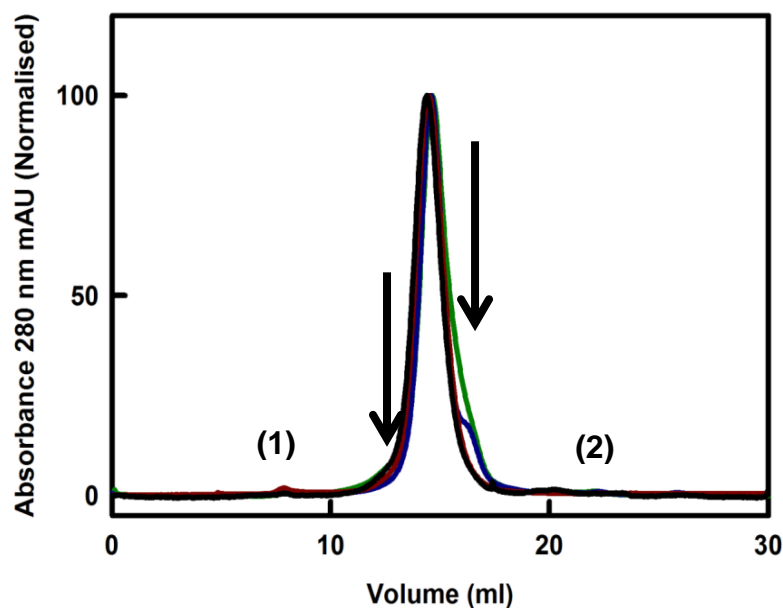


Figure 3.05 – Overlaid gel filtration elution profiles of monomeric IgA1 samples 1-4 (mAU normalised). Pooled fractions containing mIgA1 were ‘polished’ immediately prior to structural experiments by subjection to gel filtration on a Superose 6 column. Aggregates and degraded IgA1 are indicated (1 and 2, respectively). Arrows indicate mIgA1 fractions selected.

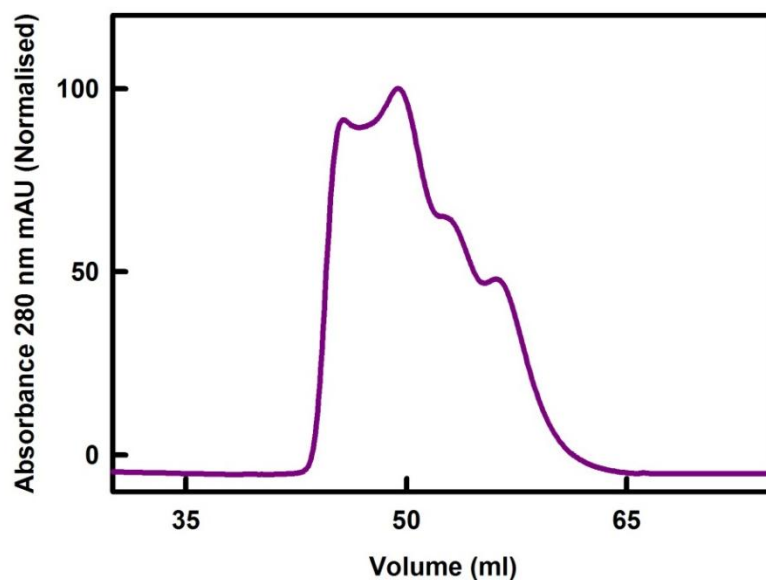


Figure 3.06 – Gel filtration of HMW polymeric IgA1 fraction (mAU normalised). Polymeric IgA1 encompasses various, high molecular weight components of generally >350 kDa. Shown here is the separation of the healthy control pIgA (Figure 3.03 (1)) at 0.5 ml/min.

3.1.3 SDS-PAGE

In order to determine adequate molecular weight separation of mIgA1 by FPLC, SDS-PAGE analysis was performed on eluted fractions (Figure 3.07). Fractions were appropriately diluted and mIgA1 and pIgA1 was separated on a 6% gel and blotted onto a nitrocellulose membrane. The membrane was then probed with goat α -IgA1 polyclonal antibody. Ideal separation of pIgA1, dIgA and mIgA1 can see through fractions 26-30 (Figure 3.07). This is in agreement with the FPLC elution profile absorbance.

Following a polishing using Superose 6 FPLC, the isolated mIgA1 samples were resolved using a 4-12% gradient gel. This was performed to confirm IgA1 molecular weight, purification and monodispersity. The purified mIgA1 was visualised with Coomassie Blue staining under non-reducing (Figure 3.08(A)) and reducing (Figure 3.08 (B)) conditions. Resolved bands on the reducing gel were of expected molecular weight, corresponding to the IgA1 α -heavy chain around 62 kDa, and the κ/λ light chains at around 30 kDa. Non-reduced mIgA1 remained intact and did not separate.

Jacalin agarose purified IgA1 proteins can also contain contaminating IgG, which co-purifies both directly to the agarose and also through IgA1-IgG immune complexes. Purified IgA1 was subjected to affinity chromatography using a staphylococcal protein G immobilized on agarose. Following removal of IgG and IgA1-IgG complex removal, the purity of the IgA1 preparations was assessed by membrane probing with mouse α -IgG monoclonal antibody (not shown).

Non-reduced HMW IgA1 proteins obtained by FPLC (Figure 3.06) were also concentrated and resolved using a 4-12% gradient gel to demonstrate purification (Figure 3.09).

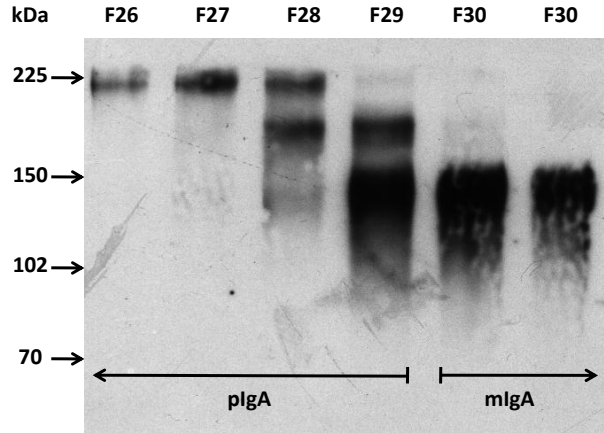


Figure 3.07– 6% SDS-PAGE Western blot of total IgA1 FPLC fractions (F20-F30). Nitrocellulose membrane was probed with goat anti human IgA1 in order to confirm FPLC fractions containing the correct weight species of IgA1. The appropriate fractions were pooled and concentrated for further structural experiments.

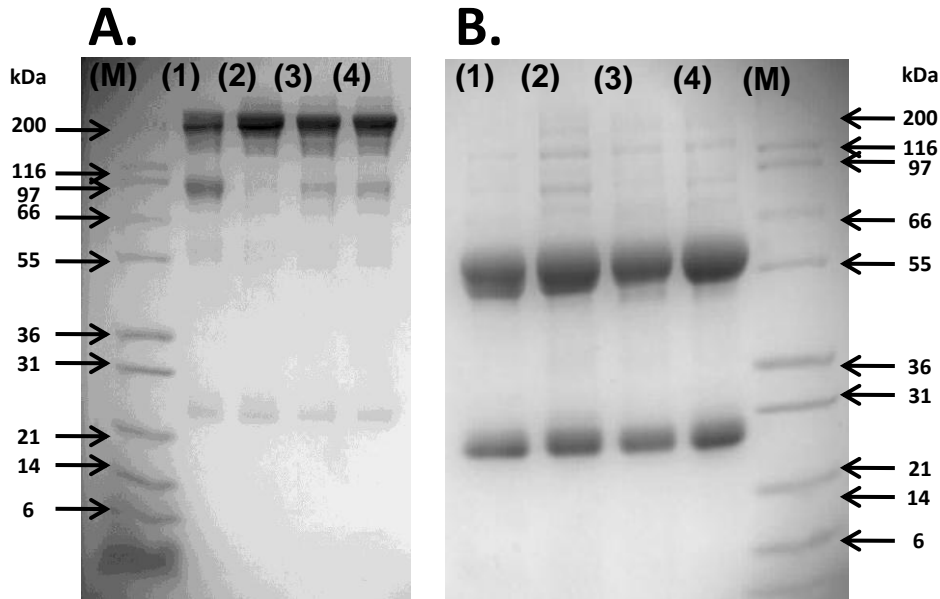


Figure 3.08 –G-250 Coomassie blue stained 4-12% SDS-PAGE of purified monomeric IgA1 samples 1-4. FPLC isolated and concentrated monomeric IgA1 resolved under non-reducing (A) and reducing (B) conditions. Samples were loaded in positions (1) – Control, lane (2) – Patient 2, lane (3) – Patient 3, lane (4) – Patient 4. Molecular weight markers are indicated (M).

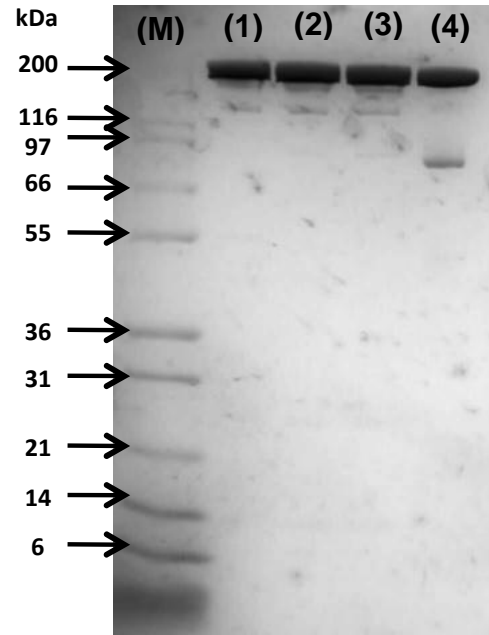


Figure 3.09 – G-250 Coomassie blue stained SDS-PAGE of pooled HMW IgA1. Gel filtrated and concentrated high molecular weight IgA1 fractions loaded onto a 4-12% gradient Tris-glycine SDS-PAGE gel. Samples were loaded in positions; **(1)** – Control, **(2)** – Patient 2, **(3)** – Patient 3, **(4)** – Patient 4. Molecular weight markers are indicated **(M)**.

3.2 Analytical ultracentrifugation

For mIgA1 samples, AUC-SV experiments were performed to identify the conformational and interactional properties of altered galactosylation in mIgA1. Data was acquired overnight for 16 hours at 20,000, 30,000, 40,000 and 50,000 rpm in a concentration series using absorbance and interference optics. The lower rotor speeds demonstrated the optimal condition to observe sedimentation for mIgA1 – higher rotor speeds resulted in the protein pelleting to the bottom of the cell with too few scans for valuable data acquisition.

Processing the AUC-SV absorbance and interference scan data was performed using the software SEDFIT, which after analysis produce $c(s)$ distribution plots. These scans identify all sedimenting species present in a given sample, and produce a sedimentation coefficient (S) for each species. The sedimentation coefficient provides an independent measure of macromolecular elongation to the R_G value from X-ray scattering. All the experimental fitted data for the mIgA1 boundaries showed good visual agreement with satisfactory root-mean-square deviation (RMSD) values.

Firstly, control mIgA1 from a healthy donor (Figure 3.10) was analysed at varying concentrations (Table 3.02) in order to establish monodispersity and confirm its sedimentation coefficient. When analysed with SEDFIT the resulting $c(s)$ distribution plots for both absorbance (Figure 3.10 (A-B)) and interference (Figure 3.10 (C-D)) showed a single predominant sedimenting species (indicated monomer) that was present at 6.2 S. The small black circles represent the experimental data and the continuous black lines represent the fits. In order to achieve clarity of the Lamm fit results only every fifth scan of the 120 scans recorded at 5 min intervals are shown (Figure 3.10 (A-B)). The corresponding $c(s)$

distribution plots are also shown (Figure 3.10 (B, D)) from which the sedimentation coefficient for mIgA1 was determined to be 6.2 S.

In addition to the predominant monomer species at 6.2 S, a smaller higher molecular weight peak was reproducibly observed (indicated as dimer). This had a variable sedimentation value of ~9 S. SEDFIT Conversion of the $c(s)$ plots to molecular mass distributions $c(M)$ showed that this species corresponded to a molecular mass value of 320 (± 11) kDa. This value agrees well with the compositionally derived molecular weight for dIgA1 (Bonner et al, 2008). No higher molecular weight species was detected. This observation indicates the presence of an interaction of mIgA1, producing a dimer at a much smaller, secondary peak at ~9 S. This was unexpected due to the high degree of mIgA1 purification obtained through gel filtration and observed by SDS-PAGE. It had also not previously been reported for mIgA1.

Further analysis of interference and absorption data SEDFIT $c(s)$ distribution analysis was performed for the three IgAN patient samples representing under-galactosylated mIgA1 (Figures 3.11 and 3.13) and elevated-galactosylated mIgA1 (Figure 3.12). For clarity Lamm fit results show every fifth scan of the 120 scans recorded at 5 min intervals. From the $c(s)$ distribution plots the sedimentation coefficient was shown to be similar and reproducible to that for healthy control mIgA1 at 6.2 S. In addition to a single sedimenting mIgA1 species (indicating monomer), a secondary peak was also seen at ~9 S that was attributed to dimer.

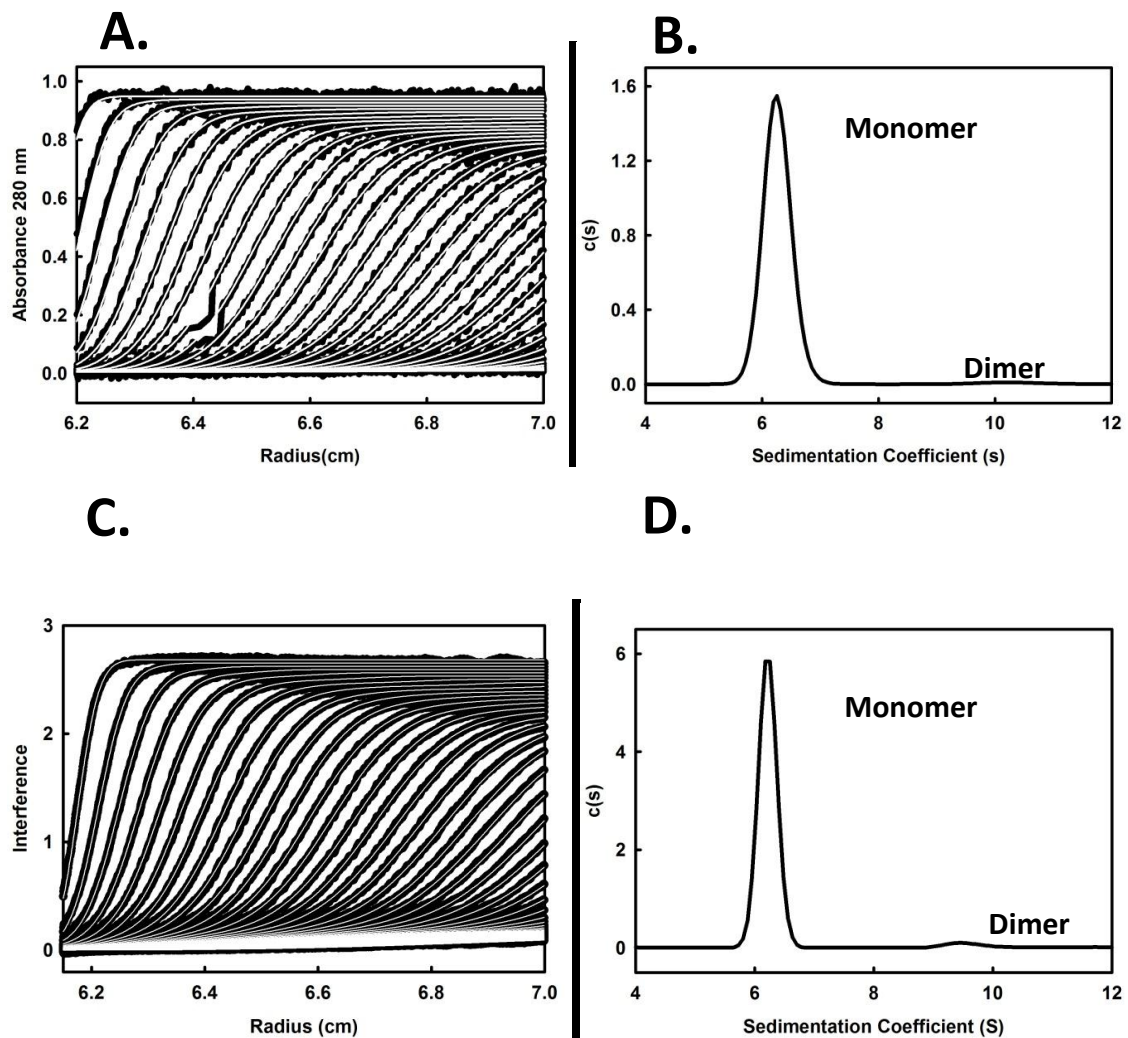


Figure 3.10– Sedimentation velocity of Healthy control sample 1. Absorbance scans recorded at 280 nm for mIgA1 at a concentration of 0.9 mg/ml and a rotor speed of 40,000 r.p.m. are shown in (A), the corresponding interference scans are shown in (C). The $c(s)$ distribution plots for absorbance and interference are also shown in (B, D) respectively. All scans were recorded at 5 min intervals.

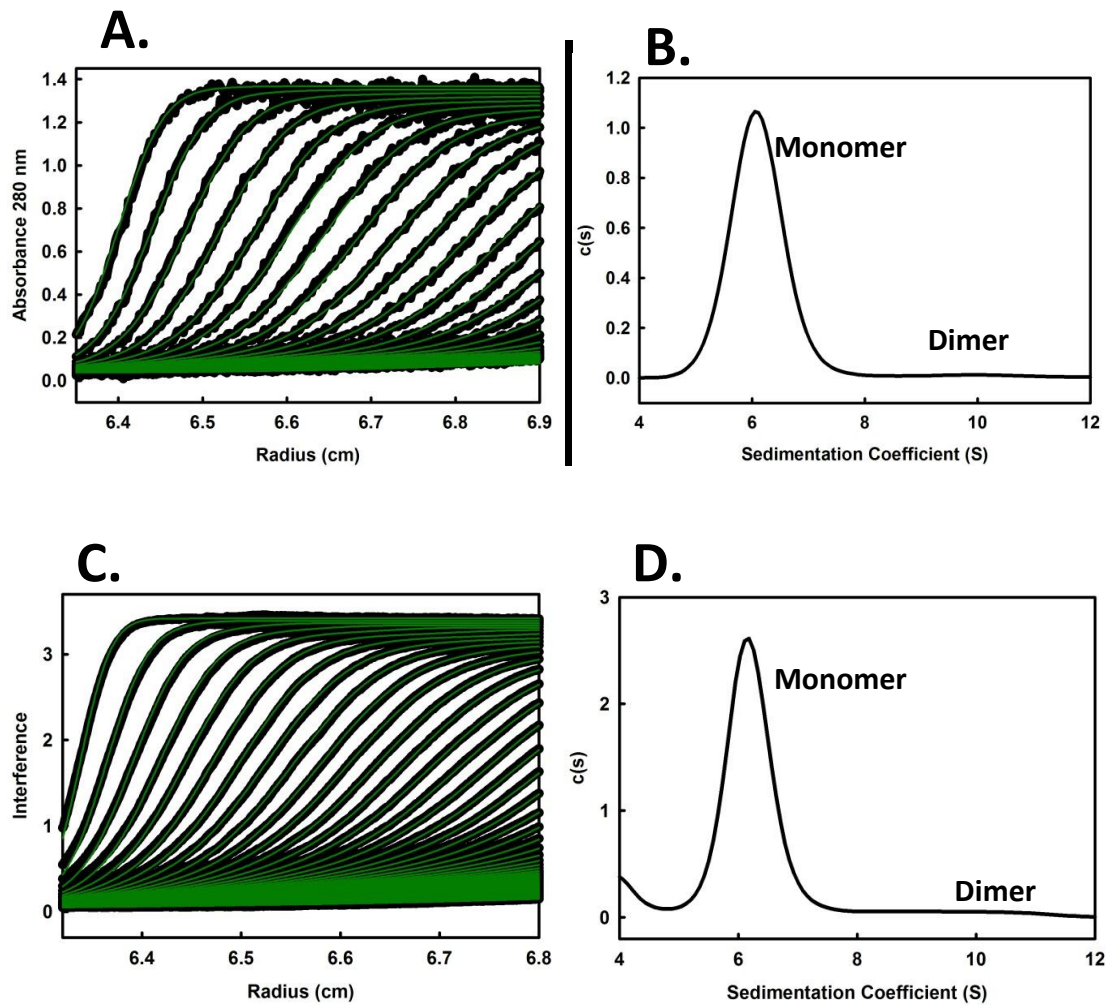


Figure 3.11 – Sedimentation velocity IgAN patient sample 2. Absorbance scans recorded at 280 nm for mIgA1 at a concentration of 1.15 mg/ml and a rotor speed of 40,000 r.p.m. are shown in (A), the corresponding interference scans are shown in (C). The $c(s)$ distribution plots for absorbance and interference are also shown in (B, D) respectively. All scans were recorded at 5 min intervals.

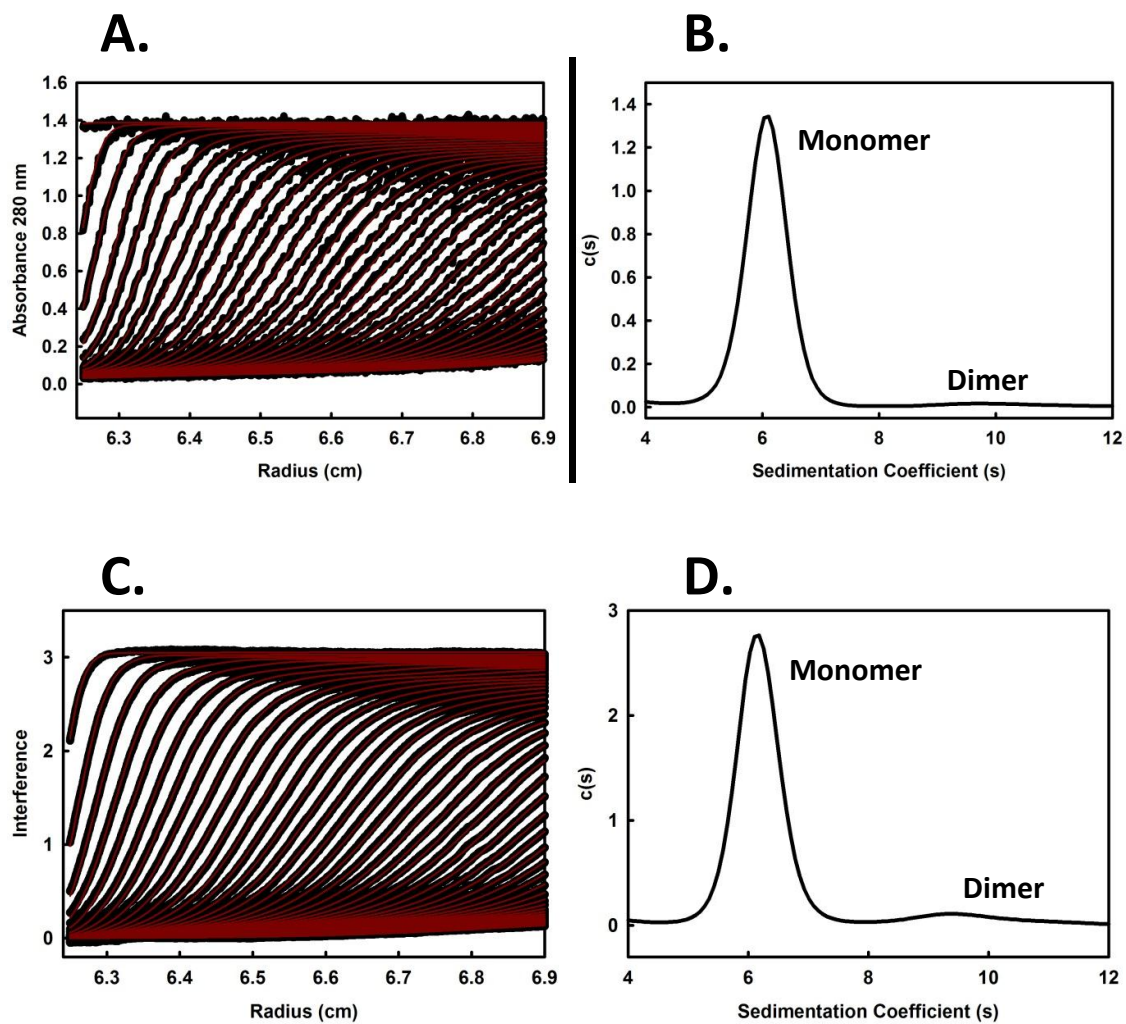


Figure 3.12 – Sedimentation velocity of IgAN patient sample 3. Absorbance scans recorded at 280 nm for mIgA1 at a concentration of 1.11 mg/ml and a rotor speed of 40,000 r.p.m. are shown in (A), the corresponding interference scans are shown in (C). The $c(s)$ distribution plots for absorbance and interference are also shown in (B, D) respectively. All scans were recorded at 5 min intervals.

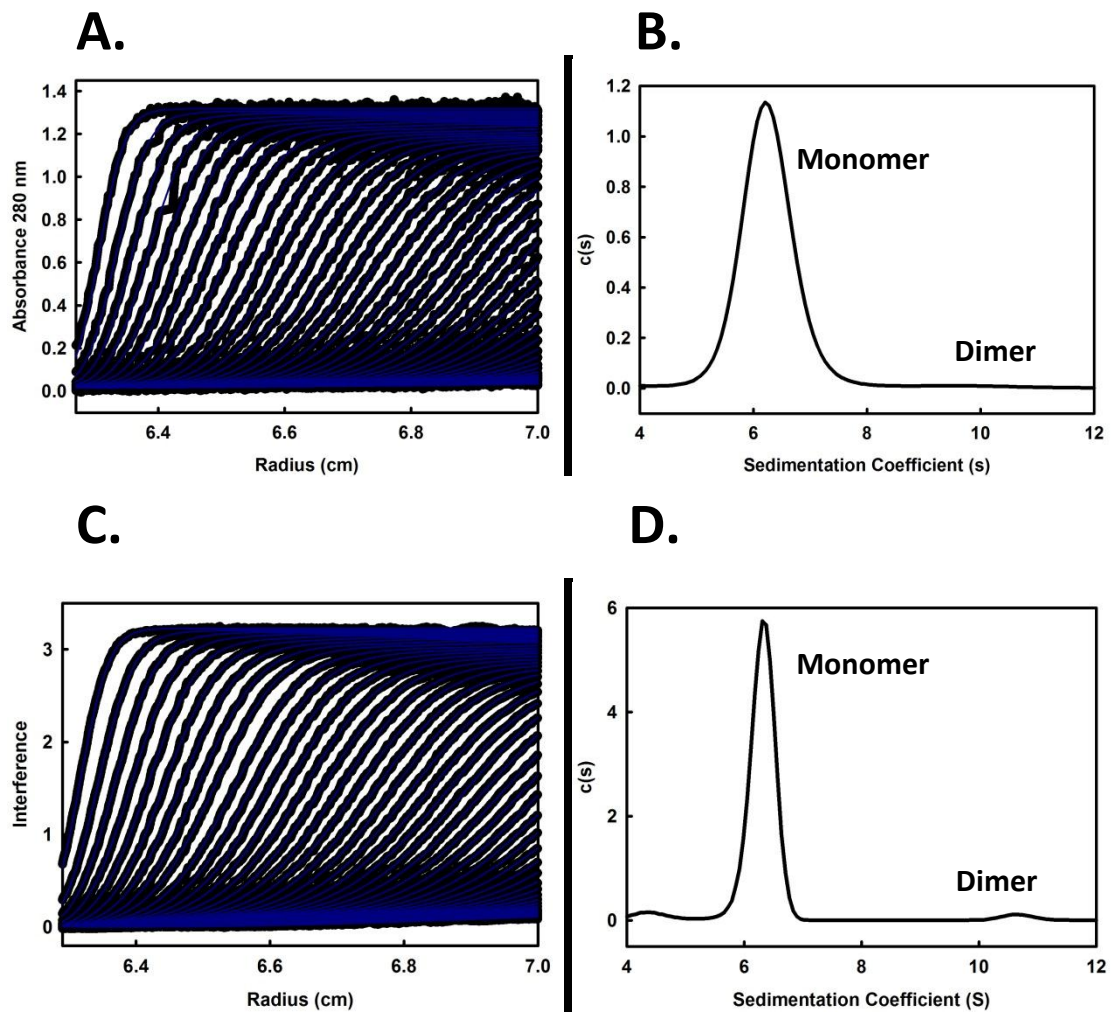


Figure 3.13 – Sedimentation velocity of IgAN patient sample 4. Absorbance scans recorded at 280 nm for mIgA1 at a concentration of 1.13 mg/ml and a rotor speed of 40,000 r.p.m. are shown in (A), the corresponding interference scans are shown in (C). The $c(s)$ distribution plots for absorbance and interference are also shown in (B, D) respectively. All scans were recorded at 5 min intervals.

Both the predominant monomer species and smaller dimer species peaks were further analysed in order to identify whether a mIgA1 conformation concentration-dependence existed, and thus the sedimentation coefficient varied. Figure 3.14 (A) illustrates all samples analysed by AUC-SV at 40,000 r.p.m. and their respective sedimentation value. Healthy control 1 and IgAN patients 2-4 are represented as a black circle, green star, red triangle and blue square respectively. The sedimentation coefficients for healthy control and patient mIgA1 (Figure 3.14 (A), bottom line) were shown to remain stable across all concentrations and ranged from 6.13 S to 6.33 S. The dimer species however did show variability, and its sedimentation coefficient value ranged between 8.01 S and 10 S at the concentrations analysed. The stability and reproducibility of the monomer species illustrates that the sedimenting mIgA1 species was the same across all sample preparations and was in agreement with that reported previously (Boehm et al, 1999).

The $c(s)$ distribution peak areas for both sedimenting peaks were converted to a percentage area using SEDFIT and plotted against concentration (Figure 3.14 (B), top line). This was performed in order to identify whether the proportion of dimer species increased with increasing mIgA1 concentration. This was of particular relevance in the case for IgAN patient samples with undergalactosylated IgA1 hinge regions in determining whether the modified hinge region induced greater aggregation. X-ray scattering for proteins at high concentrations has been linked to aggregation (Perkins et al, 1999). The predominant mIgA1 species ranged between 91 to 98% of the total $c(s)$ distribution plot data. The percentage for healthy control and IgAN patient samples was unaltered with increases in concentration. It was interesting to note that the proportion of healthy control mIgA1 was slightly reduced at lower concentrations (Figure 3.14 (B), top line black circles). The

smaller dimeric peak (Figure 3.14 (B), bottom line) remained low at 2% to 3% of the total $c(s)$ distribution plot.

Molecular weight conversion of the $c(s)$ plots to molecular mass distributions $c(M)$ (Figure 3.14 (C)) using the SEDFIT software was performed to identify whether multimerisation of the IgA1 molecule was associated with a doubling of the molecular weight. The observed molecular weights also showed some variability with the mIgA1 peak (Figure 3.14 (C), bottom line) ranging from 120 kDa to 188 kDa and the dimeric peak was doubled as expected to between 250 kDa and 385 kDa.

In conclusion, the monomer sedimentation coefficients for healthy control and IgAN patient mIgA1 remained stable and no identifiable trend was observed between mIgA1 preparations, although the presence of a secondary sedimenting species was seen that was attributable to dimer formation.

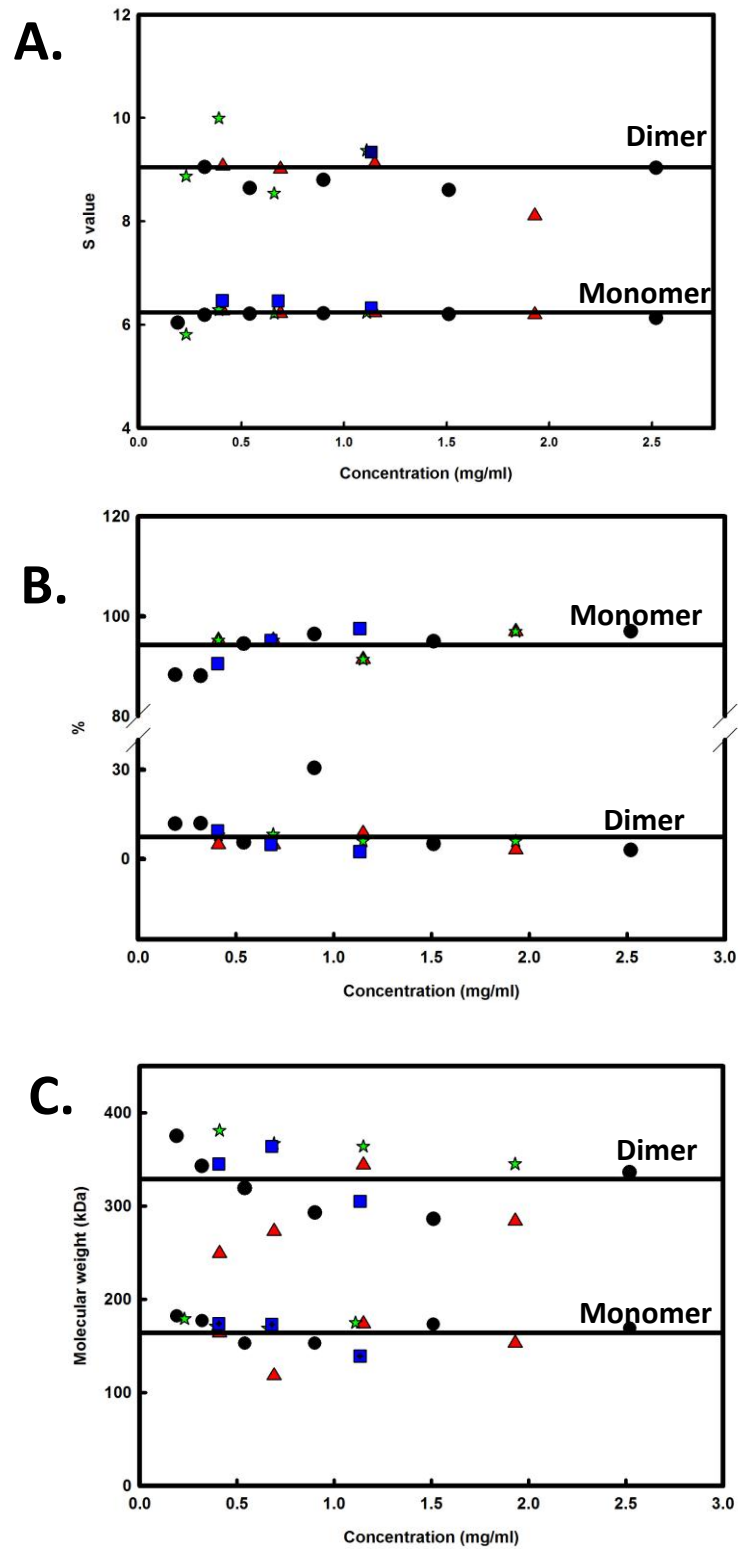


Figure 3.14 - Figure legend overleaf.

Figure 3.14 – Concentration-dependence plots for AUC-SV monomer and dimer peaks. The sedimentation coefficient (**A**), peak area percentage (**B**) and molecular weights (**C**) obtained from SEDFIT $c(s)$ distribution analysis were compared against concentration. Black circle – healthy control 1, green star – IgAN patient sample 2, red triangle – IgAN patient 3 and blue square – IgAN patient 4.

3.3 Small-angle X-ray scattering

The averaged solution structures for the healthy control and IgAN mIgA1 monomers were analysed using X-ray scattering data, and comparing this to X-ray data previously obtained for mIgA1 (Boehm et al, 1999). This experiment was performed in order to identify whether hinge region glycosylation alterations result in conformational changes in the mIgA1 solution structure.

Data was collected at mIgA1 concentrations of 0.25 mg/ml to 1.02 mg/ml, 0.16 mg/ml to 1.33 mg/ml, 0.12 mg/ml to 0.97 mg/ml and 0.15 mg/ml to 1.26 mg/ml for healthy control and the IgAN patients 2, 3 and 4 respectively (Table 2.02). Data was collected at the ESRF, Grenoble on two separate occasions to ensure consistency between beam time experiments. Comparison of collected data obtained from the first single time frame exposure with the average from all ten consecutive time frames showed that the X-ray Guinier regions were unaffected by the exposure time (Figure 1.14). This was initially determined alternating the maximum radiation exposure time to identify large linear increases in the $I(Q)$ curve during data collection, but also by overlapping sequential time frames to identify if the protein was damaged. These indicated that radiation damage or X-ray induced aggregation effects were absent and as such suitable exposure collection time per frame was used enabling the best signal-noise ratios during data acquisition. It was possible to use the time-averaged runs for data analyses. Hinge region glycosylation is indicated in all figures.

The low Q value range selected for Guinier radius of gyration (R_G) was $0.13 - 0.25 \text{ nm}^{-1}$, where analyses of $\ln I(Q)$ against Q^2 resulted in linear plots for all mIgA1 samples, yielding the R_G value from the slope (Figures 3.15 A-D). At larger Q values, analyses of $\ln I(Q)Q$

against Q^2 yielded the R_G value of the cross-section (R_{XS-1} and R_{XS-2}). This Q range was selected by comparison to ranges used previously (Boehm et al, 1999) to be $0.28 - 0.51 \text{ nm}^{-1}$ (Figure 3.16 A-D) and $0.56 - 1.01 \text{ nm}^{-1}$ (Figure 3.17 A-D) respectively. If the mIgA1 molecule were to be represented as an elliptical cylinder, then the R_{XS-1} and R_{XS-2} values correspond to the Fc and Fab regions respectively. Open circles correspond to the data points, and the filled circles and lines between the QR_G ranges (arrowed) correspond to the data points used that were used to determine R_G values for each sample. The average R_G values for the healthy control and the IgAN samples 2-4 were 6.1 nm, 6.2 nm, 6.1 nm and 6.3 nm respectively (Figure 3.18).

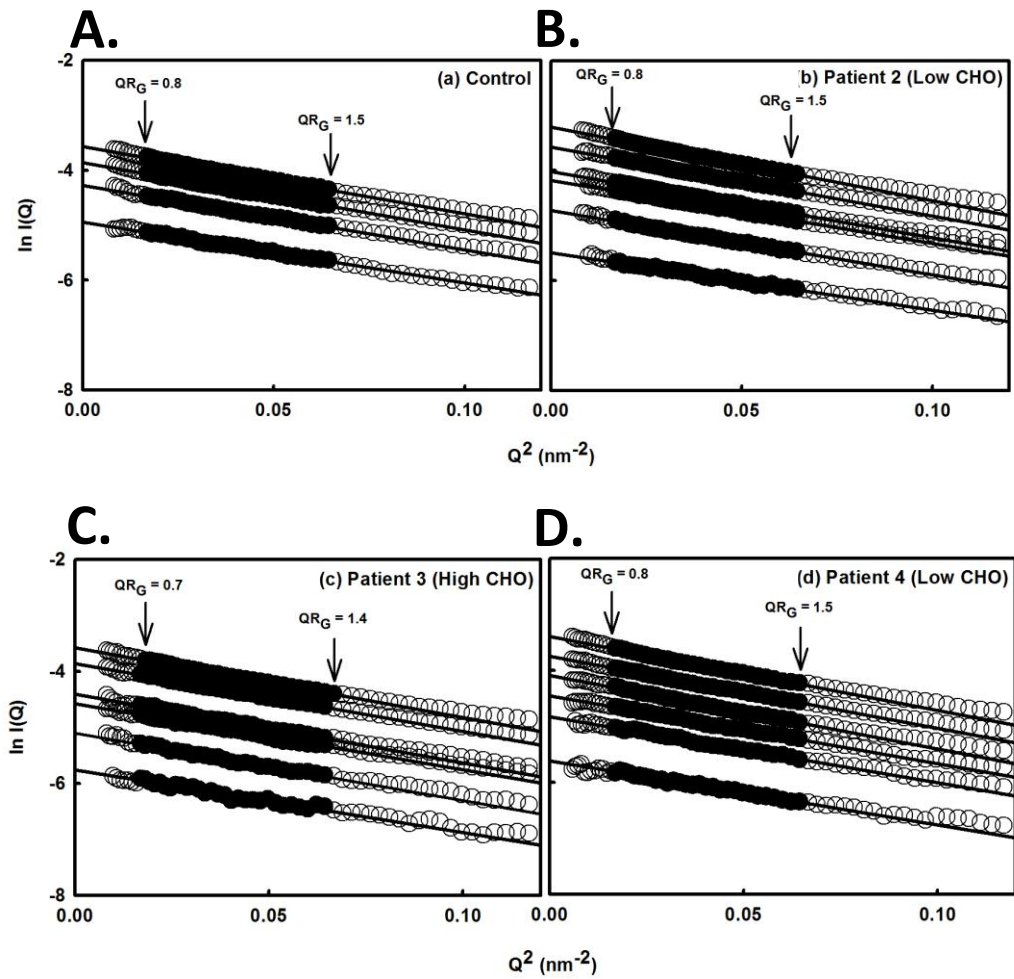


Figure 3.15 – SAXS Guinier analyses for healthy control and IgAN patient mIgA samples. In these Guinier analyses, the open circles correspond to the data points, and the filled circles and lines between the QR_G ranges (arrowed) correspond to the data points used that were used to determine R_G values for each sample. The Q range used 0.13 to 0.25 nm^{-1} . **A** – Healthy control, **B** – IgAN patient 2 (low CHO), **C** - IgAN patient 3 (high CHO) and **D** – IgAN Patient 4 (low CHO).

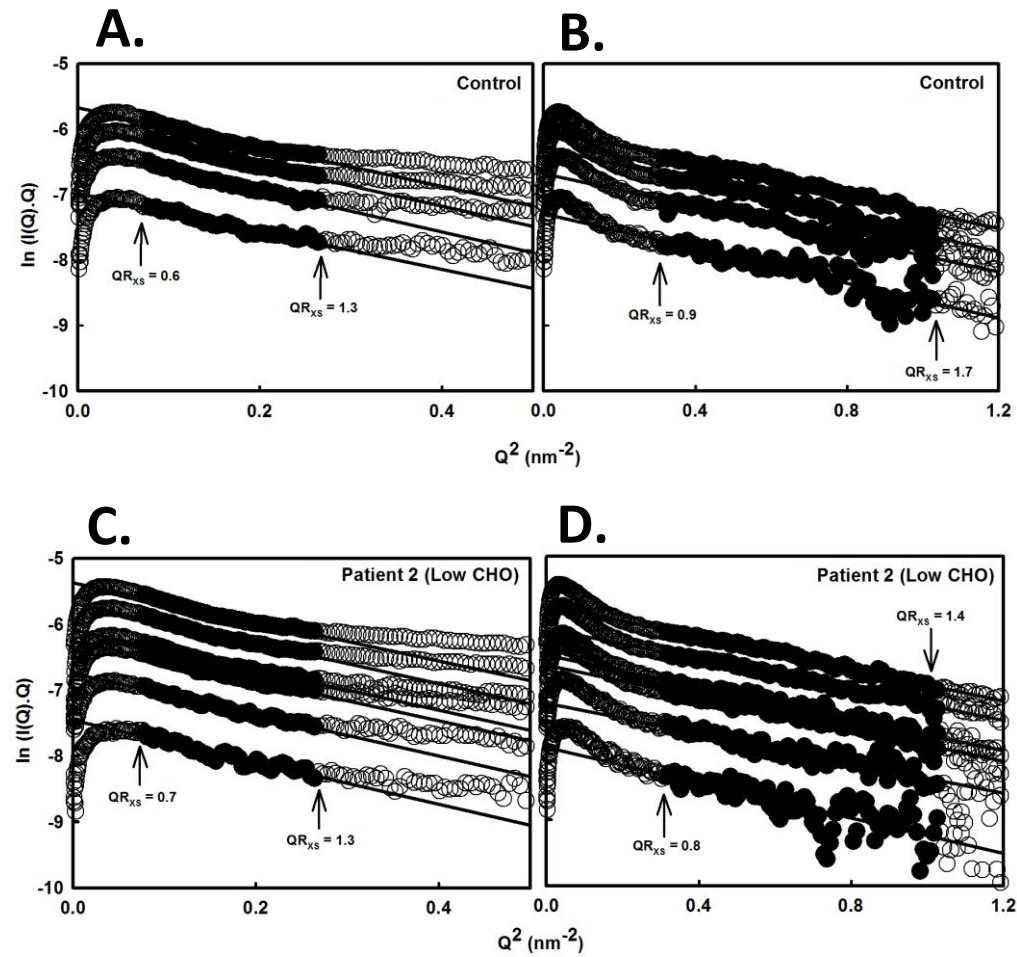


Figure 3.16 – R_{XS-1} and R_{XS-2} plots for healthy control and IgAN patient 2 mIgA1. The filled circles between the QR_G ranges (arrowed) show the data points obtained from SAXS used to determine R_G , R_{XS-1} and R_{XS-2} values. The Q range used for R_{XS-1} (A and C) and R_{XS-2} (B and D) values were 0.28 to 0.51 nm⁻¹ and 0.56 to 1.01 nm⁻¹ respectively.

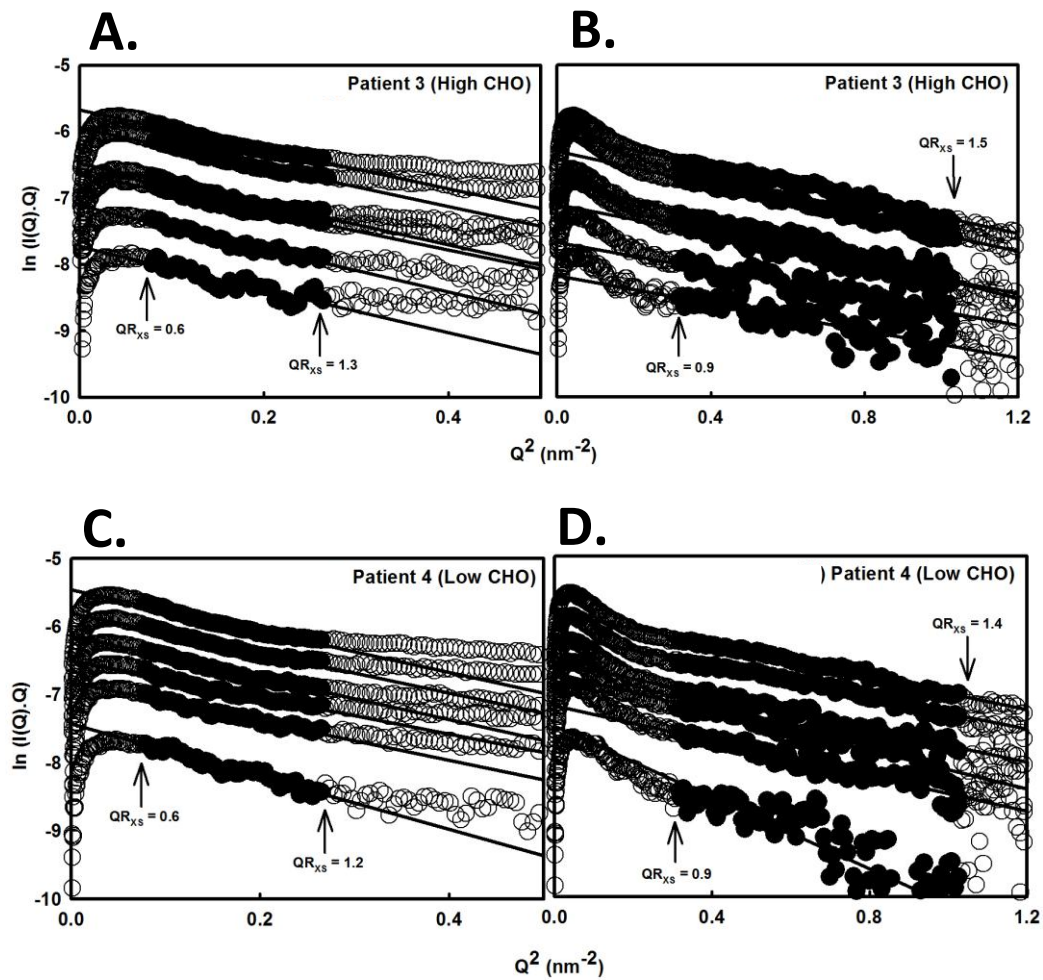


Figure 3.17 – R_{XS-1} and R_{XS-2} plots for IgAN patients 3 and 4 mIgA1. The filled circles between the QR_G ranges (arrowed) show the data points obtained from SAXS used to determine R_G , R_{XS-1} and R_{XS-2} values. The Q range used for R_{XS-1} (A and C) and R_{XS-2} (B and D) values were 0.28 to 0.51 nm^{-1} and 0.56 to 1.01 nm^{-1} respectively.

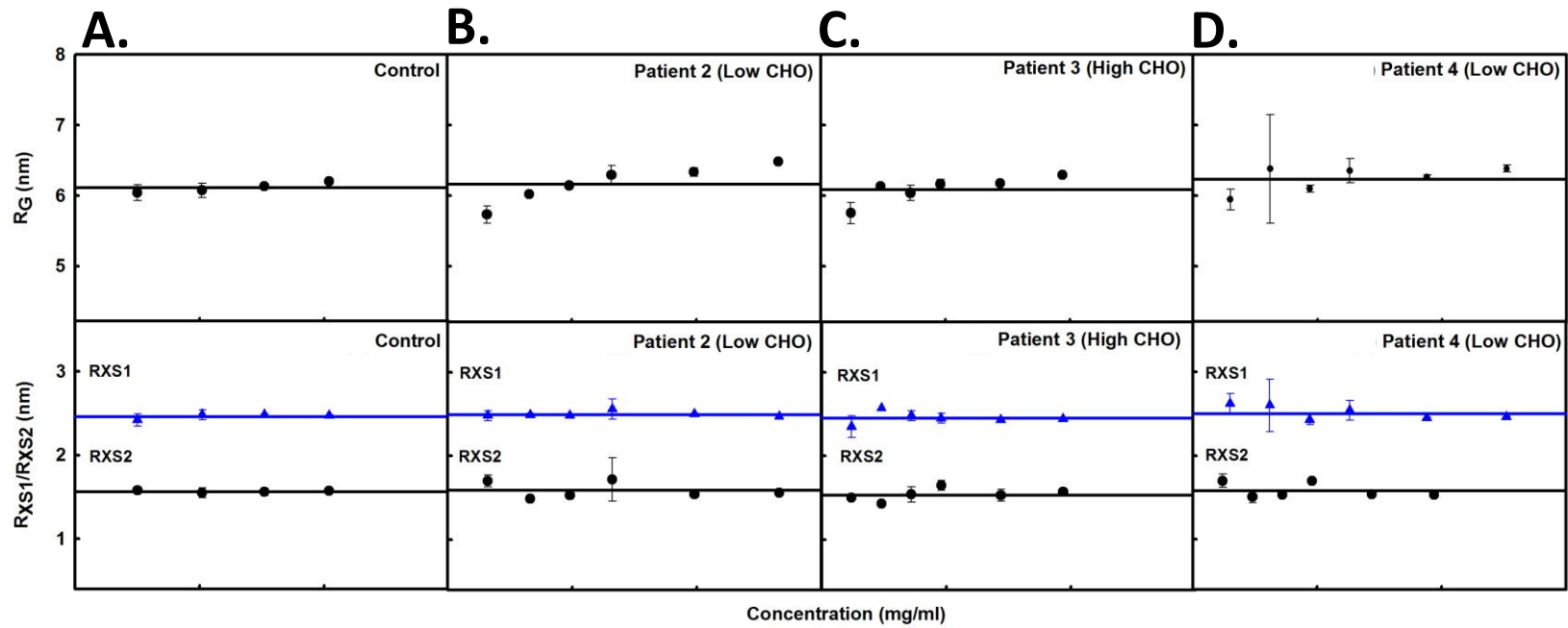


Figure 3.18 – X-ray Guinier R_G , R_{XS-1} and R_{XS-2} lengths for mIgA1 samples 1-4 over concentration - A – Healthy control, B – IgAN patient 2 (low CHO), C - IgAN patient 3 (High CHO) and D – IgAN Patient 4 (Low CHO).

Structural dimensions of molecules analysed by SAXS are provided by the transformation of the $I(Q)$ curve into the distance distribution function $P(r)$ curve. This curve provides valuable information pertaining to molecules by converting the scattered data into reciprocal space, revealing data on its length L . In addition to L , the mean R_G values for all mIgA1 samples were determined and compared to those from Guinier analysis.

The $P(r)$ curves for all samples (Figure 3.19 A-D) showed the presence of a double peak and are labelled maxima M1 and M2. The maxima peaks and their positions depict the two most frequently occurring distance within the mIgA1 structure and relate to an abundance of interatomic vectors within the mIgA solution structure. The M1 peak is assigned to the most commonly occurring distance within a single Fab or Fc region, given that each is approximately 8 nm long. Previous solution structure analysis revealed the M1 peak to be consistent with the presence of distinct Fab and Fc regions in mIgA1. For the healthy control mIgA1 (Figure 3.20 A) at all SAXS concentrations (Table 2.02), the positions of M1 and M2 are 4.2 nm and 9 nm. These values are very similar and agree well with those previously reported for mIgA1 (Boehm et al, 1999). In patient samples 2 and 4 (with reduced hinge region glycosylation) the positions of M1 and M2 were slightly reduced, at between 4.1 nm and 8.4 nm (Figure 3.20 B and D).

The least frequently occurring distances observed in the molecule by SAXS are displayed towards the right of the X-axis. The maximum intermolecular length for the entire mIgA1 molecule occurs infrequently but indicates the extended length L (Figure 3.19 A-D). The L value for the healthy control mIgA1 sample was 21 nm, again this was in agreement with that determined previously for mIgA1 and provided an adequate test for the method. The L values for the IgAN patient samples were 22 nm, 25 nm and 25 nm respectively.

Interestingly increased molecular length was seen in IgAN patient samples with undergalactosylated mIgA1 (low CHO) (IgAN patients 2 and 4) at all concentrations (Figures 3.19 A-D; Figure 3.20 A-D). This suggests that the conformation of the mIgA1 in those patients exhibiting reduced hinge *O*-glycosylation was slightly extended and may have potentially unravelled.

Structural length for elevated hinge region glycosylation mIgA1 (high CHO) (IgAN sample 3) was not altered, and remained consistent with that for healthy control mIgA1. The M1 and M2 peak positions for all samples remained stable at all concentrations (Figure 3.20 A-D), however a small trend for increasing M2 with elevated concentration for IgAN patient samples may be present (Figure 3.20 B-D). Further structural analysis based on molecular modelling fits will elucidate this further.

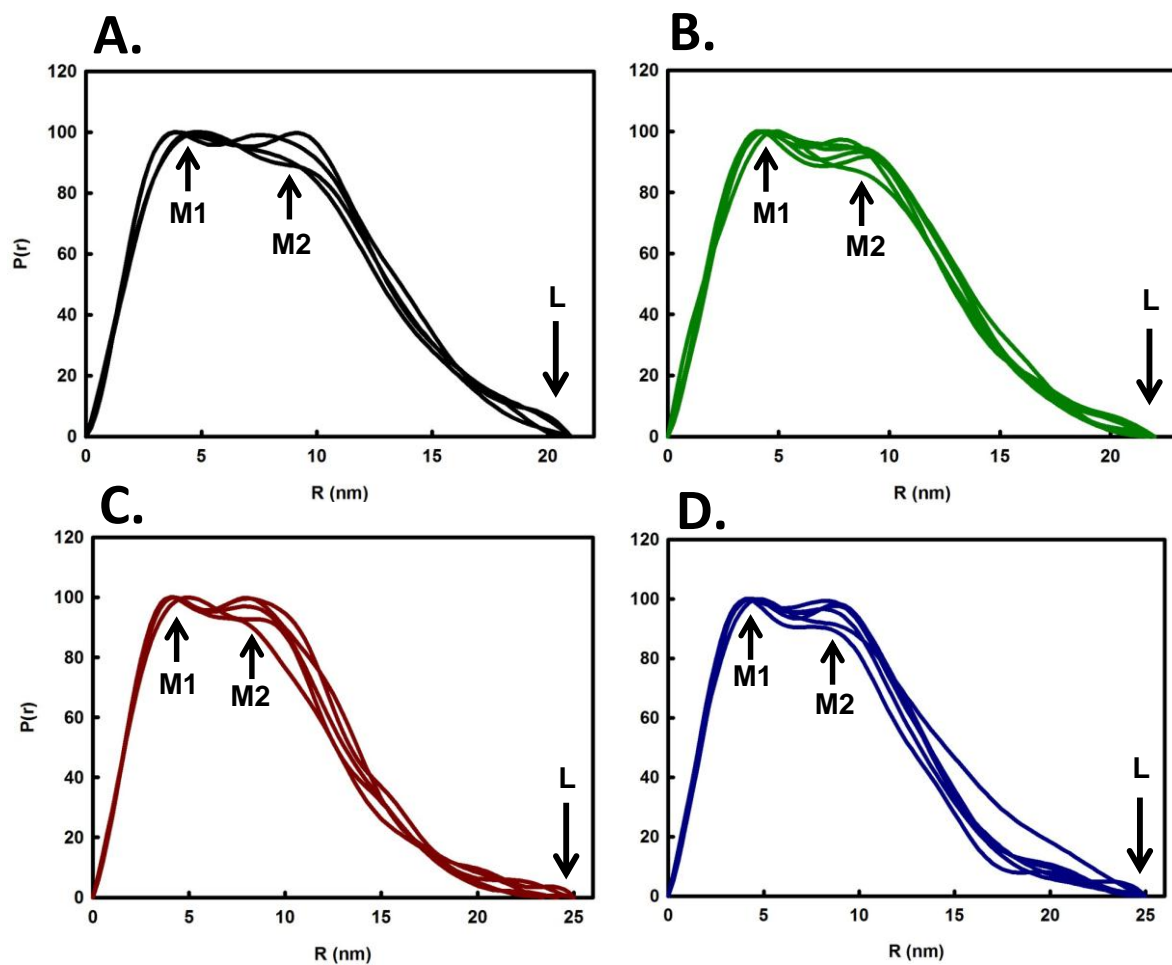


Figure 3.19 – X-ray distance distribution functions $P(r)$ for mIgA1, samples 1-4. The distance distribution function graphs represent all SAXS concentrations of mIgA1 samples for healthy control 1 (A) and IgAN patient samples 2-4 (B-D) overlaid. The two maxima peaks are indicated M1 and M2. The maximum molecular length is denoted by L .

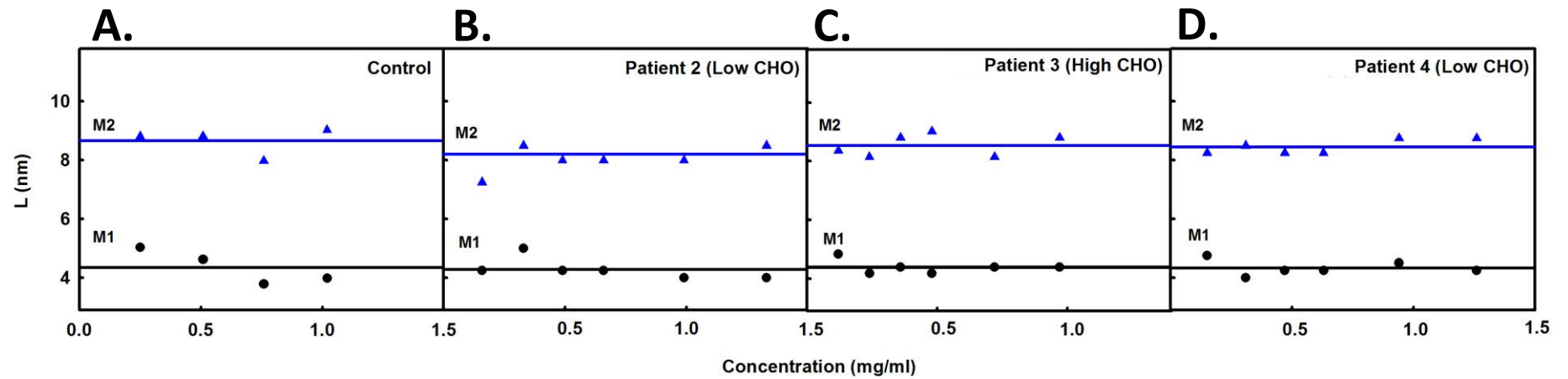


Figure 3.20 – Distance distribution M1 and M2 maxima lengths for mIgA1 samples 1-4. Distance distribution function lengths for maxima M1 and M2 at each concentration are shown. **A** – Healthy control, **B** – IgAN patient 2 (low CHO), **C** - IgAN patient 3 (High CHO) and **D** – IgAN Patient 4 (Low CHO).

Chapter Four

Discussion

4.1 Discussion

To date the precise cause and pathogenesis of IgAN remains unclear; as a disease it is diverse in presentation and has numerous potential initiation modulators that may play a role in its development and ultimate prognosis. These centre on the IgA1 molecule itself, its production, lifespan, removal or the kidneys' response to exposure/deposition of the IgA1. This project examined structural characteristics of the IgA1 molecule, in particular whether its structure is potentially altered as a result of aberrant hinge region galactosylation; and whether these alterations may play an intrinsic role in the pathogenesis of IgAN. The application of biophysical techniques such as AUC and SAS thus served a vital purpose in exploring the solution structure of important proteins, particularly those implicated in disease.

The isolation of serum IgA1 from control and patient samples was performed using Jacalin affinity chromatography purification. This is now the most widely accepted method for IgA1 purification since its original development over 20 years ago. Following removal of contaminating IgG, a SDS-PAGE staining gel and Western blotting with an anti- α -IgA1 probe confirmed the purity of the isolated mIgA1. The removal of IgG from the IgA1 preparation served to increase purity of the final product and ensured that subsequent structural experiments were homogeneous and would not be impaired by contaminating immunoglobulin species. It must be noted however that with the removal of the IgG, there is inevitably also removal of IgA1-IgG immune complexes, which was evidenced through a slight reduction in protein concentration following Protein G treatment. It may be possible that the removal of these complexes in effect removes the 'pathogenic' component of circulating serum IgA1. Therefore the subsequent downstream analysis is of the IgA1

without this potentially important proportion of IgA1. Structural studies such as the one performed here crucially depend on a monodisperse and homogeneous solution of the protein of interest. The presence of any IgG would have likely altered the experimental data and potentially given erroneous results. Once the healthy control and patient IgA1 was purified, FPLC gel filtration was performed to separate the mIgA1 fraction from higher molecular weight species for the ultracentrifuge and scattering experiments. The propensity for purified protein samples to aggregate is well documented, and isolated mIgA1 used in this study was without exception. Both healthy control and patient samples demonstrated aggregation with short-term storage at 4°C and even modest agitation. This was removed through successive gel filtration by FPLC immediately prior to experimentation.

Serum IgA1 is unusual in that it contains *O*-linked hinge carbohydrates; therefore careful elucidation of any structural change induced through removal of these carbohydrates is highly beneficial in the understanding of the importance they may hold in the pathogenesis of IgAN.

AUC-SV experiments were performed on isolated serum mIgA1 in order to identify disease related structural changes in the IgA1 molecule, using three different levels of hinge region galactosylation as a parameter. Analysis of the AUC-SV data for healthy and control mIgA1 does not appear to show any clear trend with *S* values of 6.2 S. This sedimentation coefficient agrees well with and confirms that previously determined (Boehm et al, 1999). The reason for there not being an observable difference between the preparations may in part be due to the low concentrations used or the partial specific volume (0.724 ml/g), which was taken using a theoretic mIgA1 molecule with a full glycosylated hinge profile (Boehm et al, 1999). It is also worth noting that AUC-SV is a low-resolution technique.

Discrimination of subtle differences between mIgA1 preparations may therefore not be adequately resolved. The AUC-SV results do however help confirm the FPLC and SDS-PAGE purification status of mIgA1.

Analysis of the AUC-SV experiments with SEDFIT identified the presence of low amounts (2-3%) of a larger molecular weight dimeric species in healthy control and IgAN samples. It is important to note that different AUC-SV analysis software was employed when the AUC experiments were originally performed on mIgA1 in 1999. This analysis software was based on 4-20 scans at the centre of the sedimentation experiment using the $g(s^*)$ method in DCDT+ software. Unlike the $c(s)$ plots obtained from SEDFIT, the $g(s^*)$ method does not identify and resolve all sedimenting species within an individual sample. It is therefore highly likely that the presence of a dimeric sedimenting species was not originally identified even though this was present.

X-ray scattering data was performed on a concentration series of healthy control and patient mIgA1. Data was collected during two beam sessions in sixteen-bunch mode on Instrument ID02 at the ESRF, Grenoble, France. The purpose of these experiments was to identify with greater precision whether there were any structural differences between the mIgA1 preparations. The average R_G values for all sample preparations were similar, with R_G values for healthy control and IgAN samples 2-4 were 6.1 nm, 6.2 nm, 6.1 nm and 6.3 nm respectively and no observable trend was identified.

The X-ray $P(r)$ analysis demonstrates a reproducible pattern of two maxima M1, and M2 in agreement with that previously determined. They also appear to show that the maximum molecular length L of the IgAN patient mIgA1 was greater than 21 nm, which was

previously determined for healthy serum mIgA1 and reproduced in this work. An increase in length was seen for IgAN samples 2 and 4. This is particularly interesting as both samples are undergalactosylated, with HAA lectin values of 31 and 33 respectively.

The $P(r)$ distribution function is derived from the one-dimensional data and is converted to reciprocal space using a direct Fourier transformation. It is a valuable tool in understanding molecular structures and interactions and provides revealing information relating to the conformational state of a protein. Unravelling of the mIgA1 structure through reduced glycosylation, from a 'T'-shaped molecule to a more 'Y' shaped would result in increased length and would indeed be an explanation for the increased macromolecular lengths in these samples. Analysis of the $P(r)$ data effectively compares M1 and M2 peaks from all samples. This illustrates that for IgAN patient 2, an undergalactosylated sample, the average M2 peak is slightly shorter than that of the other mIgA1 preparations, potentially indicating that the internal 'T' shaped conformation may be altered. This is in agreement with the increased maximum molecular length, which is the most interesting outcome of this project, and suggests an alteration and potential unravelling of the protein. Evidently, more work is required in the production of molecular models of the solution structure for the proteins analysed in this study and this will be the next phase in ascertaining a three-dimensional model of IgA1 in IgAN. The modelling will need to explain the change in the L values, while leaving the S values and R_G values mostly unaltered.

In summary, using the application of well-established biophysical techniques, this project investigated the potential structural aberration of mIgA1 isolated from patients suffering from IgAN at a variety of concentrations. Although this work investigated the implication of hinge region glycosylation using HAA binding, an altered structure may have indeed

been caused by another variable associated with IgAN. One explanation for the lack of differences observed for mIgA1 isolated from IgAN patients may be attributed to the fact this study has initially focussed on mIgA1 and not pIgA. Higher molecular weight immune complexes of IgA1 are widely recognised as having a greater pathogenic role in IgAN. Thus the elucidation of greater differences may be seen more clearly in higher polymerisation states of IgA1, such as the dimeric form. This experimental work is planned to be undertaken following this MPhil.

This project has opened the way for further functional studies into the importance of structurally altered IgA1 in IgAN. The continuation of this project will ultimately lead towards a clearer identification as to the state of altered IgA1 solution structure in IgAN, defining and identifying in detail the exact mechanism of action (i.e. altered receptor binding/clearance, predisposition for aggregation etc.). Evidently, the next step forward regarding this data will be the analysis and production of three-dimensional best-fit molecular models for the monomeric IgA1 molecules in the healthy control and in IgAN, providing an increased appreciation for structural differences. Likewise, with the availability of data on dimeric IgA1, these too will be subjected to modelling to see whether structural differences are seen between the different forms of the dimer.

Appendix I
Buffers and Solutions

0.175 M Tris HCl pH 7.5:

Dissolve in 1400 mL ddH₂O:

30 g Trizma base

200mL 1 M HCl

Store at 4°C

1 M Galactose in Tris HCl pH 7.5:

Dissolve in 100 mL Tris HCl pH 7.5:

18 g D-galactose

Store at 4°C

Jacalin Storage Buffer:

Dissolve in 1L ddH₂O:

10 mL 1M 4-(2-hydroxyethyl)-1-piperazineethanesulfonic acid (HEPES) solution

8.76 g NaCl

11.1 g CaCl₂

3.8 g D-galactose

0.8 g NaN₂

Store at 4°C

Substrate Solution (per plate):

Dissolve in 6mL diH₂O:

4 mg OPD

2.5 L 30% H₂O₂

Wash Buffer:

Dissolve in 1L 1xPBS:

20.75 g NaCl

1 mL Tween-20

Coating Buffer (10 plates):

Dissolve in 100 mL diH₂O:

0.378 g NaHCO₃

0.053 g Na₂CO₃

1X PBS, pH7.4, 1L

Dissolve in diH₂O:

8 g NaCl

1.15 g anhydrous Na₂HPO₄

0.2 g KCl

0.2 g KH₂PO₄

Ammonium persulphate (APS, 10%)

Dissolve in 1 ml ddH₂O

0.1 g Ammonium persulphate

SDS (10%)

To 50 ml ddH₂O

5 g Sodium dodecyl sulphate (SDS)

Electrophoresis separating gel (10%)

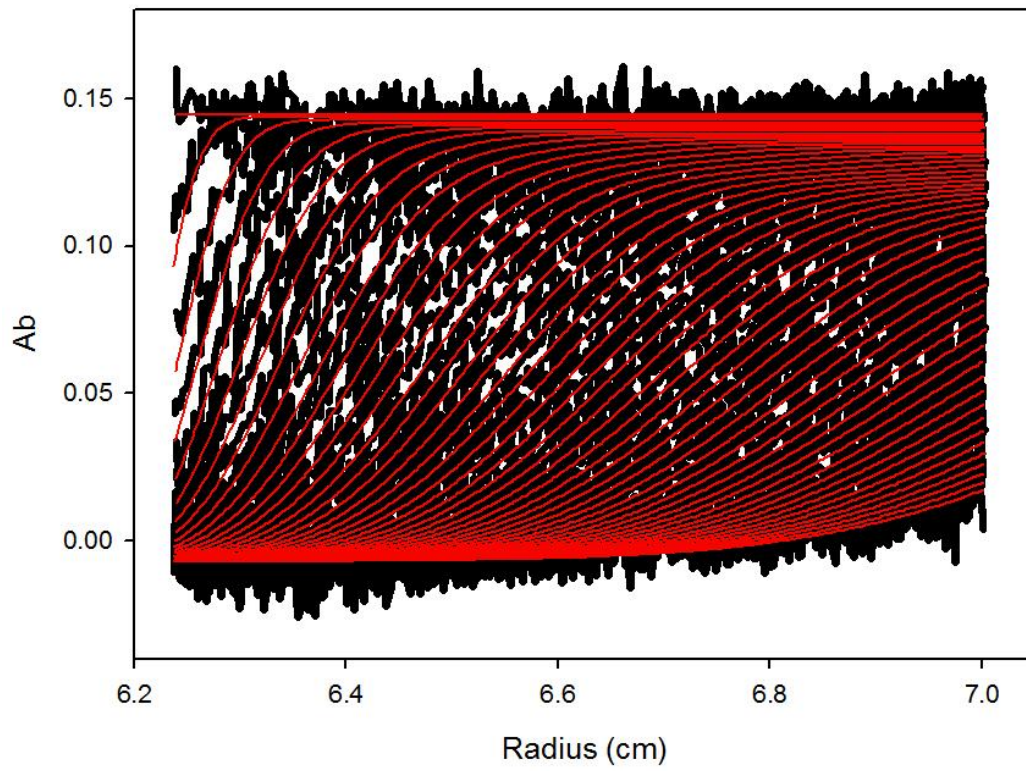
ddH ₂ O	4.1 ml
Tris buffer 1.5 M pH 8.8	2.5 ml
10 SDS	100 µl
30% Acrylamide/bis solution	3.33 ml
10% APS	50 µl
TEMED	10 µl

Electrophoresis stacking gel (4%)

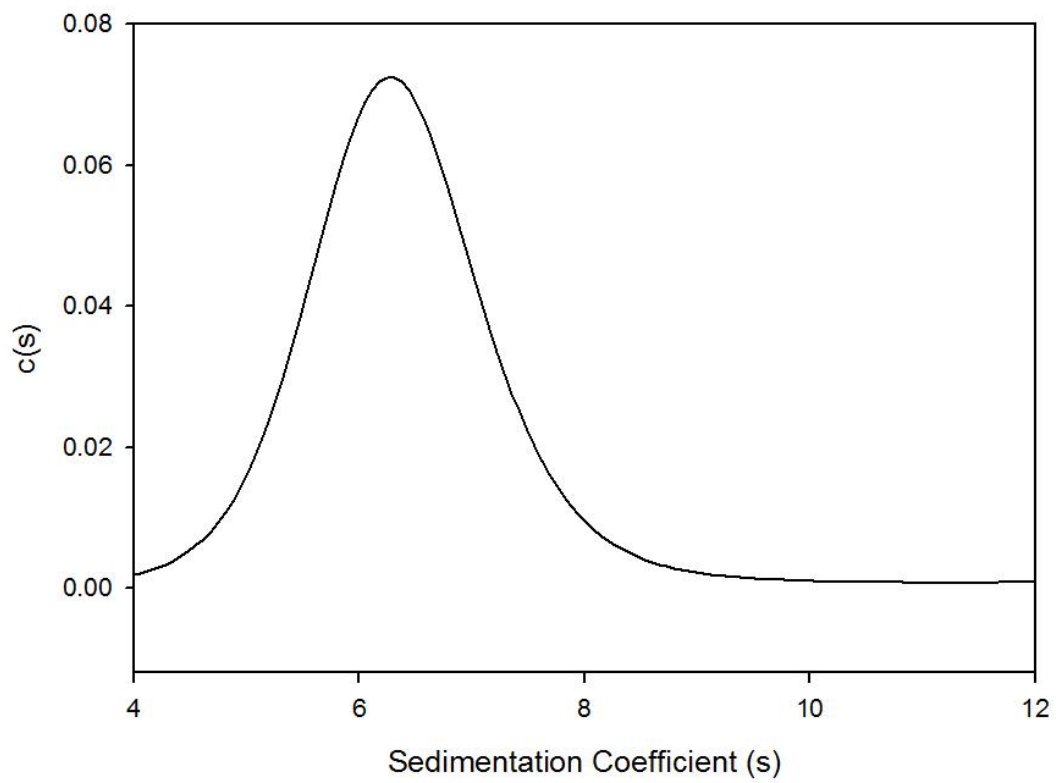
ddH ₂ O	6.1 ml
Tris buffer 0.5 M pH 6.8	2.5 ml
10 SDS	100 µl
30% Acrylamide/bis solution	1.3 ml
10% APS	50 µl
TEMED	10 µl

Appendix II
Analytical Centrifugation Analyses

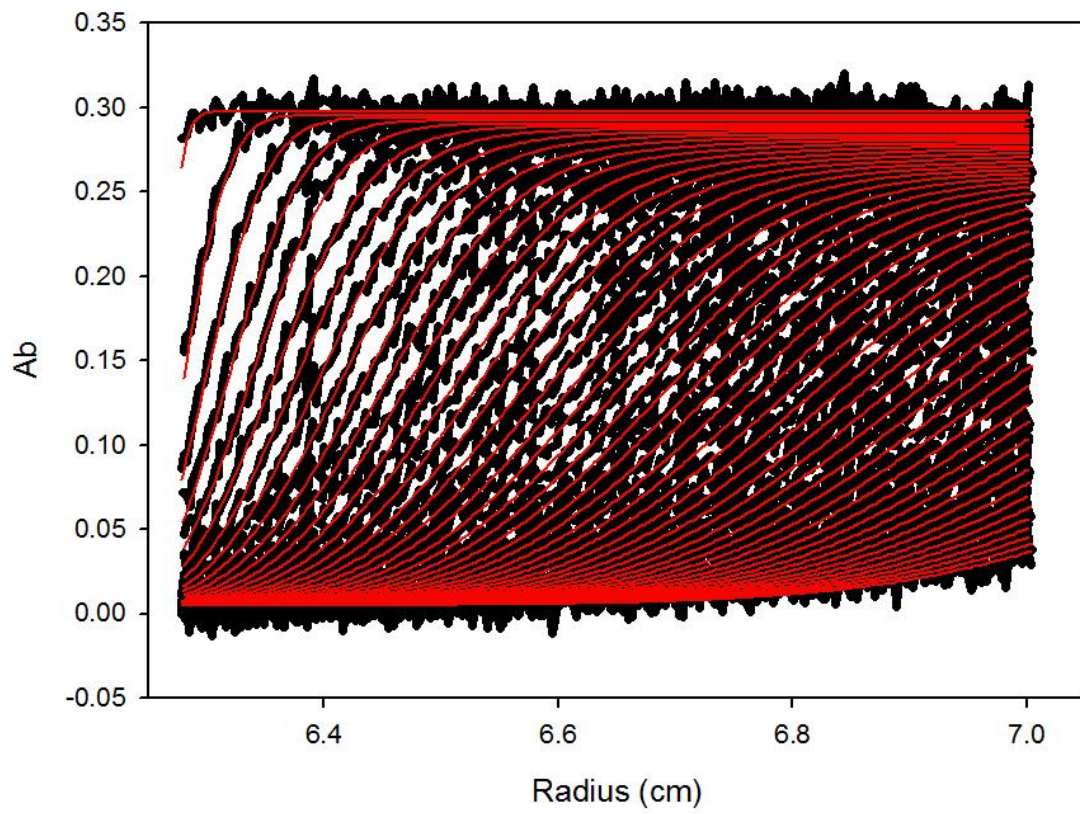
ALICE 20K AB1



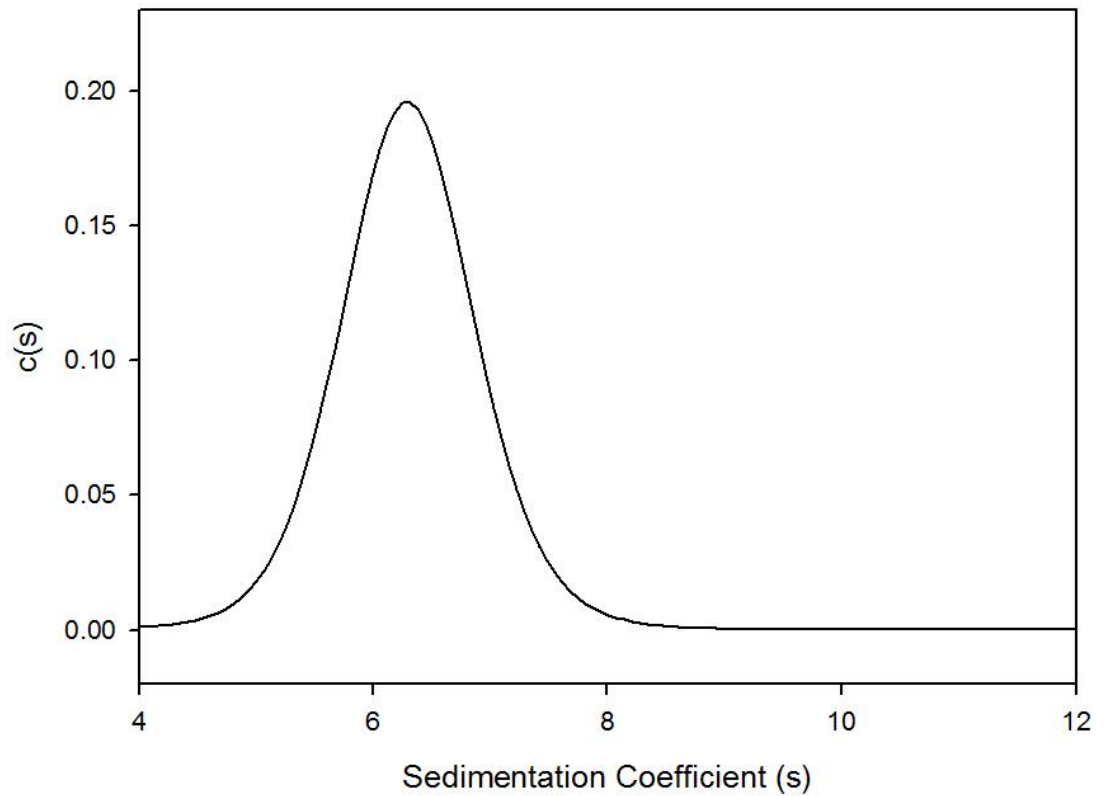
ALICE 20K AB1 c(s) distribution



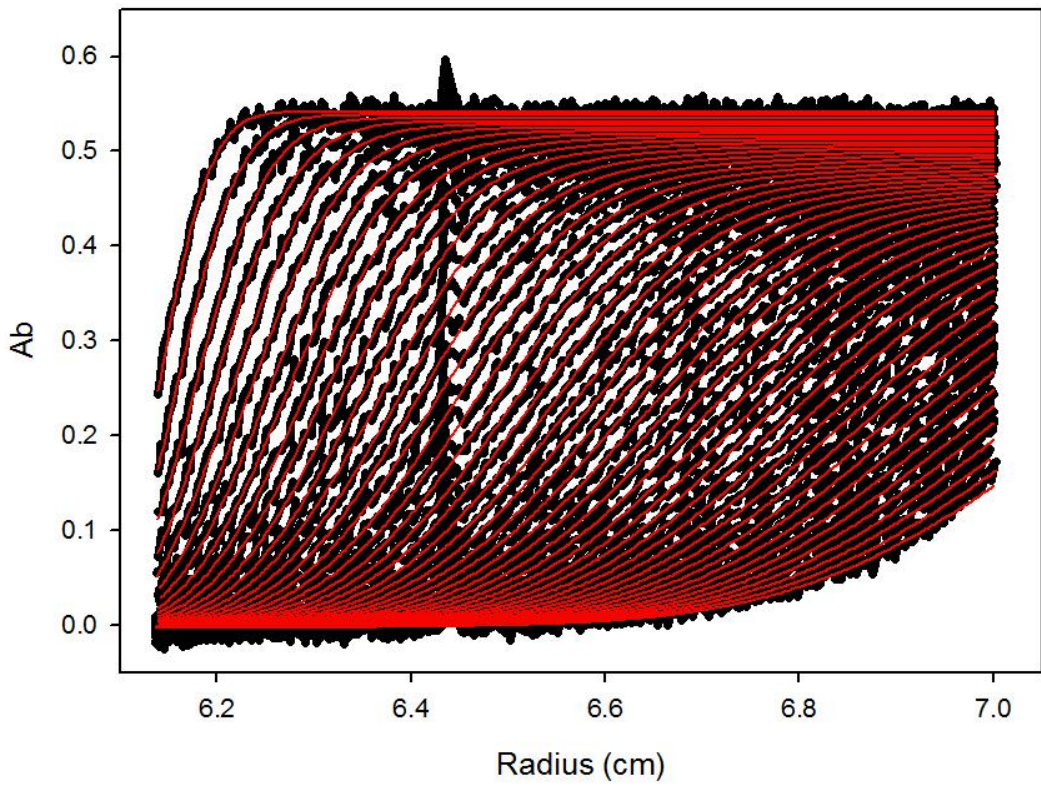
ALICE 20K AB2



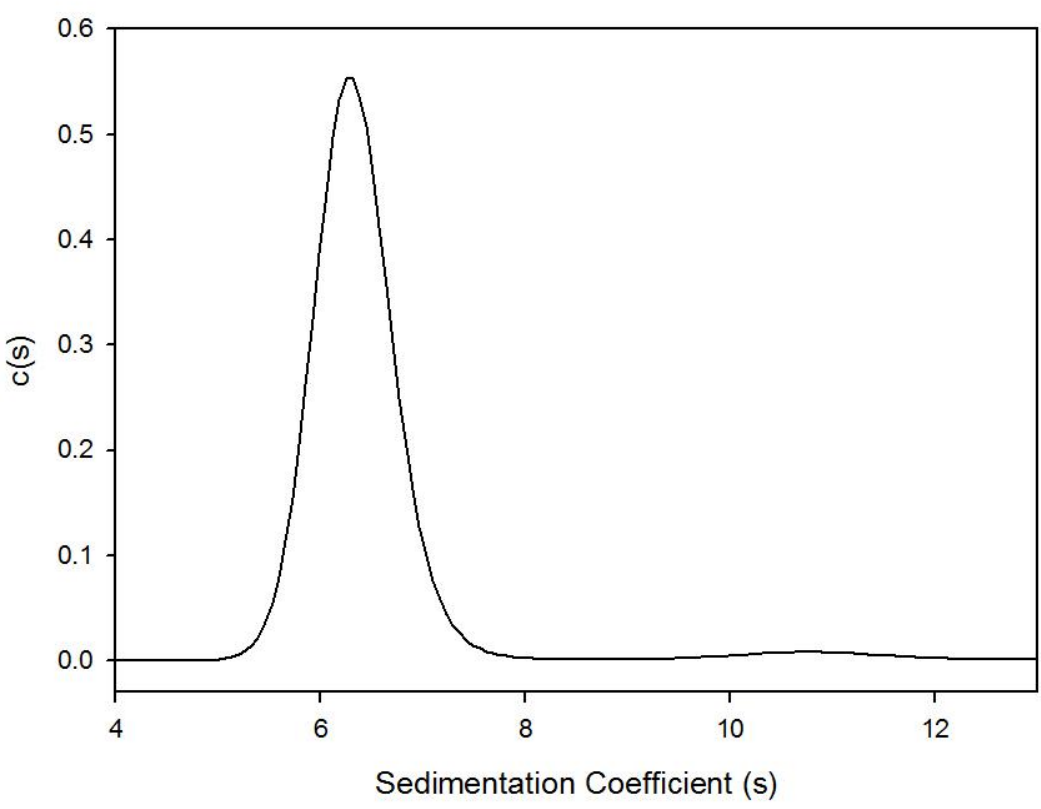
ALICE 20K AB2 c(s) distribution



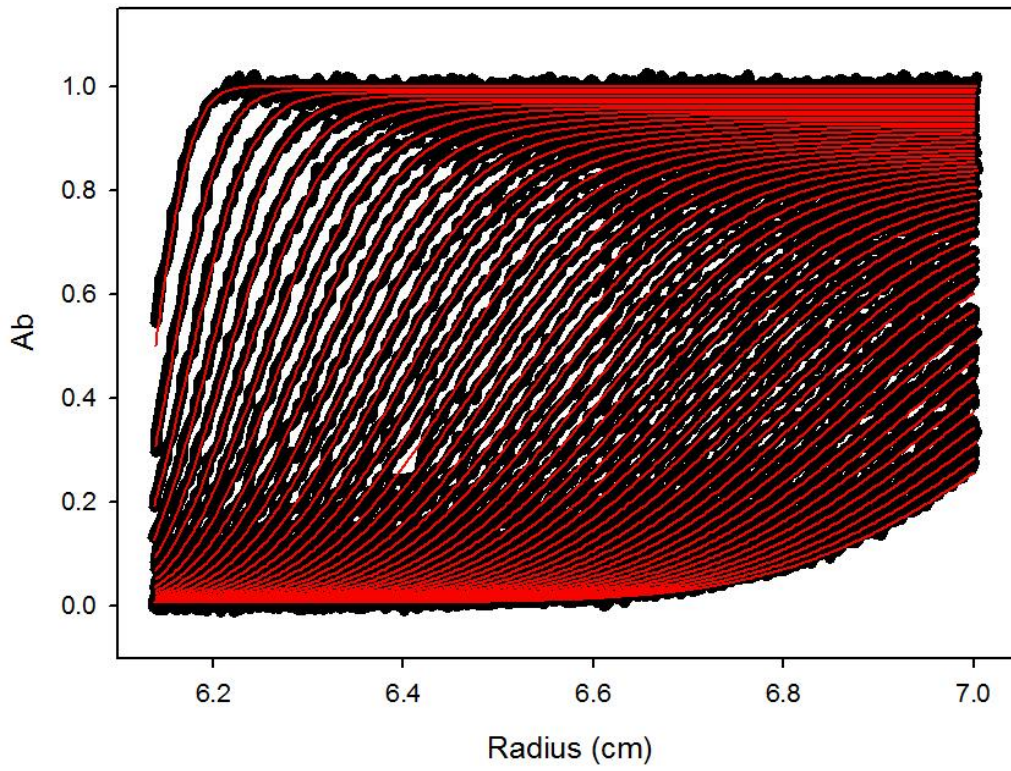
ALICE 20K AB3



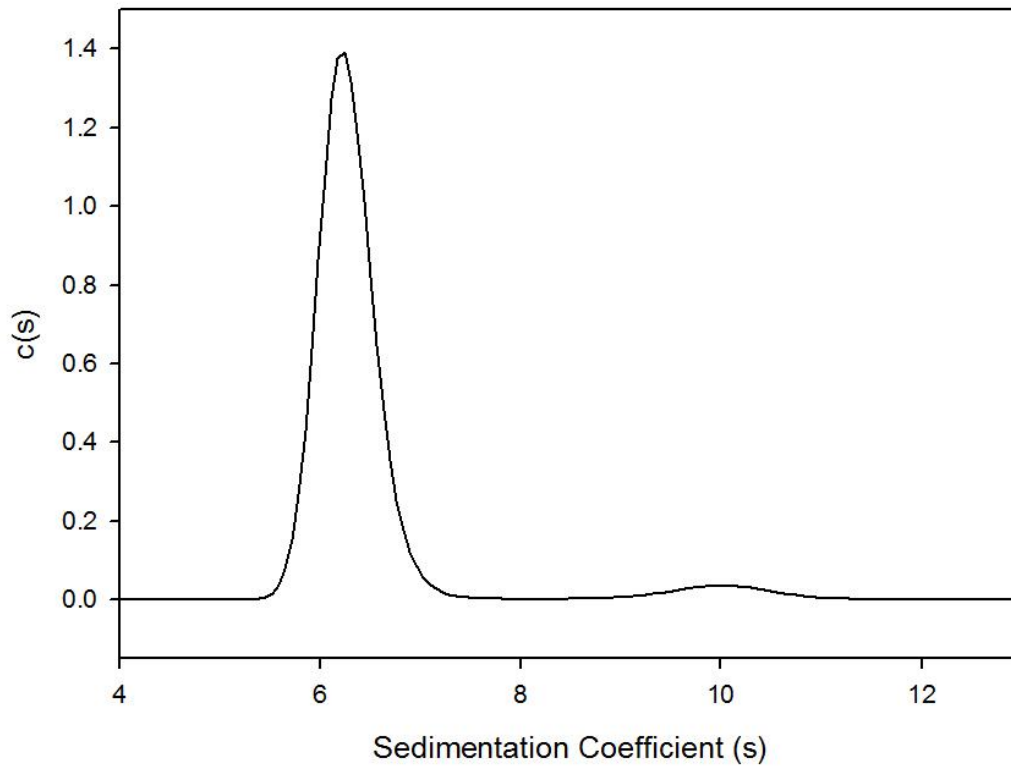
ALICE 20K AB3 c(s) distribution



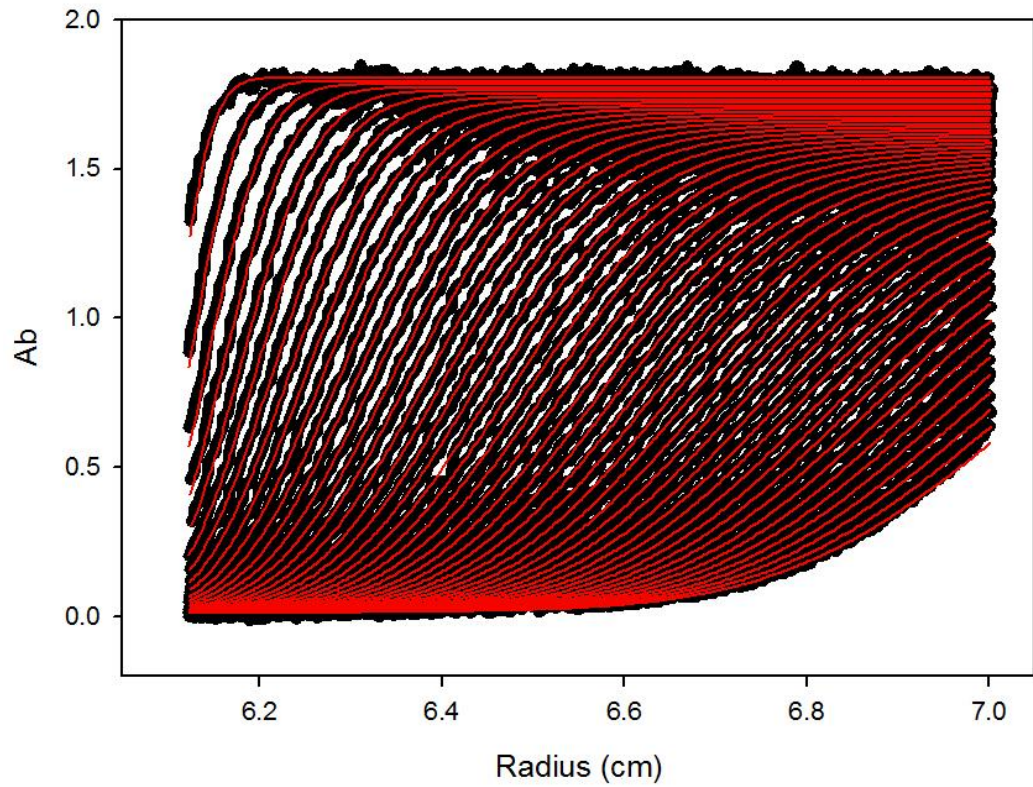
ALICE 20K AB4



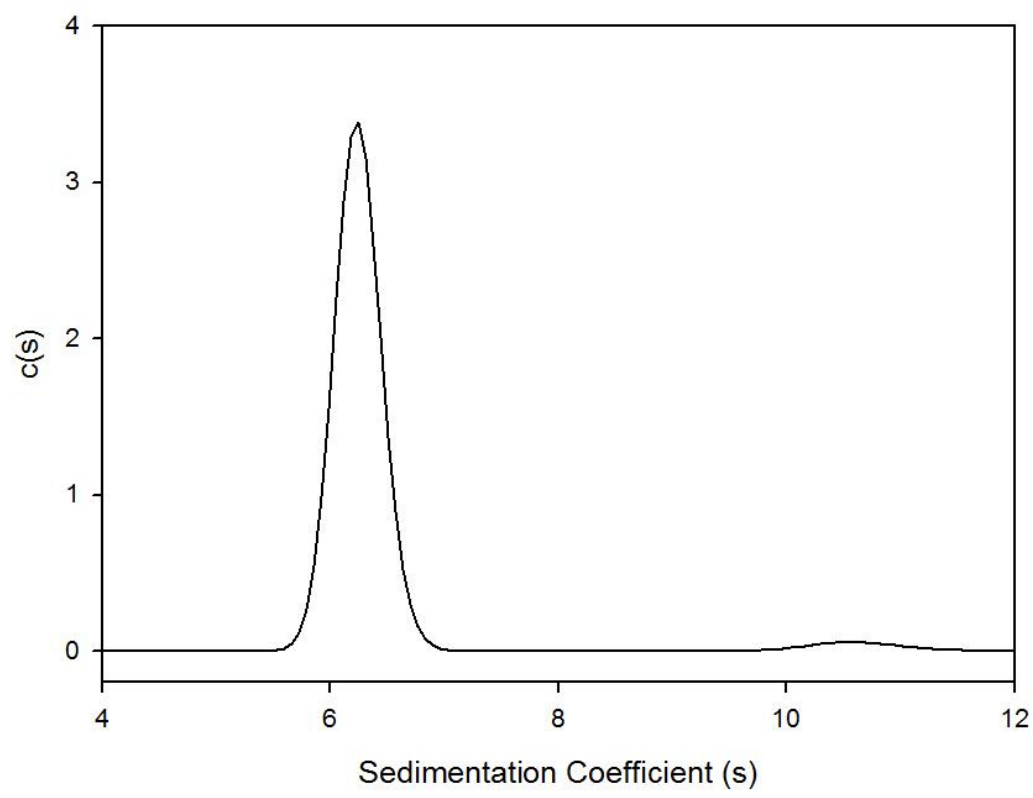
ALICE 20K AB4 c(s) distribution



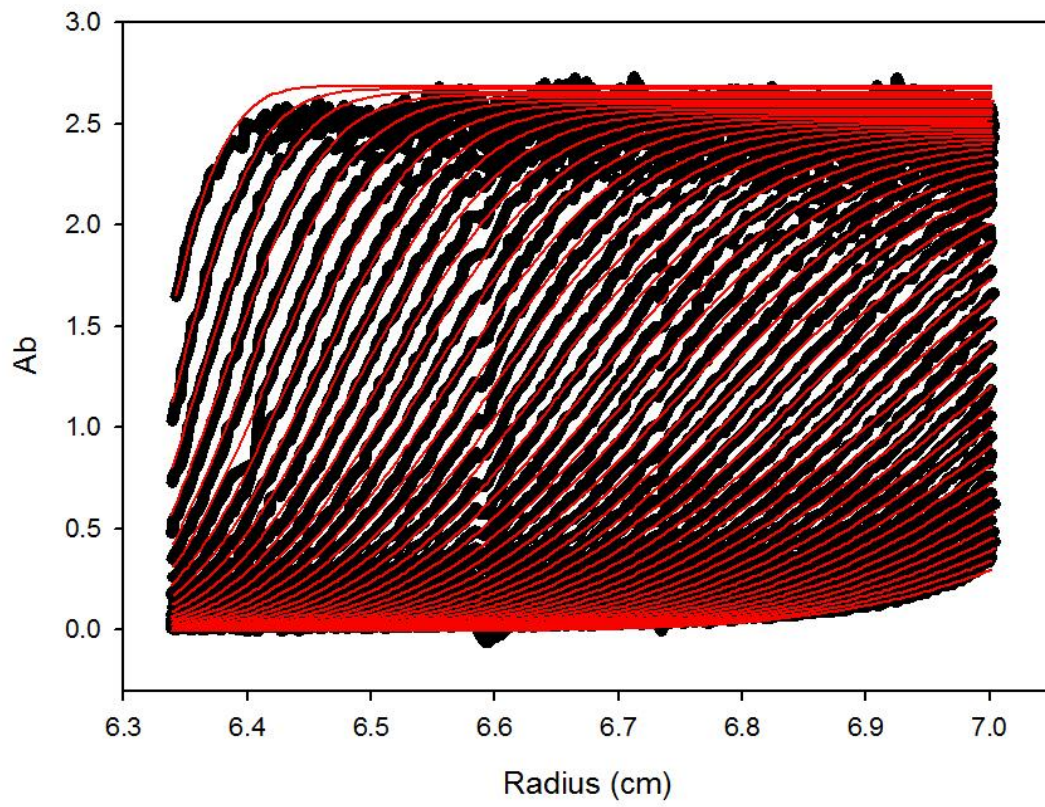
ALICE 20K AB5



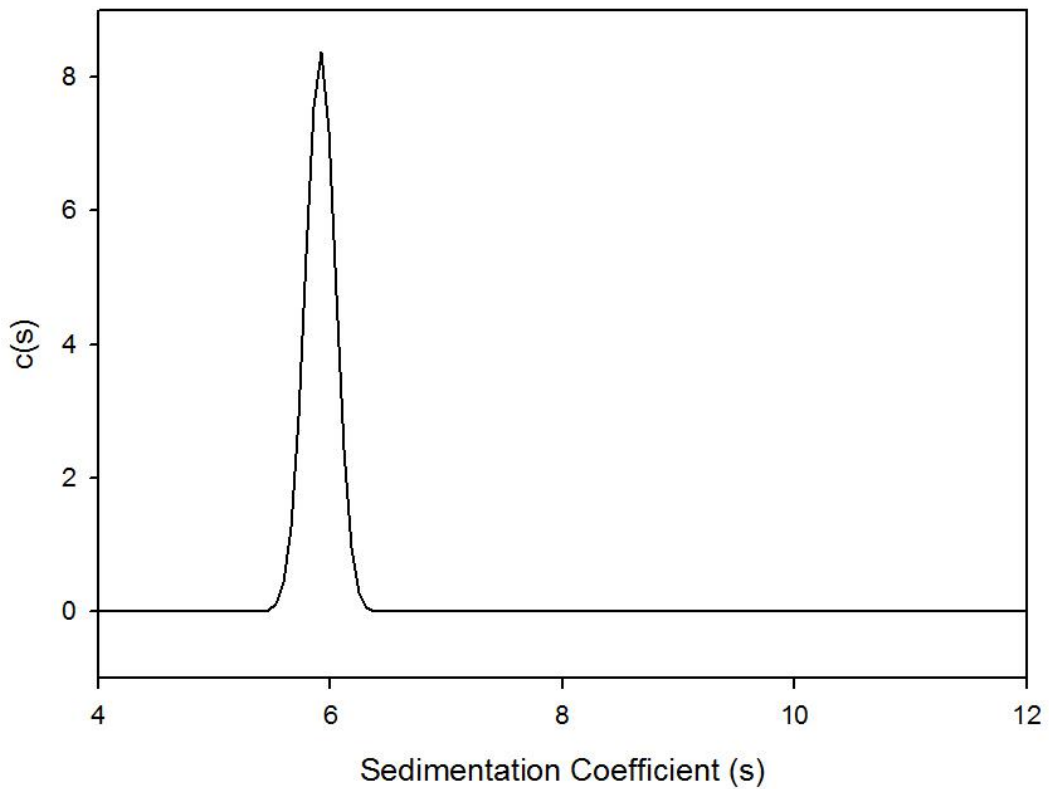
ALICE 20K AB5 c(s) distribution



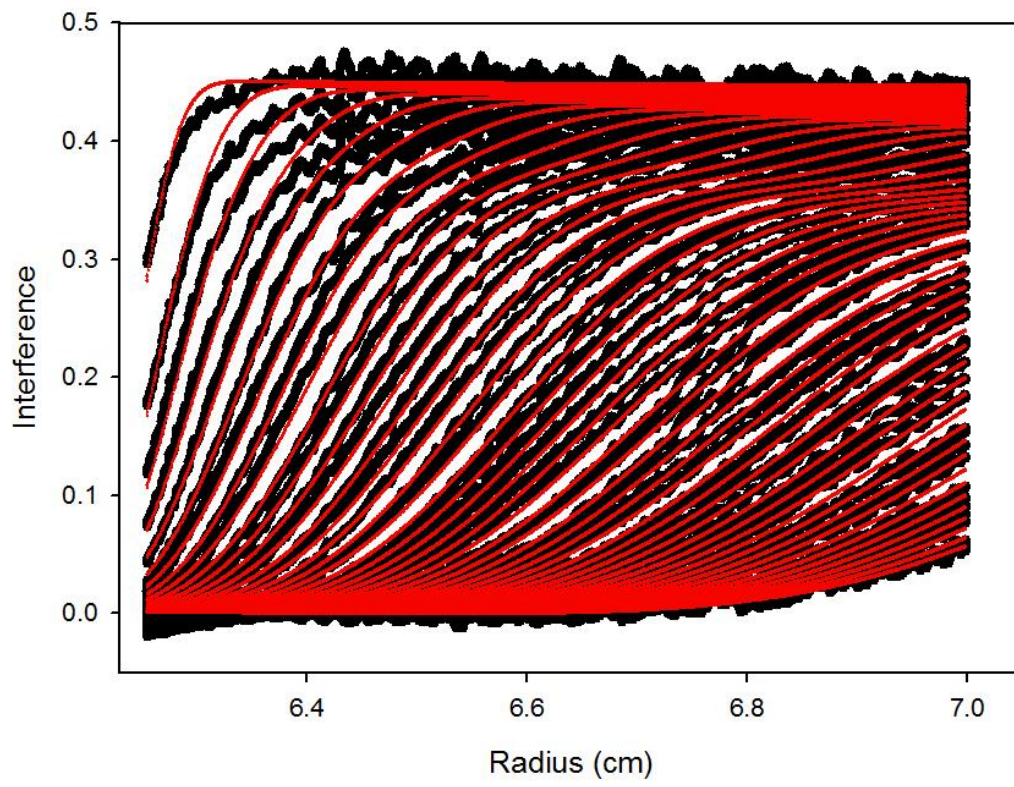
ALICE 20K AB6



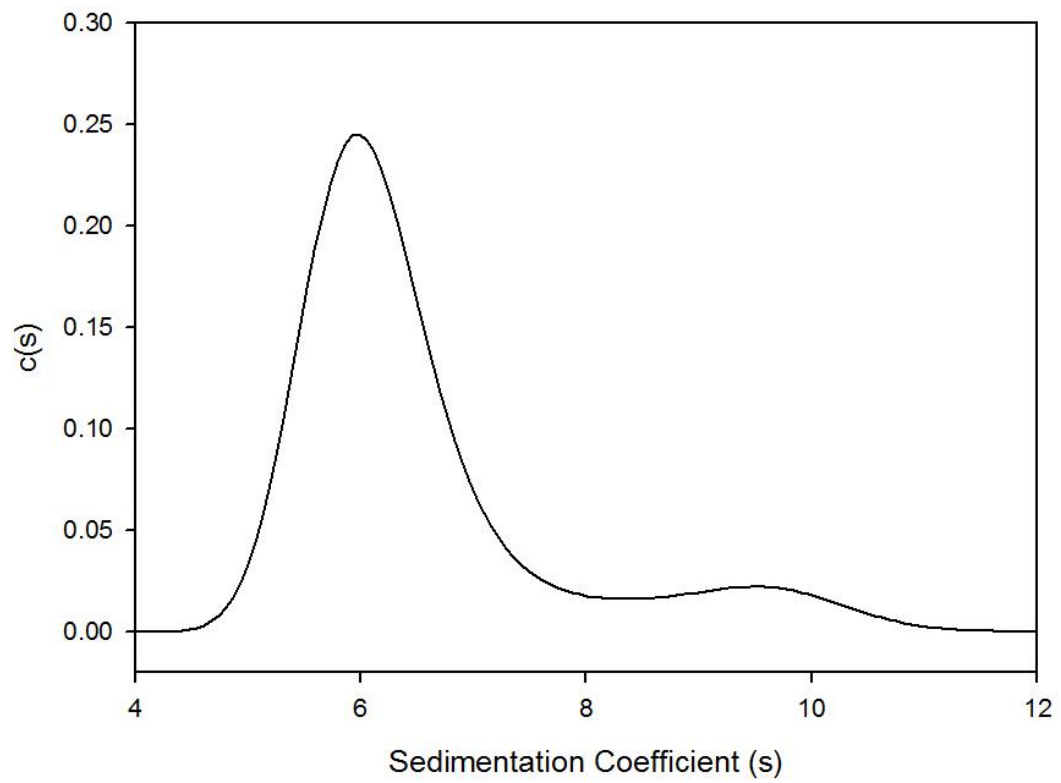
ALICE 20K AB6 c(s) distribution



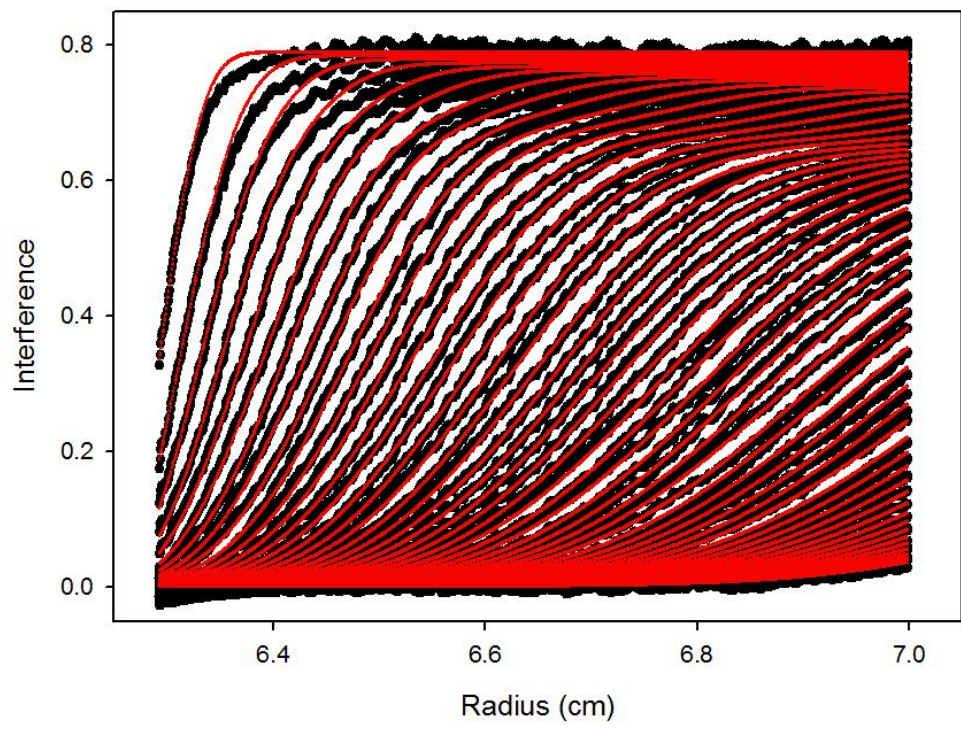
ALICE 20K IP1



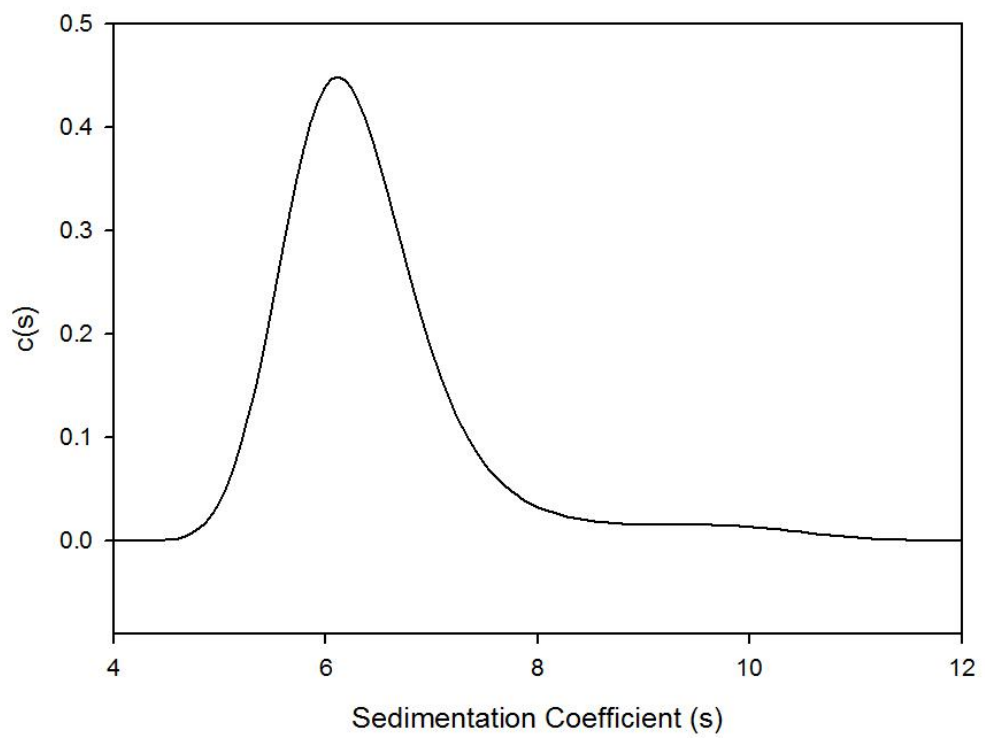
ALICE 20K IP1 c(s) distribution



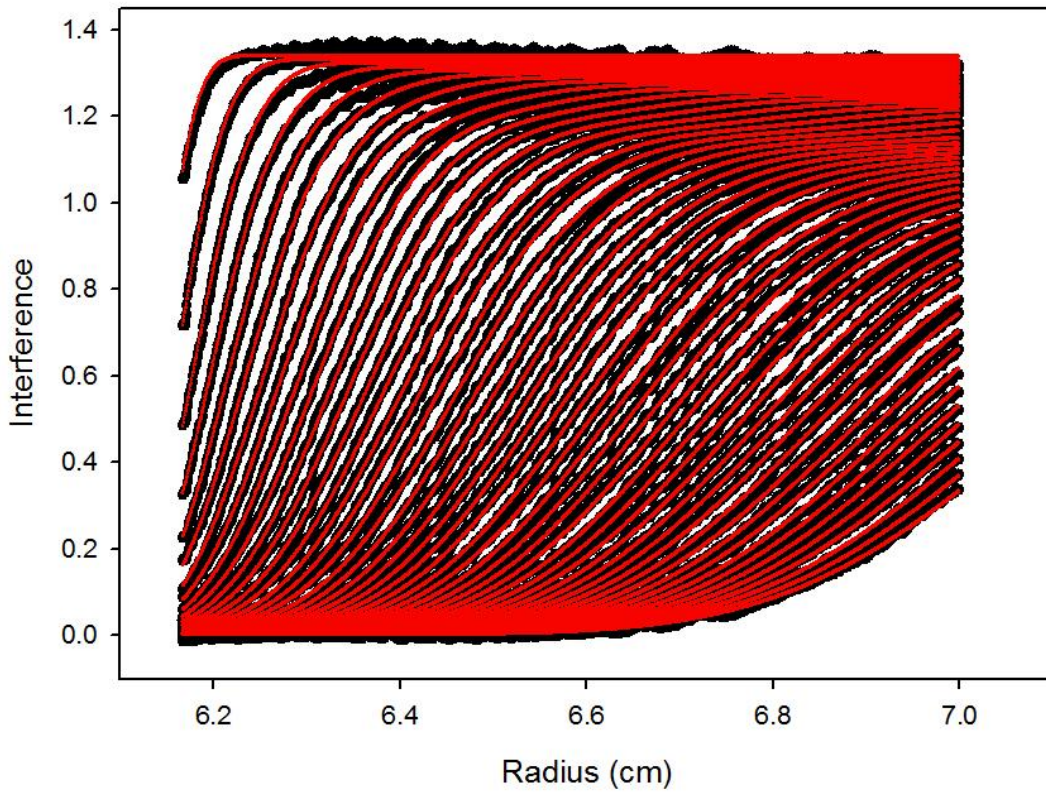
ALICE 20K IP2



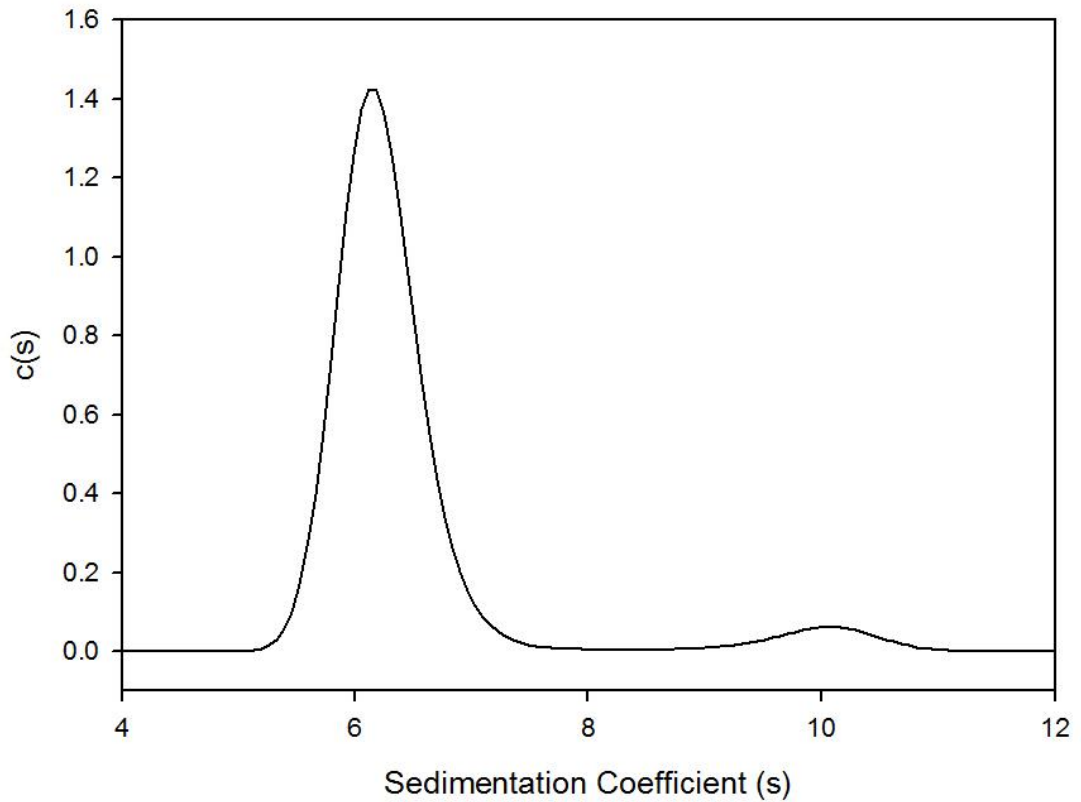
ALICE 20K IP2 c(s) distribution



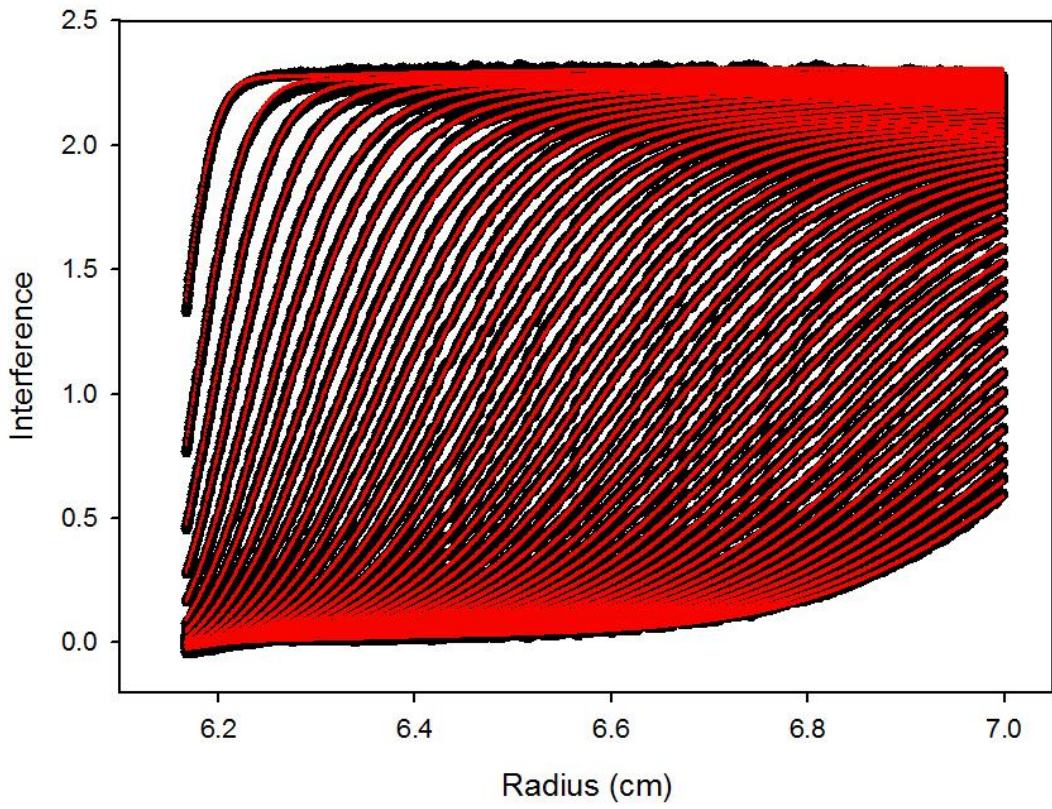
ALICE 20K IP3



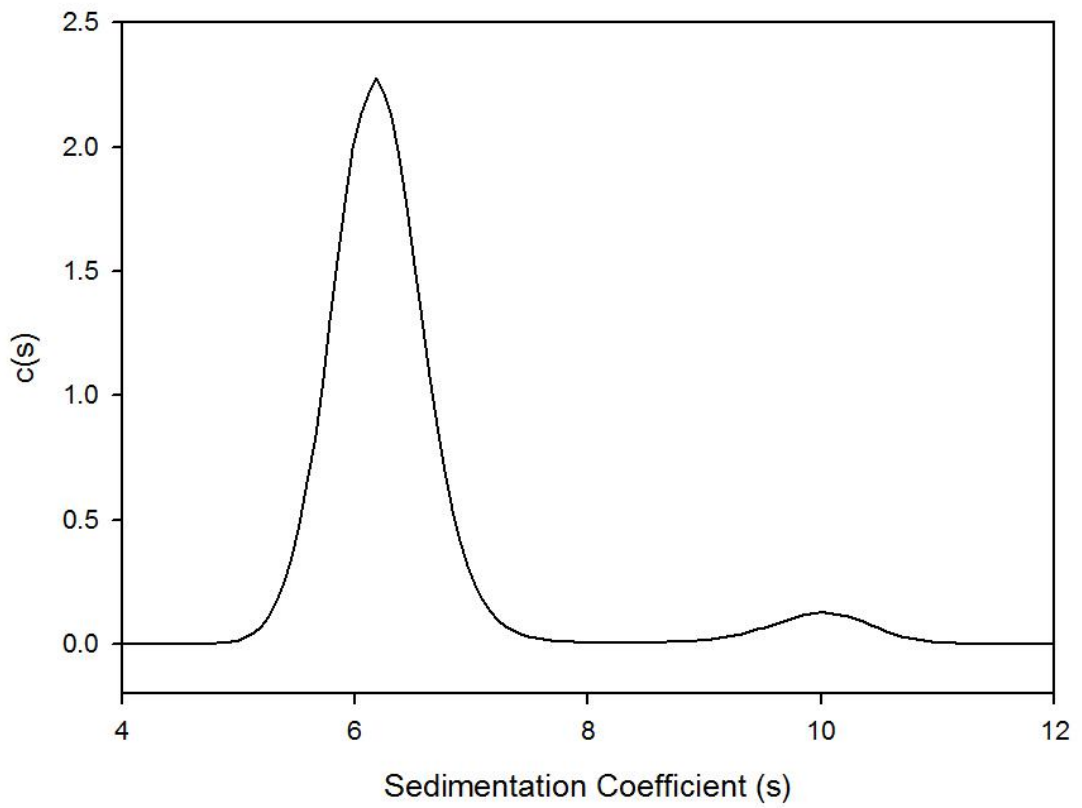
ALICE 20K IP3 c(s) distribution



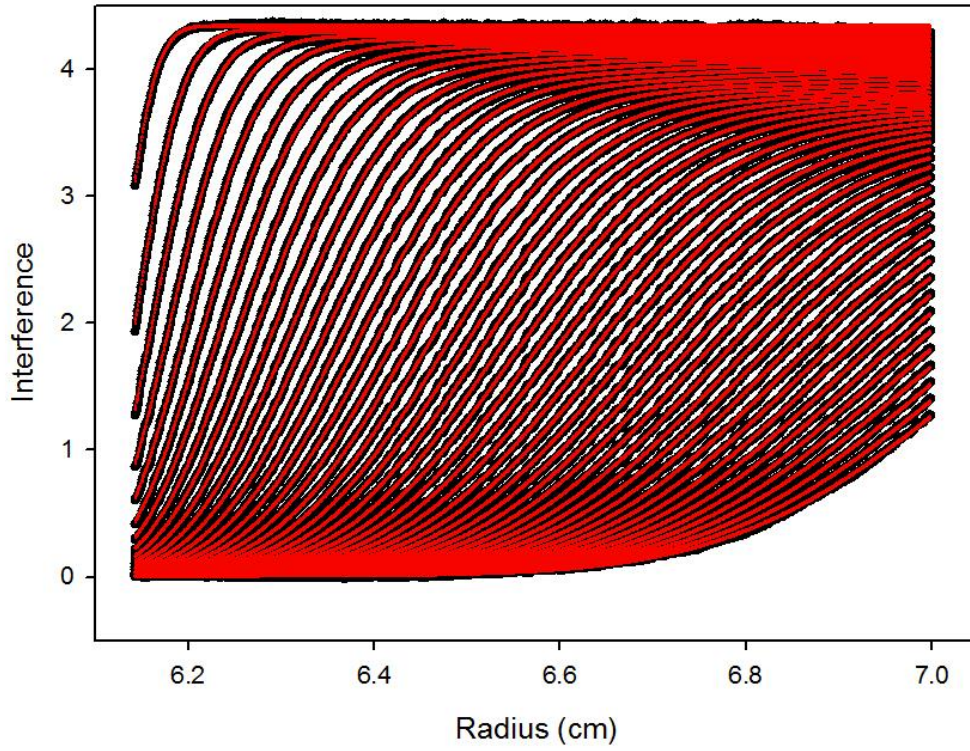
ALICE 20K IP4



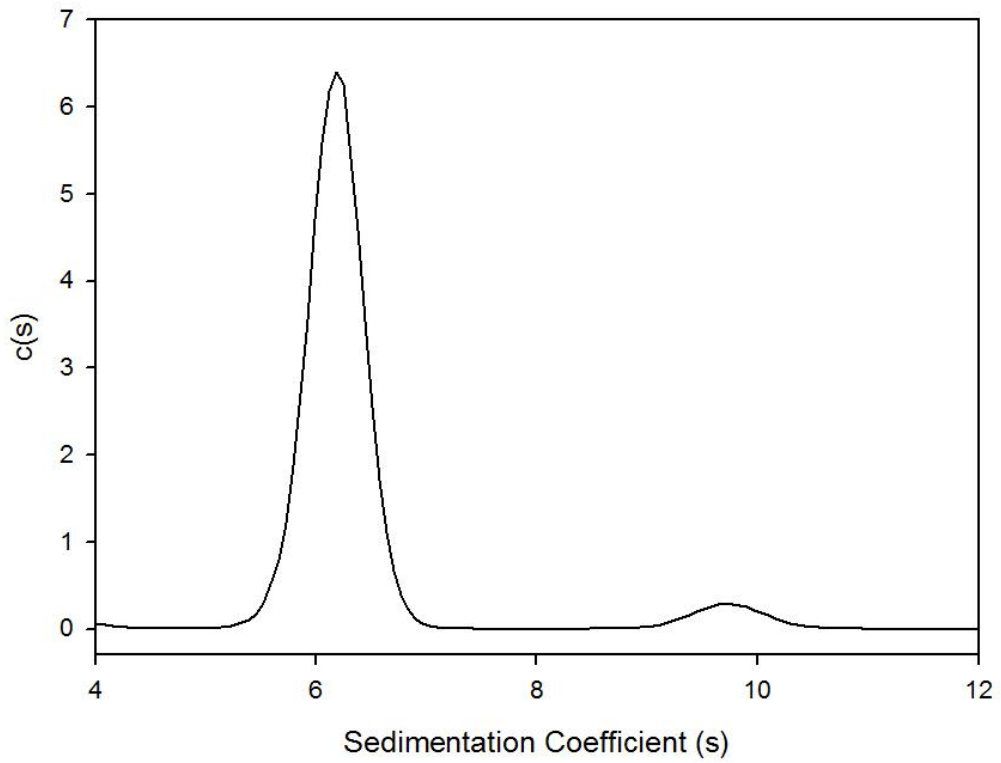
ALICE 20K IP4 c(s) distribution

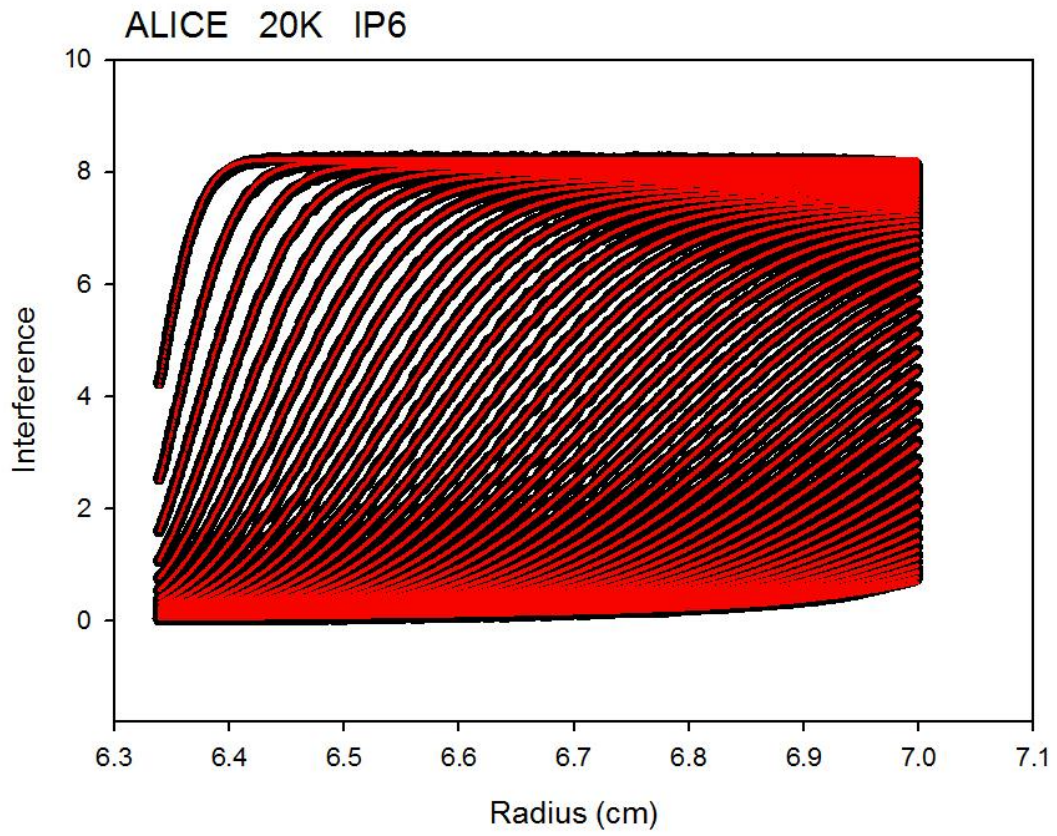


ALICE 20K IP5

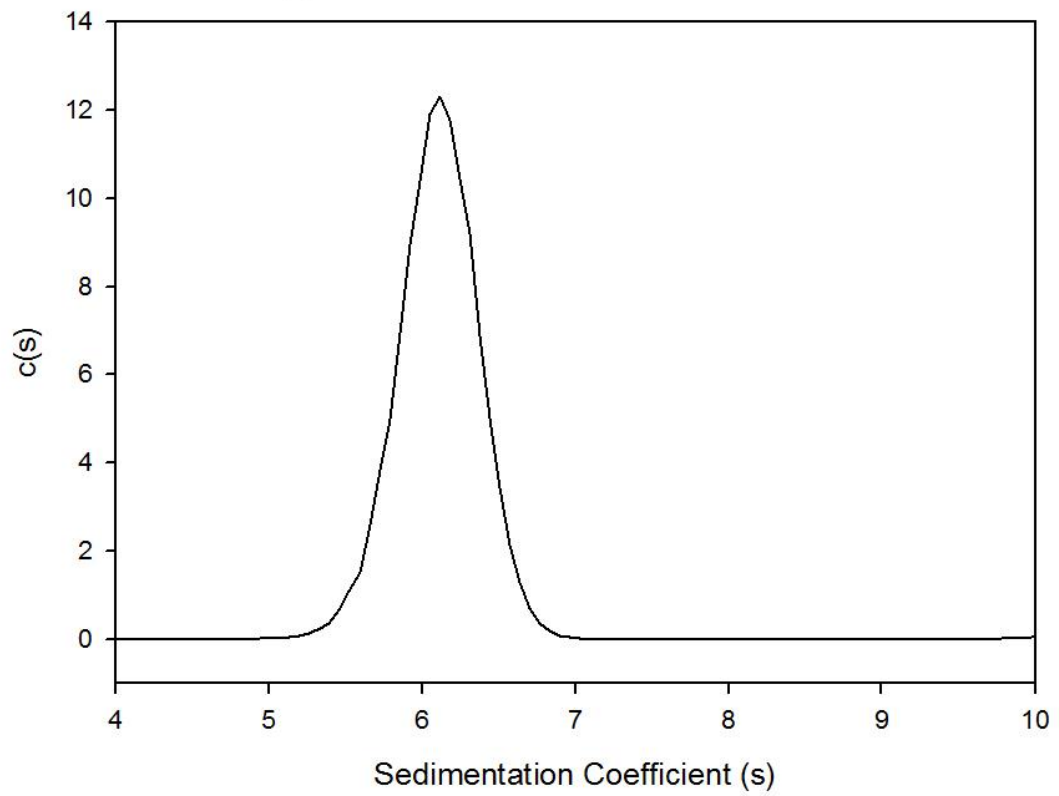


ALICE 20K IP5 c(s) distribution

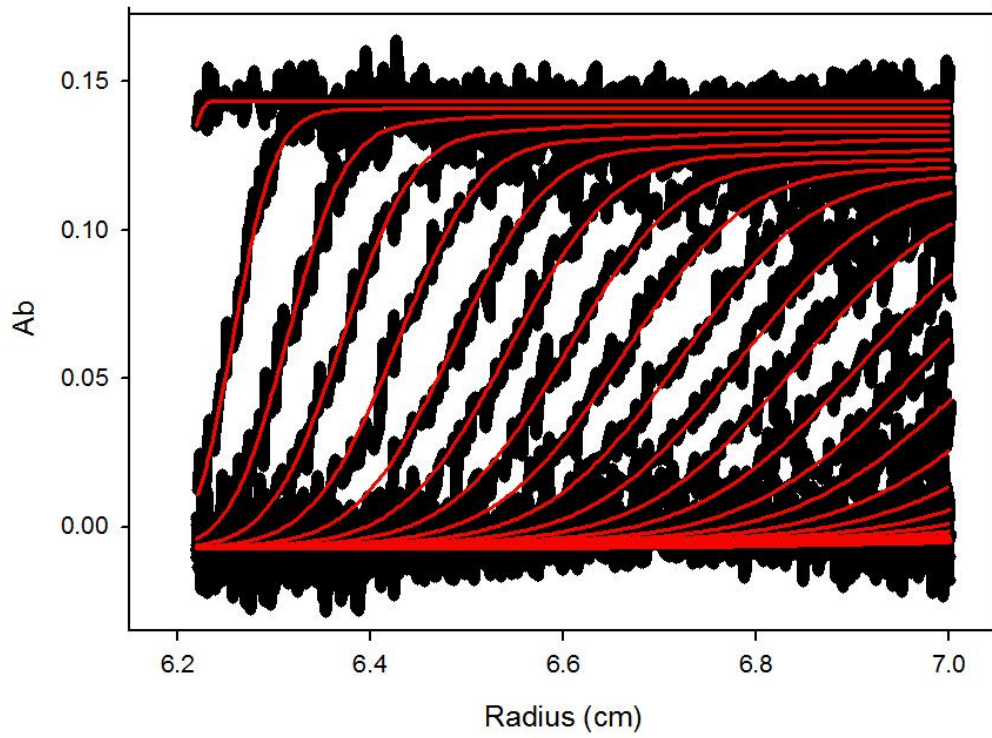




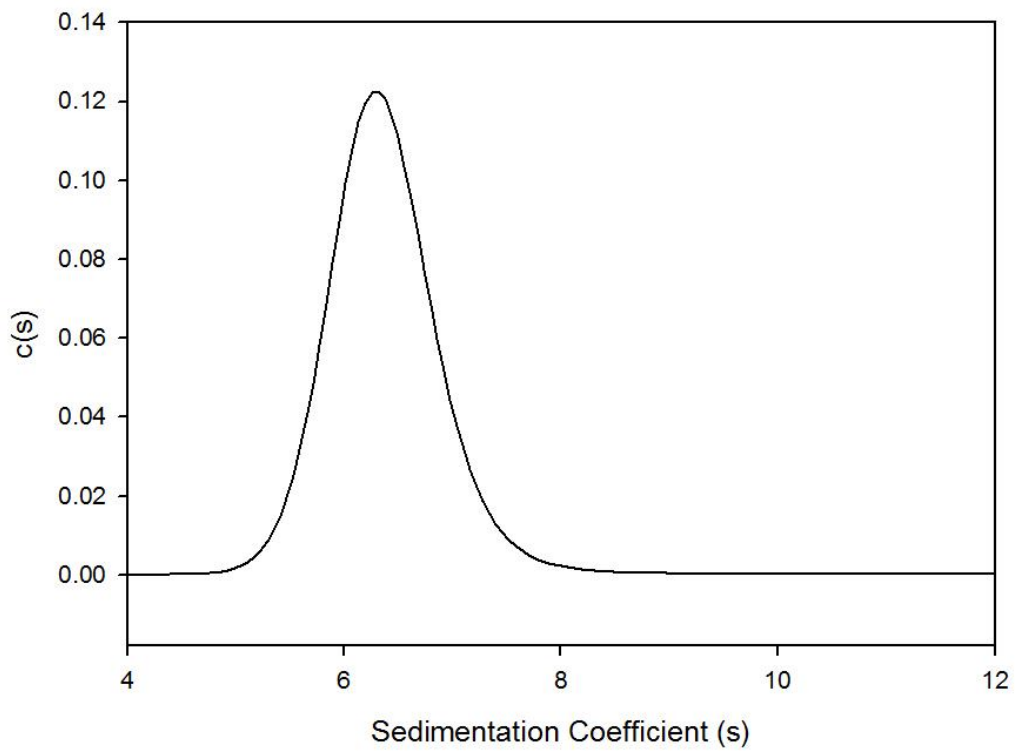
ALICE 20K IP6 c(s) distribution



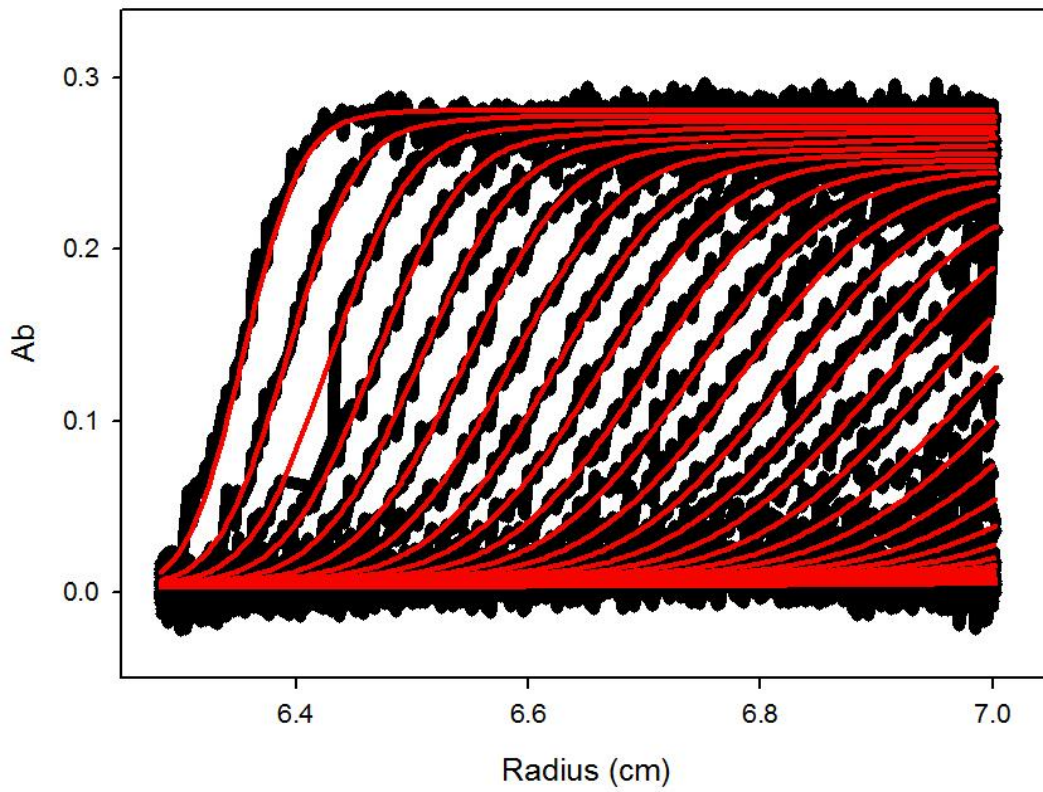
ALICE 30K AB1



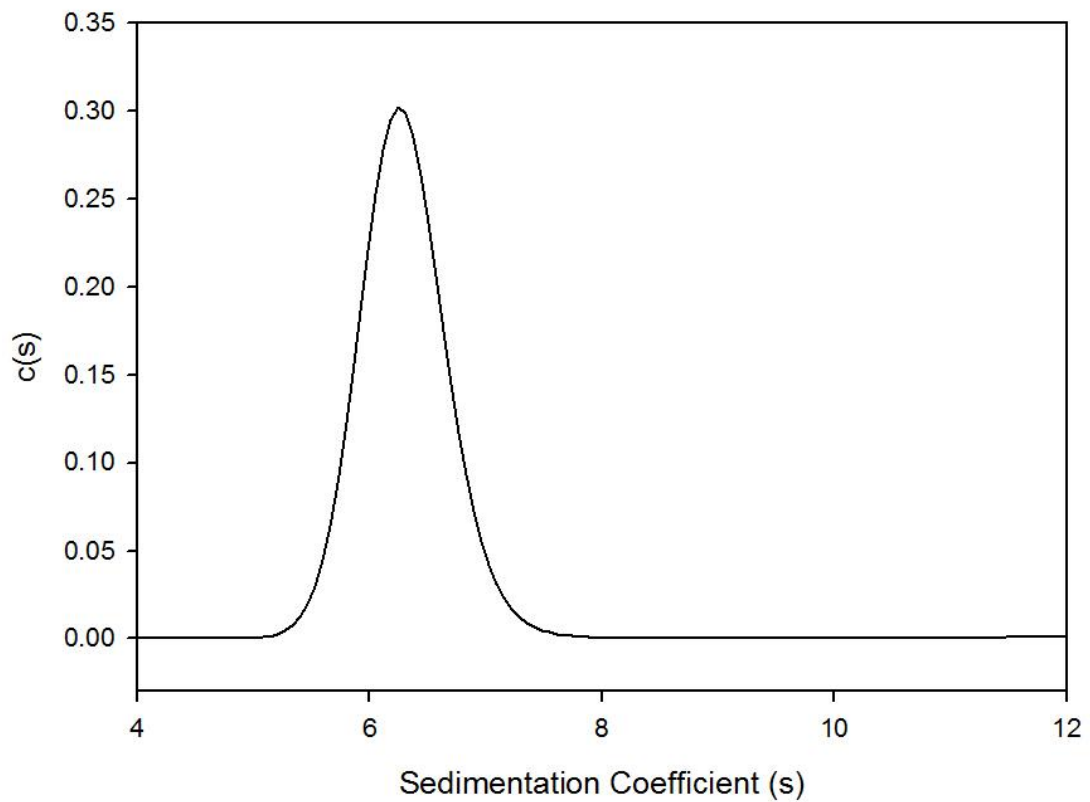
ALICE 30K AB1 c(s) distribution



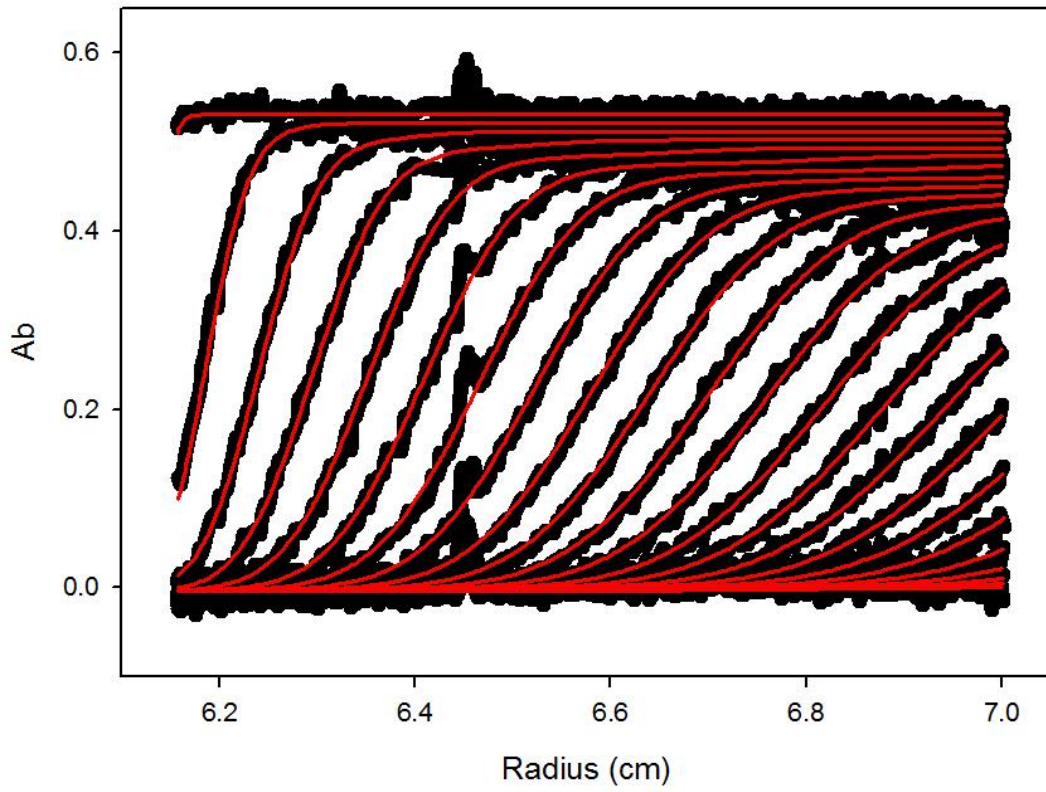
ALICE 30K AB2



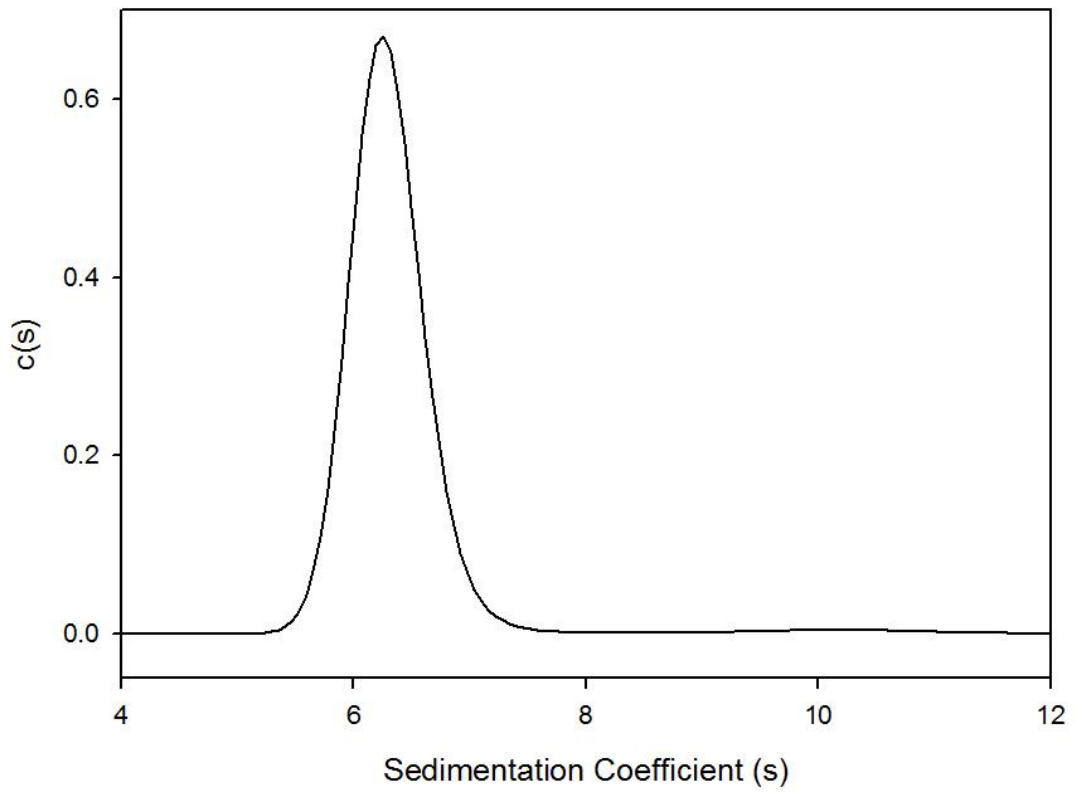
ALICE 30K AB2 c(s) distribution



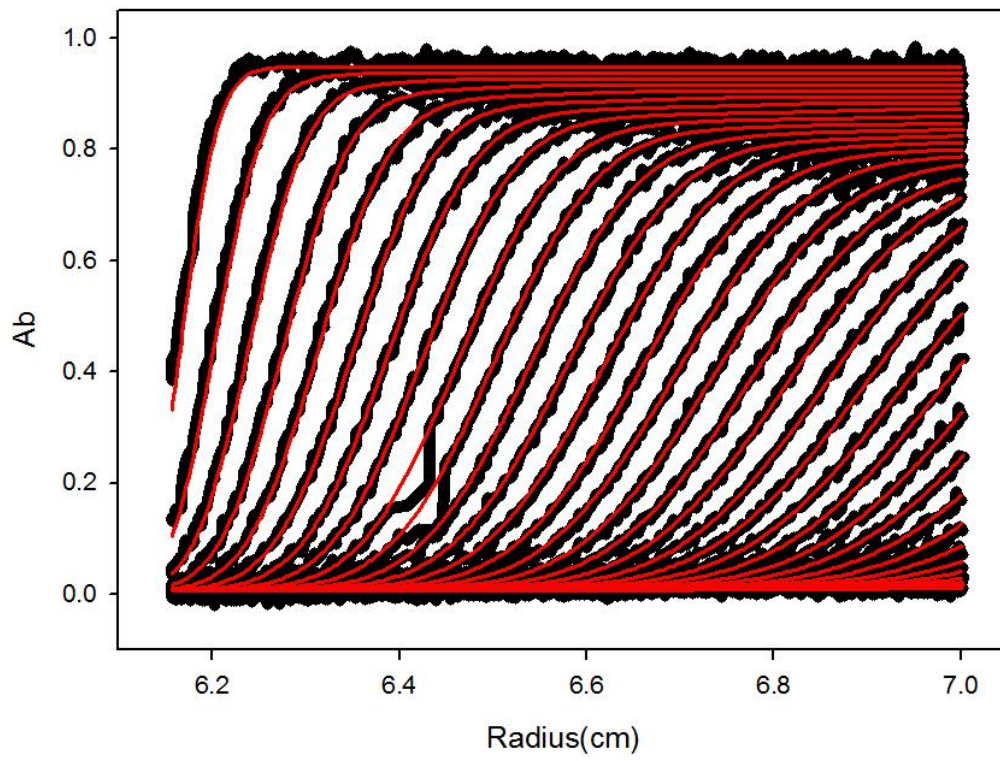
ALICE 30K AB3



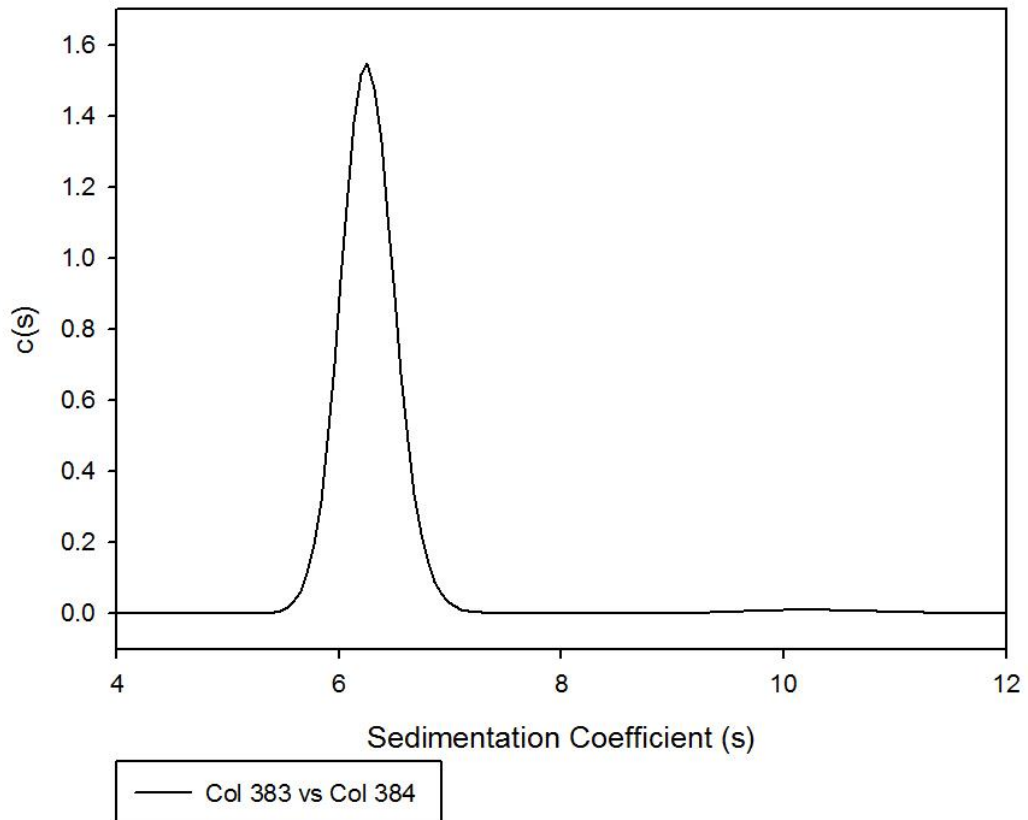
ALICE 30K AB3 c(s) distribution



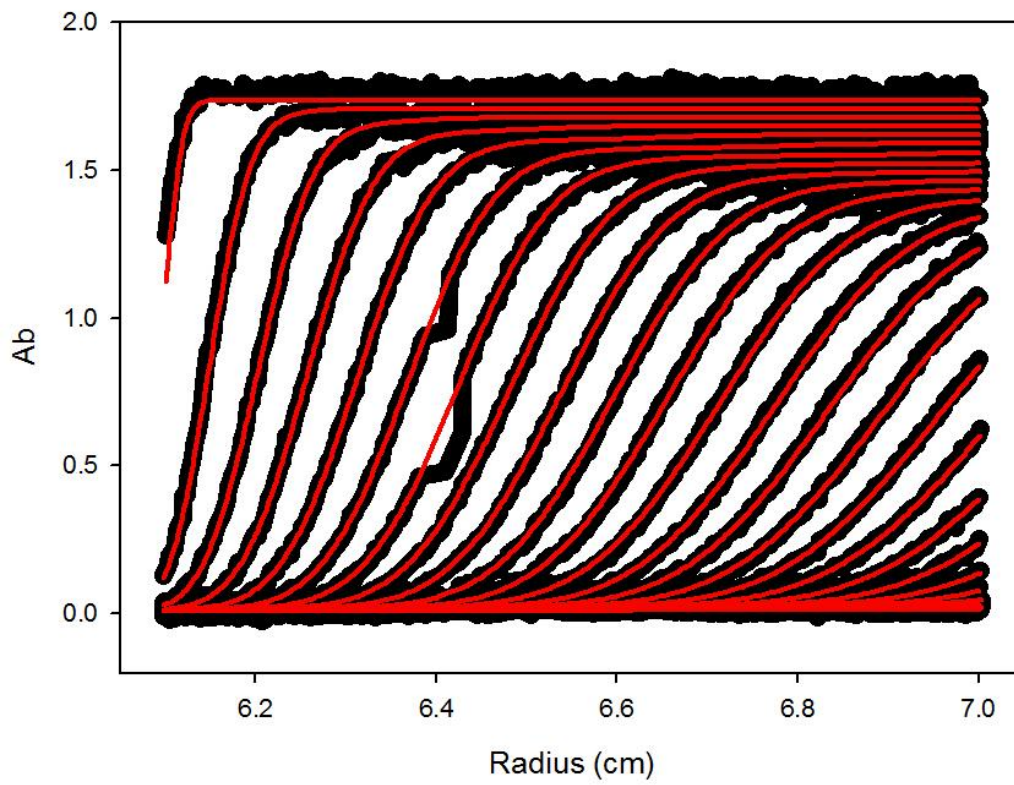
ALICE 30K AB4



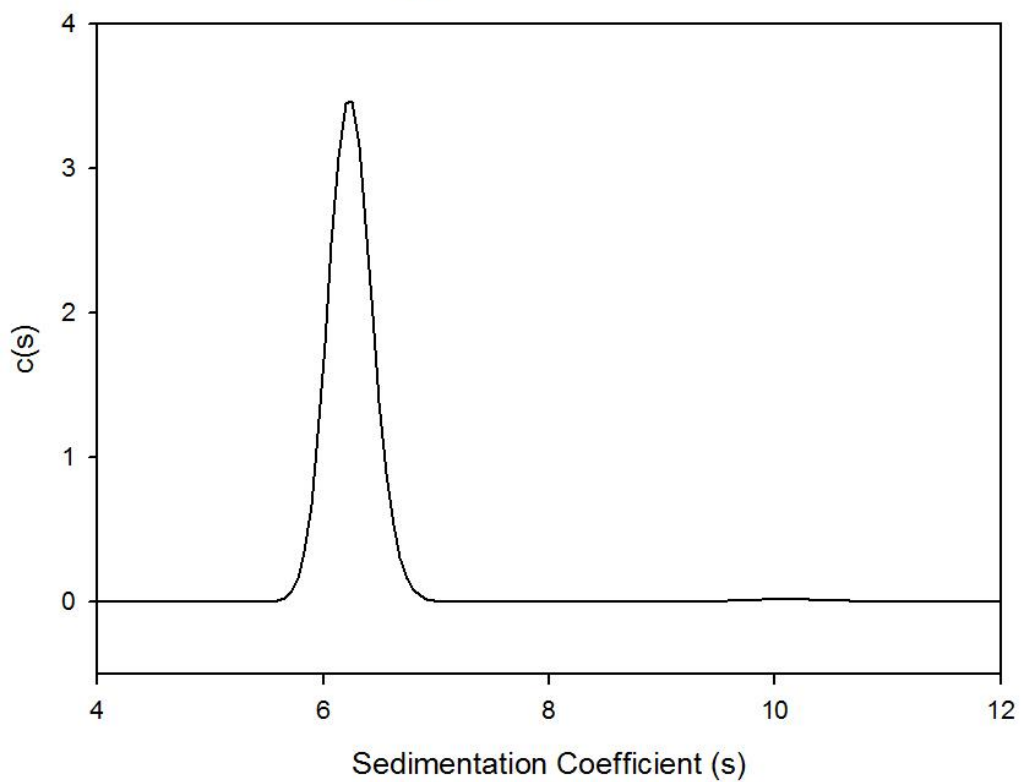
ALICE 30K AB4 c(s) distribution



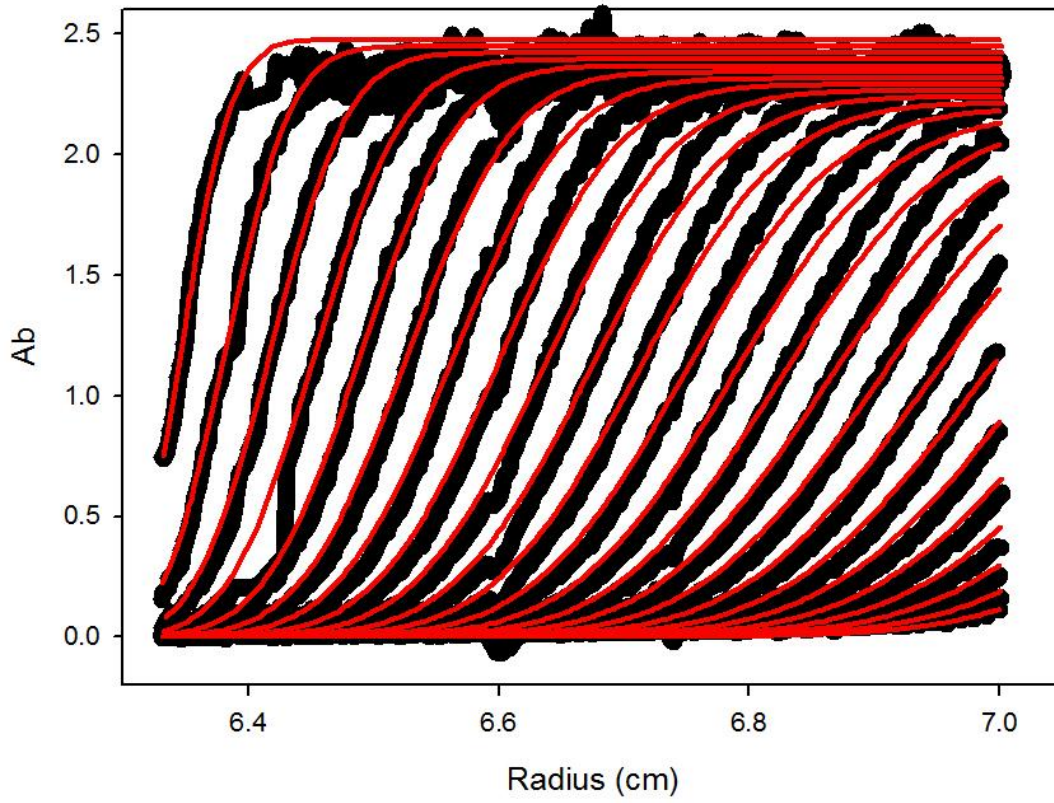
ALICE 30K AB5



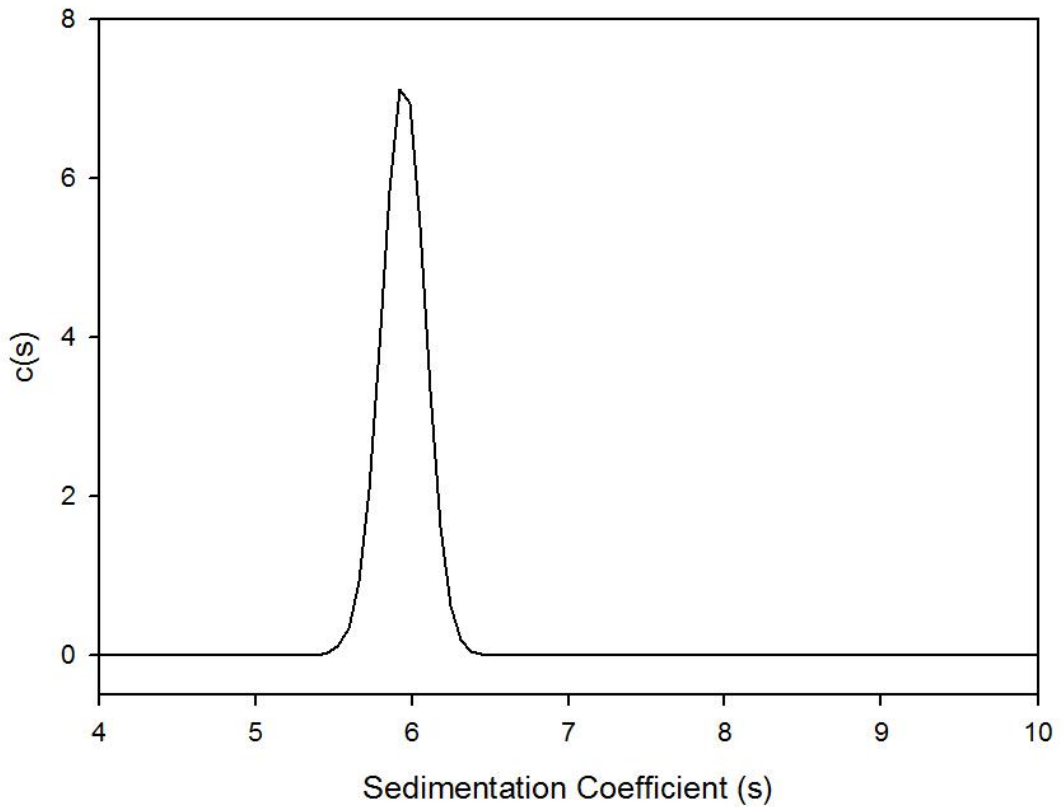
ALICE 30K AB5 c(s) distribution



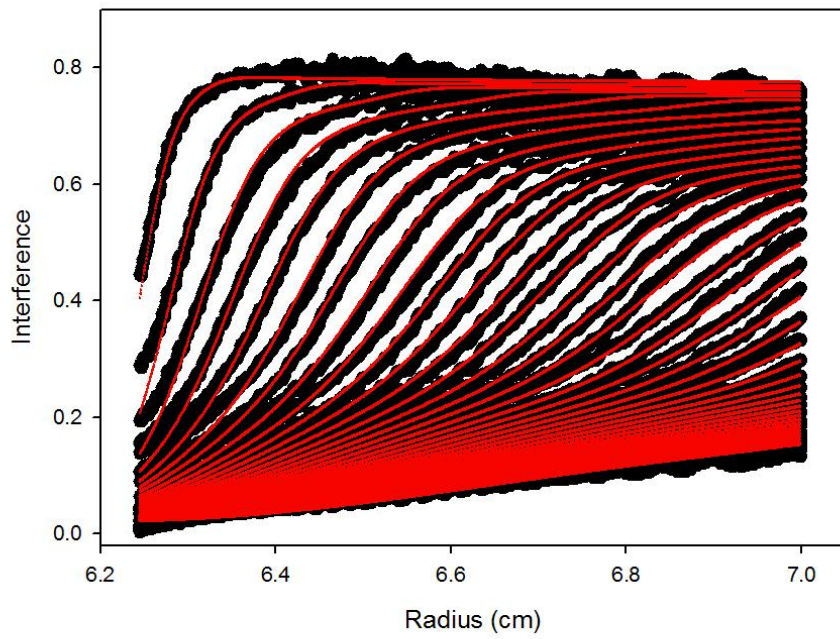
ALICE 30K AB6



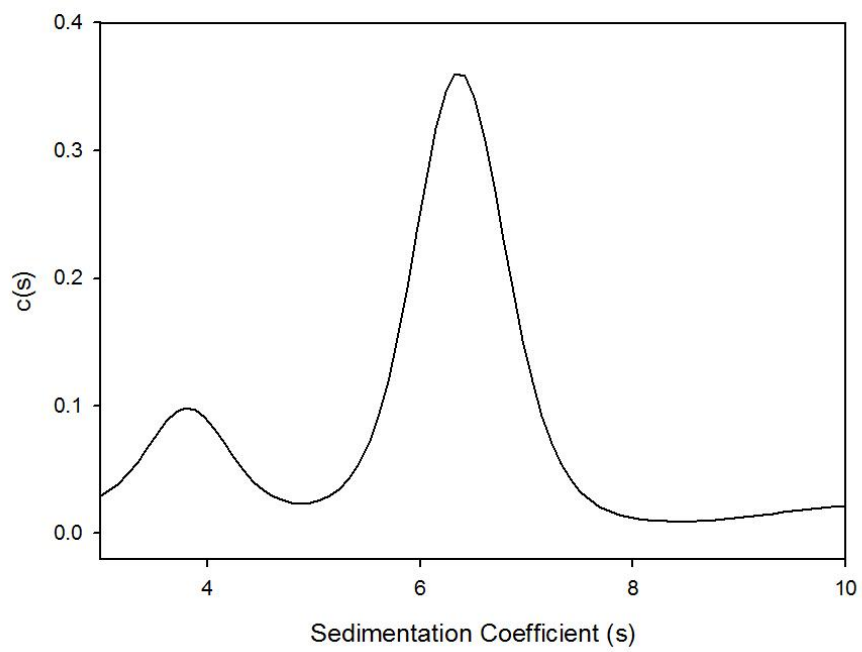
ALICE 30K AB6 c(s) distribution

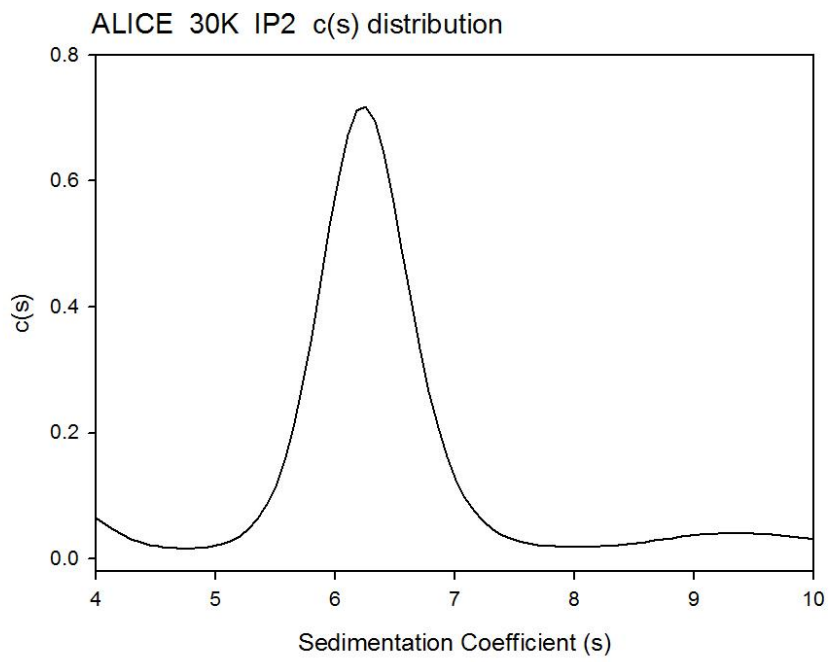
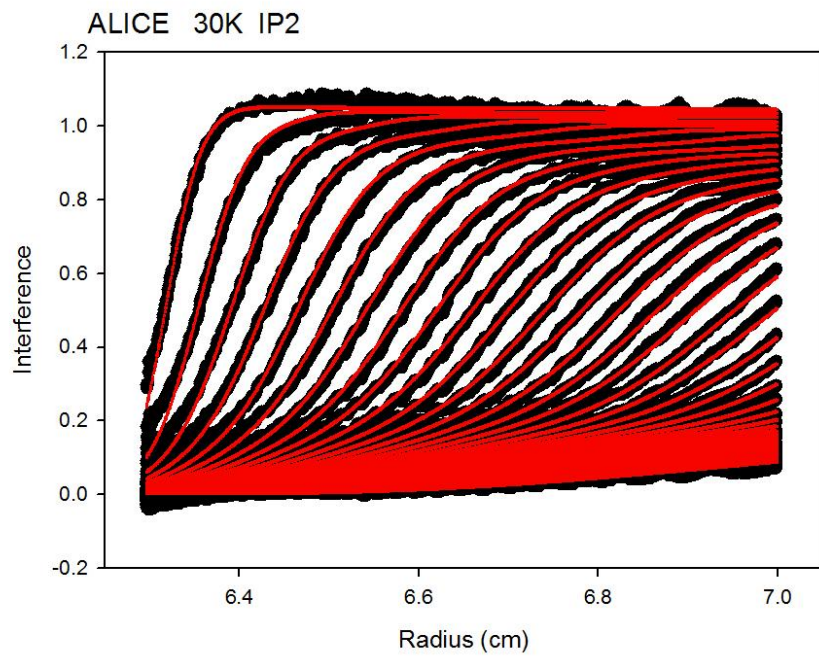


ALICE 30K IP1

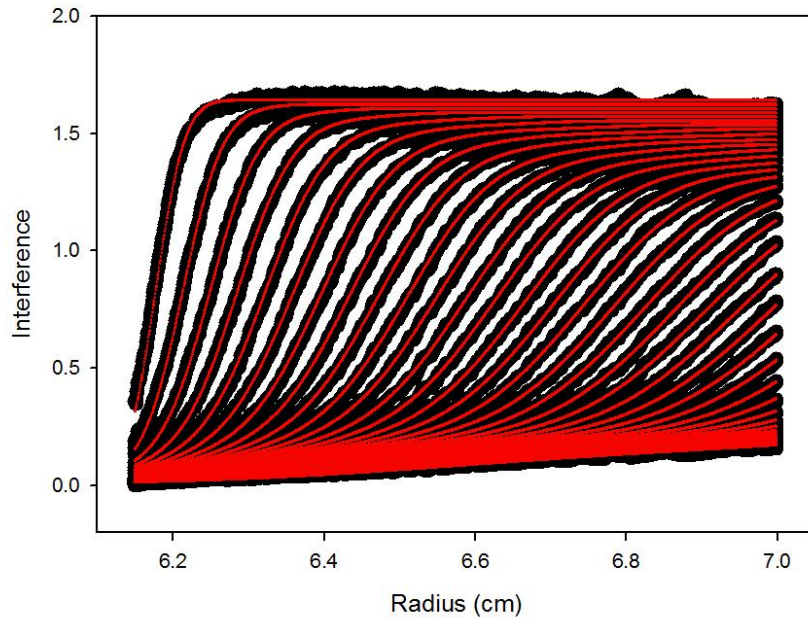


ALICE 30K IP1 c(s) distribution

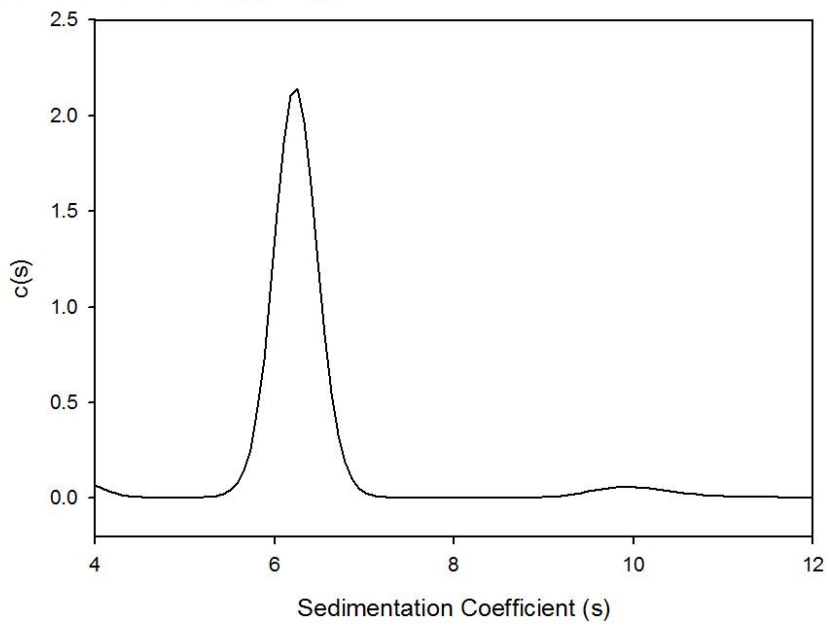




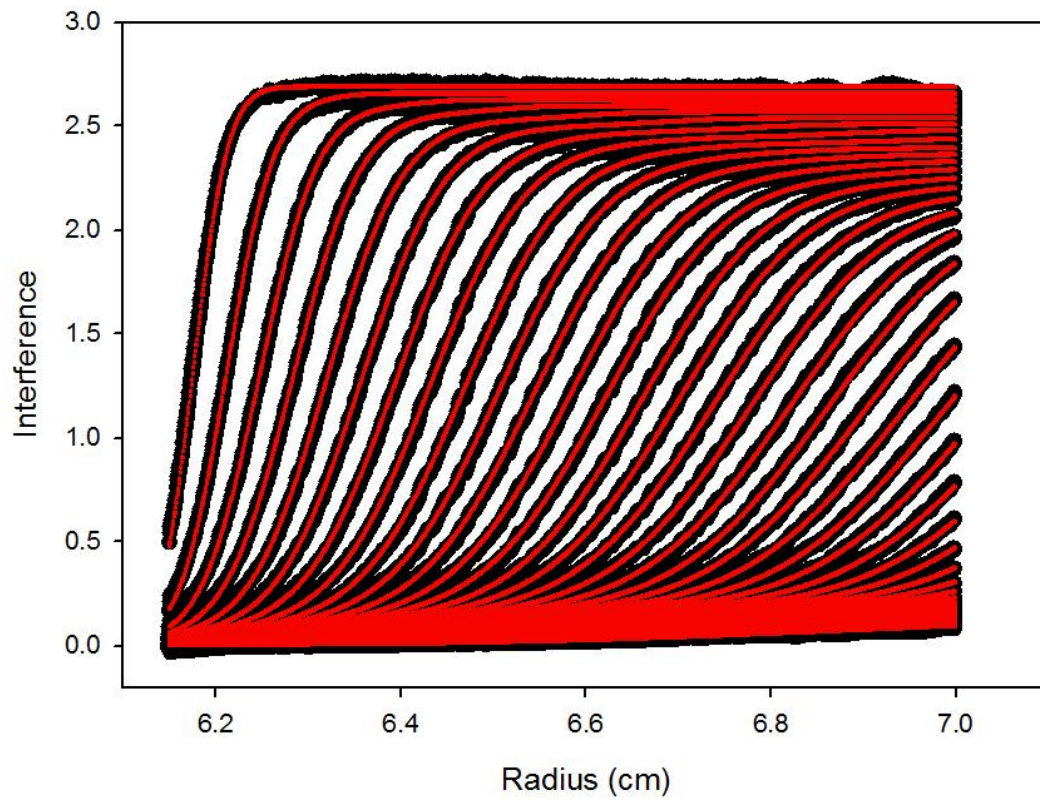
ALICE 30K IP3



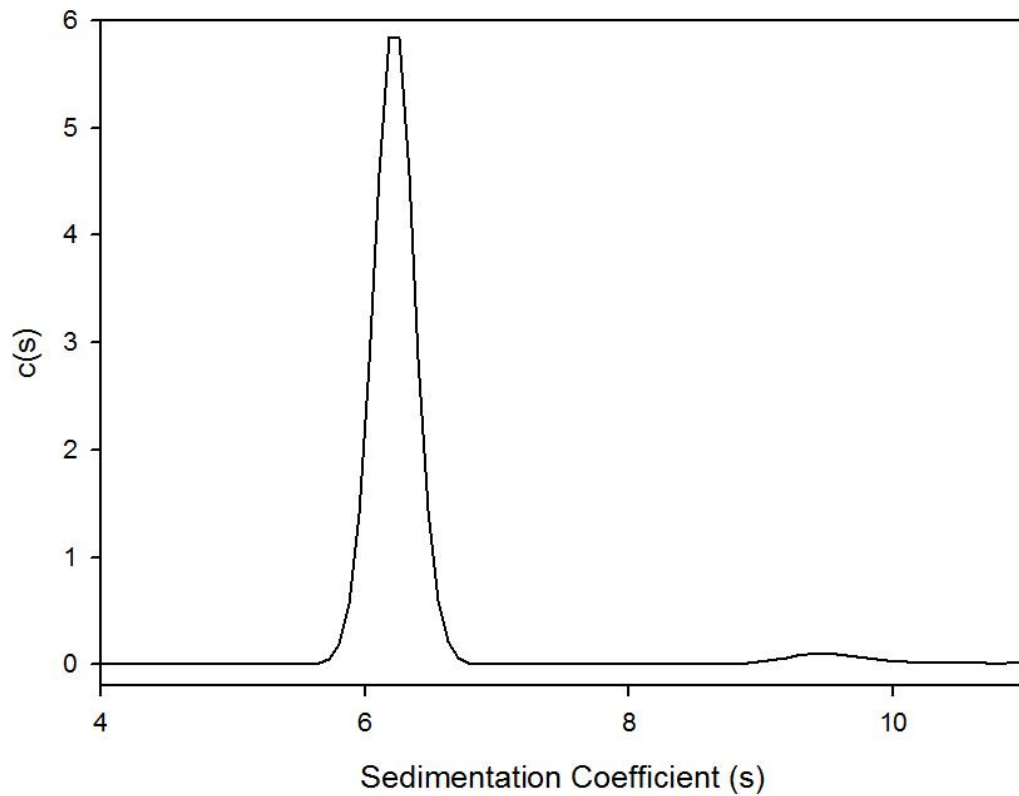
ALICE 30K IP3 c(s) distribution

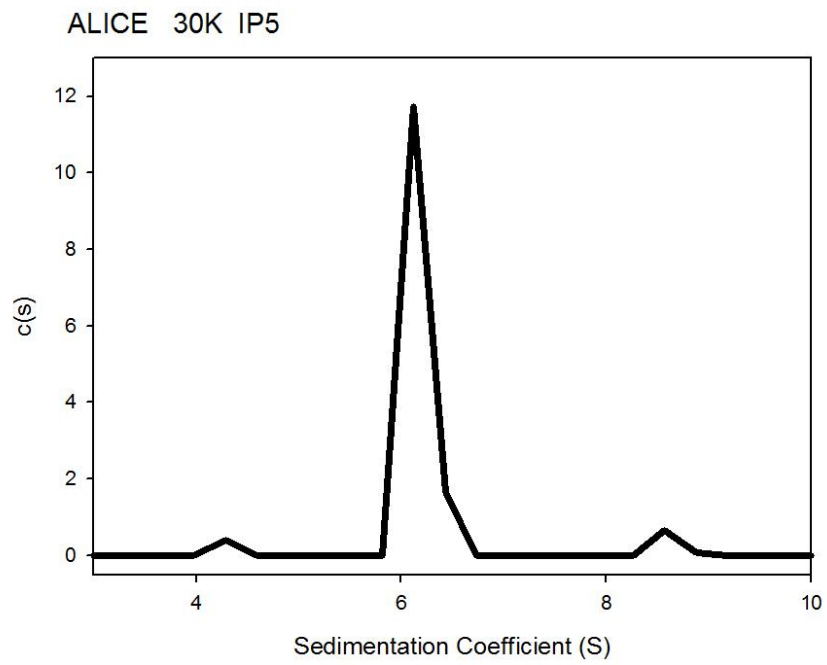
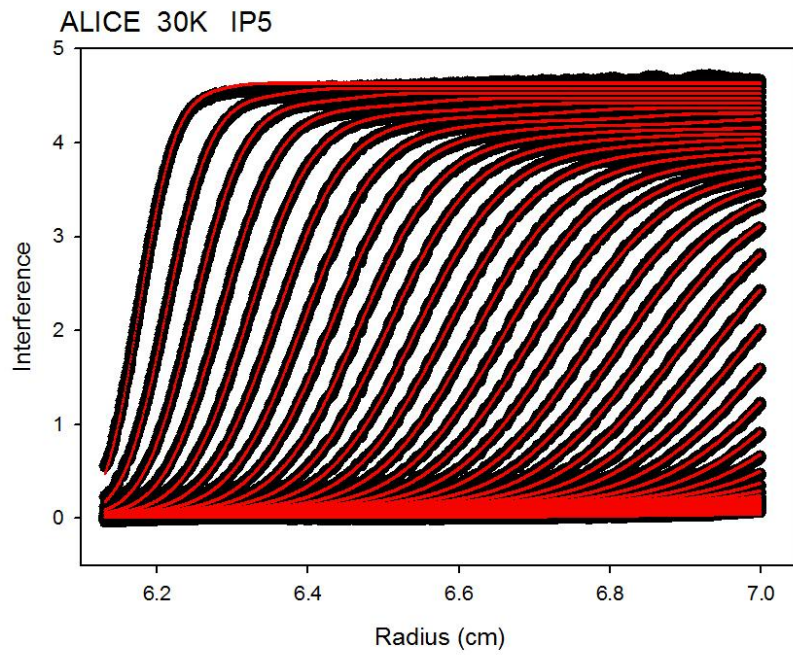


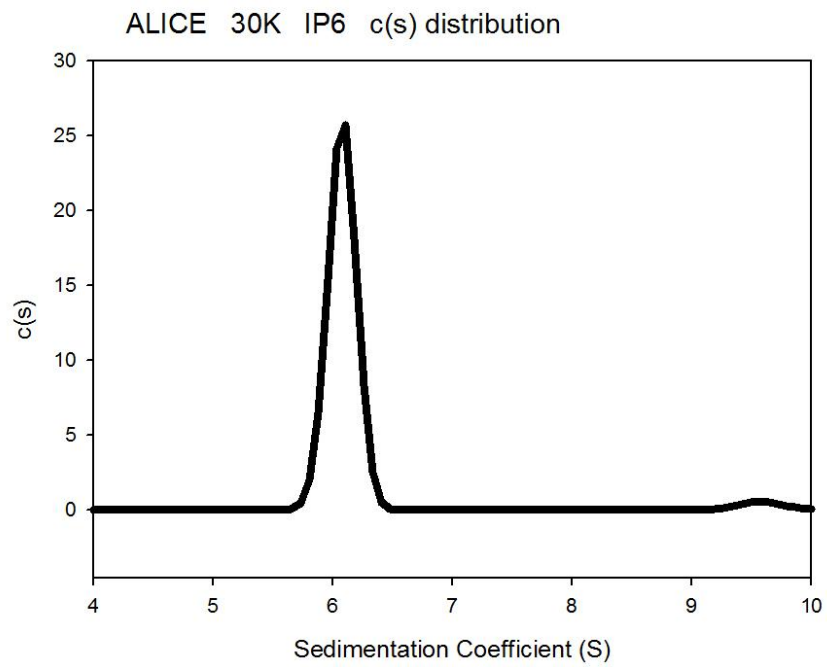
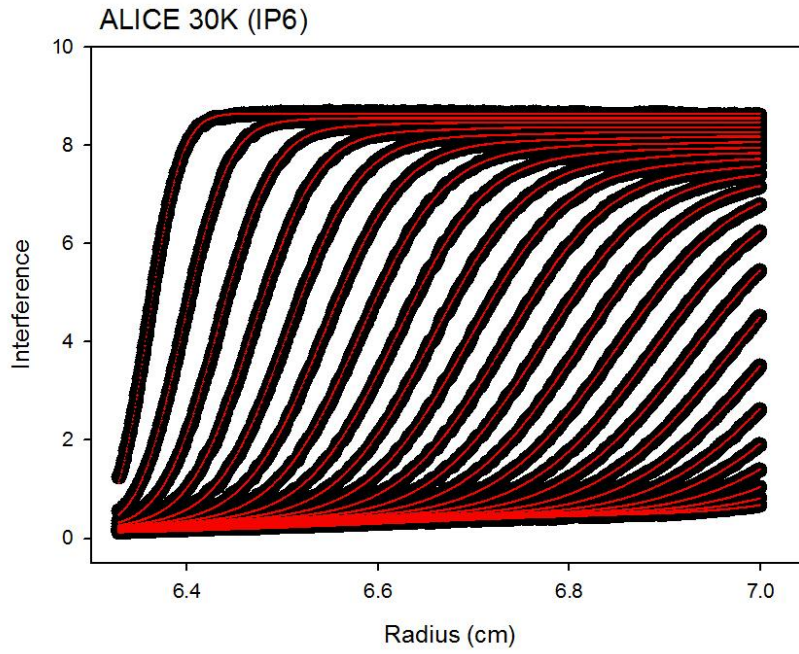
ALICE 30K IP4



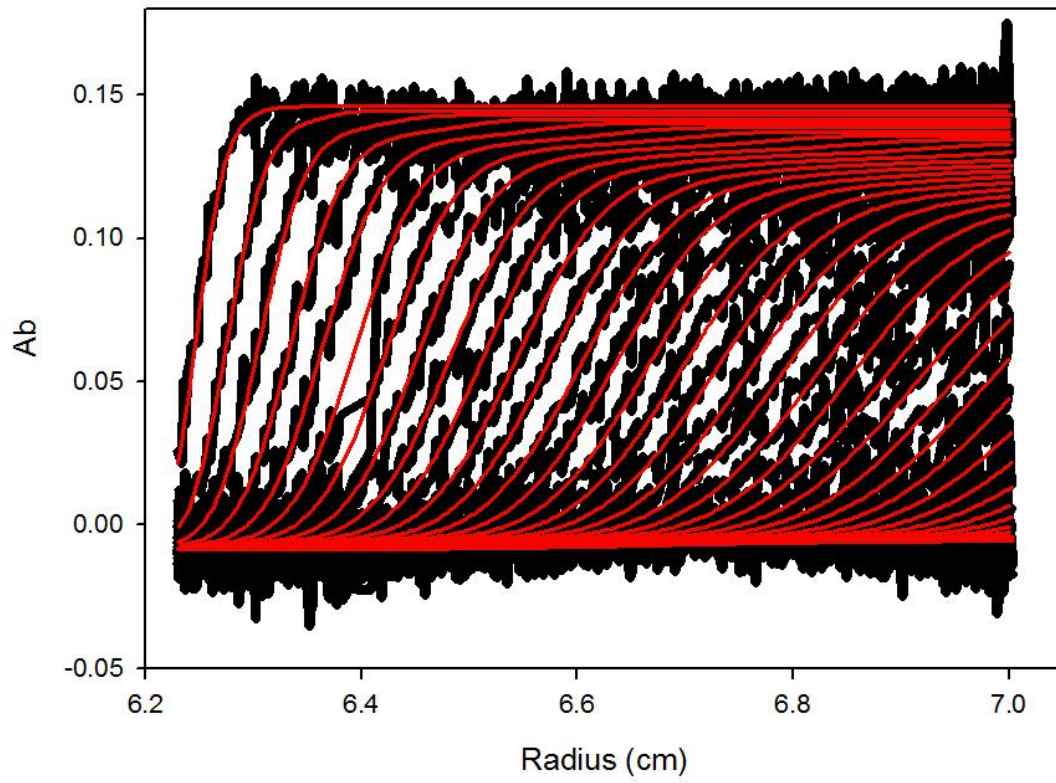
ALICE 30K IP4 c(s) distribution



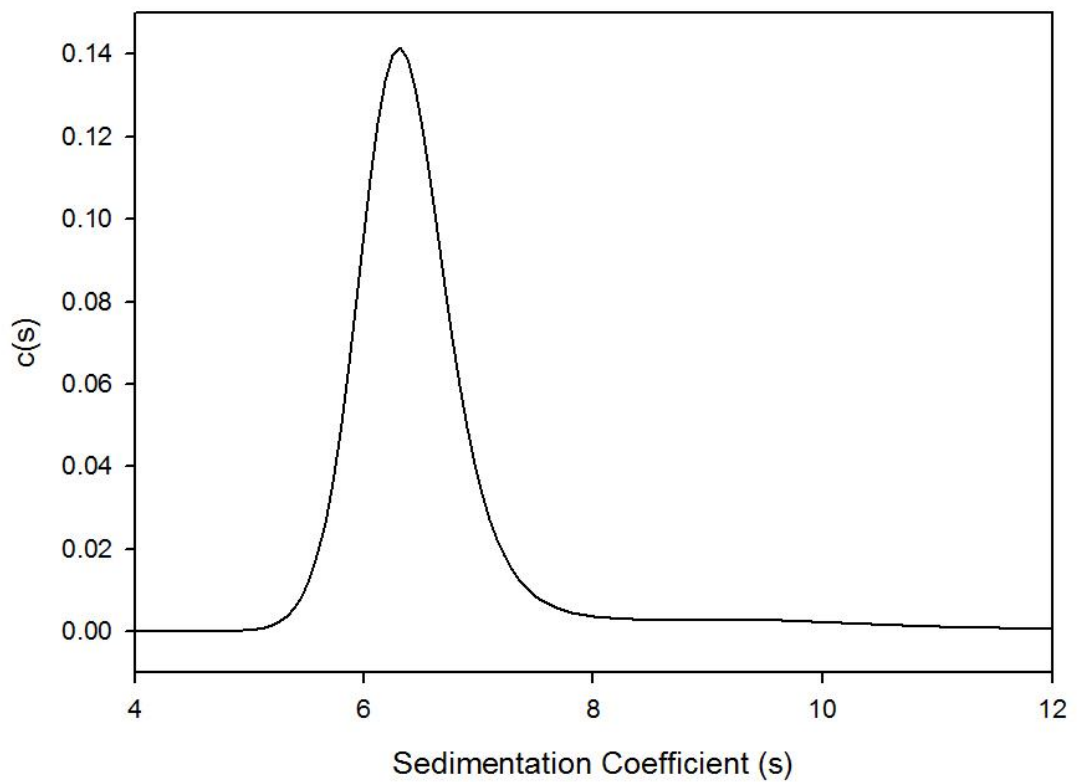




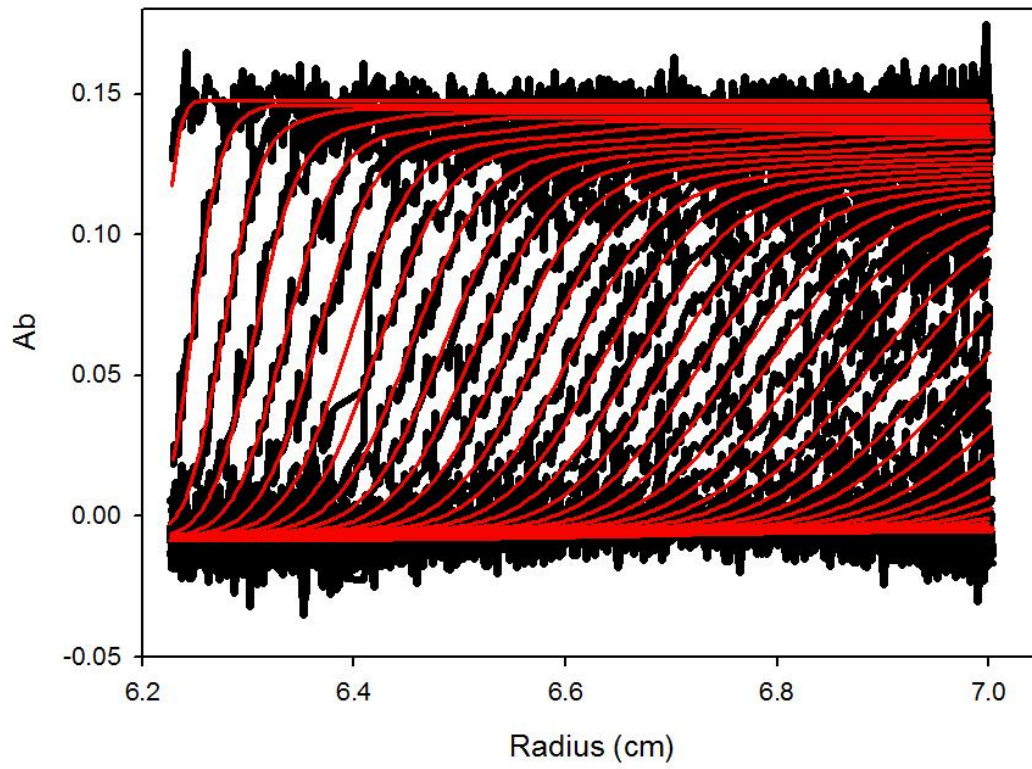
ALICE 40K AB1



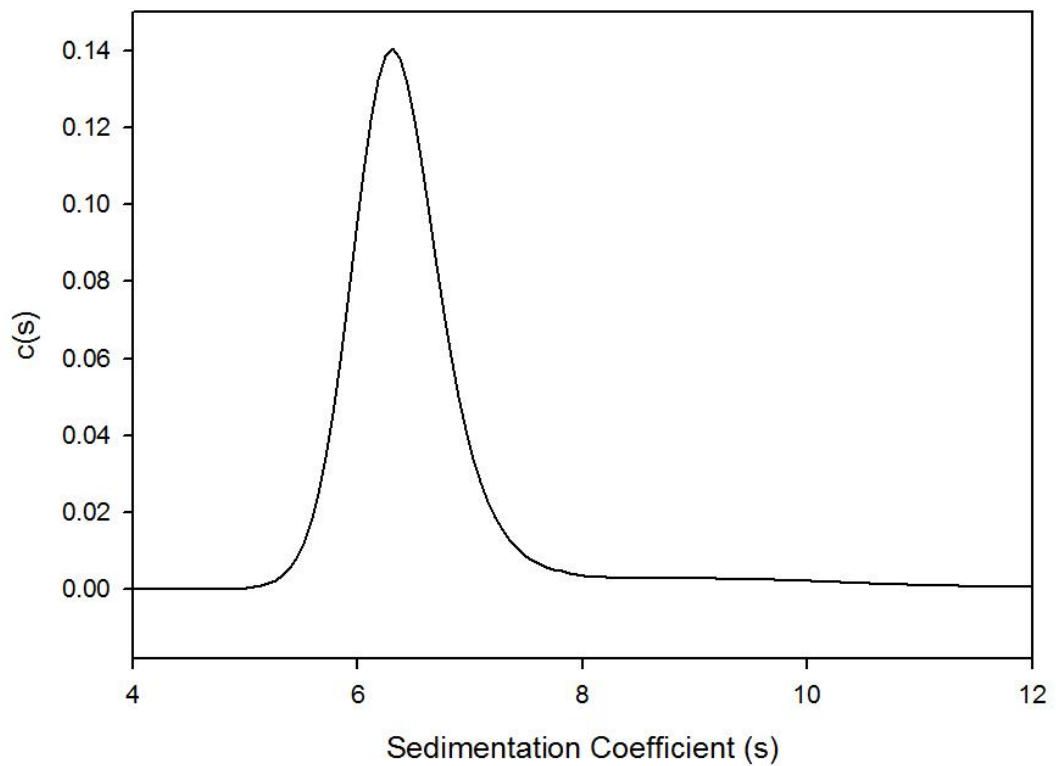
ALICE 40K AB1 c(s) distribution



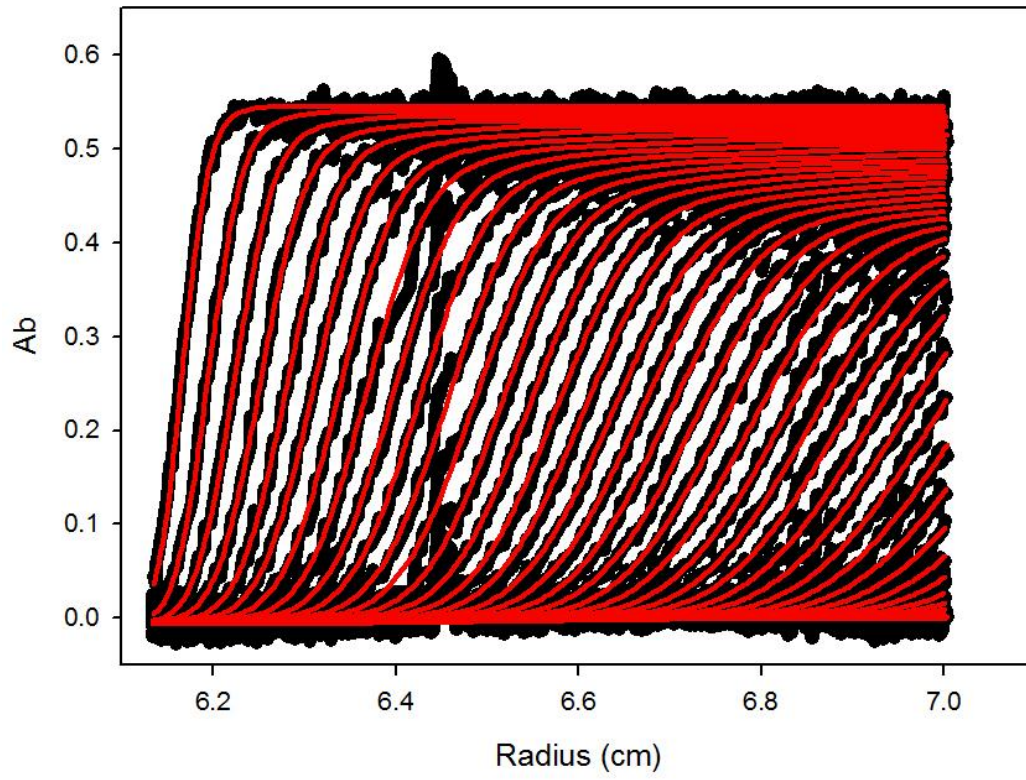
ALICE 40K AB2



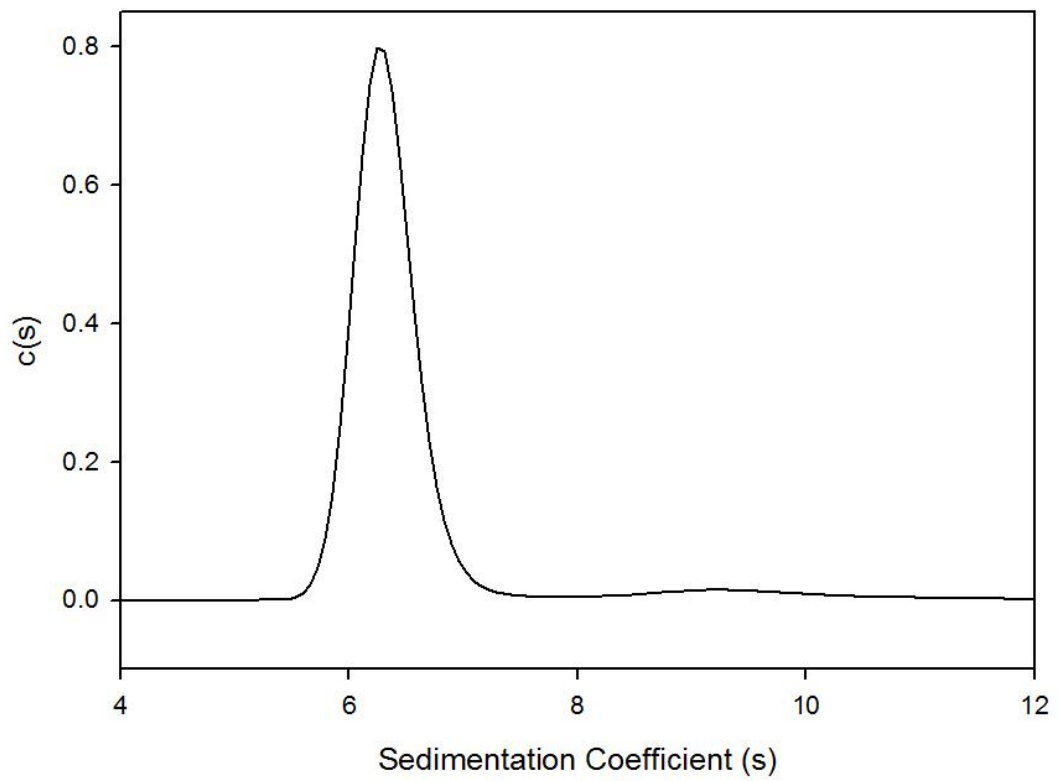
ALICE 40K AB2 c(s) distribution



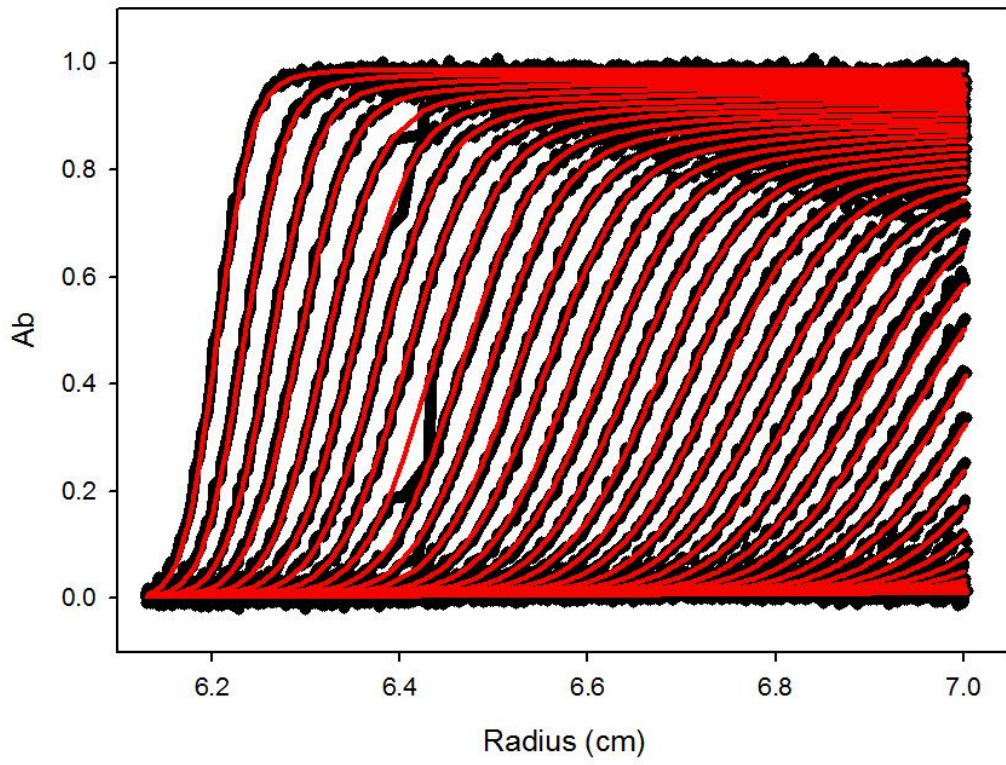
ALICE 40K AB3



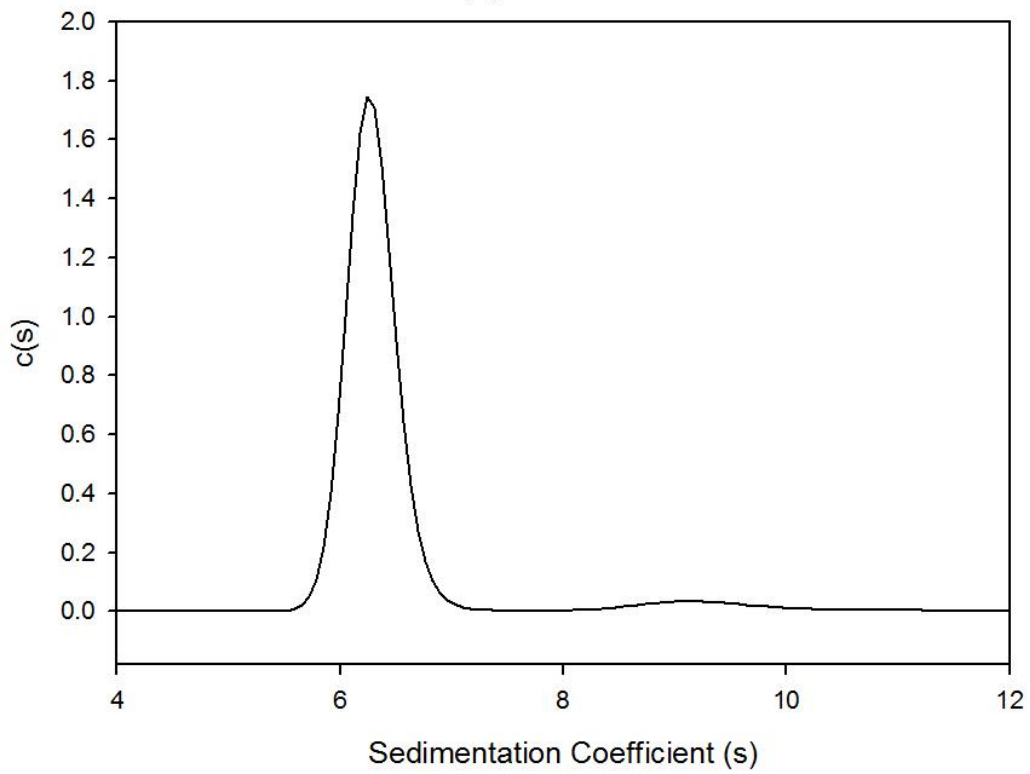
ALICE 40K AB3 c(s) distribution



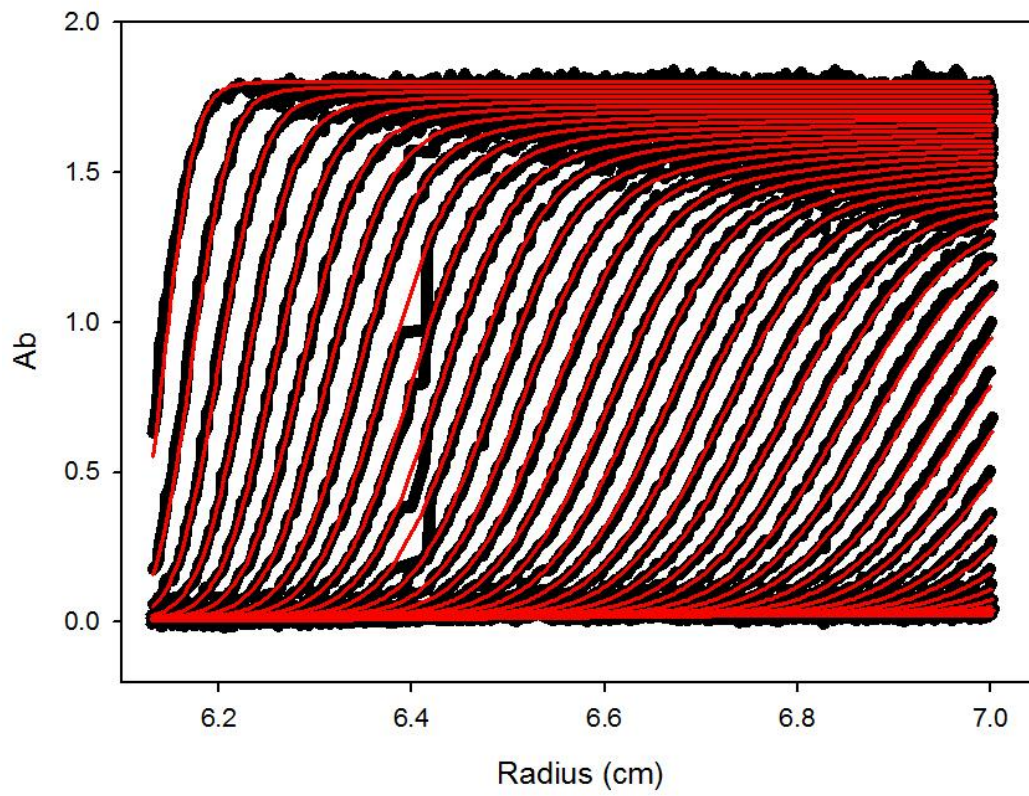
ALICE 40K AB4



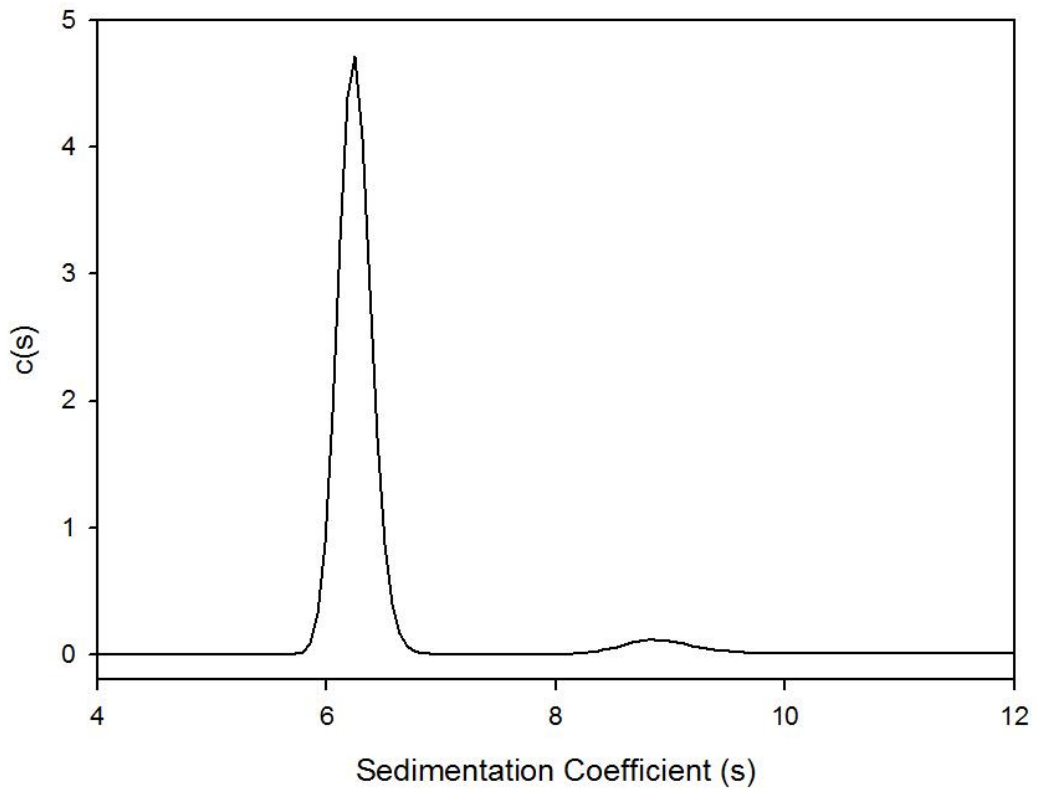
ALICE 40K AB4 c(s) distribution



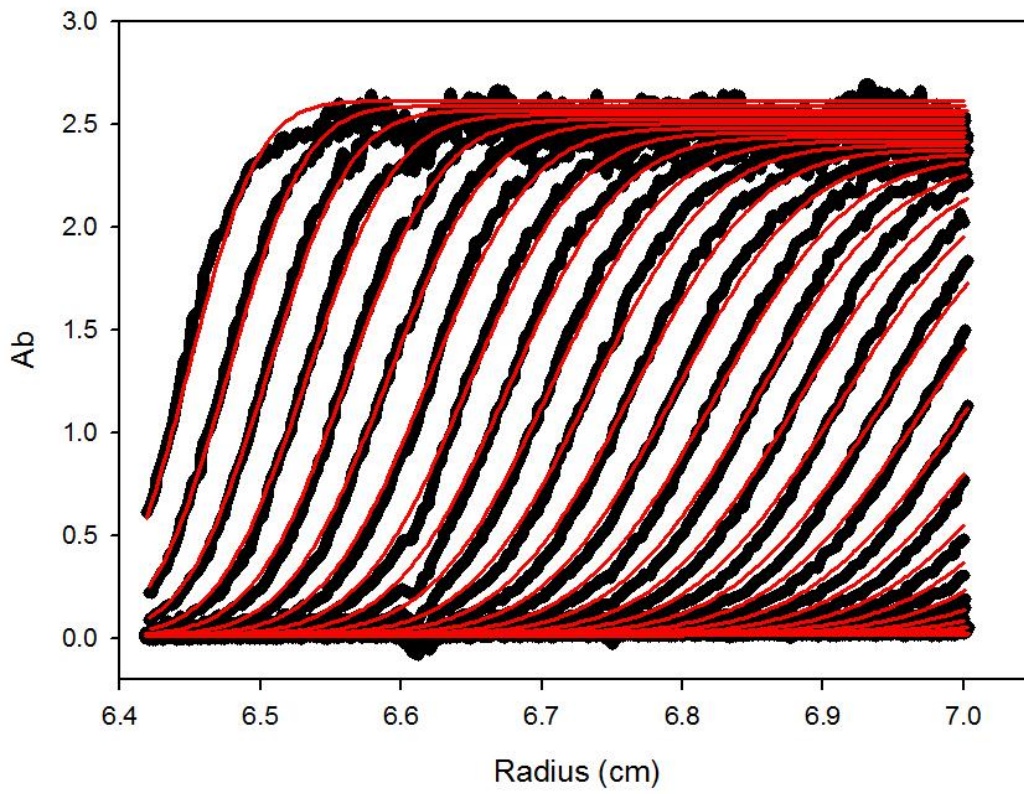
ALICE 40K AB5



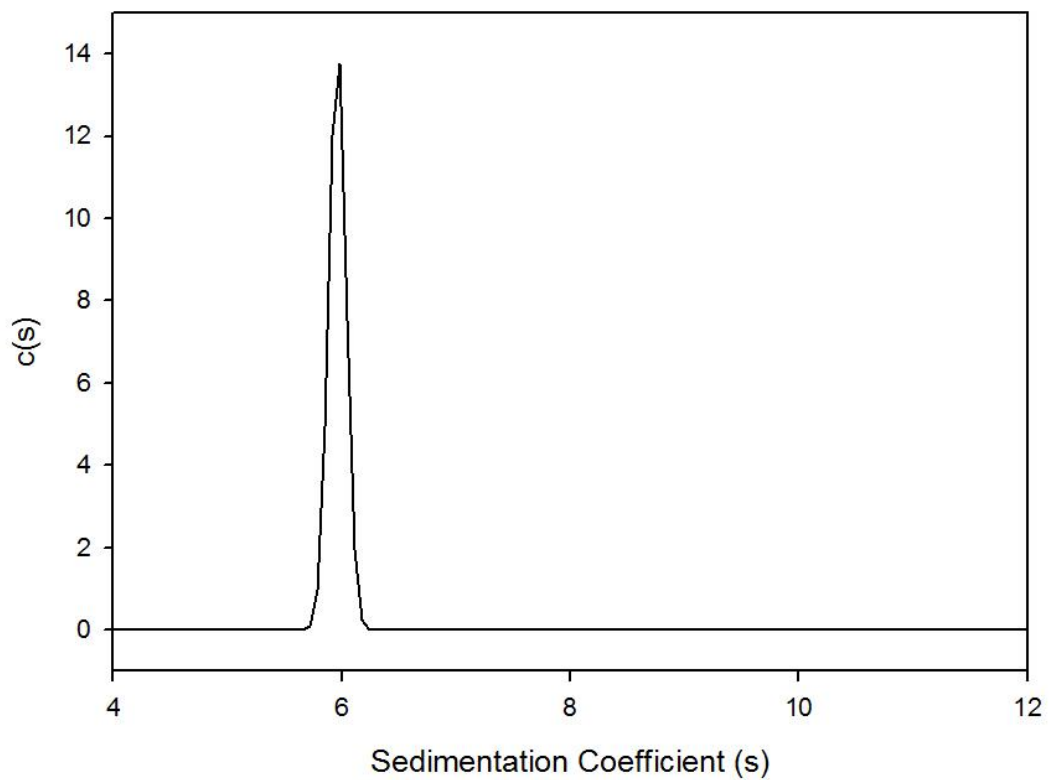
ALICE 40K AB5 c(s) distribution



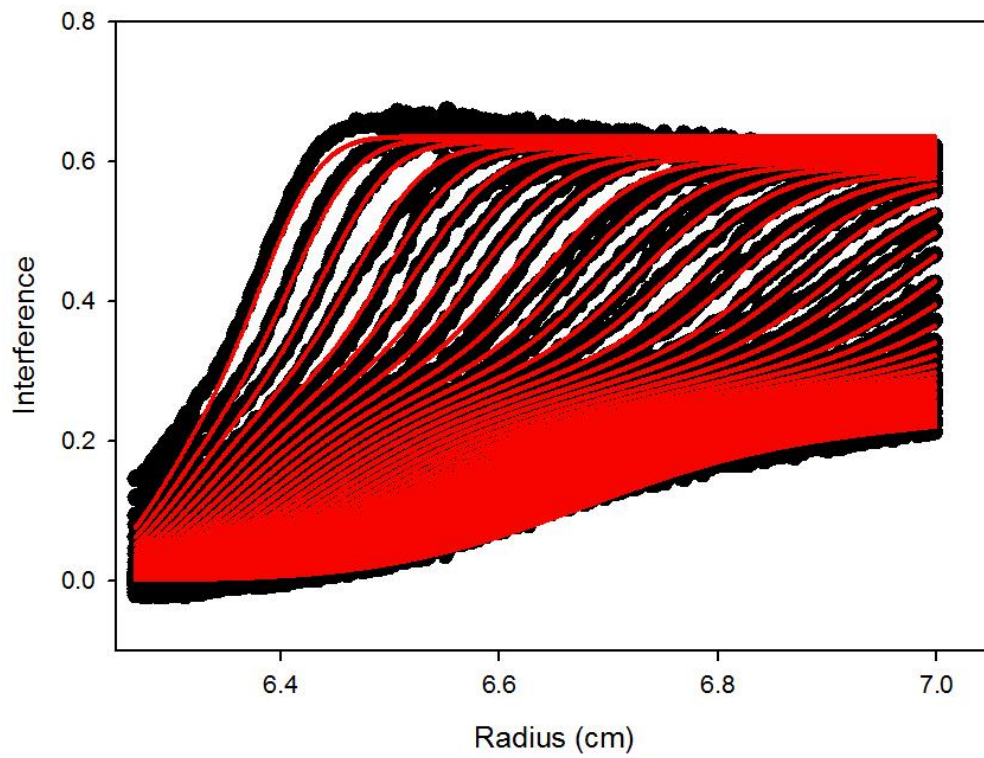
ALICE 40K AB6



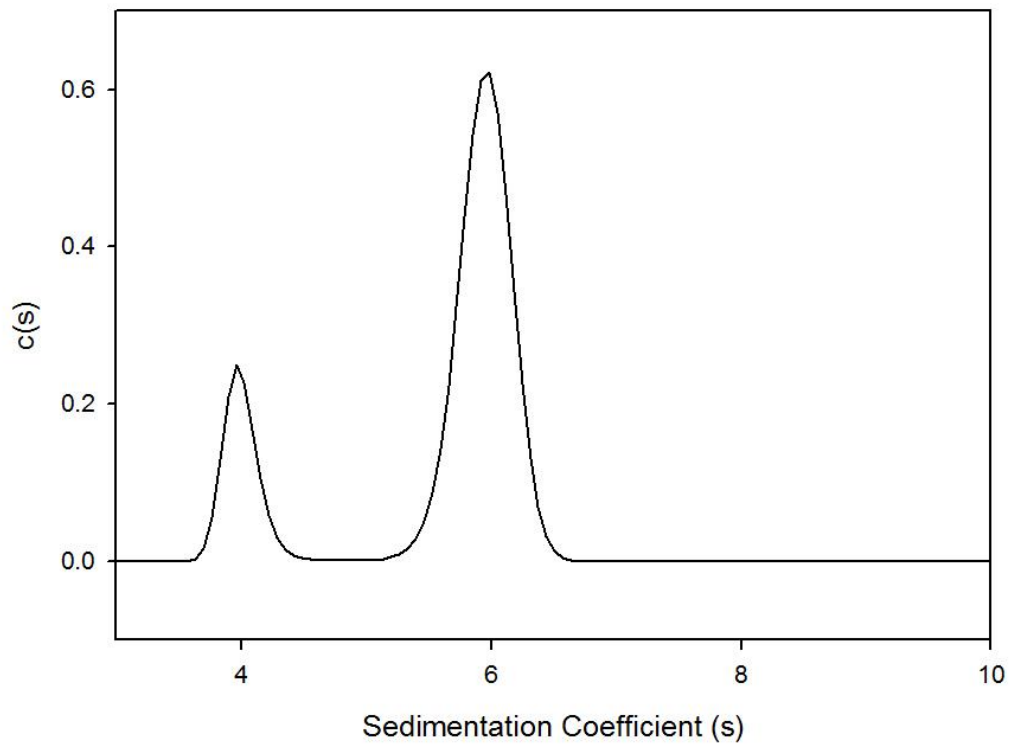
ALICE 40K AB6 c(s) distribution



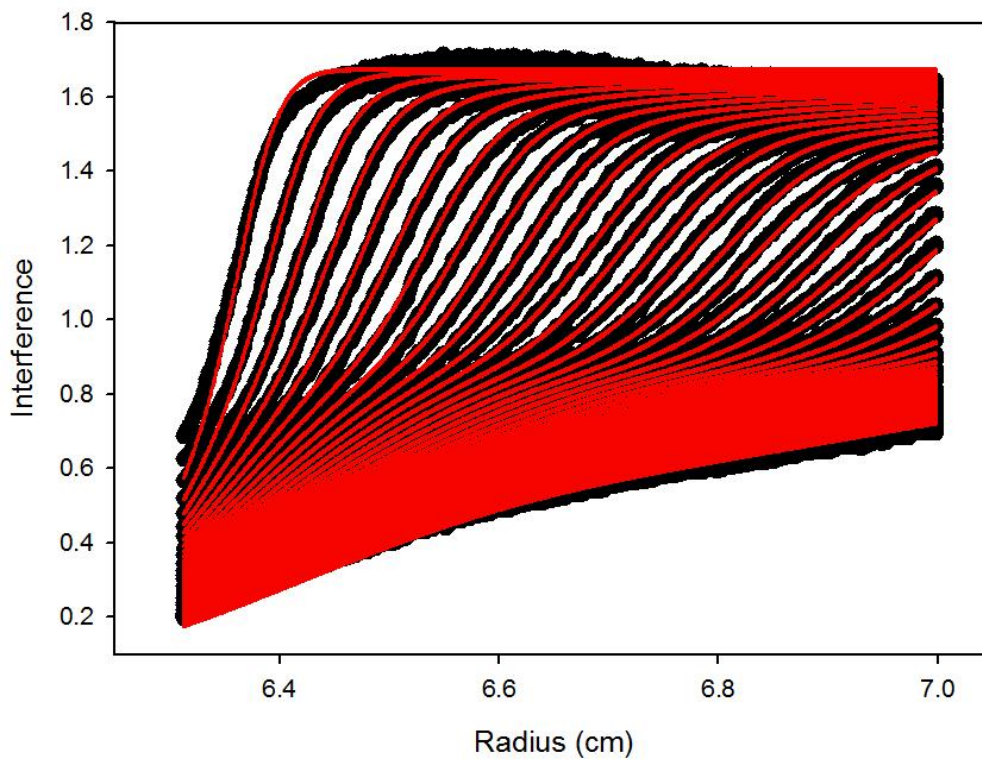
ALICE 40K IP1



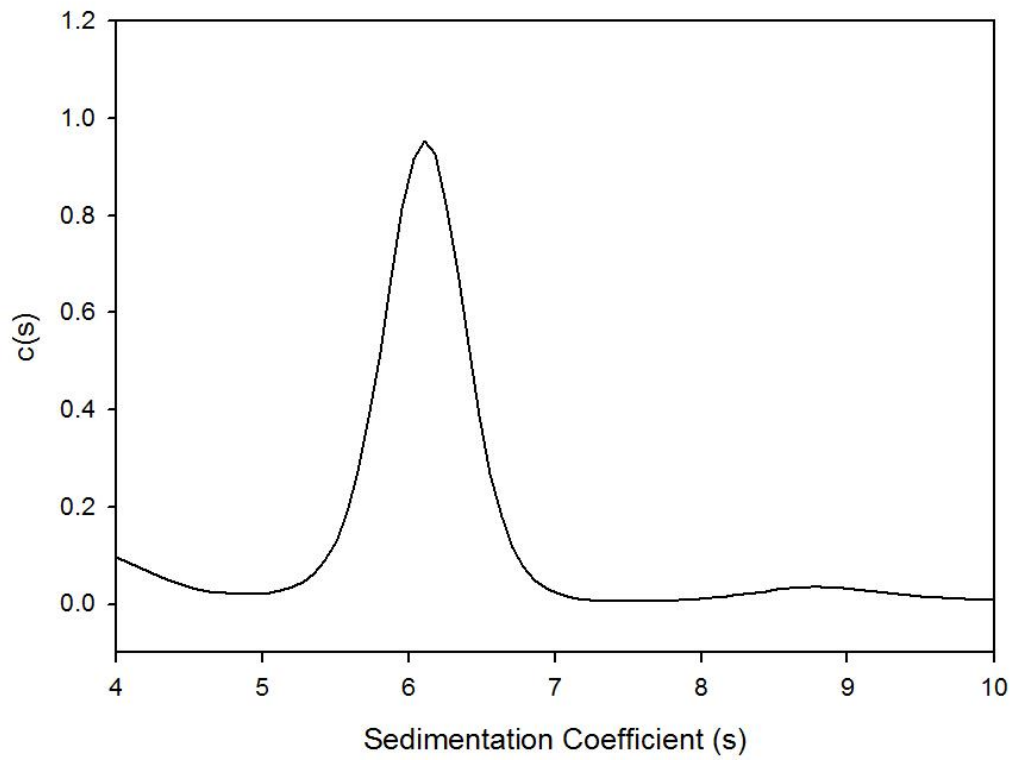
ALICE 40K IP1 c(s) distribution



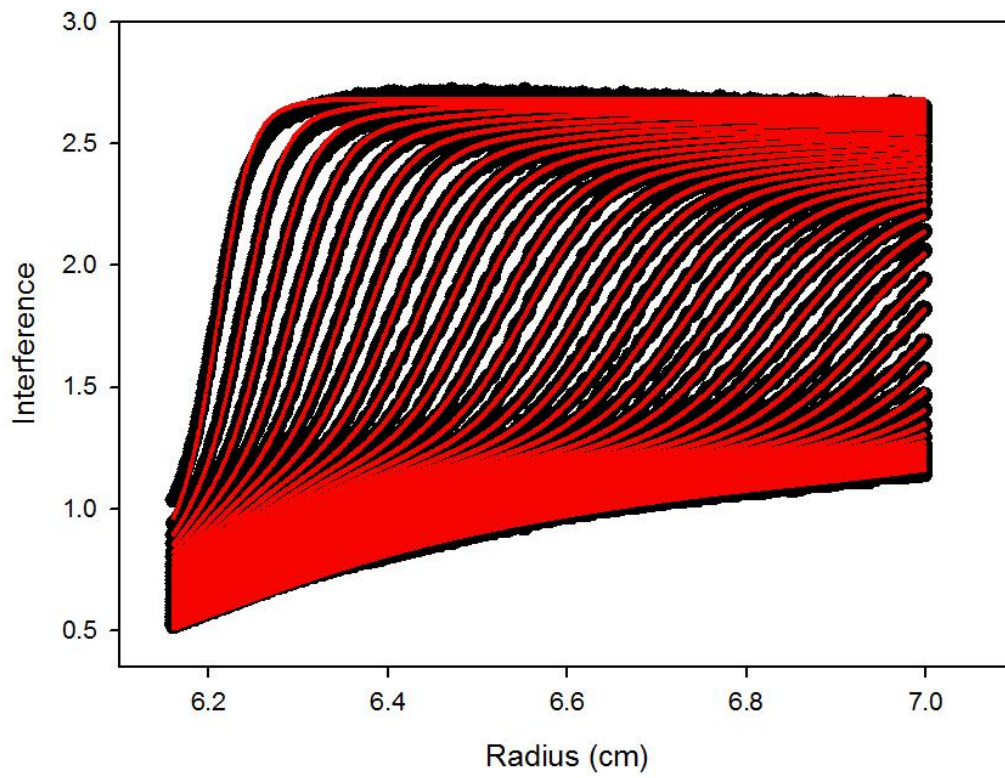
ALICE 40K IP2



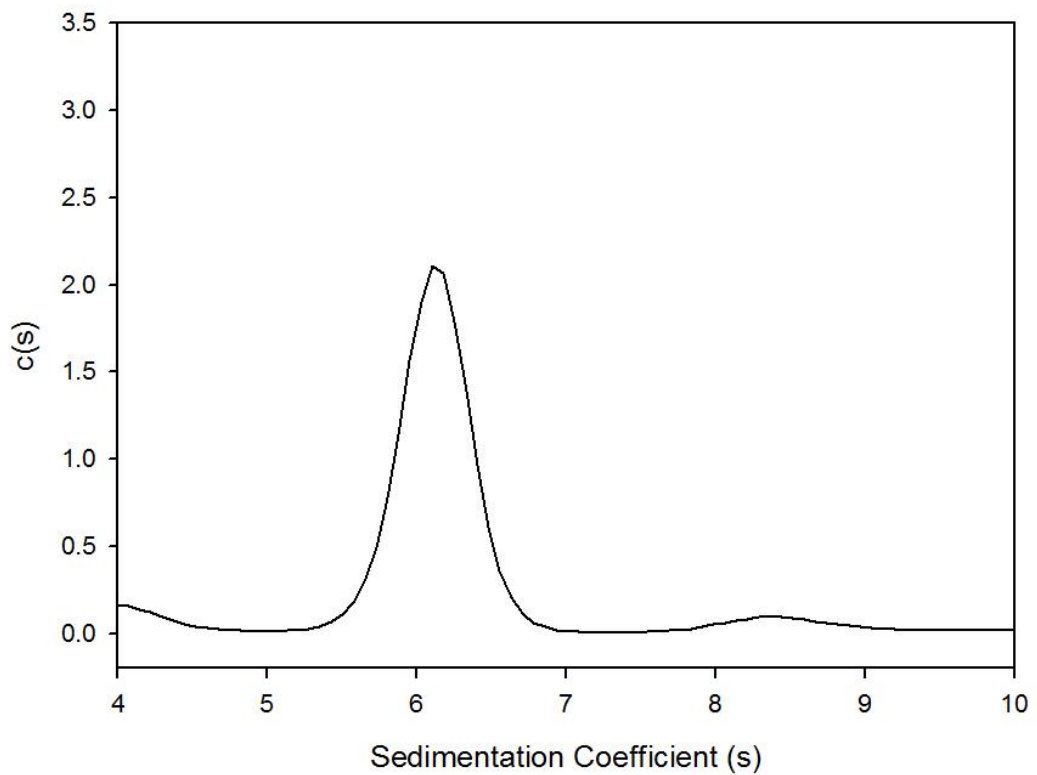
ALICE 40K IP2 $c(s)$ distribution



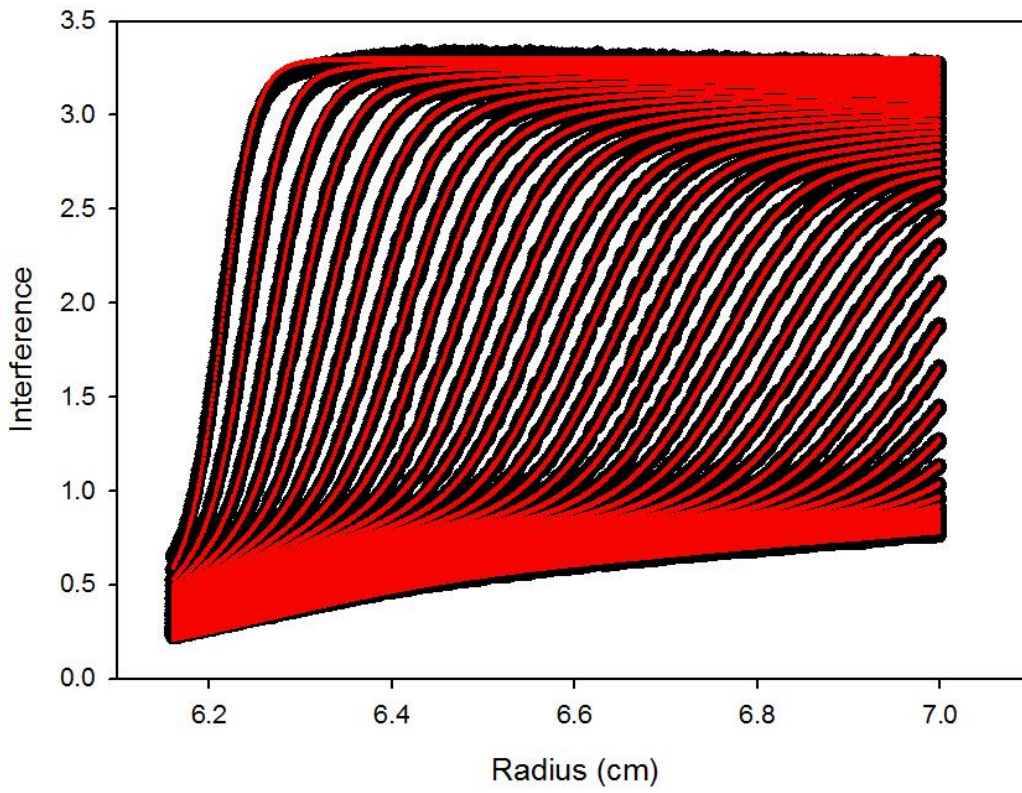
ALICE 40K IP3



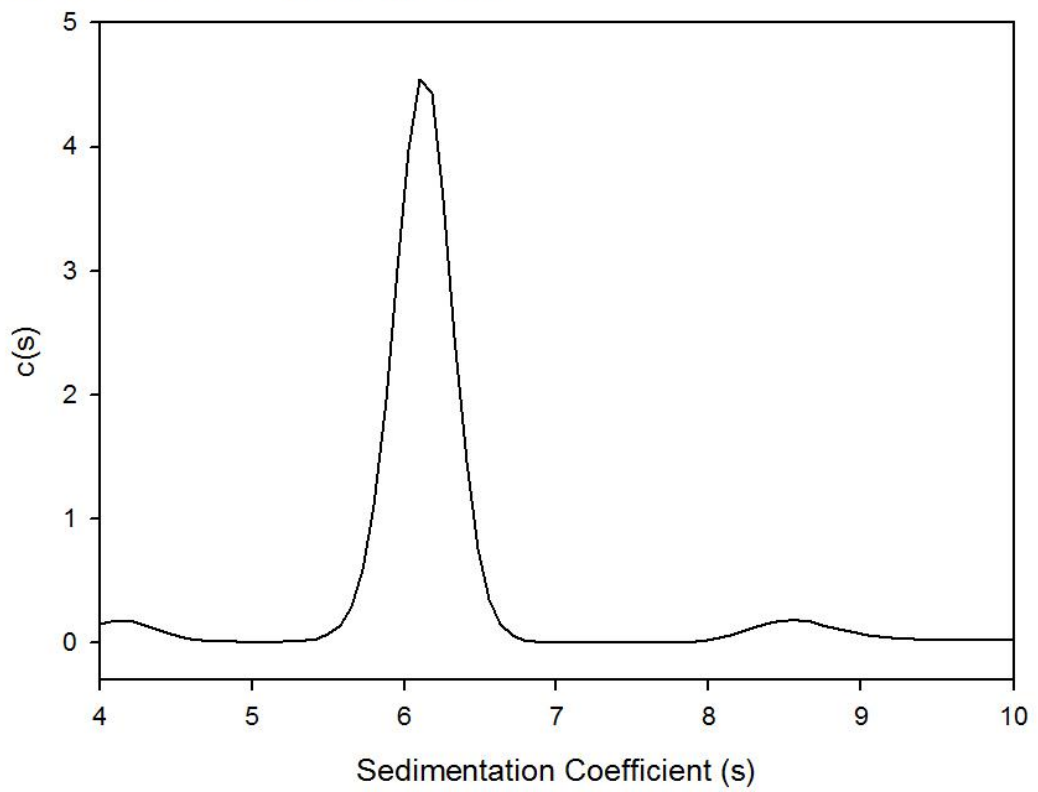
ALICE 40K IP3 c(s) distribution



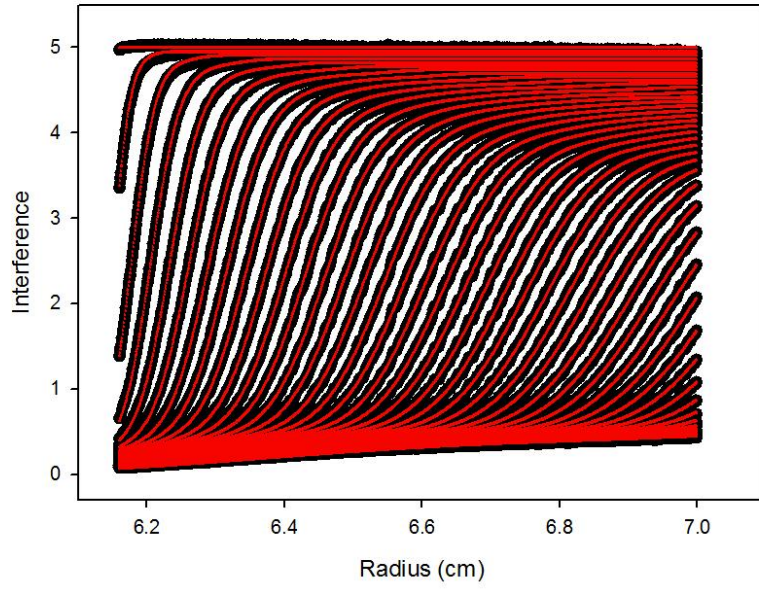
ALICE 40K IP4



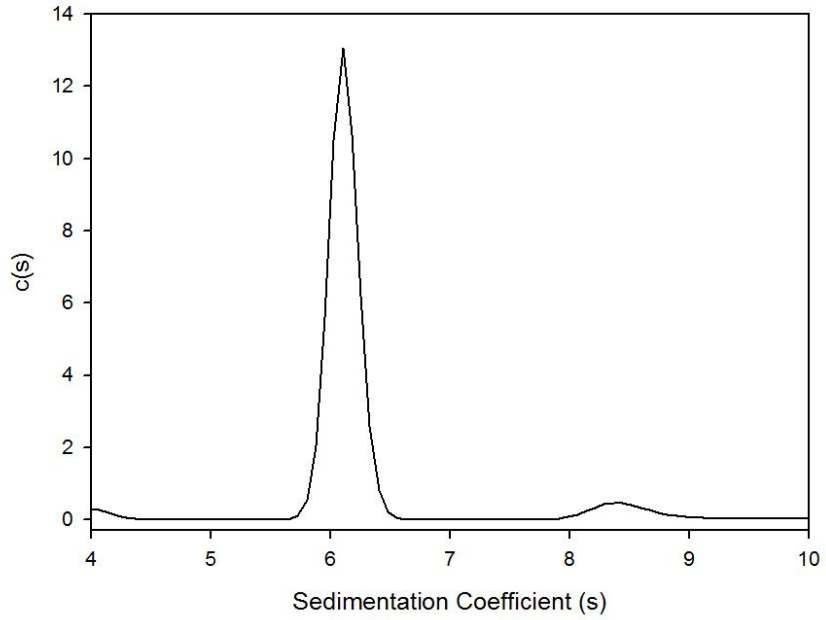
ALICE 40K IP4 c(s) distribution

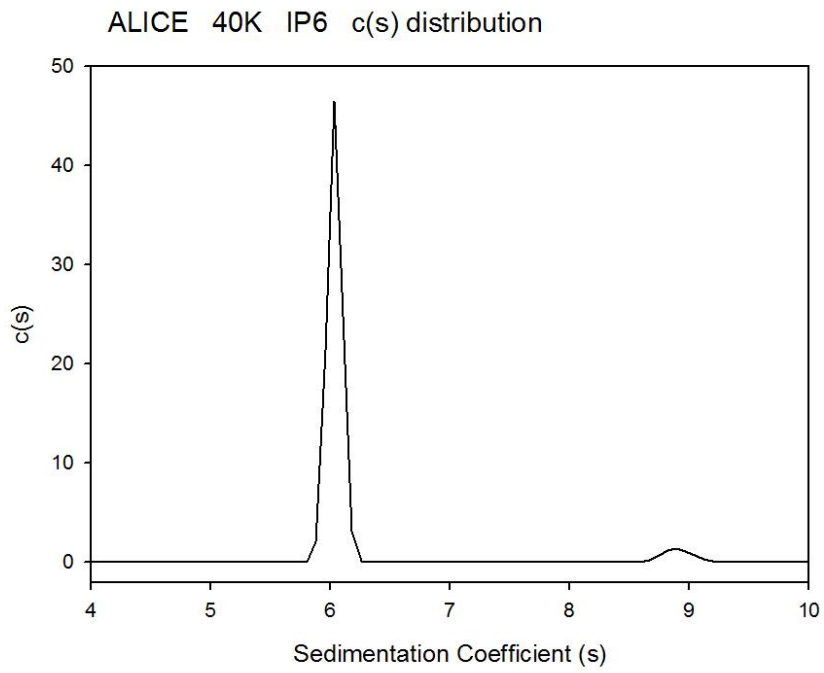
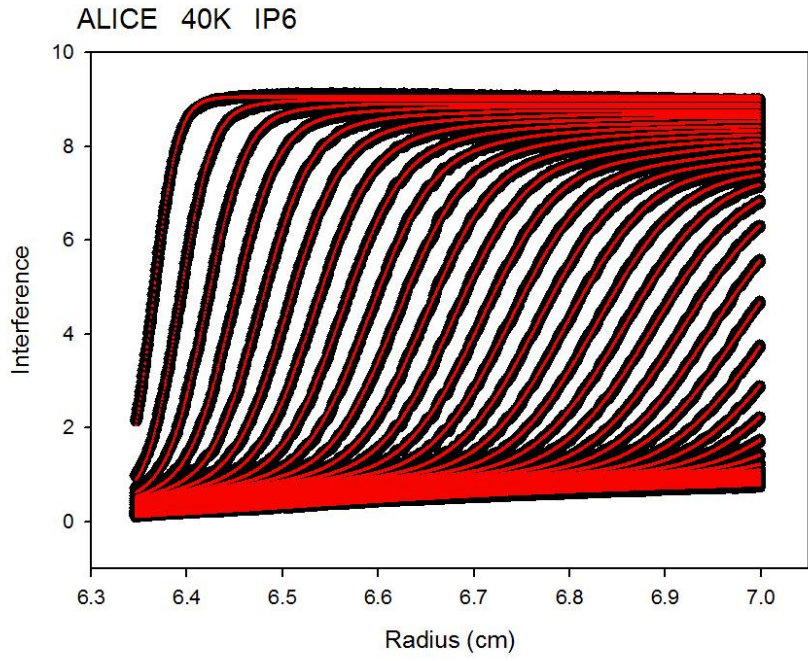


ALICE 40K IP5

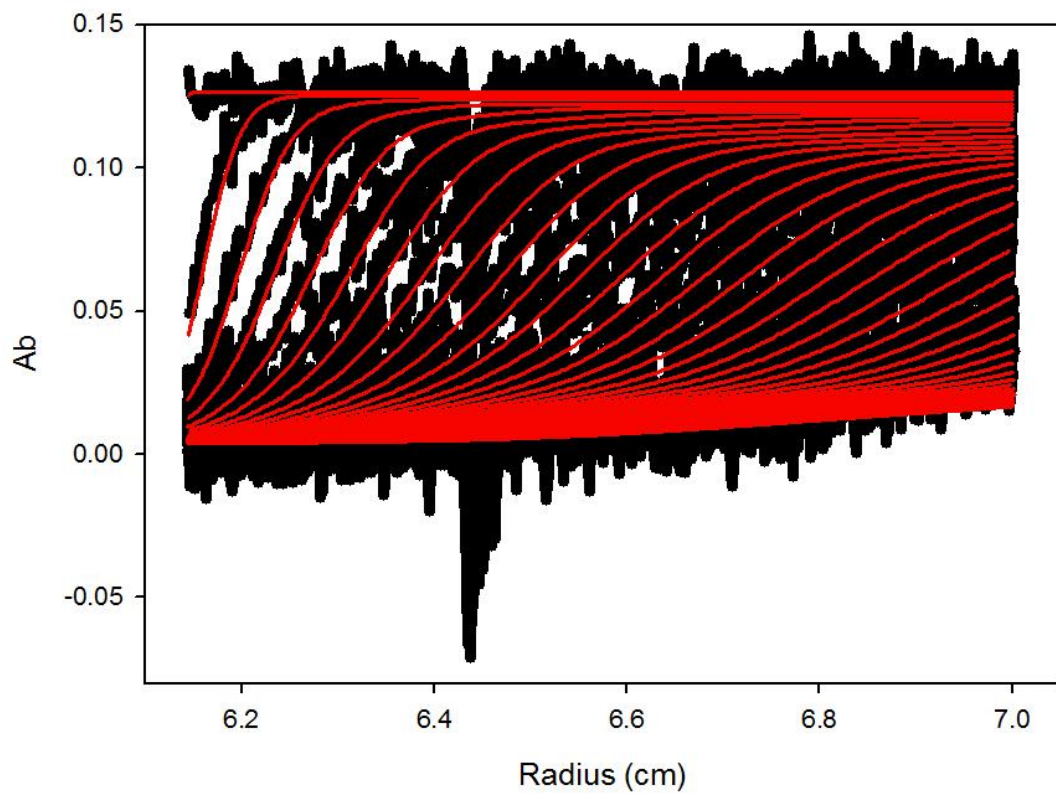


ALICE 40K IP5 c(s) distribution

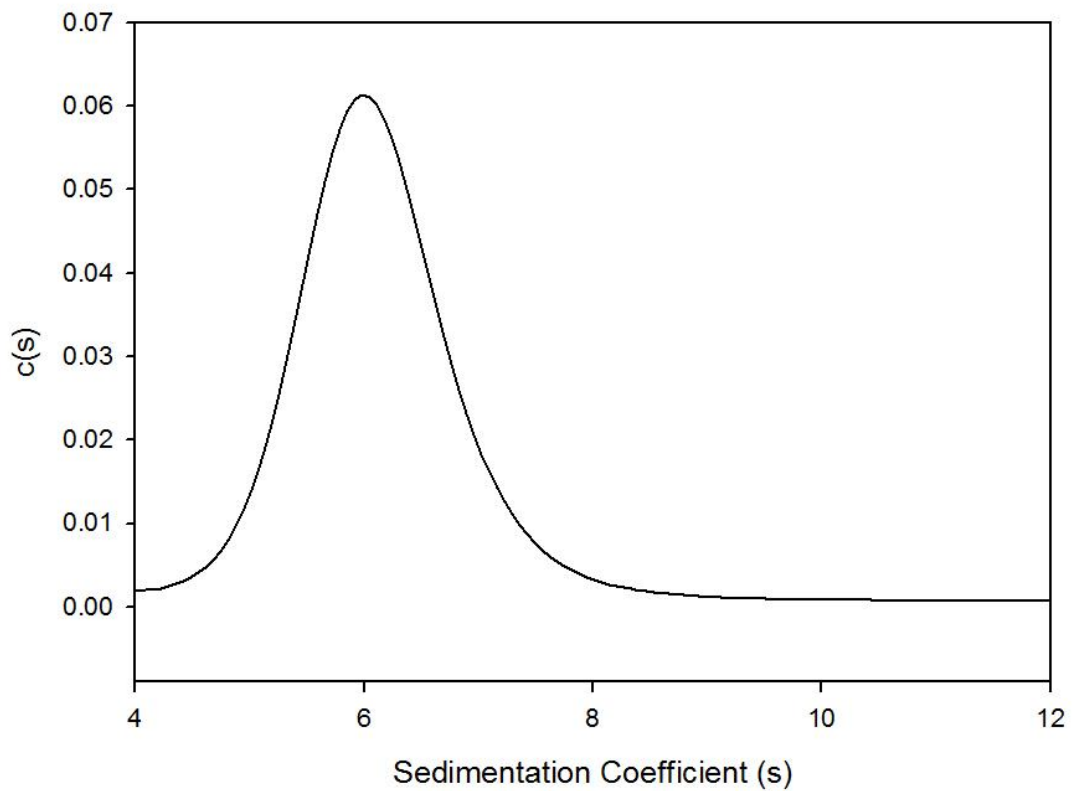




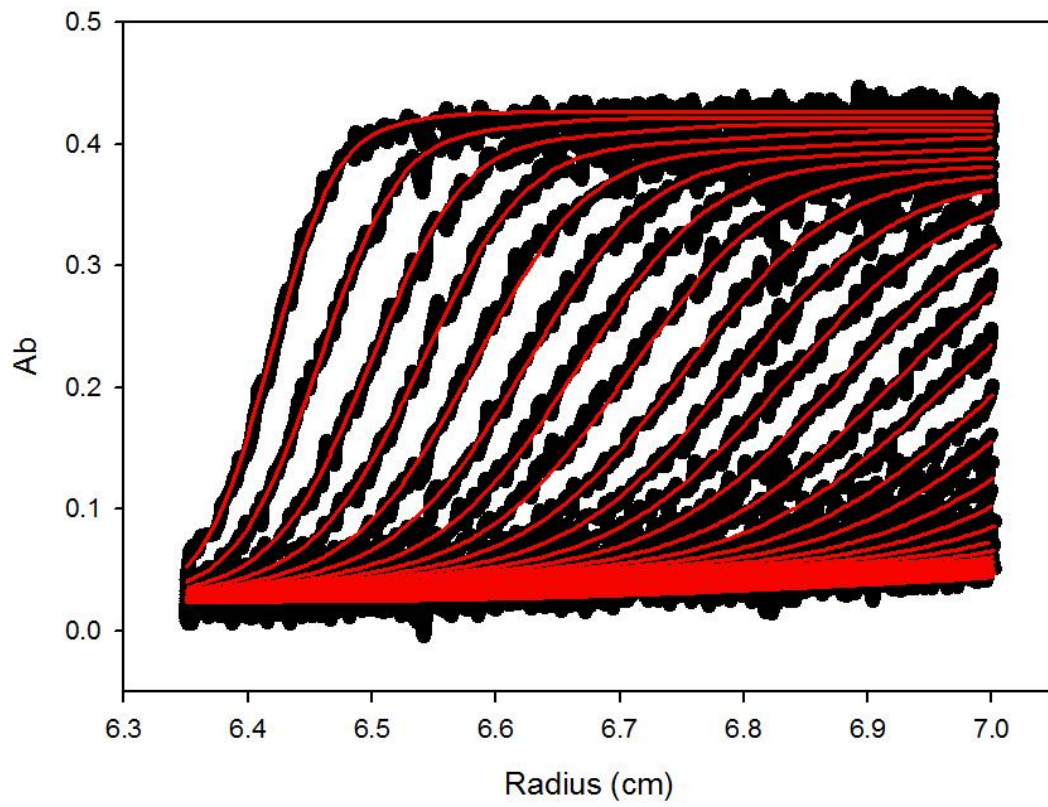
SB308 30K AB1.



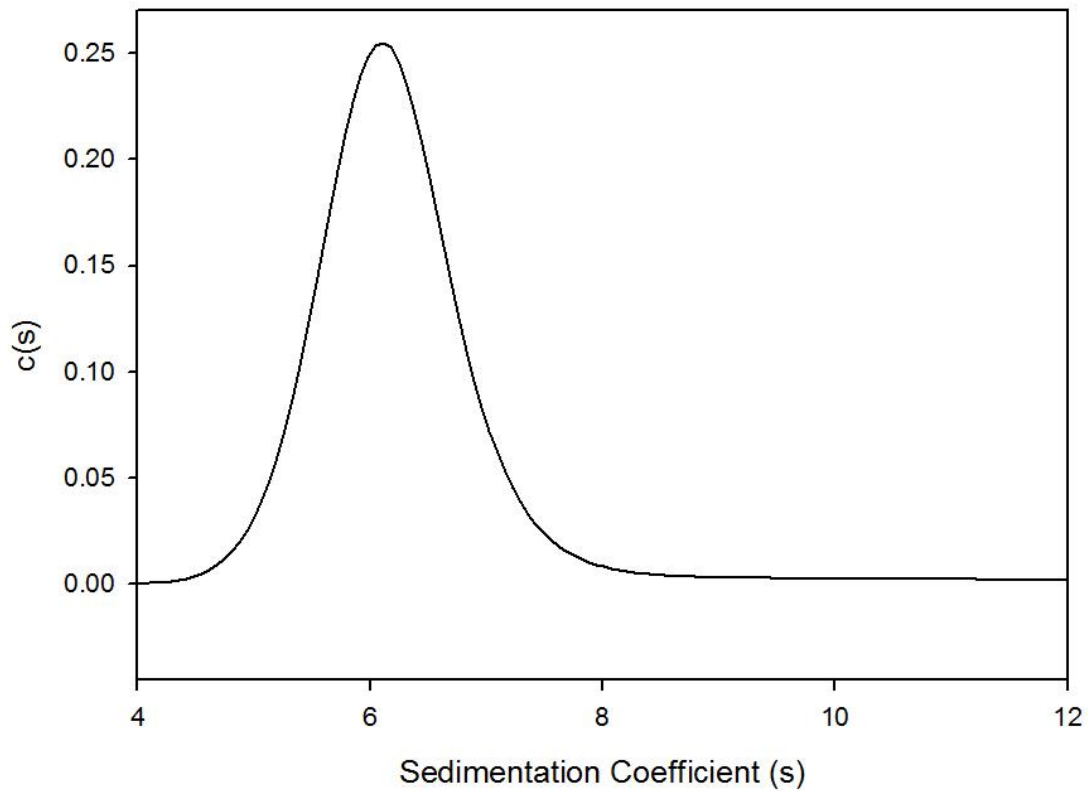
SB308 30K AB1. c(s) distribution



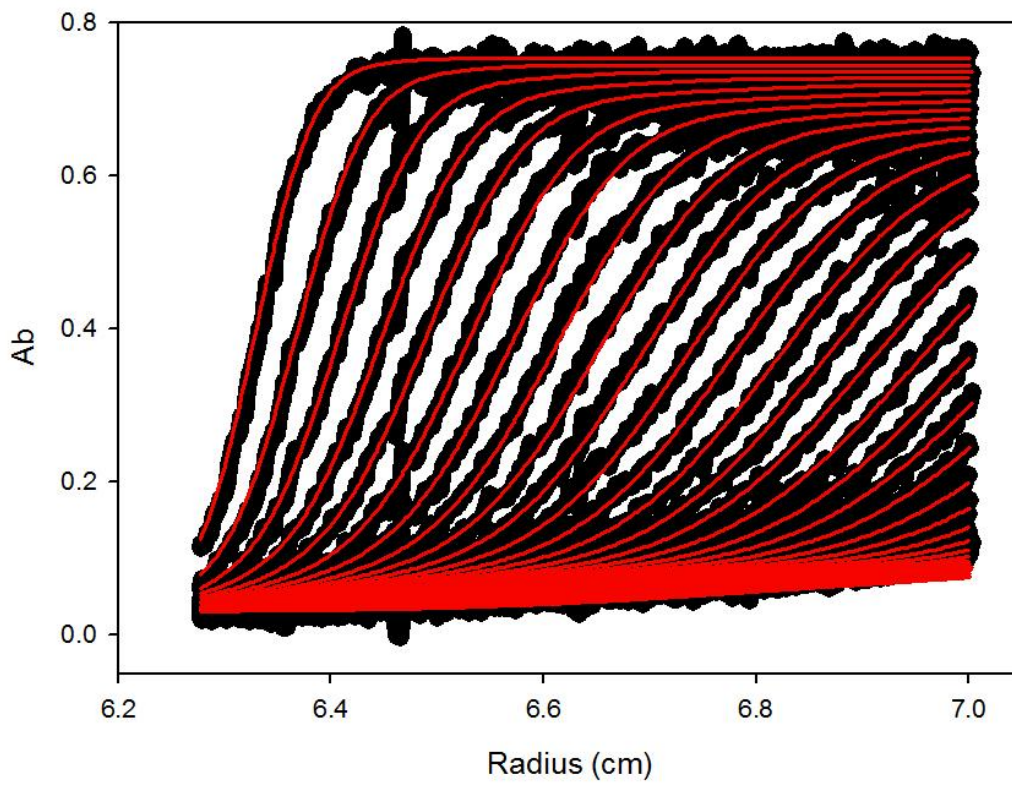
SB308 30K AB4.



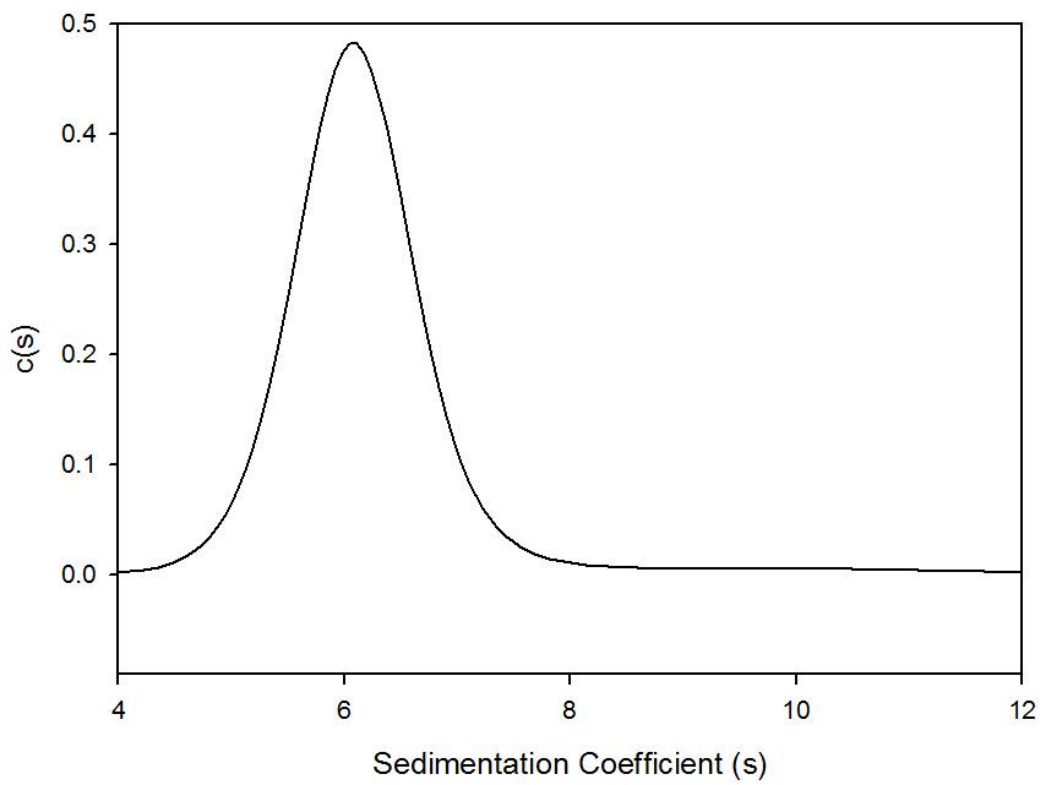
SB308 30K AB4. $c(s)$ distribution



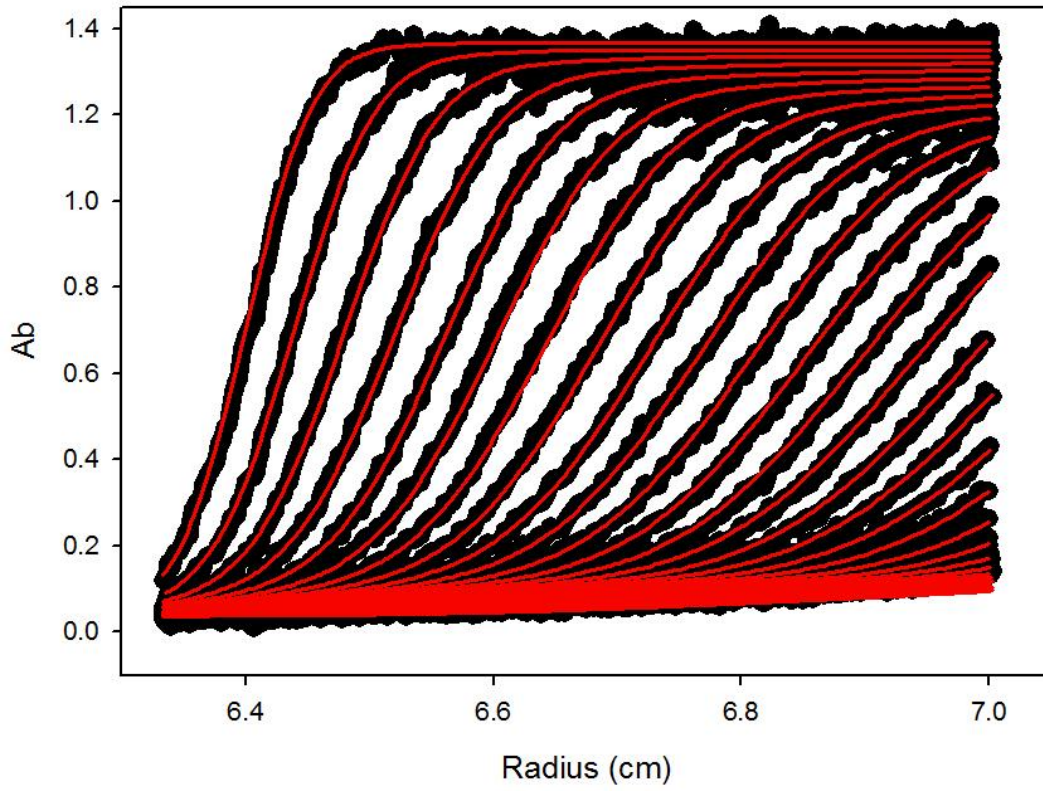
SB308 30K AB5.



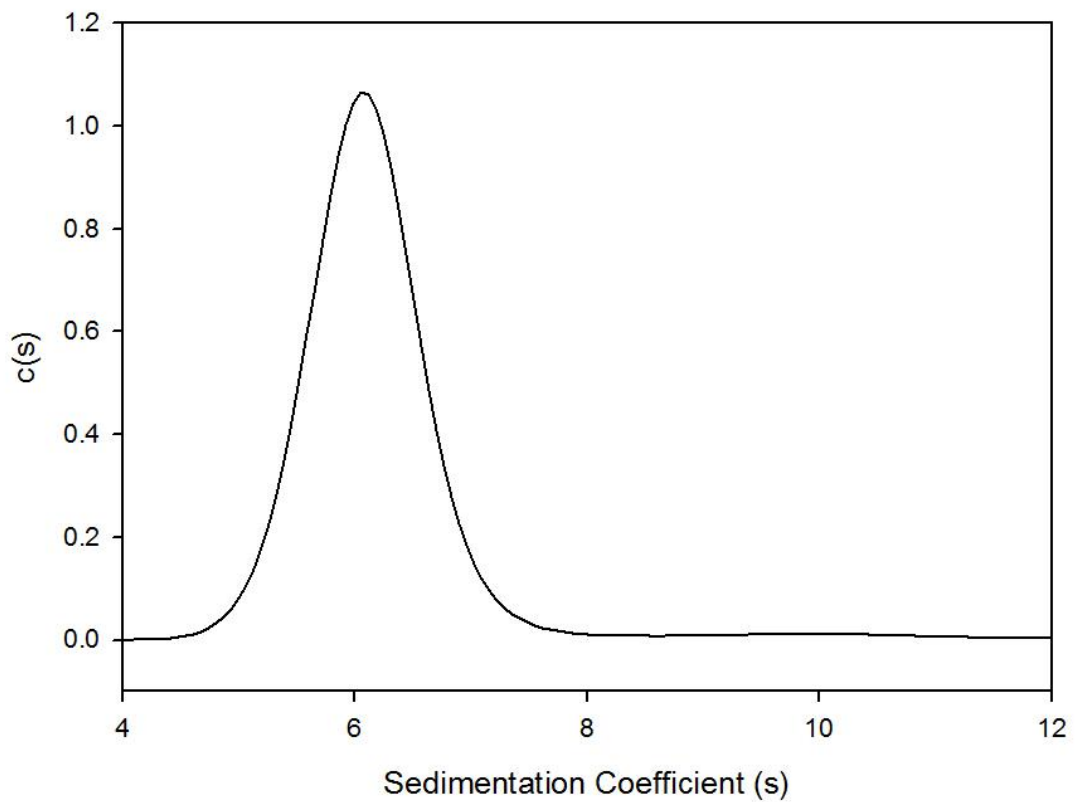
SB308 30K AB5. c(s) distribution



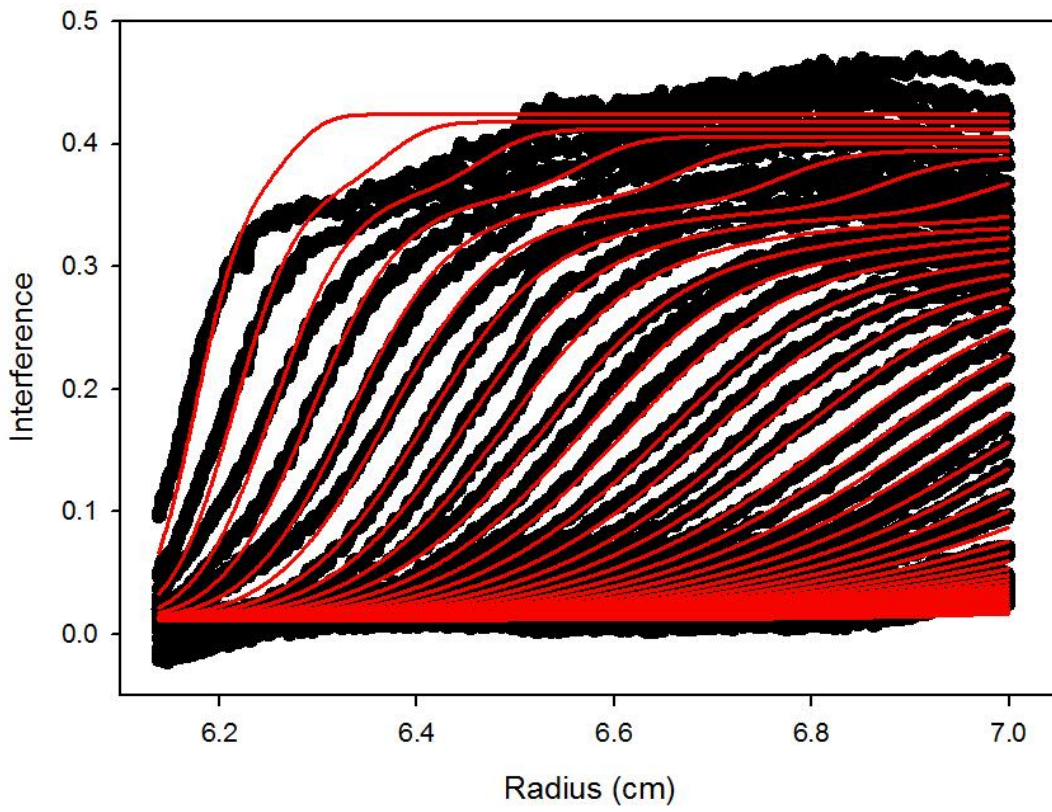
SB308 30K AB6.



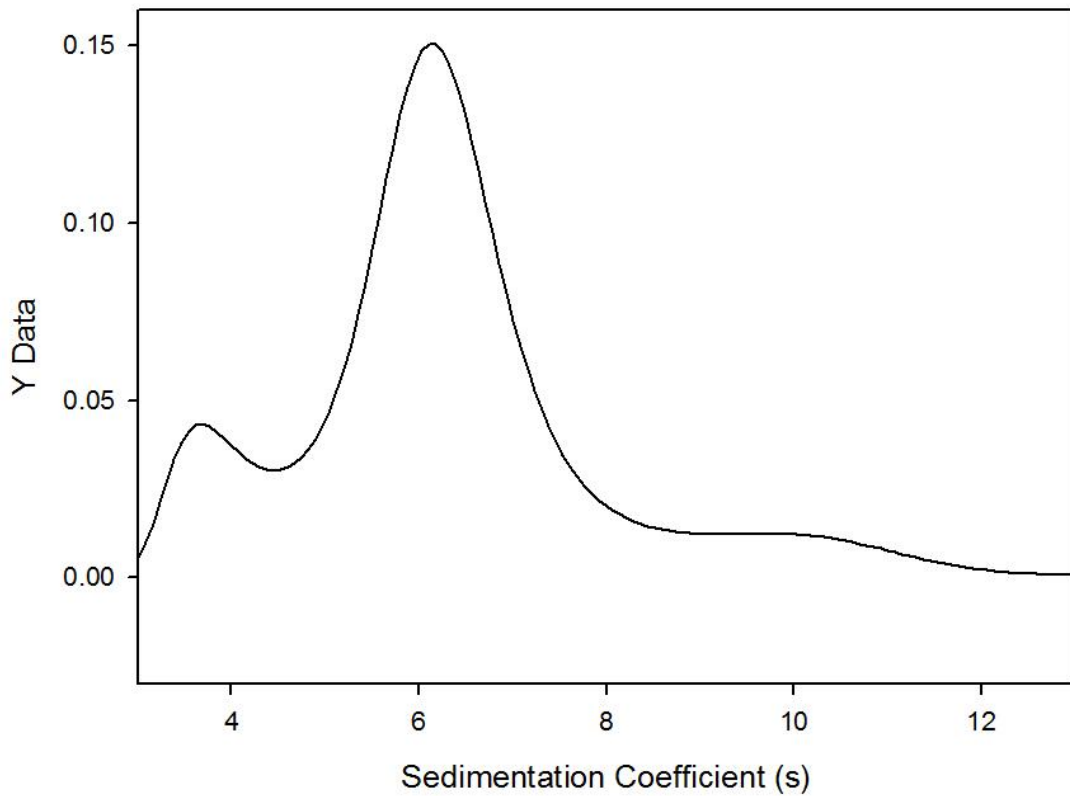
SB308 30K AB6. c(s) distribution



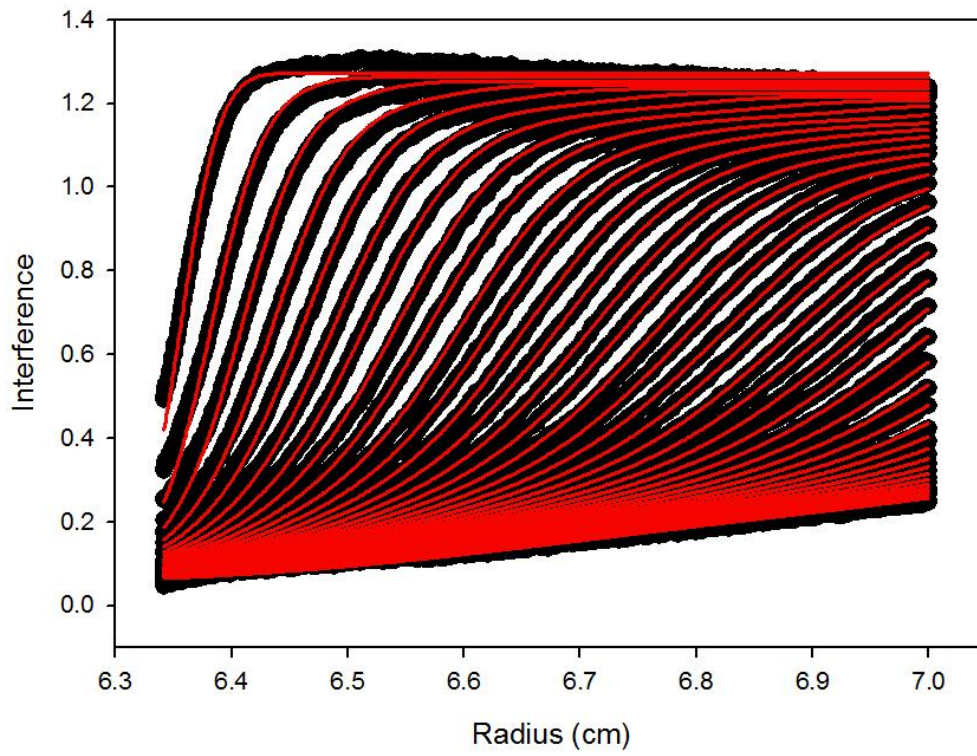
SB308 30K IP1



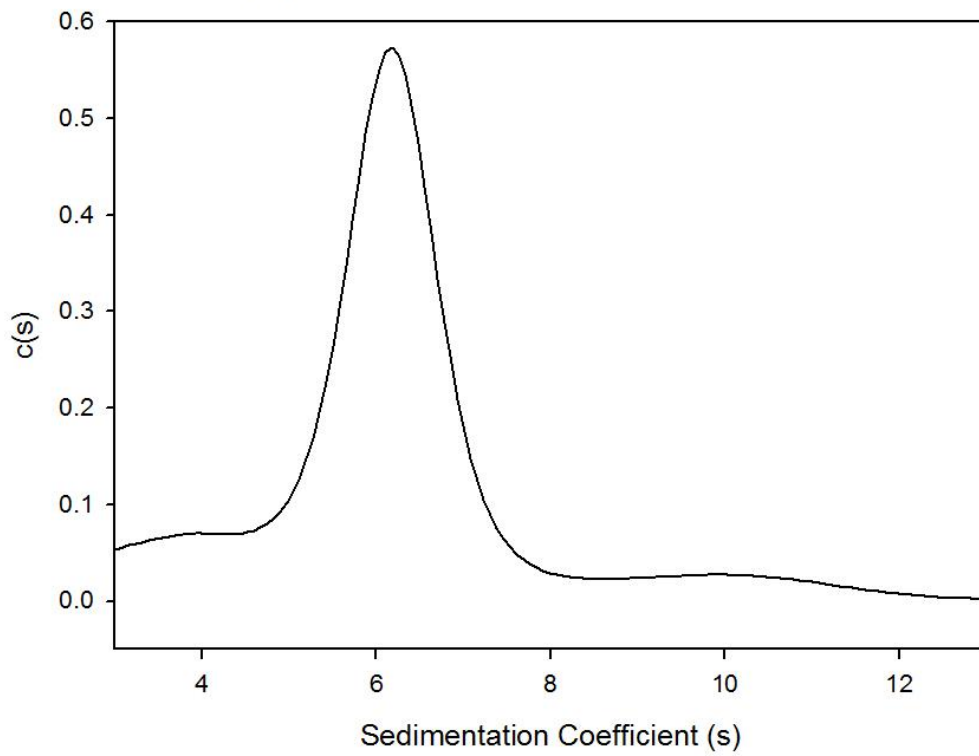
SB308 30K IP1 c(s) distribution



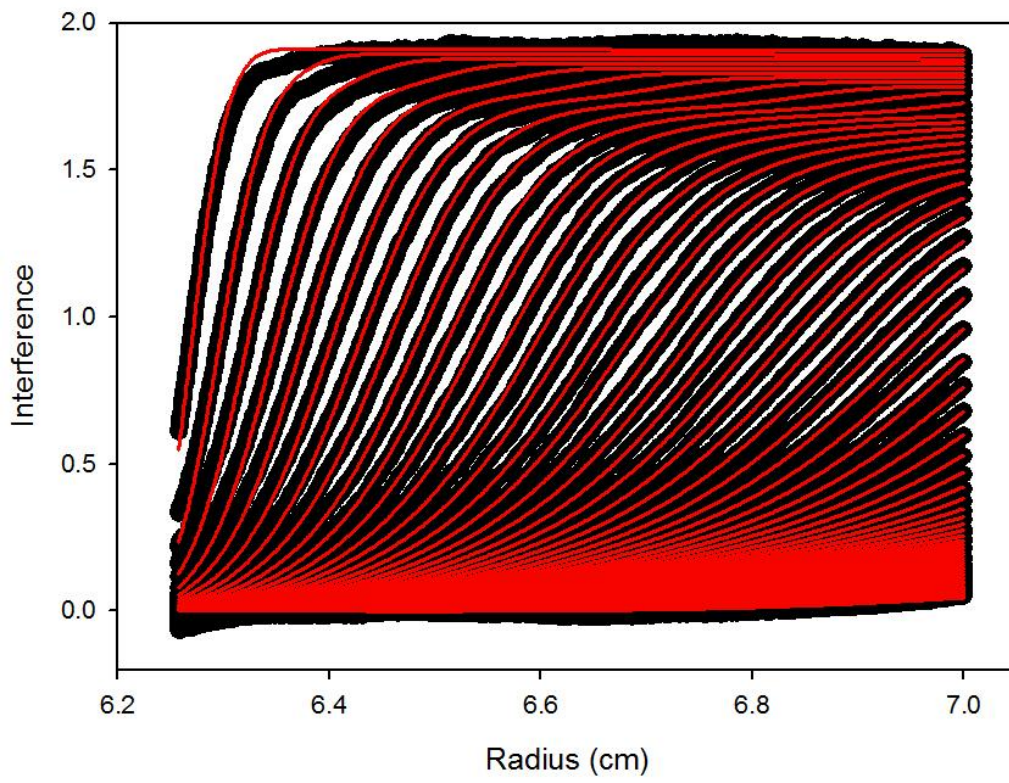
SB308 30K IP4



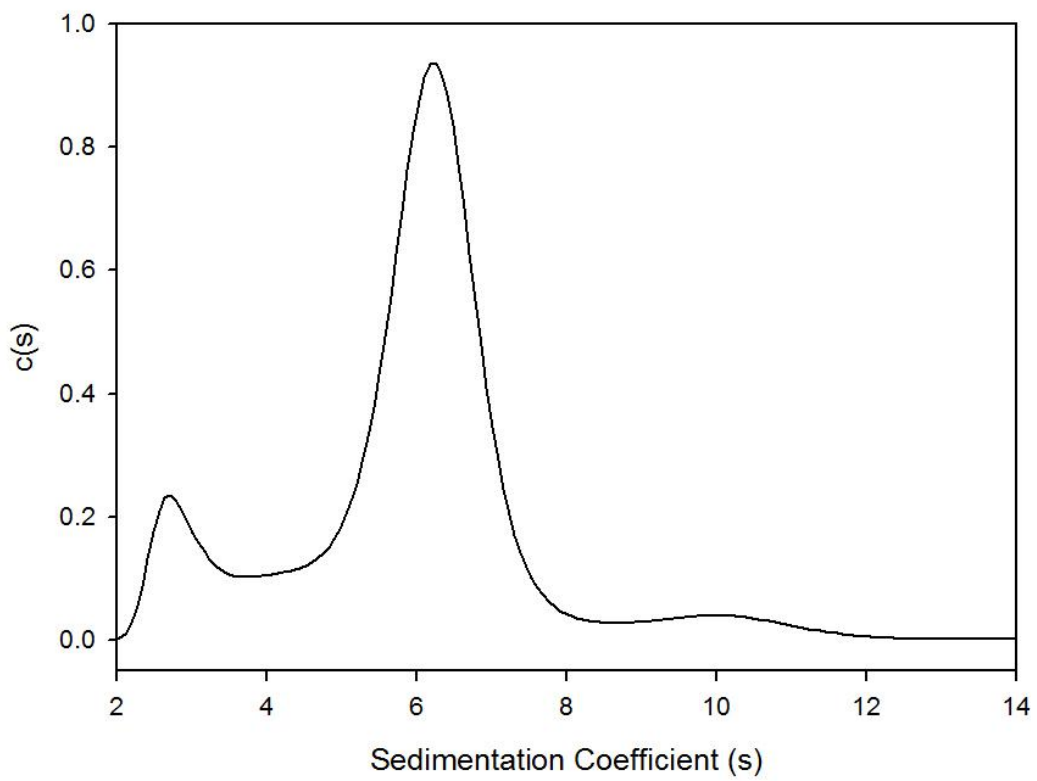
SB388 30K IP4 c(s) distribution



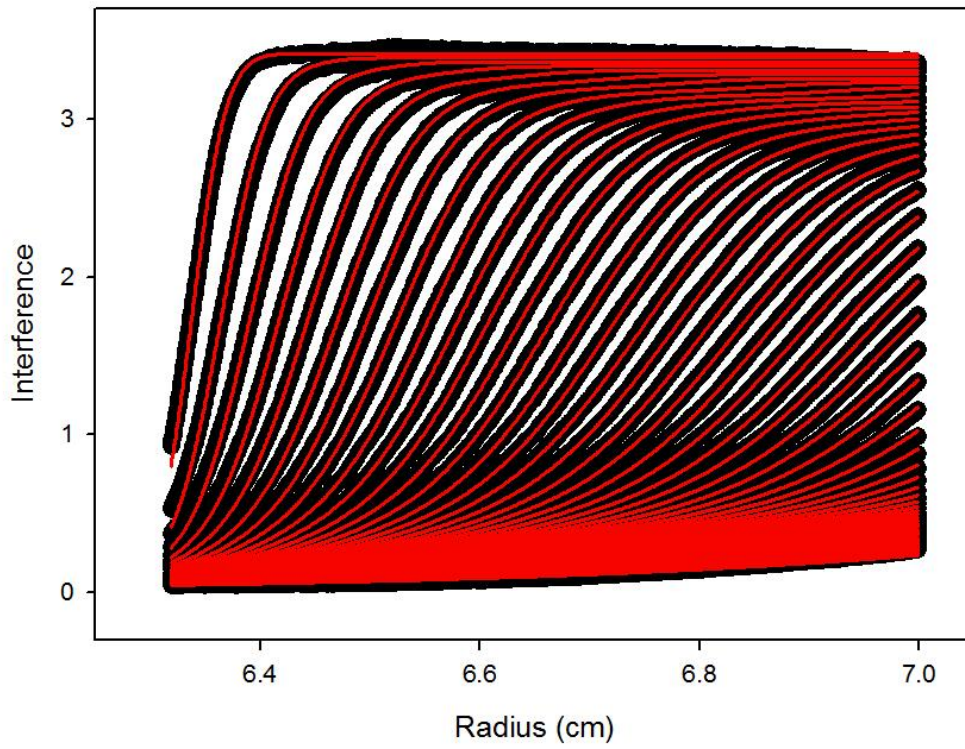
SB308 30K IP5



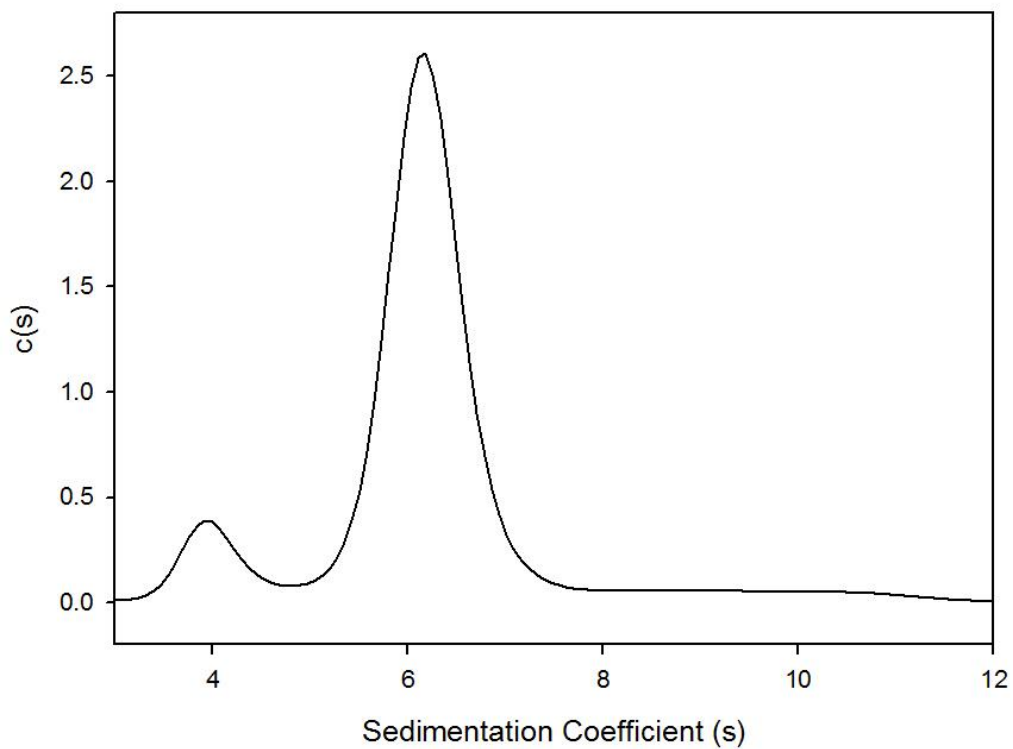
SB308 30K IP5 c(s) distribution



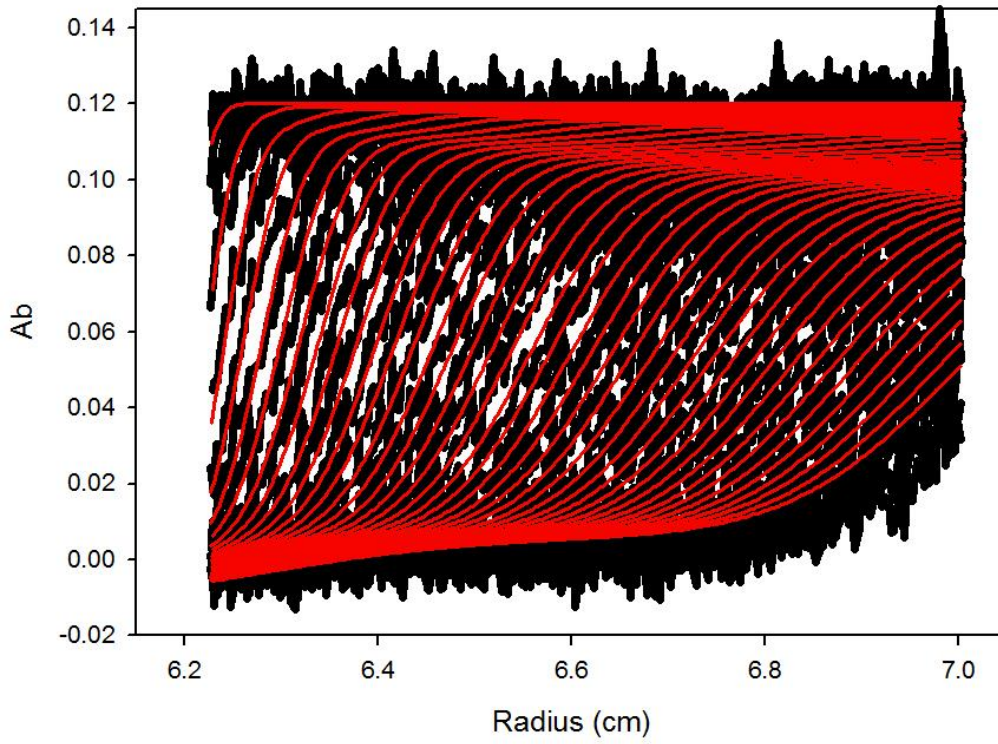
SB308 30K IP6



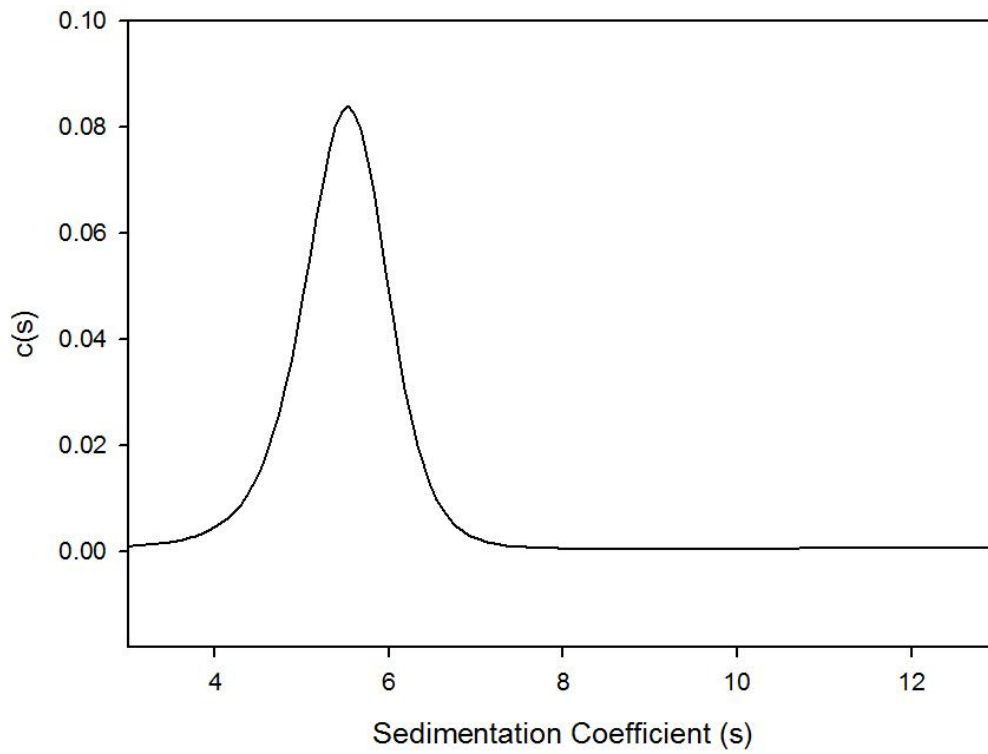
SB308 30K IP6 $c(s)$ distribution



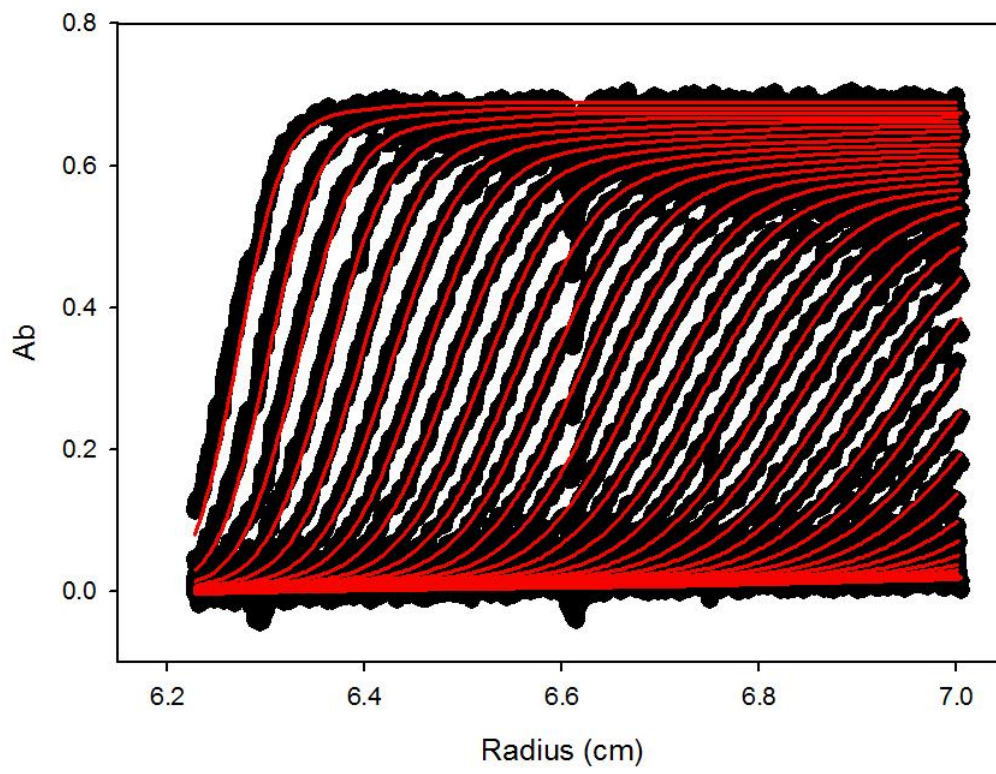
SB308 40K AB2.



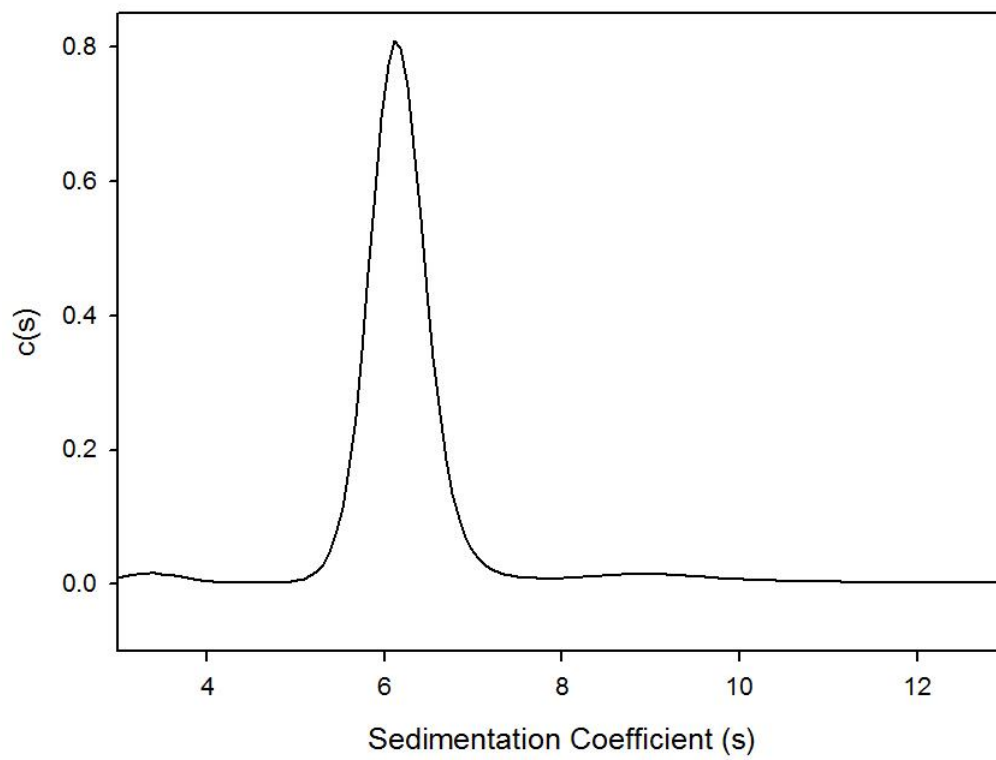
SB308 40K AB2. c(s) distribution



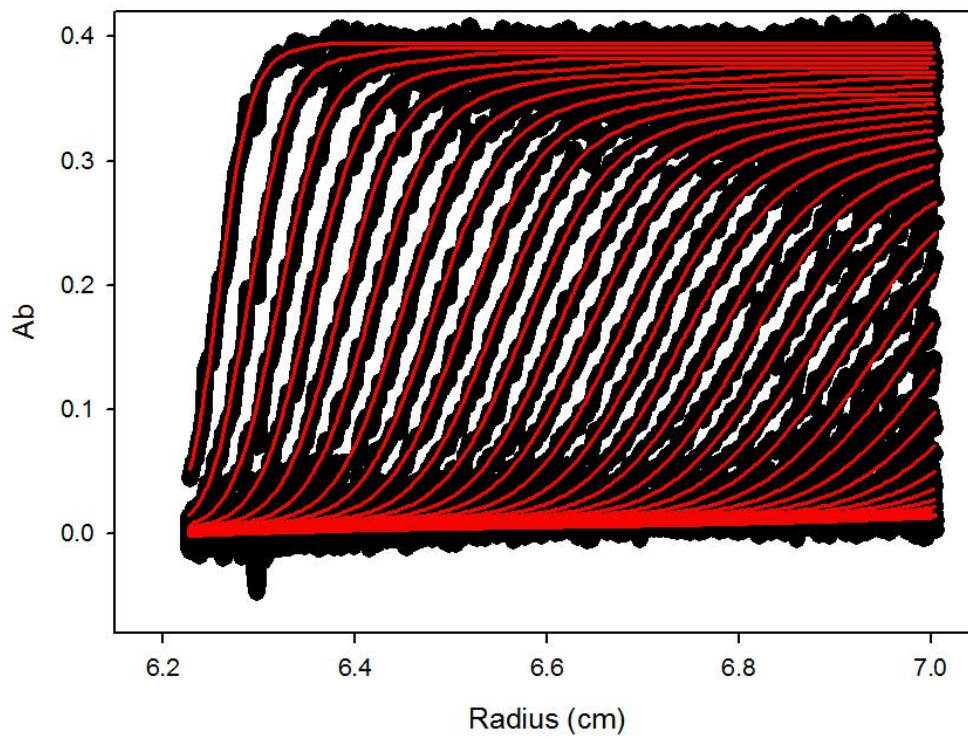
SB308 40K AB5



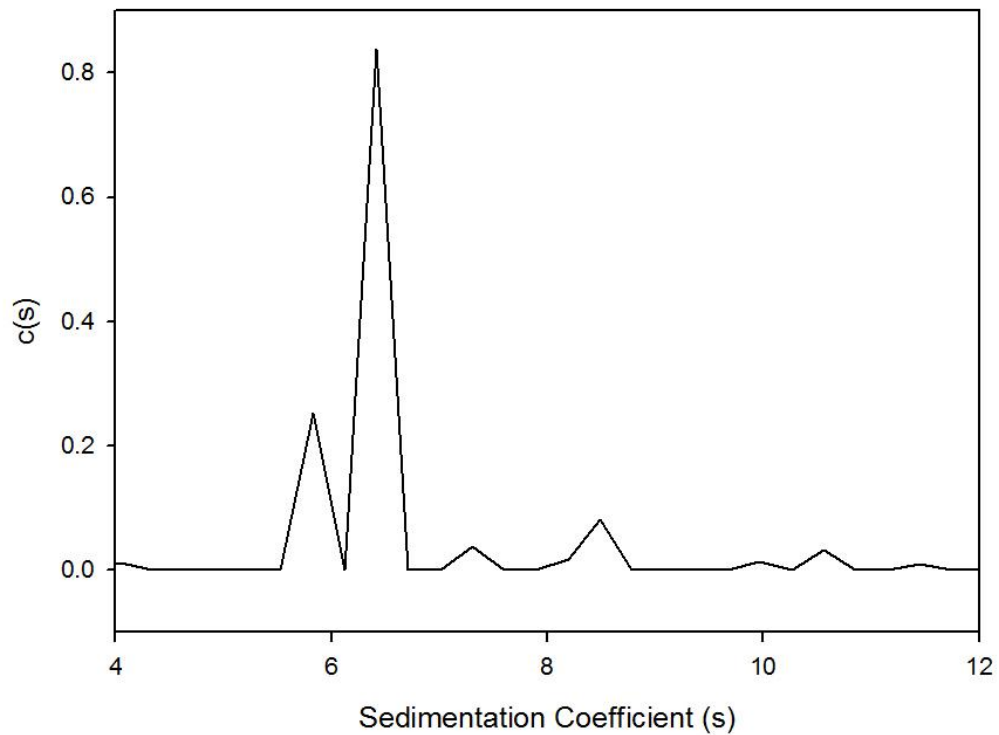
SB308 40K AB5 c(s) distribution



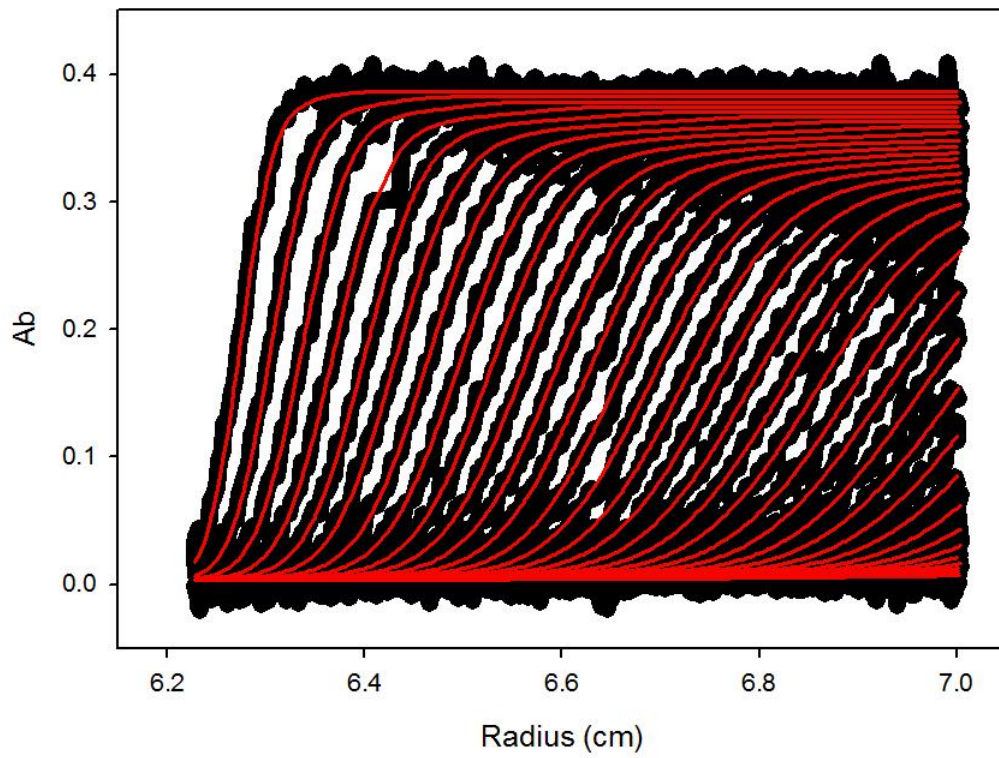
SB308 40K AB6



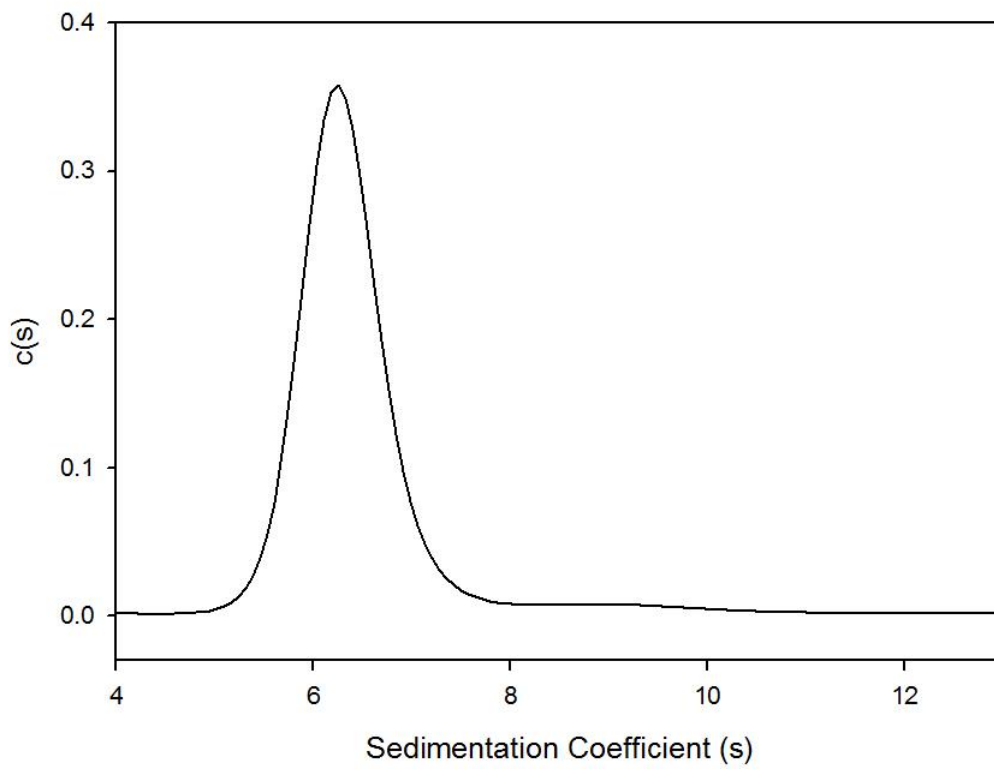
SB308 40K AB6 c(s) distribution



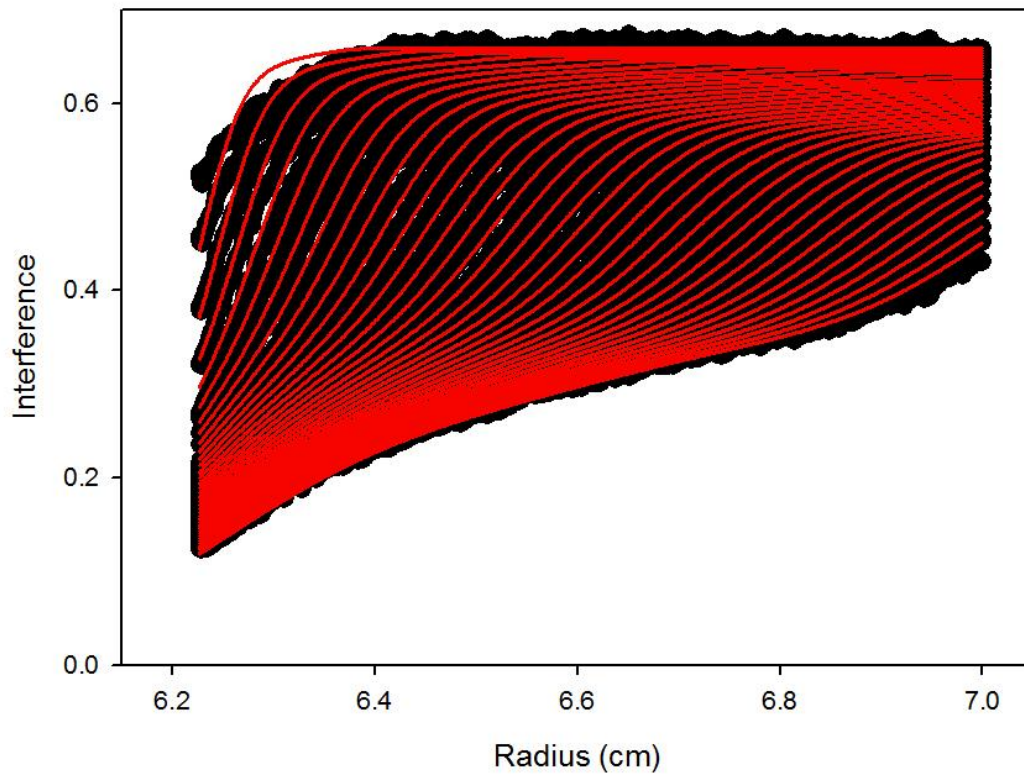
SB308 40K AB7



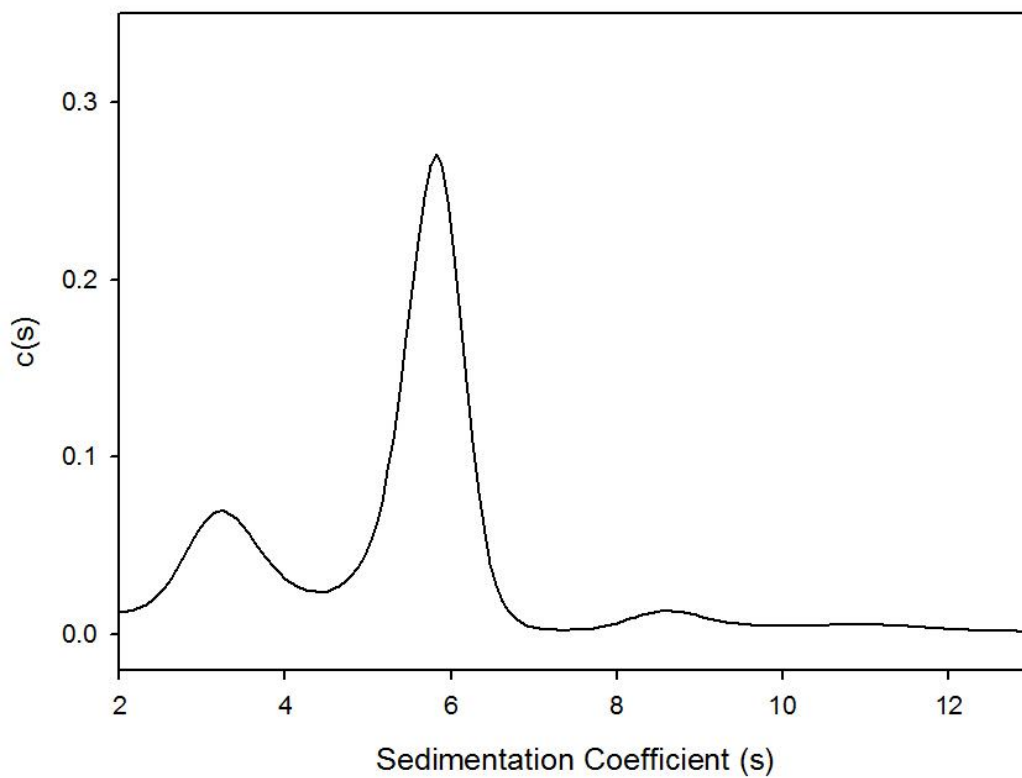
SB308 40K AB7 c(s) distribution



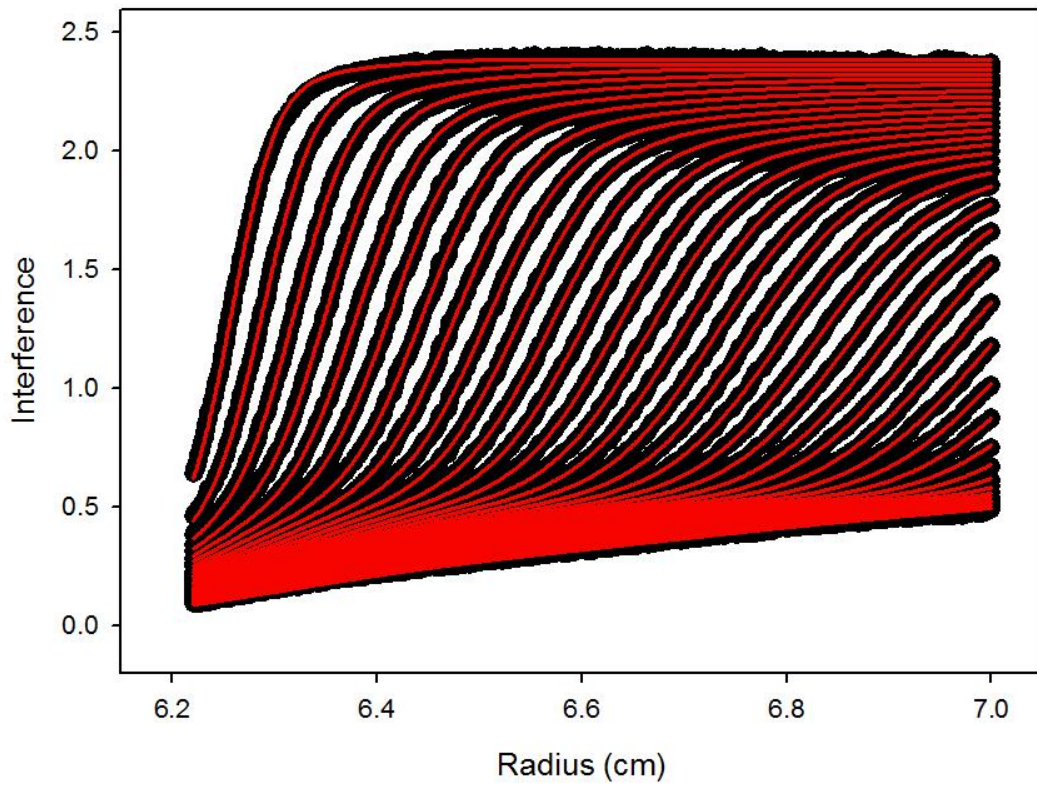
SB308 40K IP2.



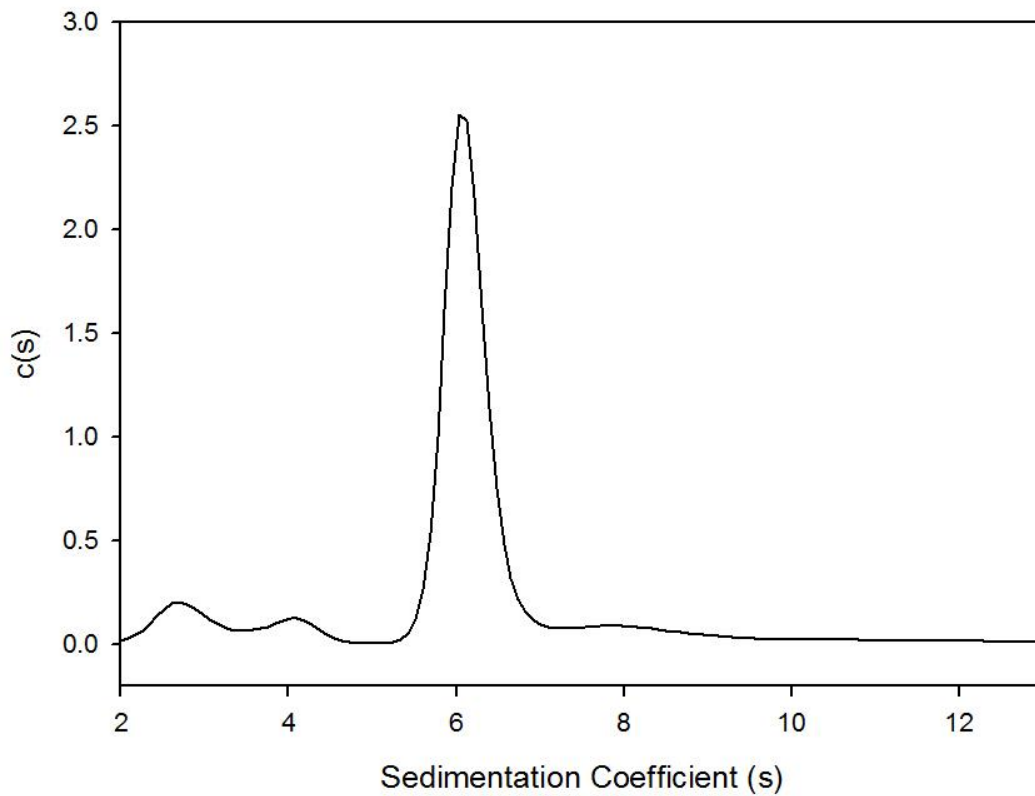
SB308 40K IP2. $c(s)$ distribution



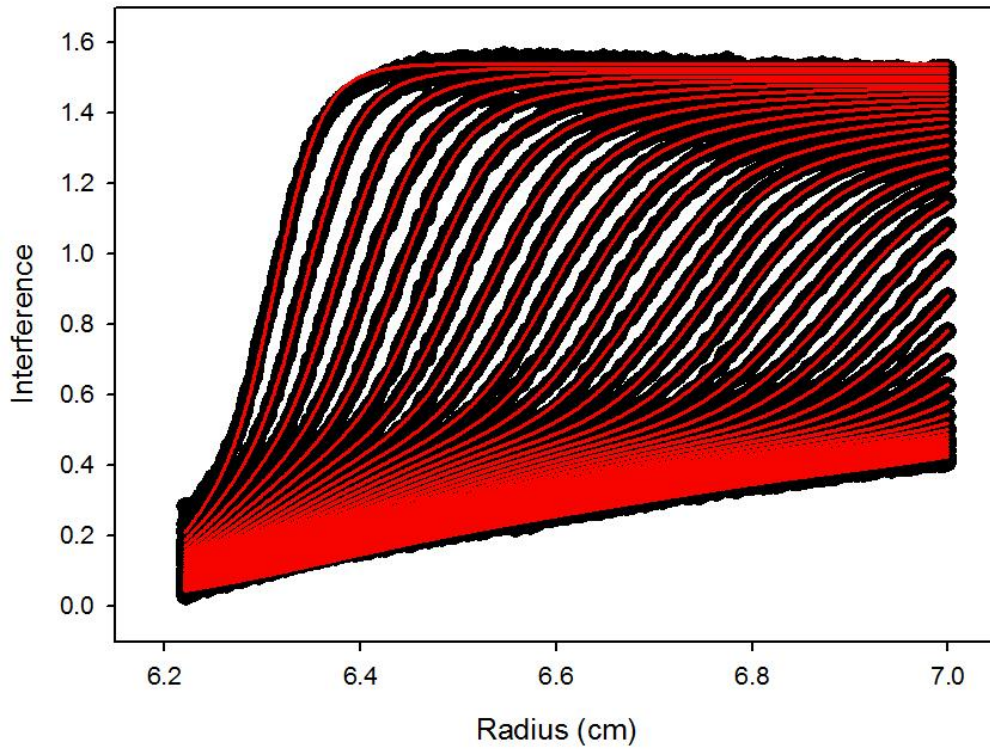
SB308 40K IP5



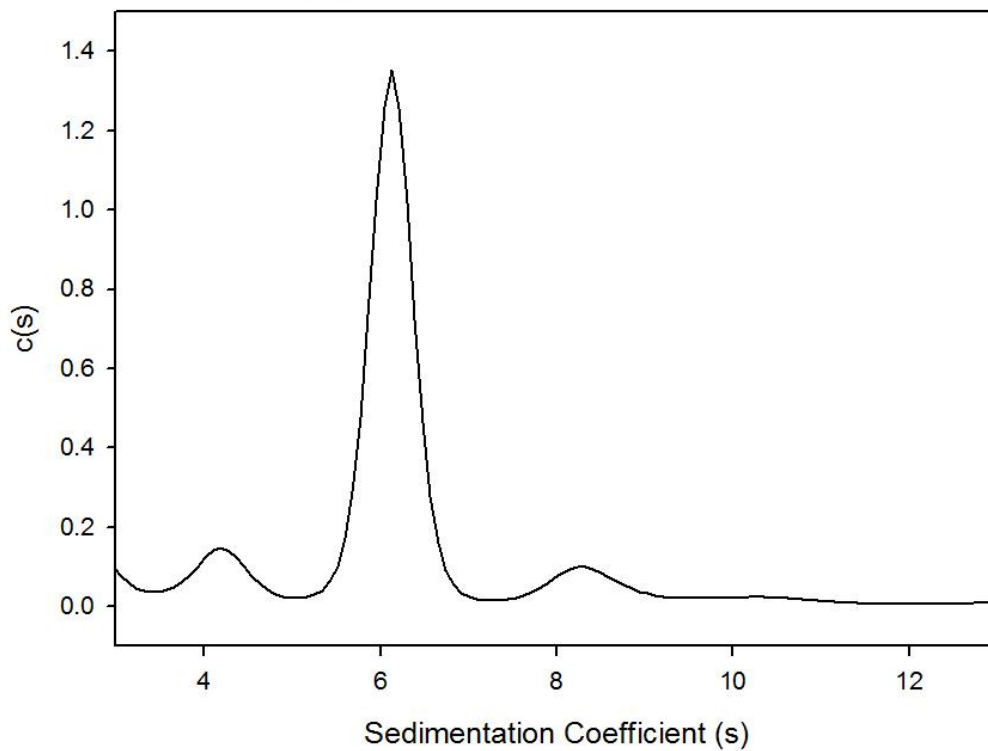
SB308 40K IP5 c(s) distribution



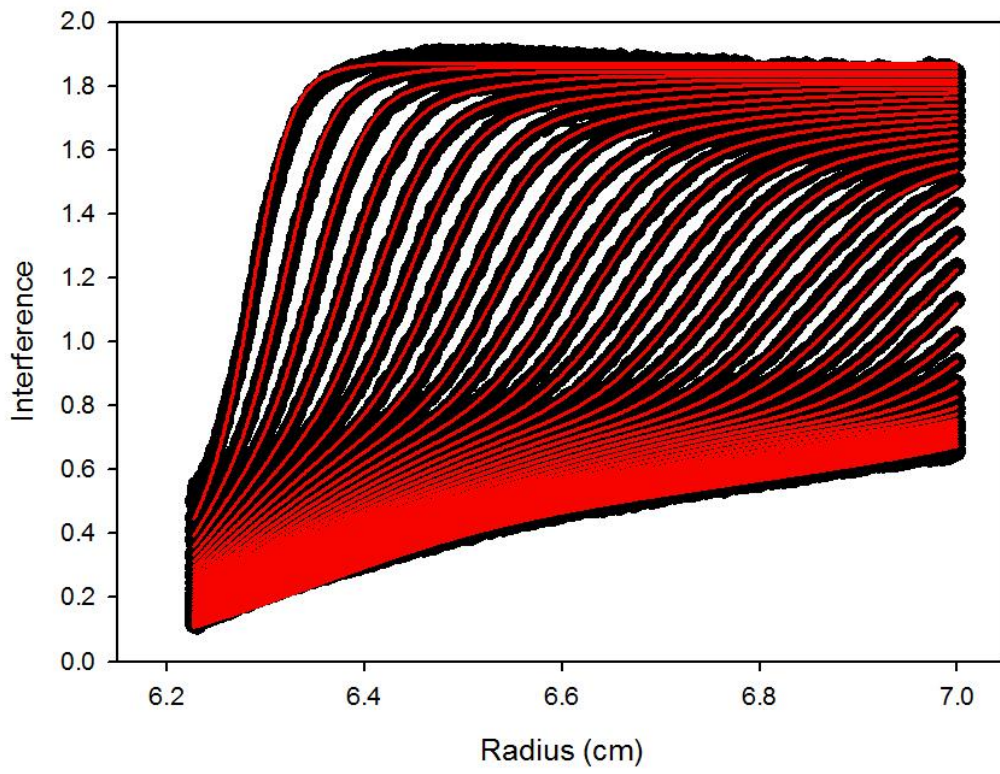
SB308 40K IP6



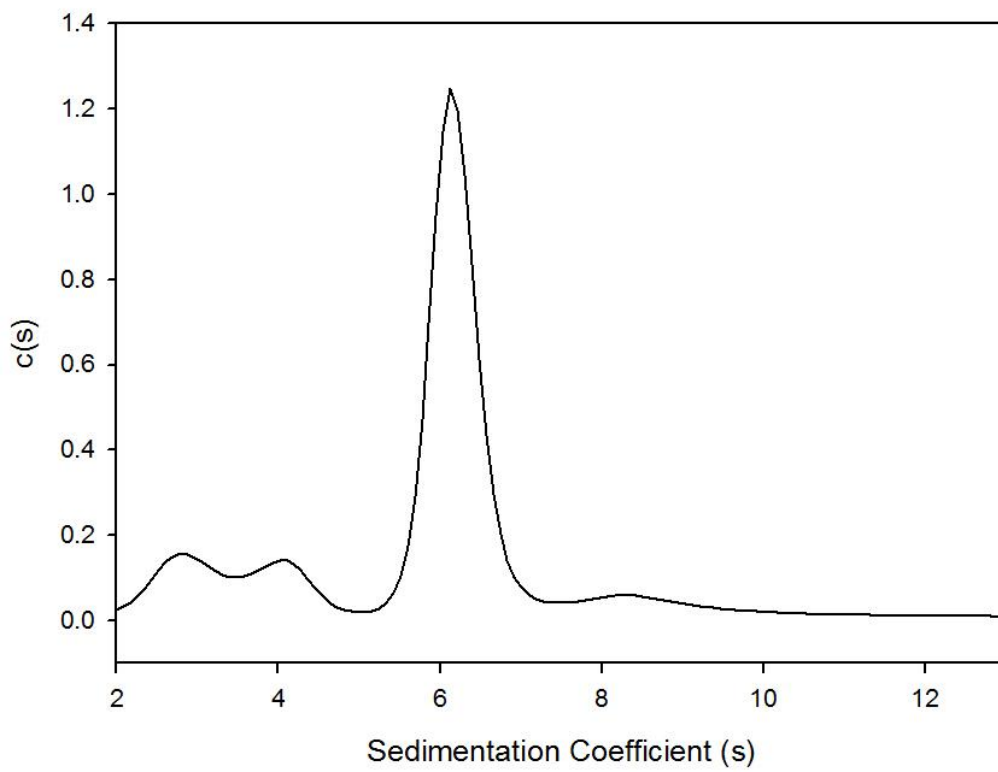
SB308 40K IP6



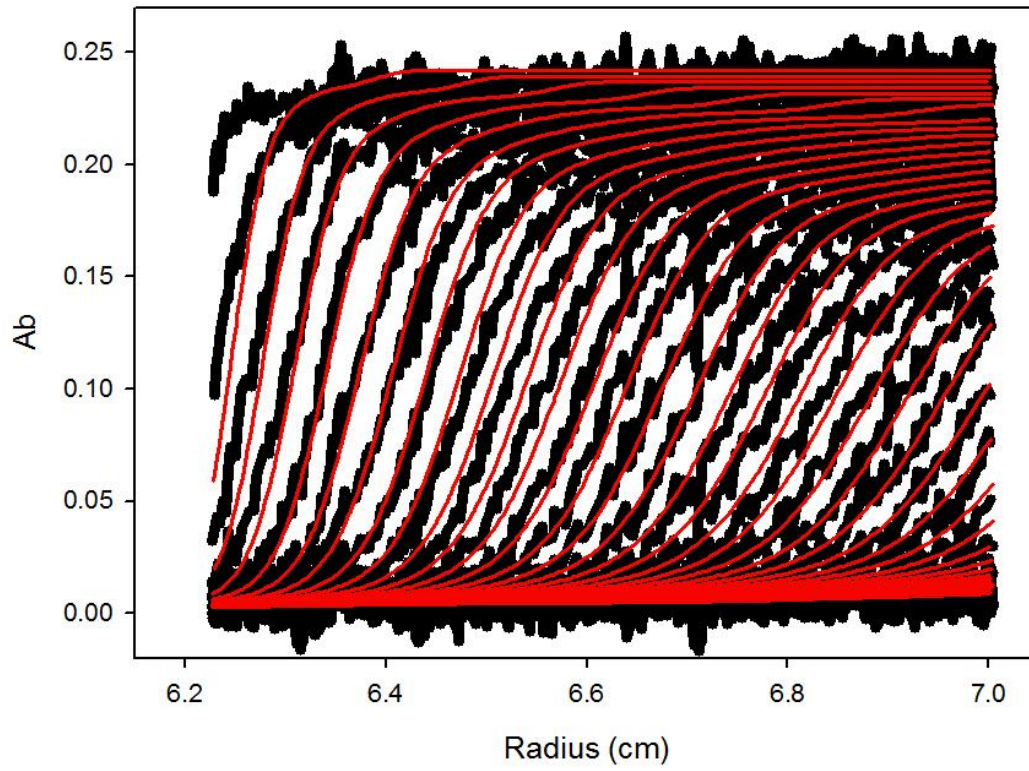
SB308 40K IP7



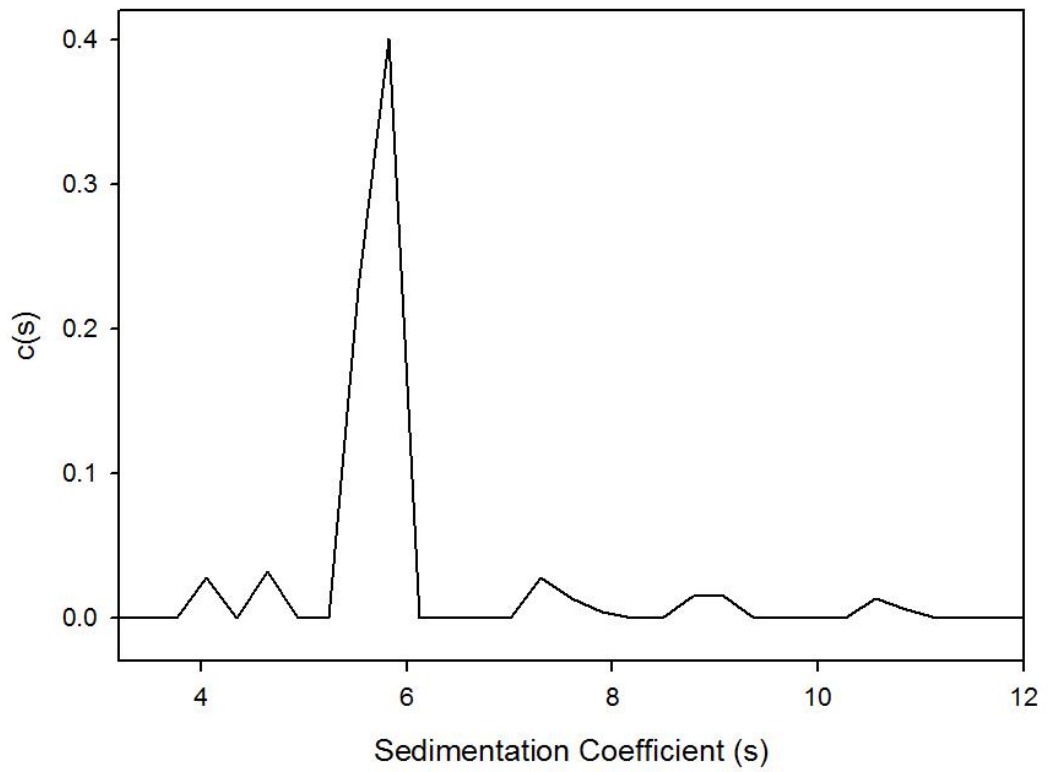
SB308 40K IP7



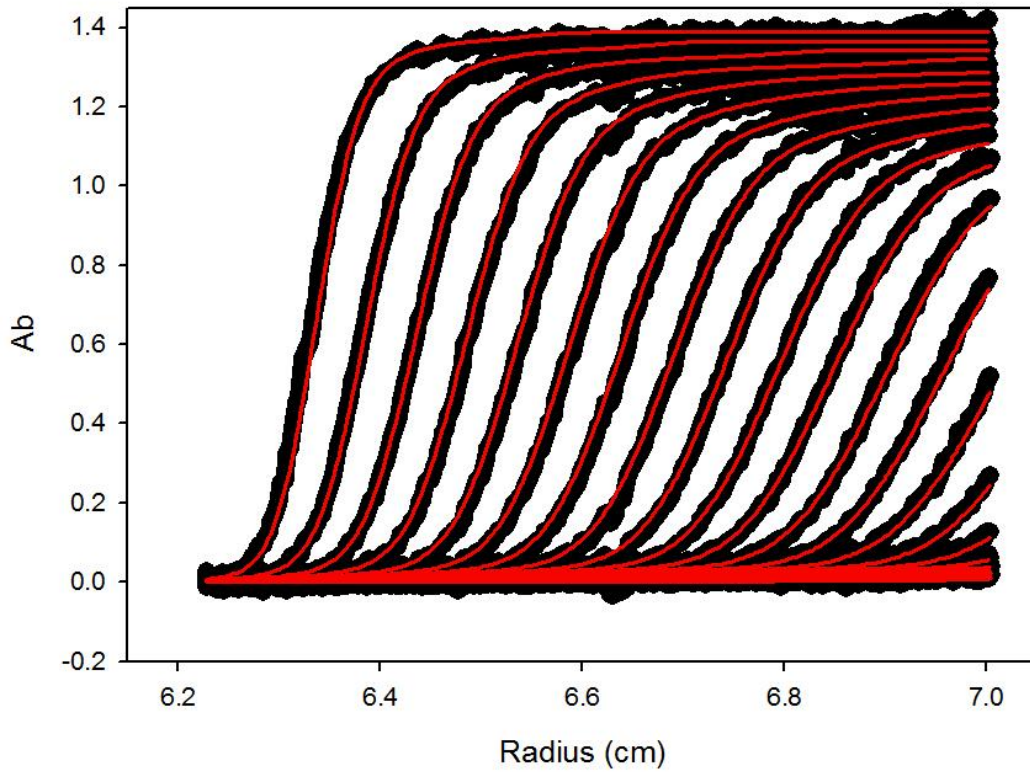
SB308 50K AB2.



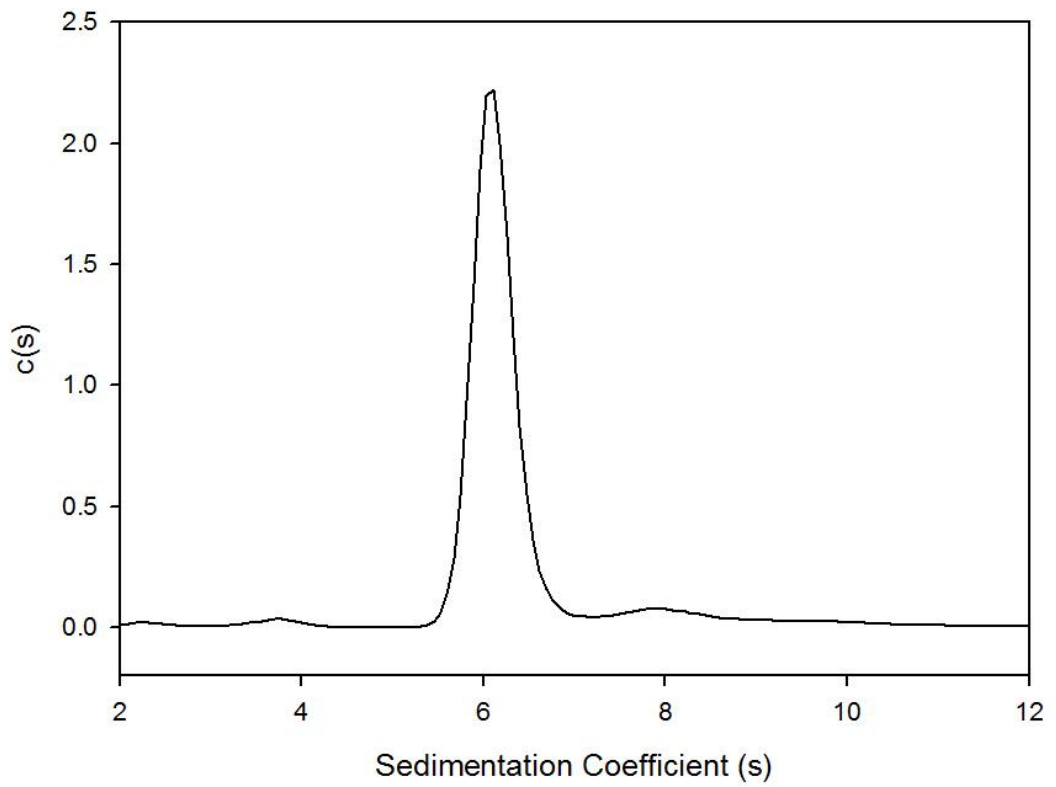
SB308 50K AB2. c(s) distribution



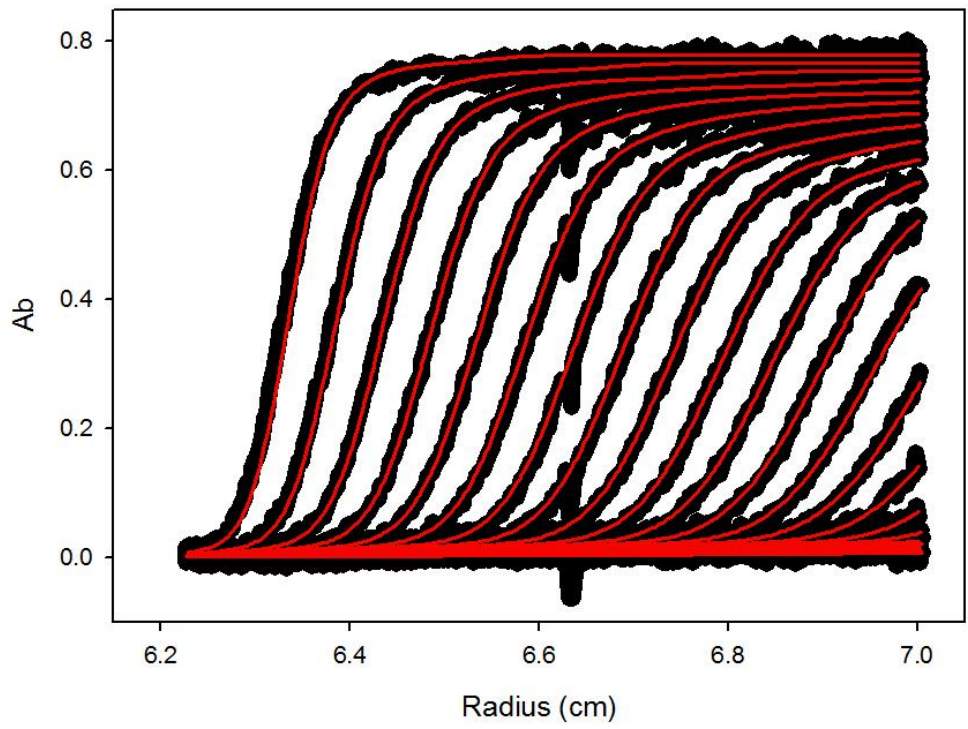
SB308 50K AB5



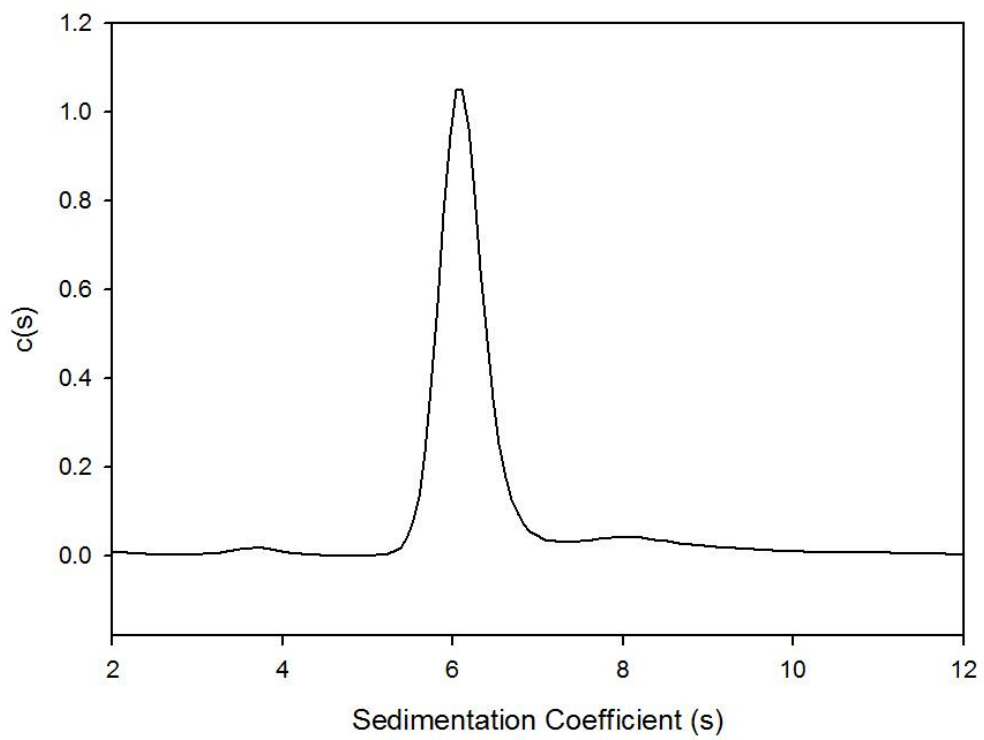
SB308 50K AB5 c(s) distribution



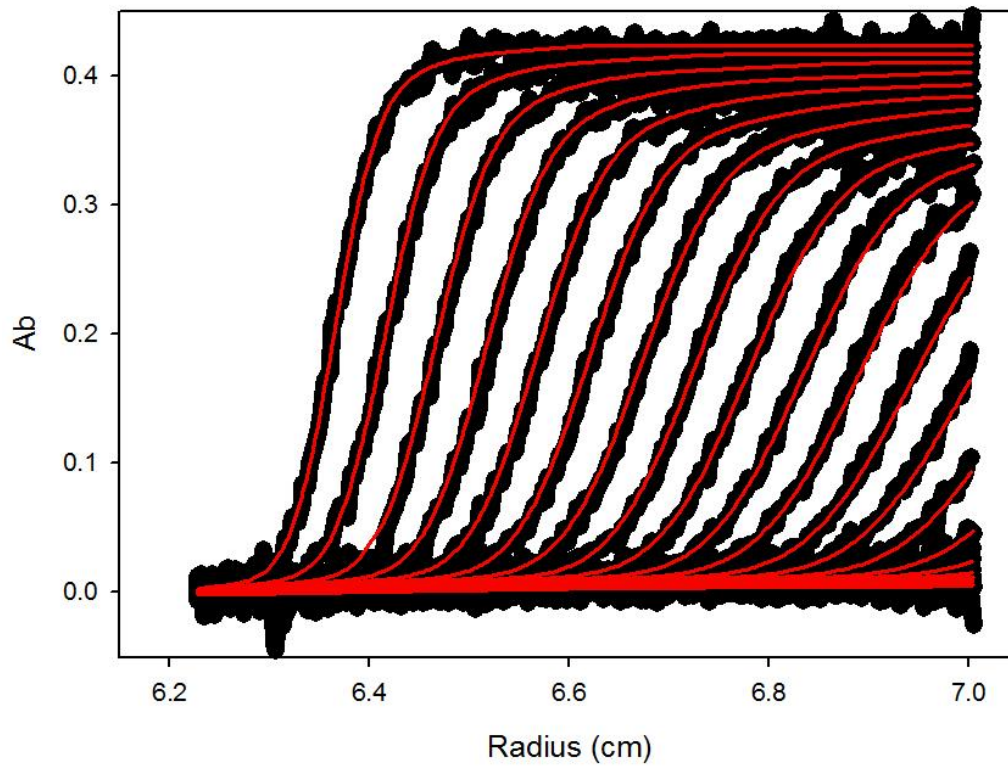
SB308 50K AB6



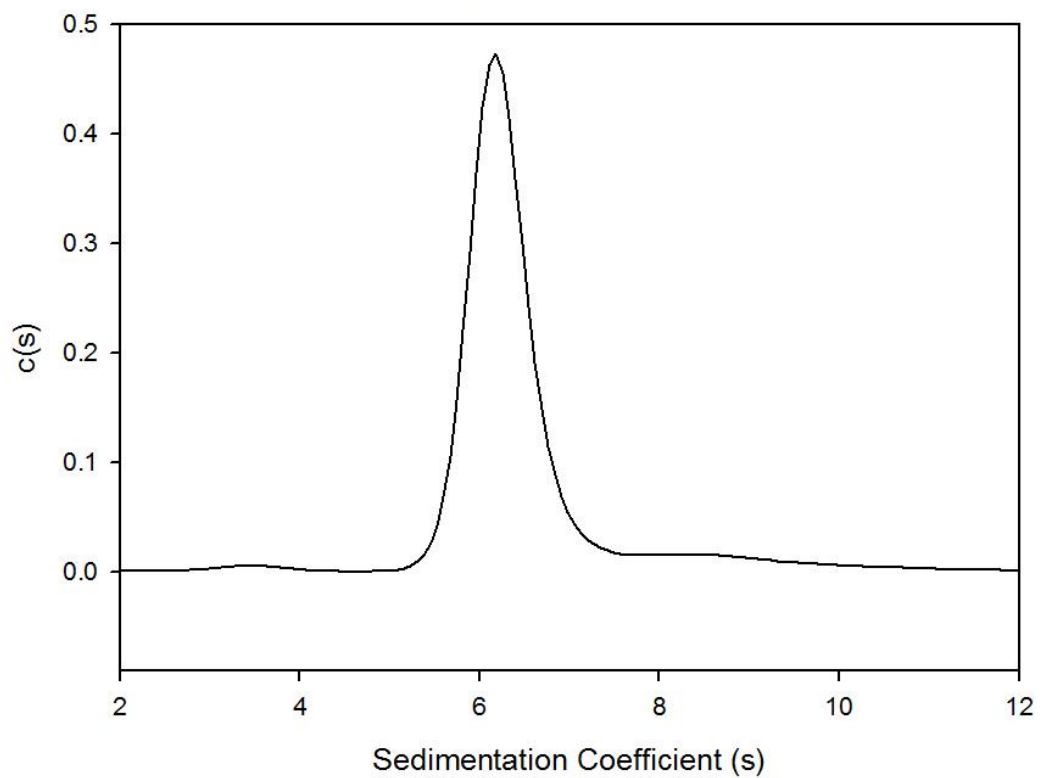
SB308 50K AB6 c(s) distribution



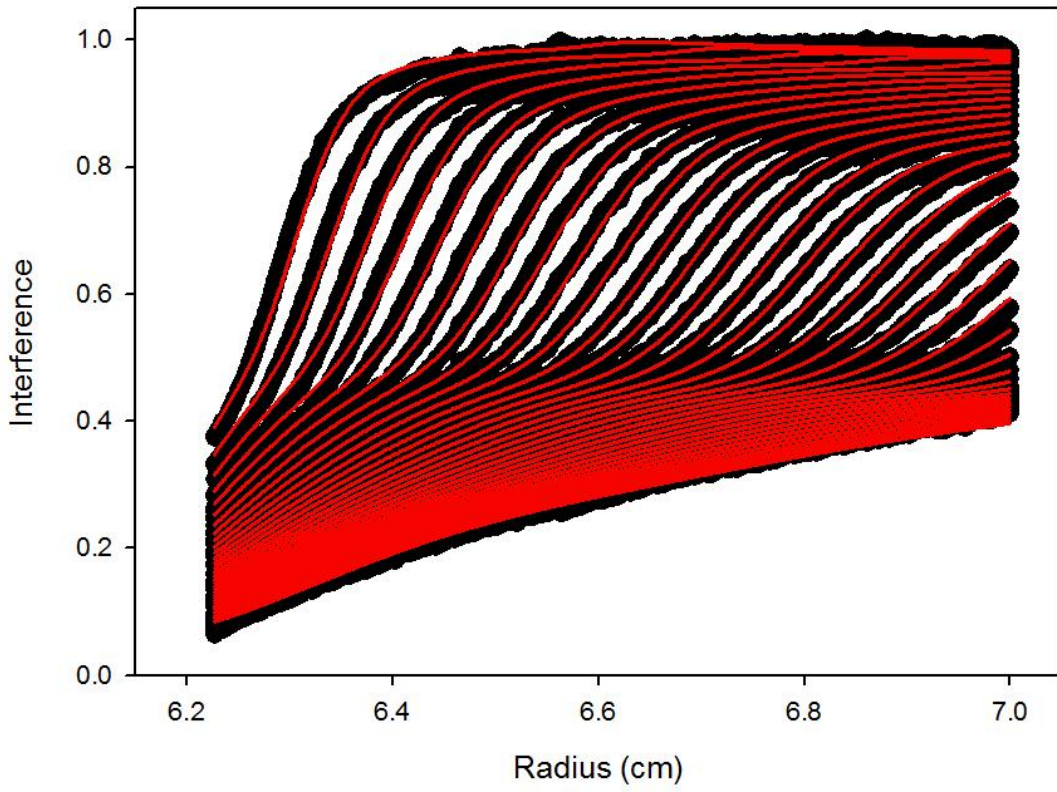
SB308 50K AB7



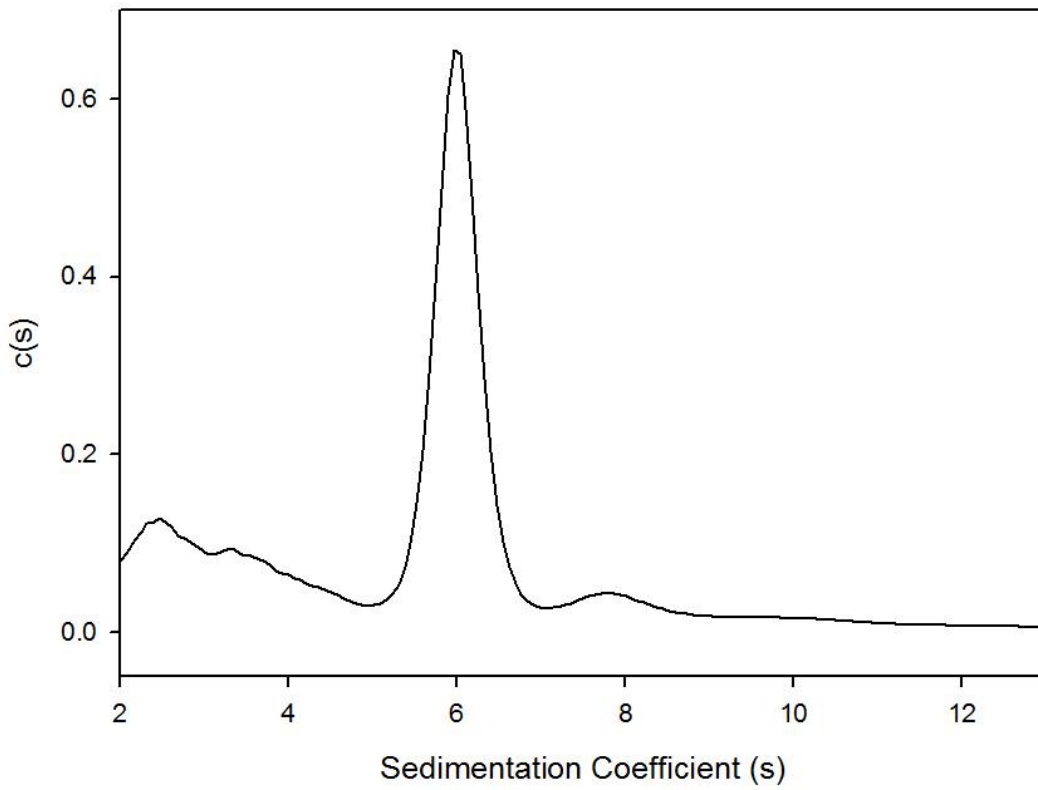
SB308 50K AB7 c(s) distribution



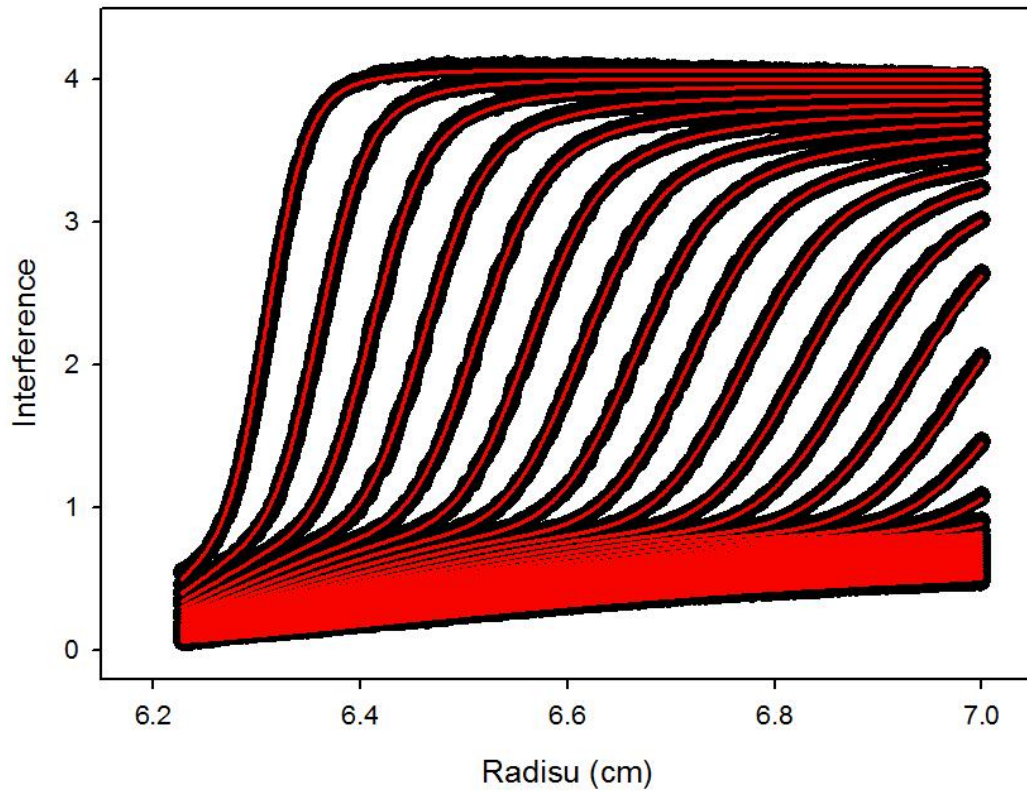
SB308 50K IP2.



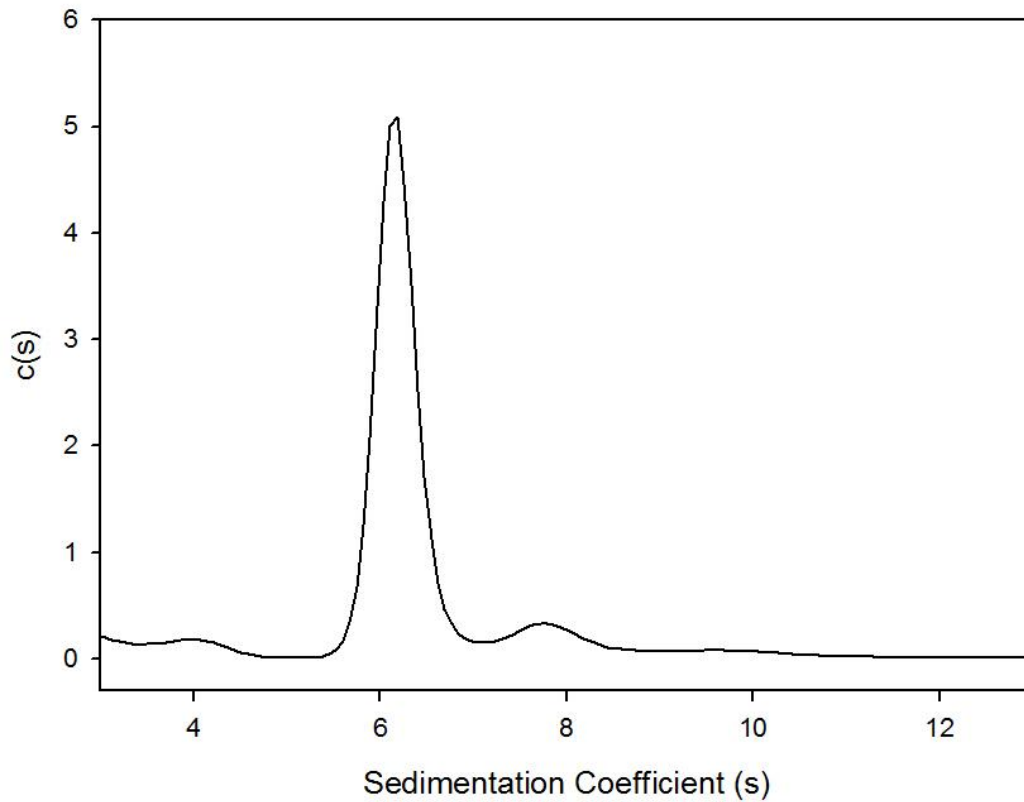
SB308 50K IP2. c(s) distribution



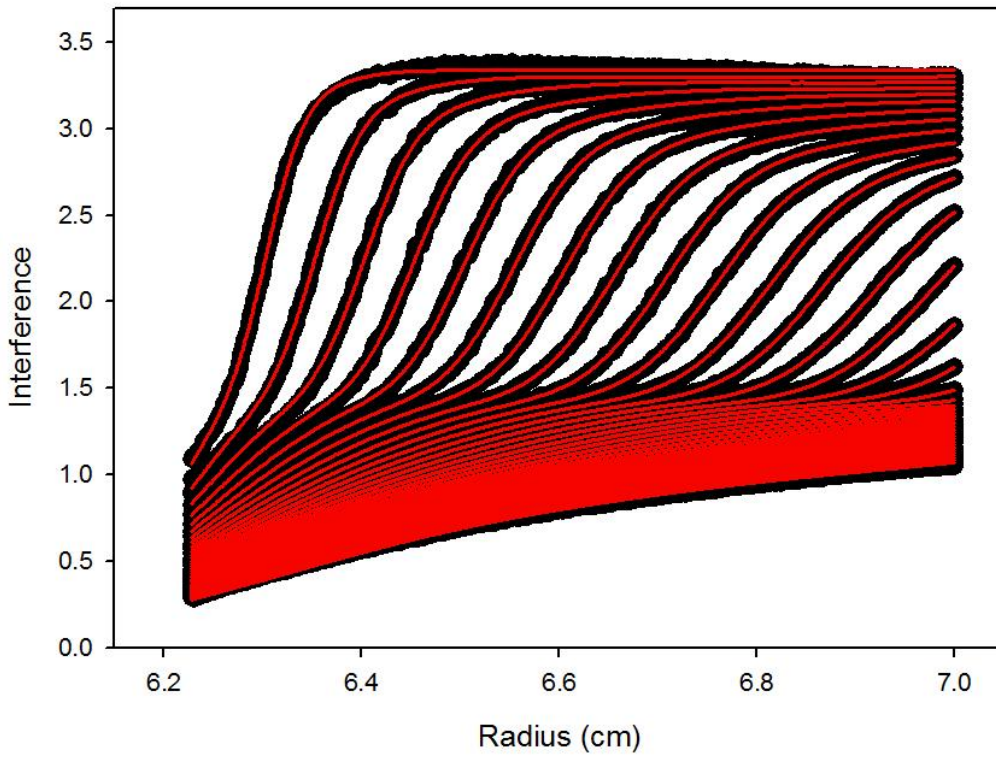
SB308 50K IP5



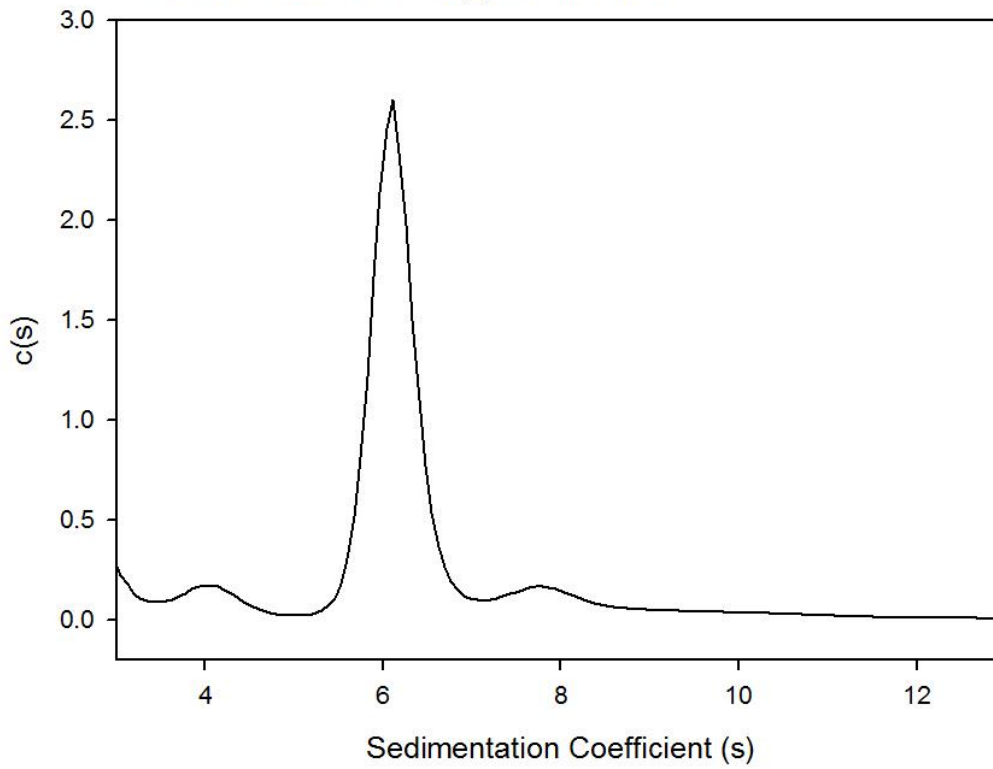
SB308 50K IP5 c(s) distribution



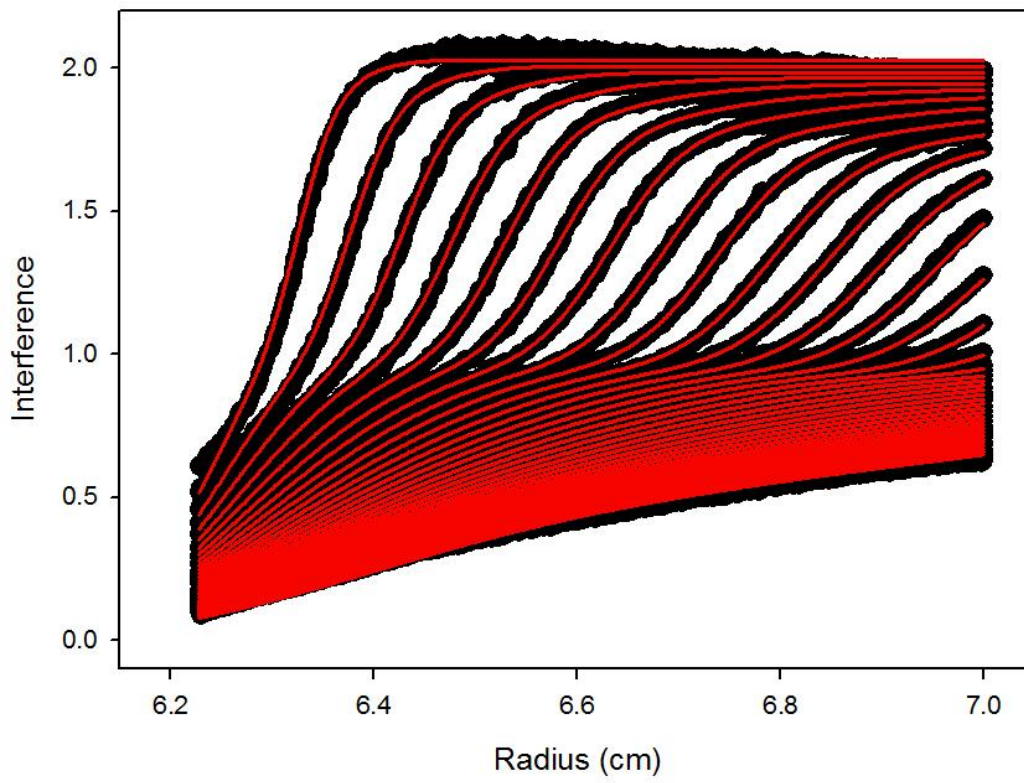
SB308 50K IP5



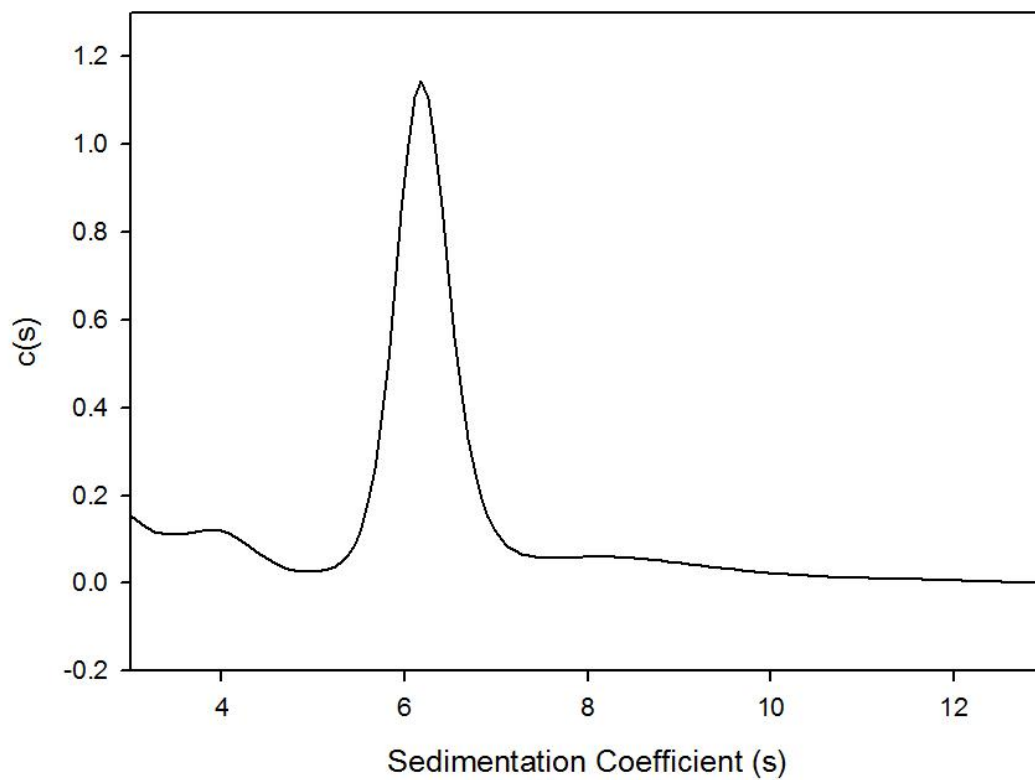
SB308 50K IP6 c(s) distribution



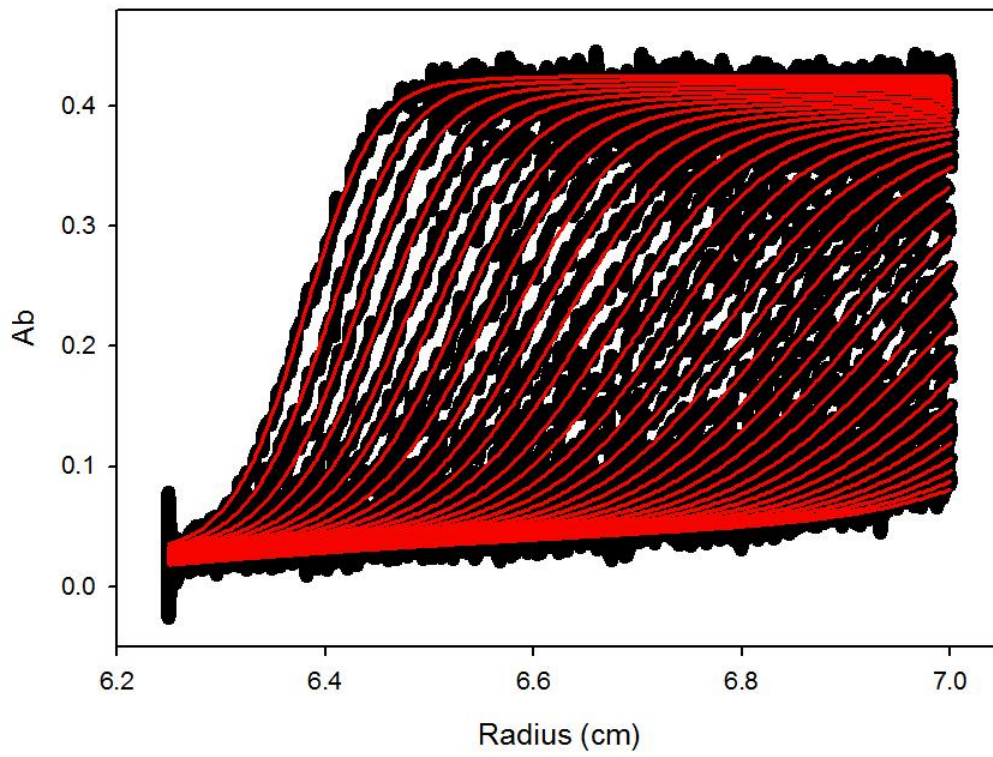
SB308 50K IP7



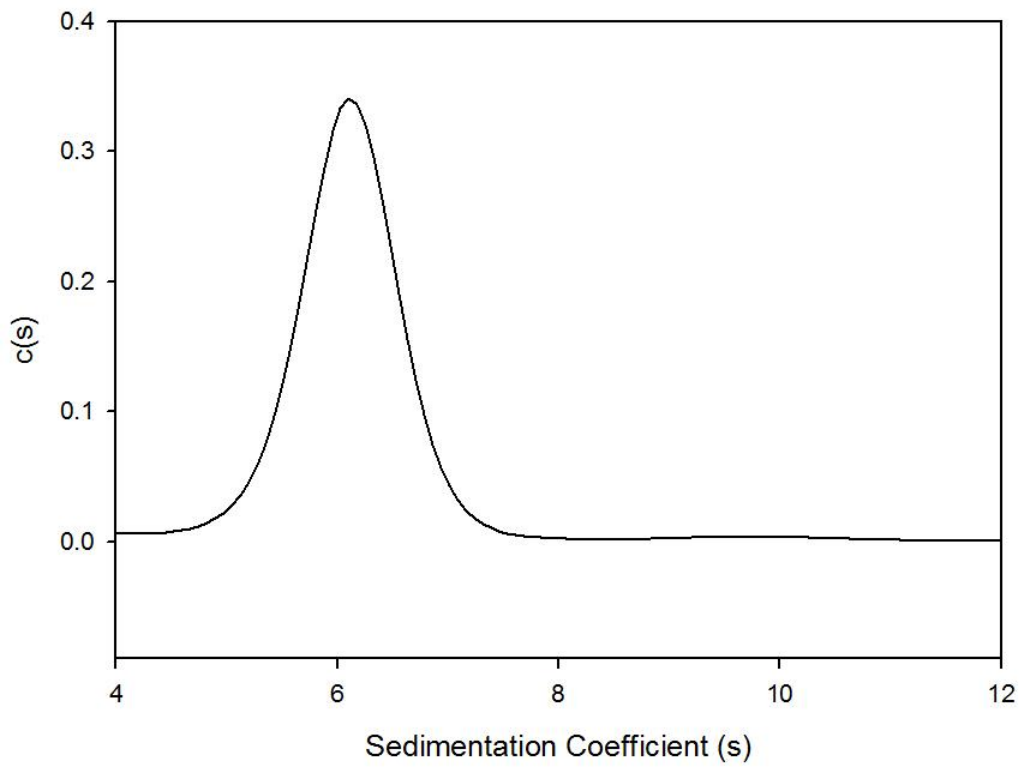
SB308 50K IP7 c(s) distribution



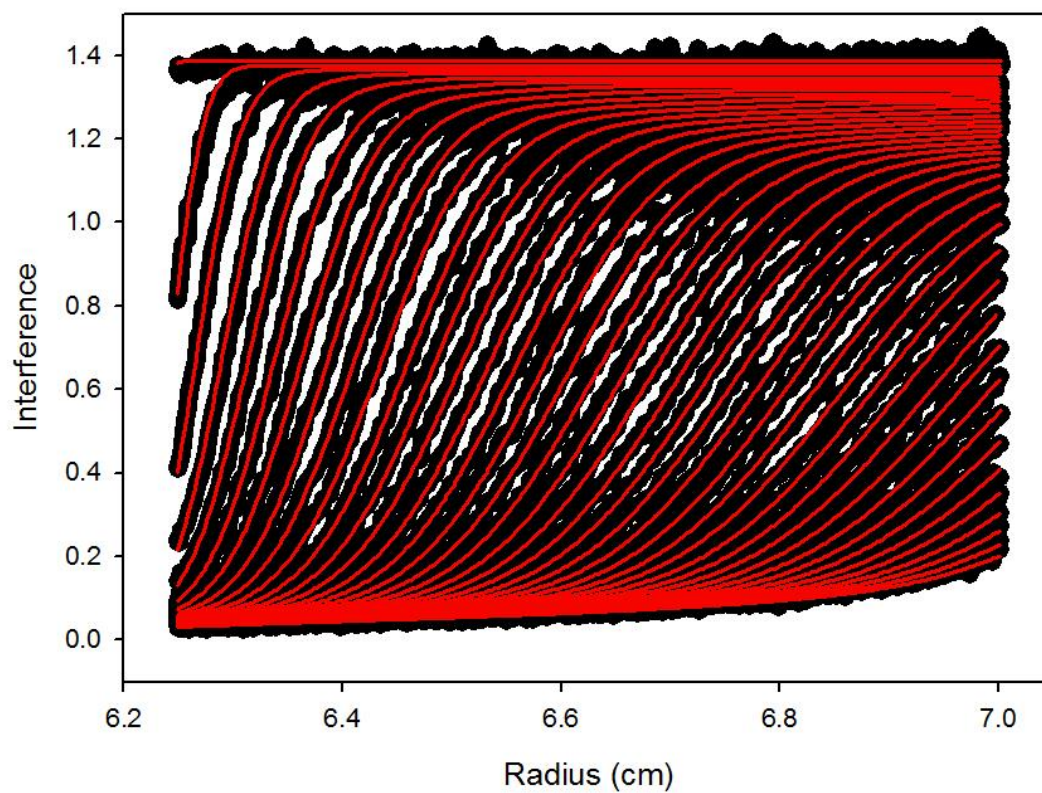
SB338 30K AB2



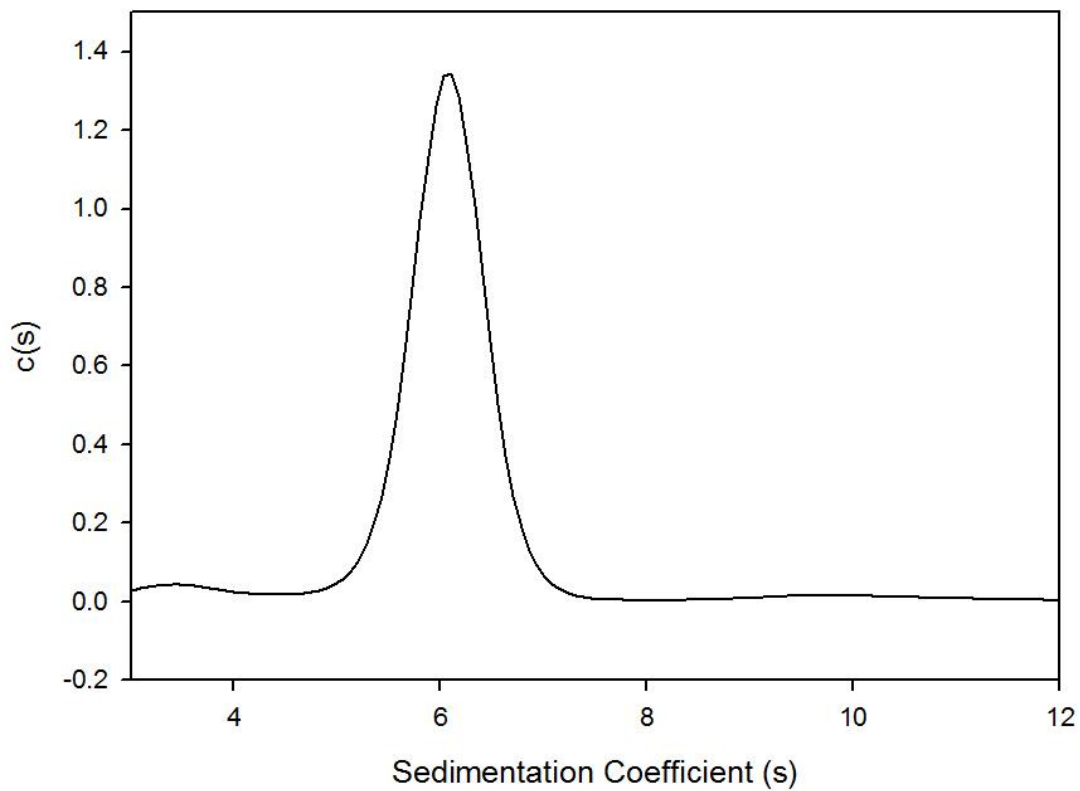
Sb338 30K AB2 c(s) distribution



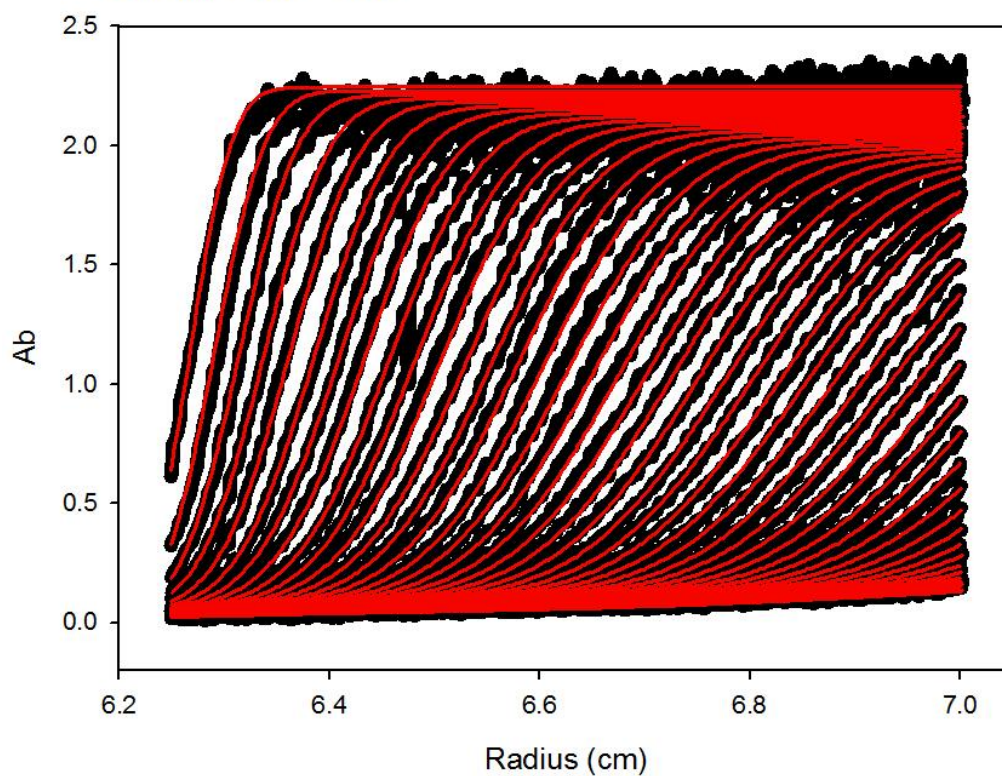
SB338 30K AB4



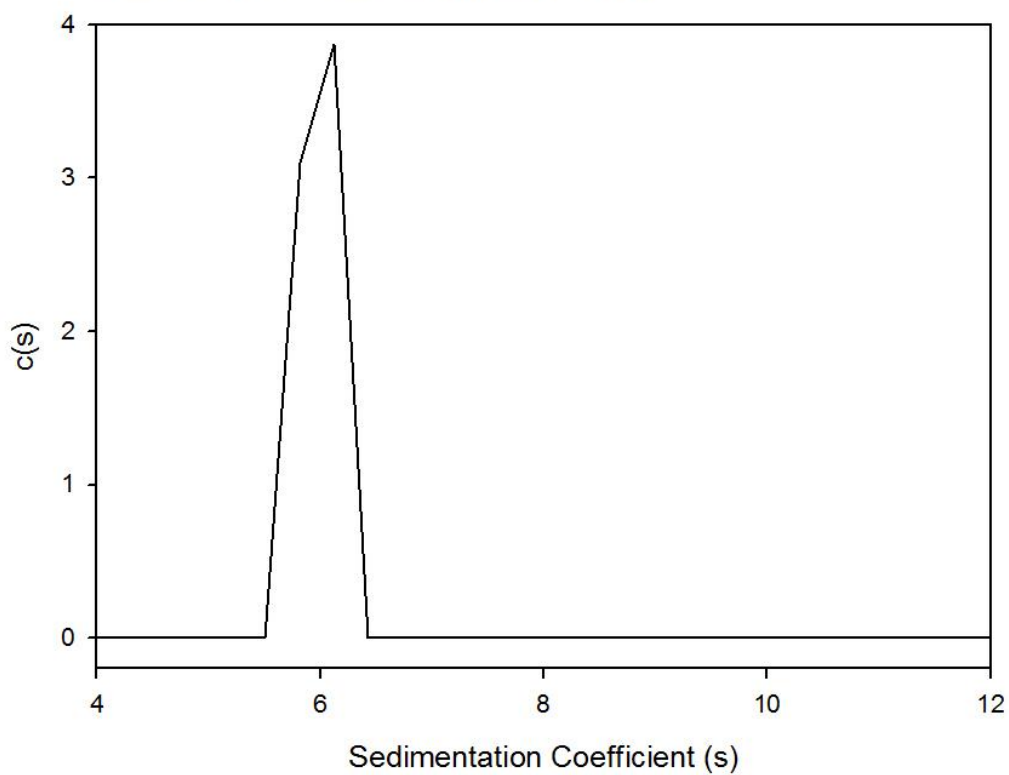
SB338 30K AB4 c(s) distribution



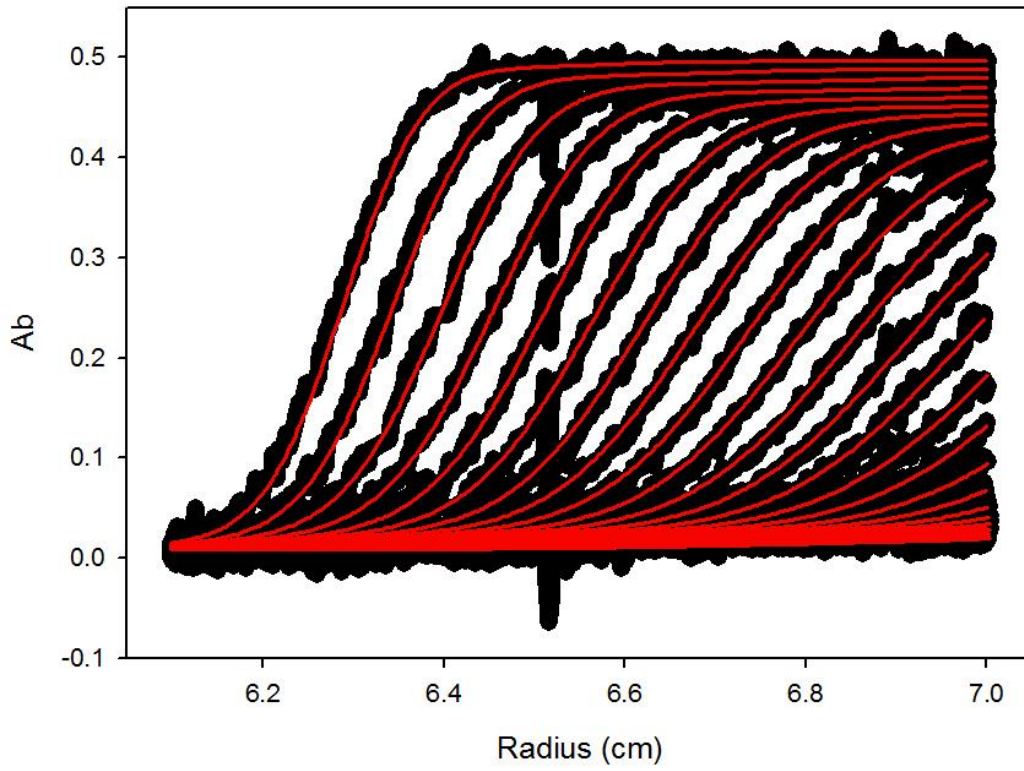
SB338 30K AB6



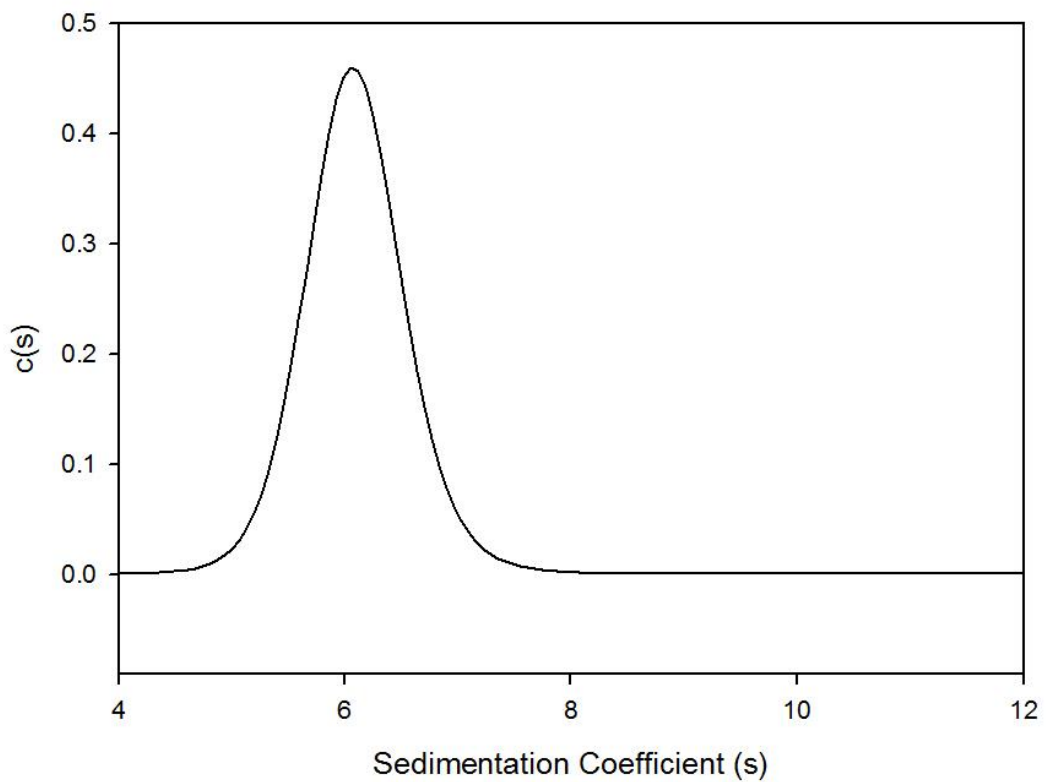
SB338 30K AB6 c(s) distribution



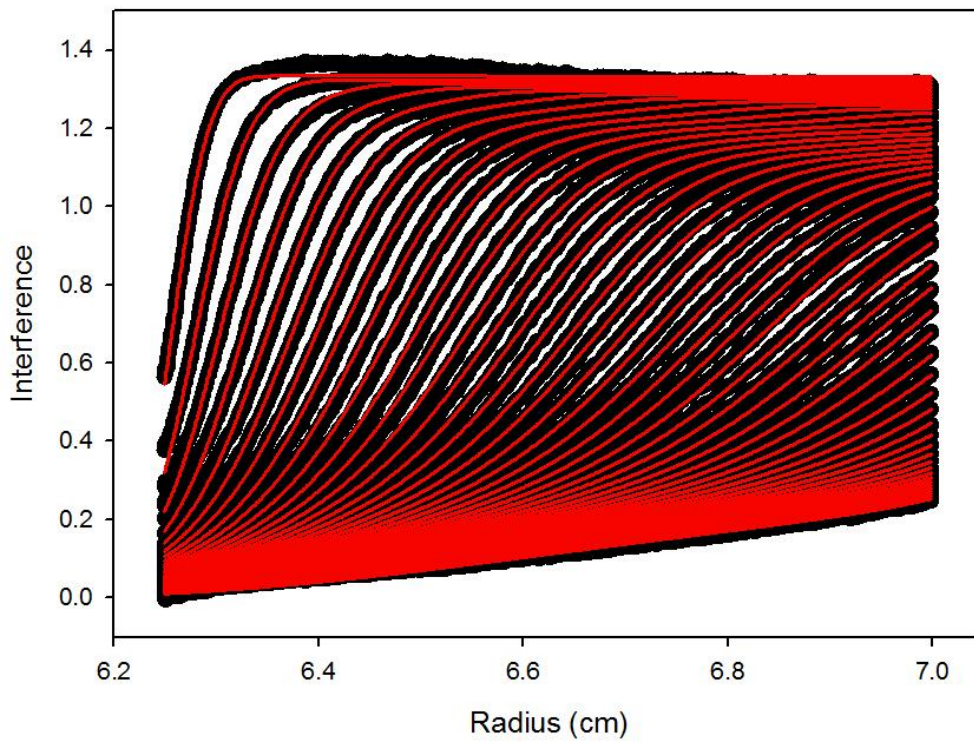
SB338 30K AB7.



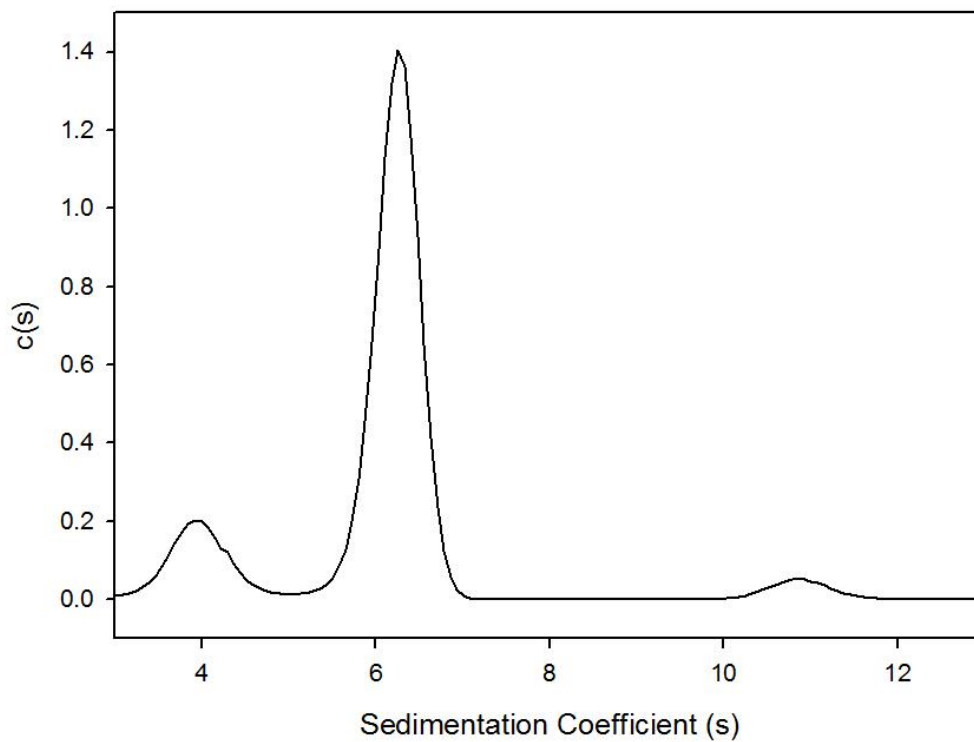
SB338 30K AB7. $c(s)$ distribution



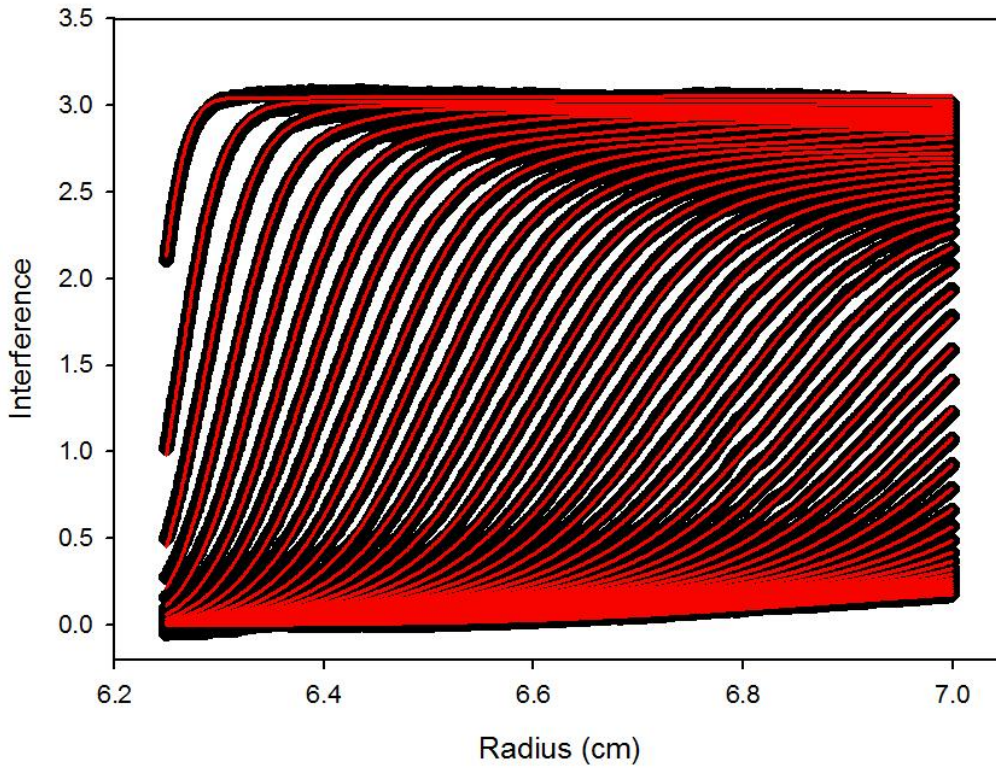
SB338 30K IP2



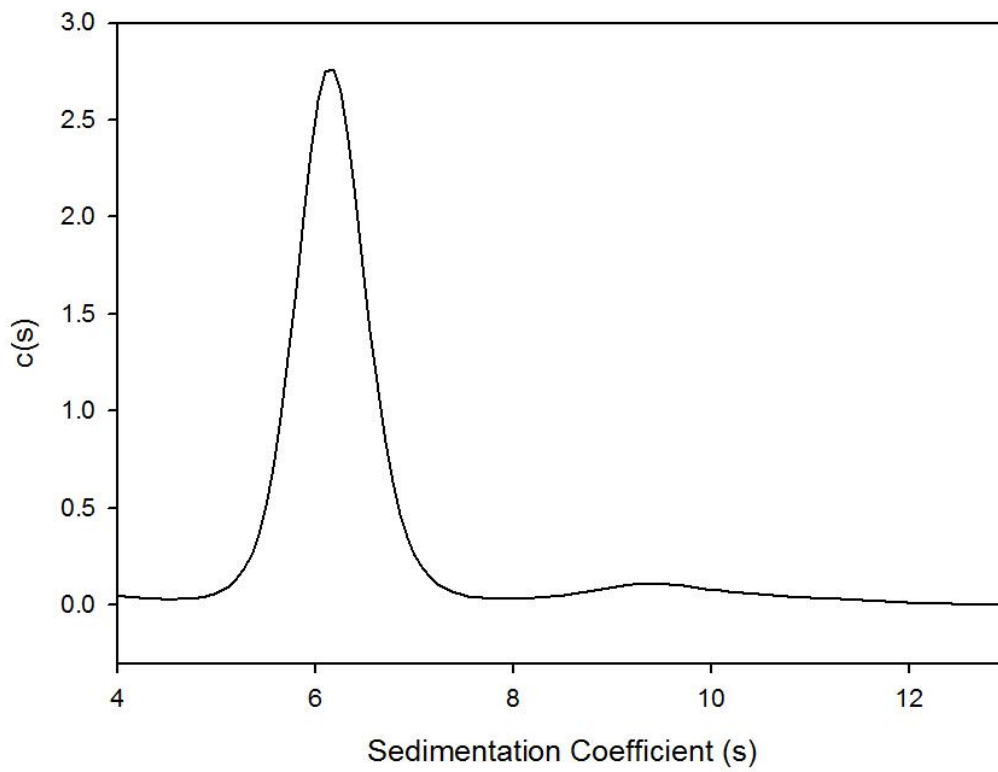
SB338 30K IP2 c(s) distribution



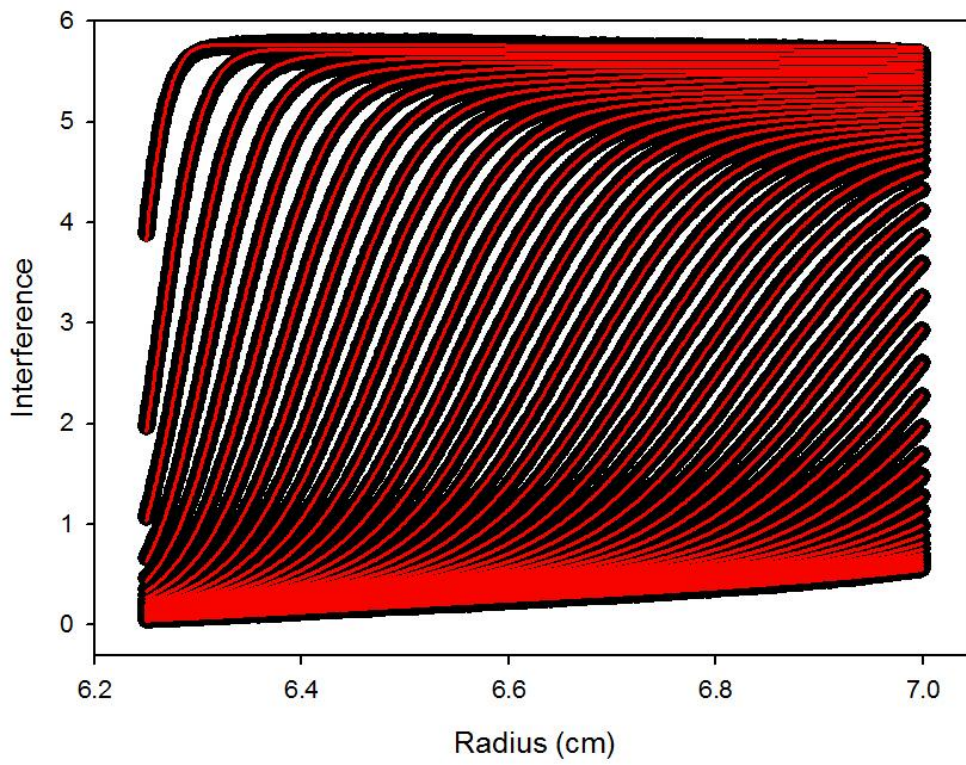
SB338 30K IP4



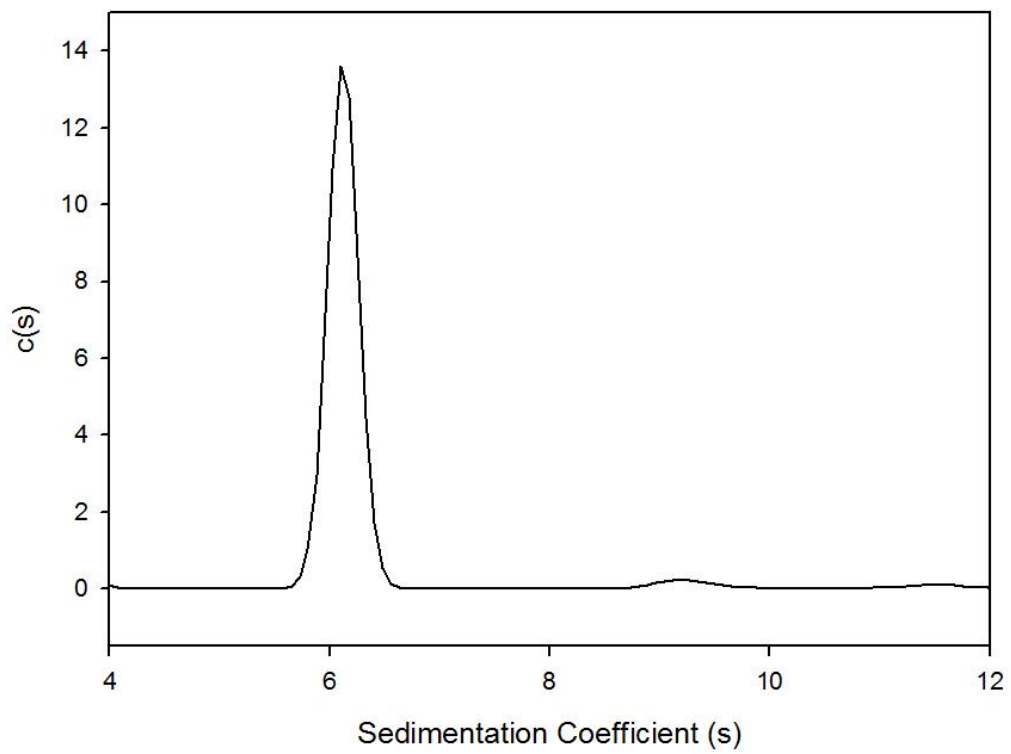
SB338 30K IP4 c(s) distribution



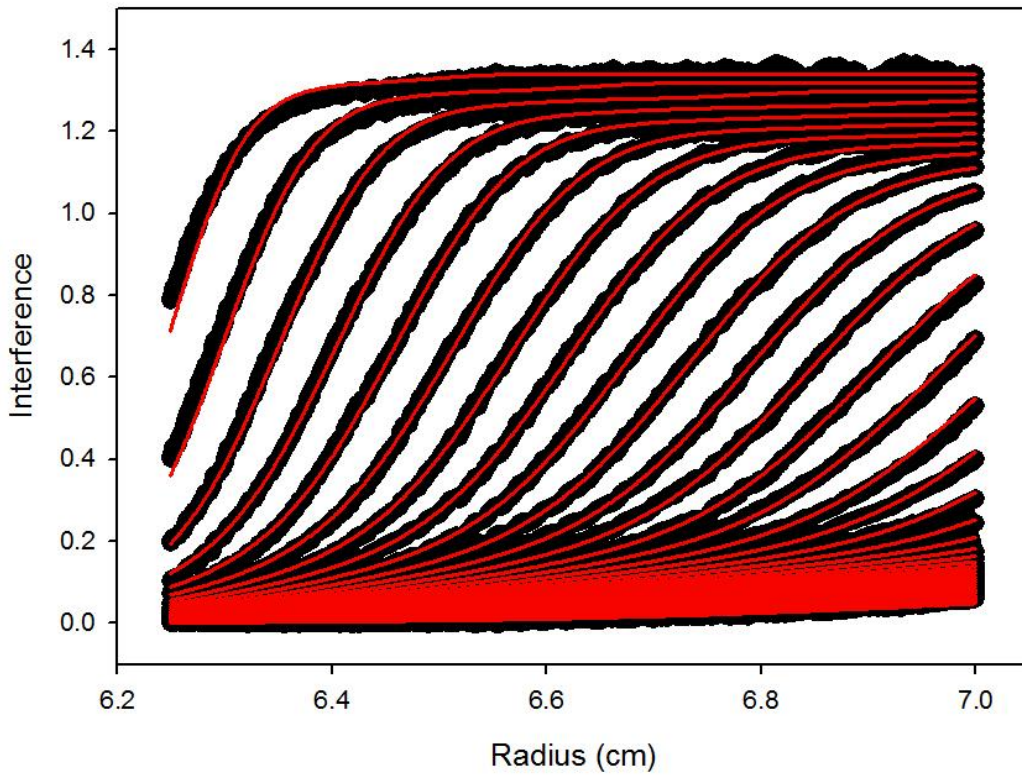
SB338 30K IP6



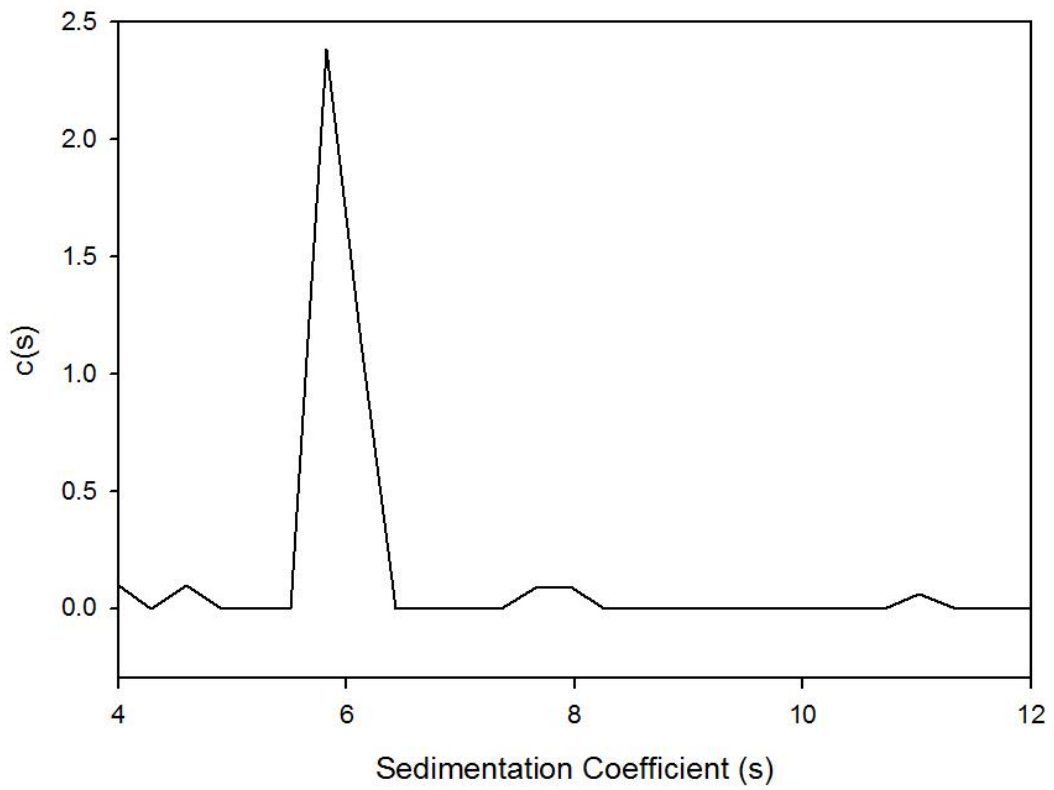
SB338 30K IP6 c(s) distribution



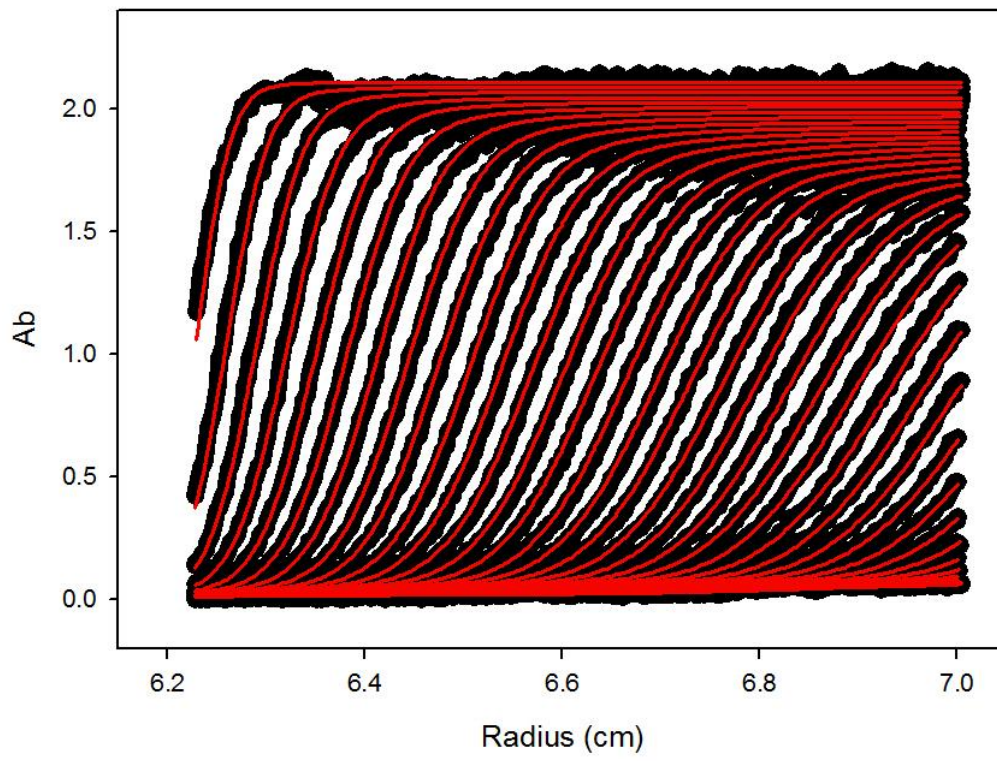
SB338 30K IP7



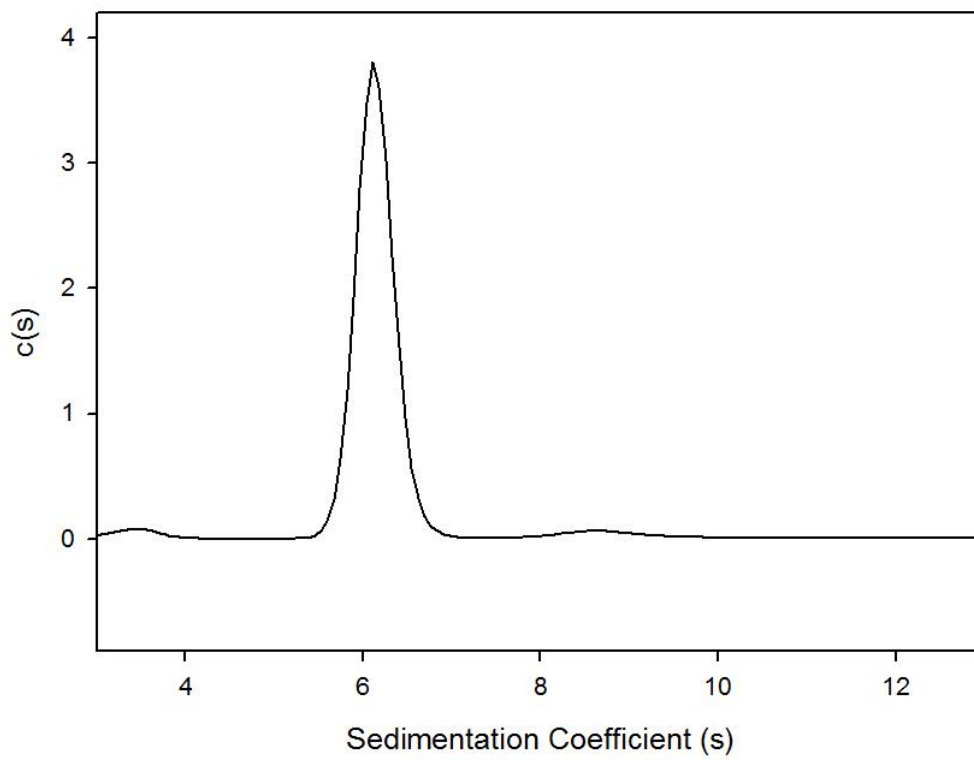
SB338 30K IP7 c(s) distribution



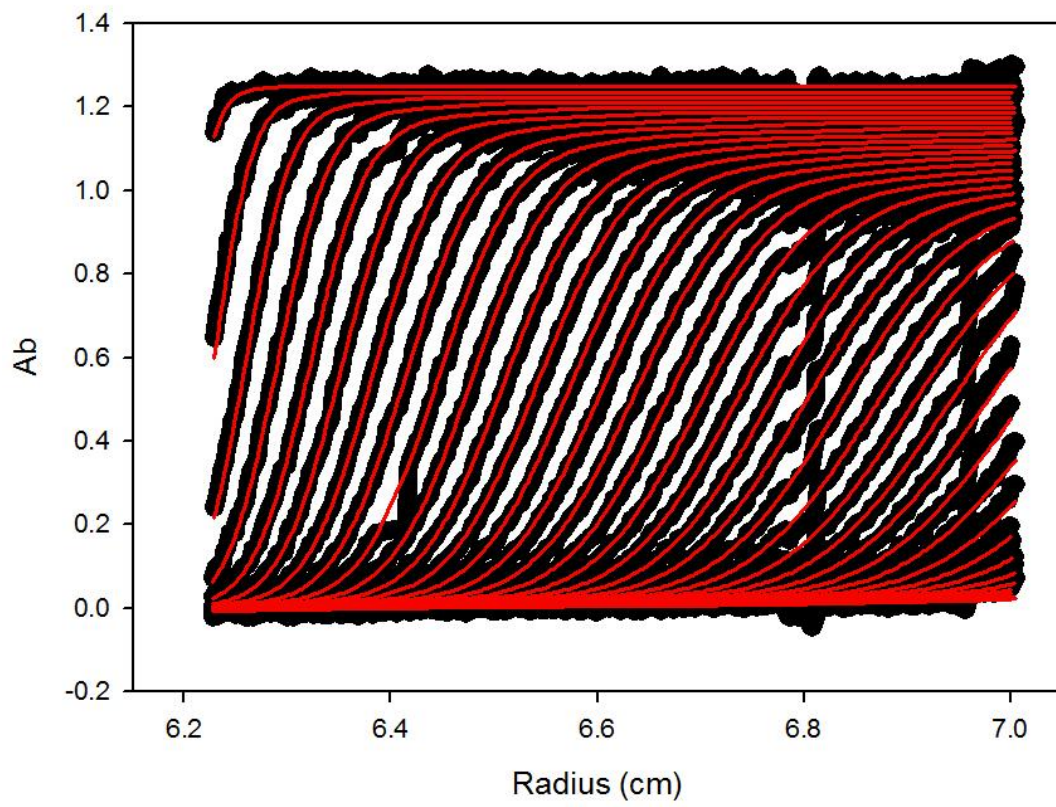
SB338 40K AB1



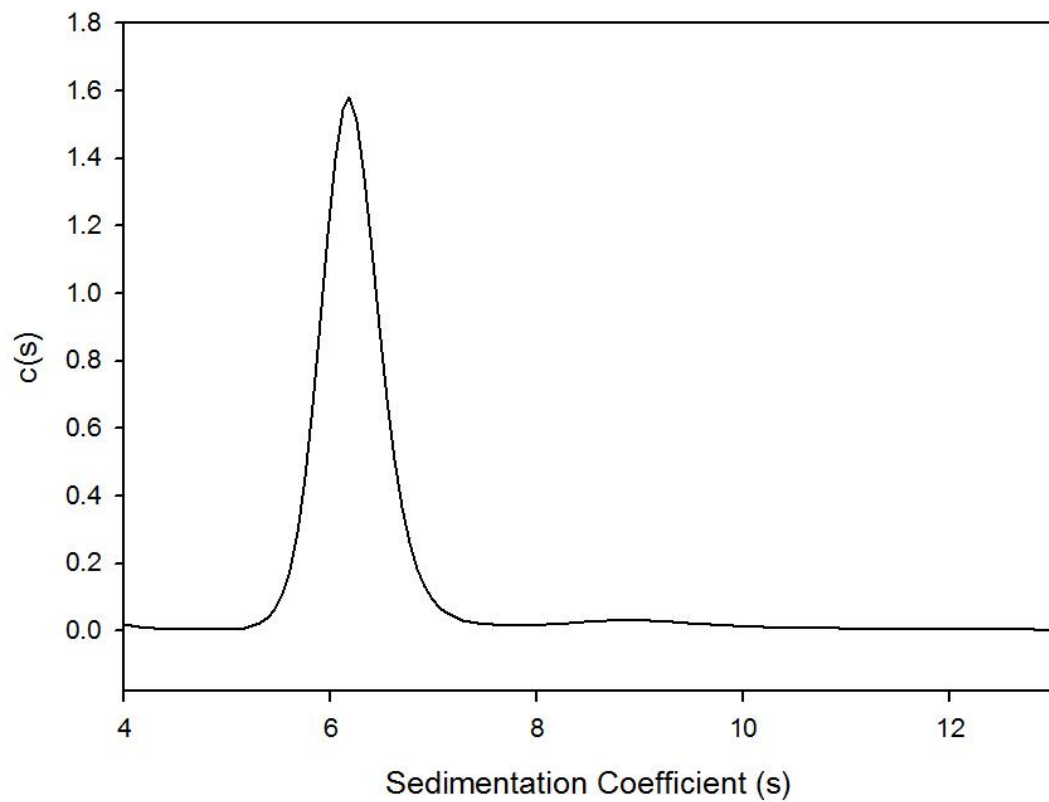
SB338 49K AB1 c(s) distribution



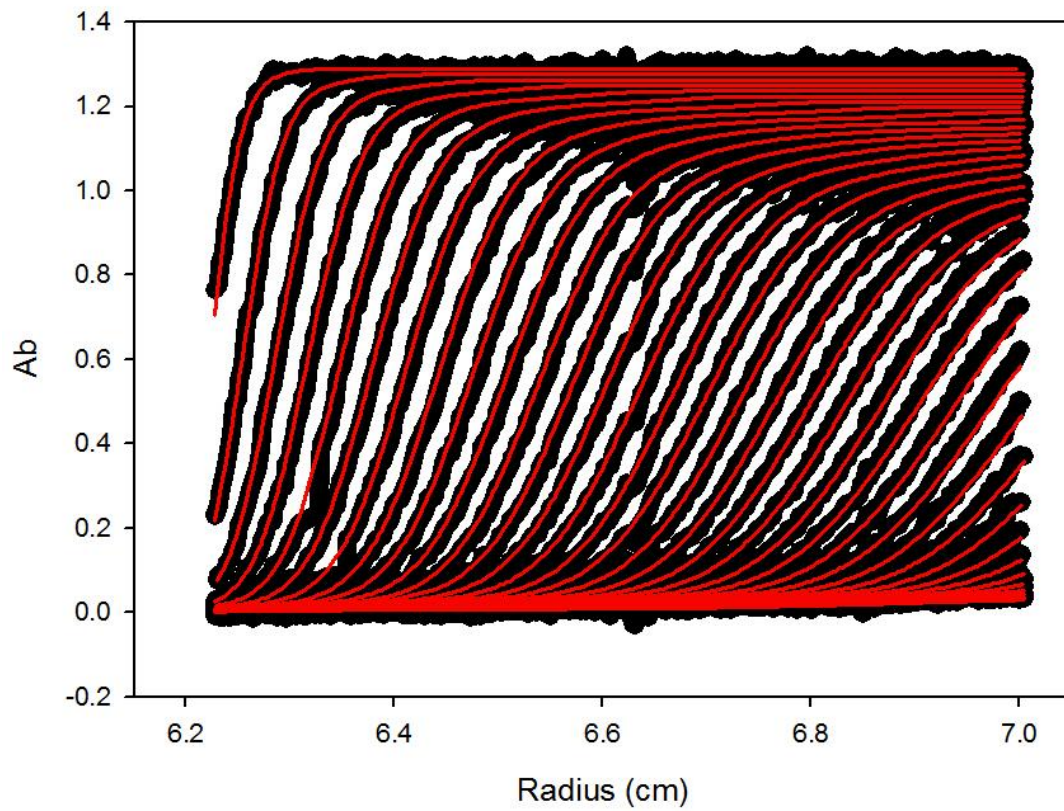
SB338 40K AB2



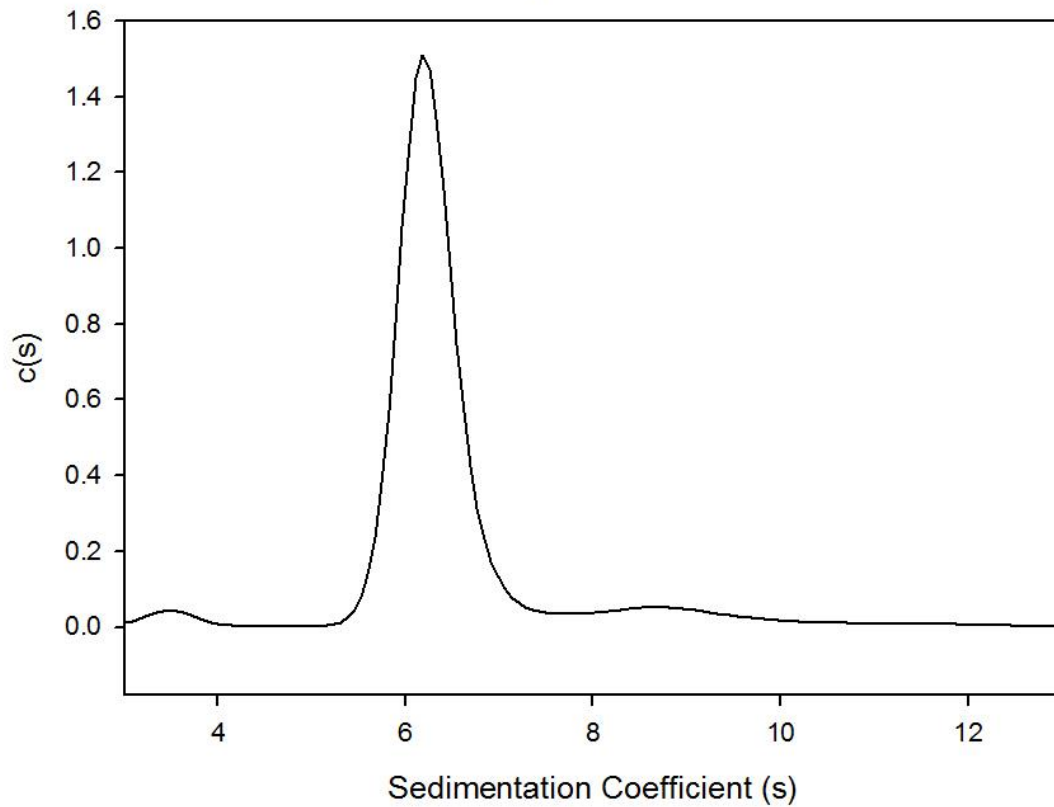
SB338 40K AB2 c(s) distribution



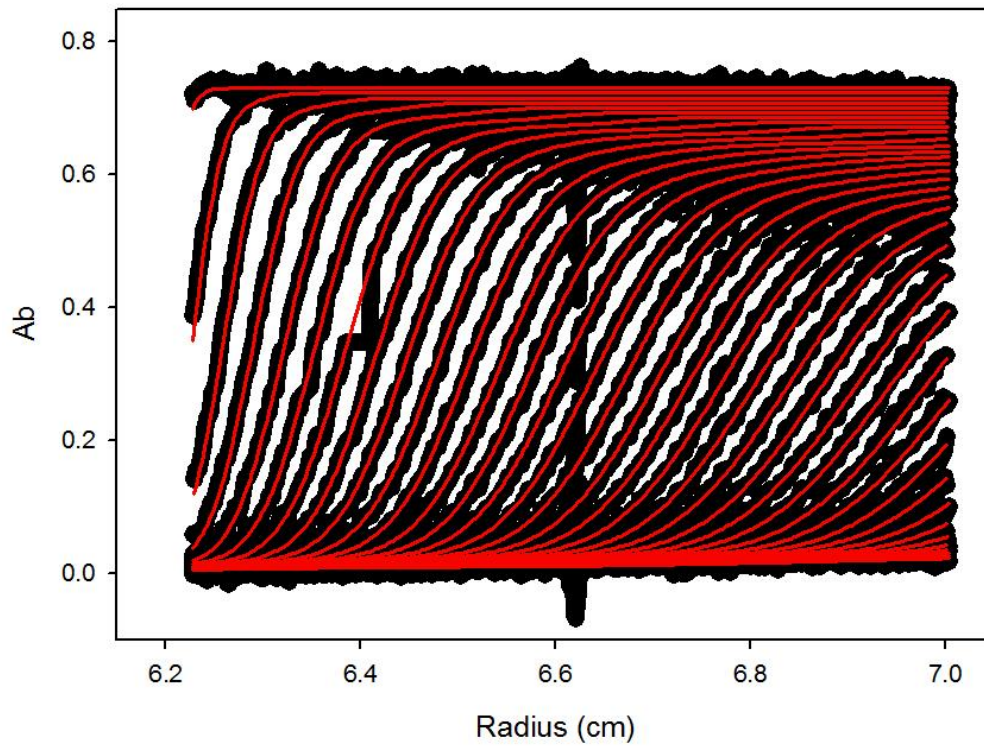
SB338 40K AB3



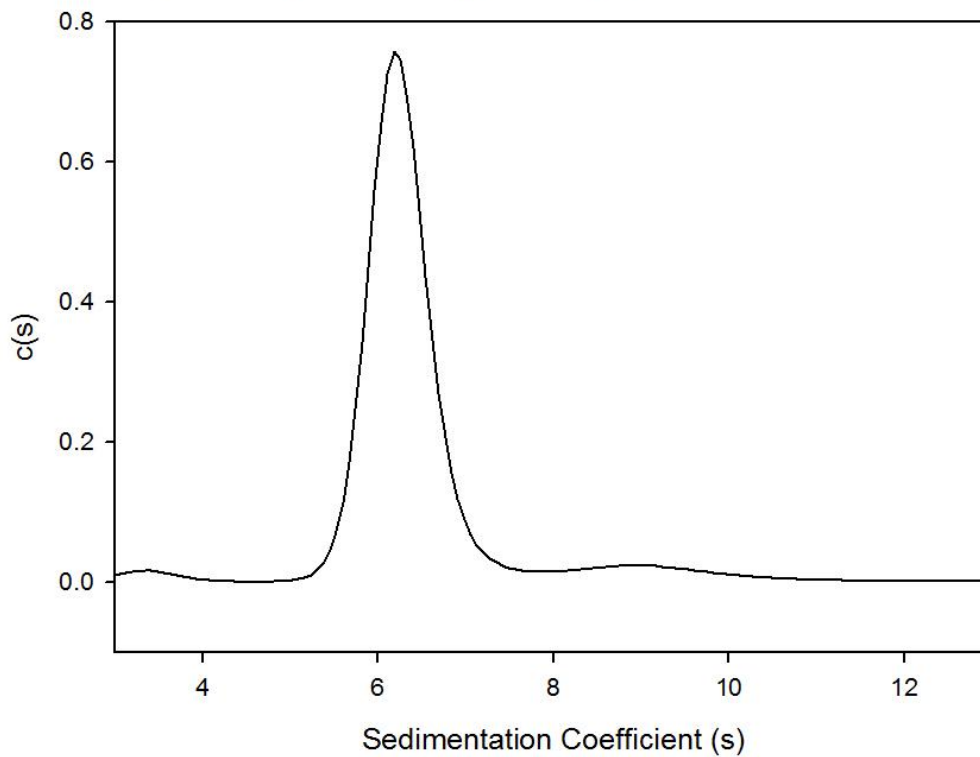
SB338 40K AB3 c(s) distribution



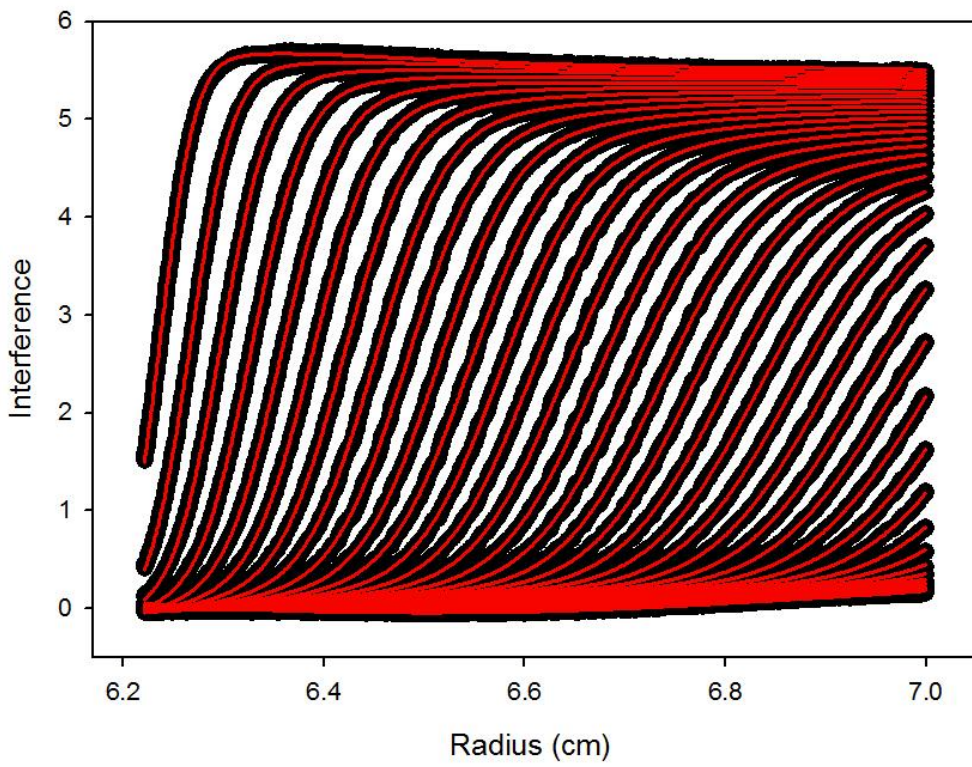
SB338 40K AB4



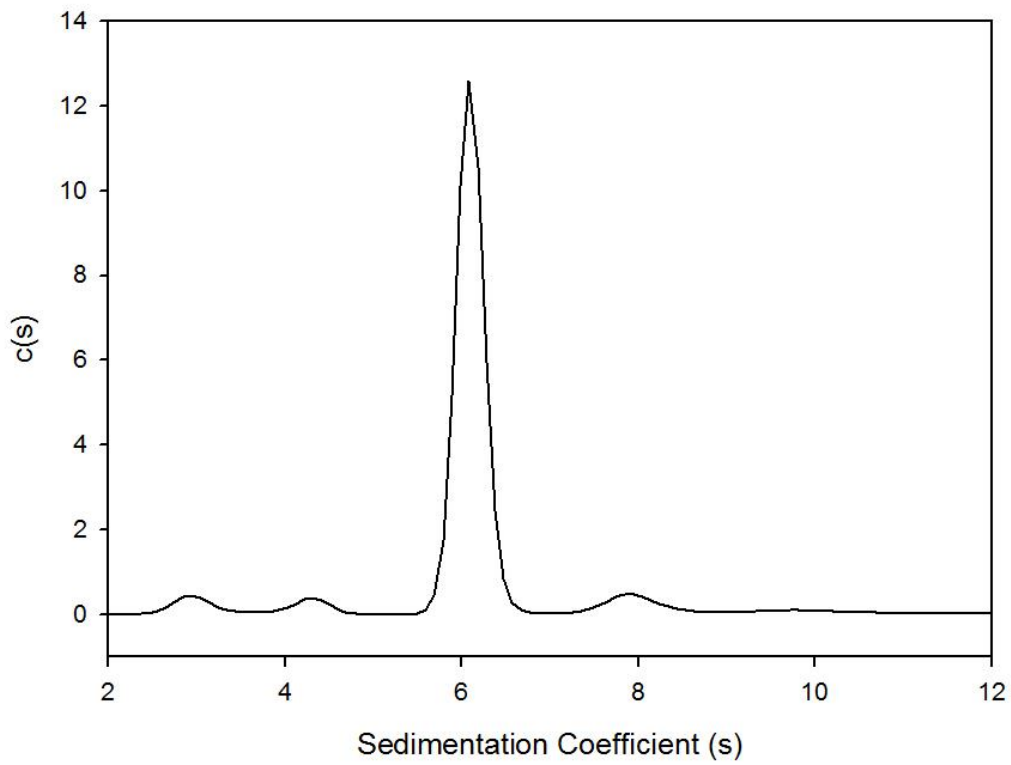
SB338 40K AB4 c(s) distribution



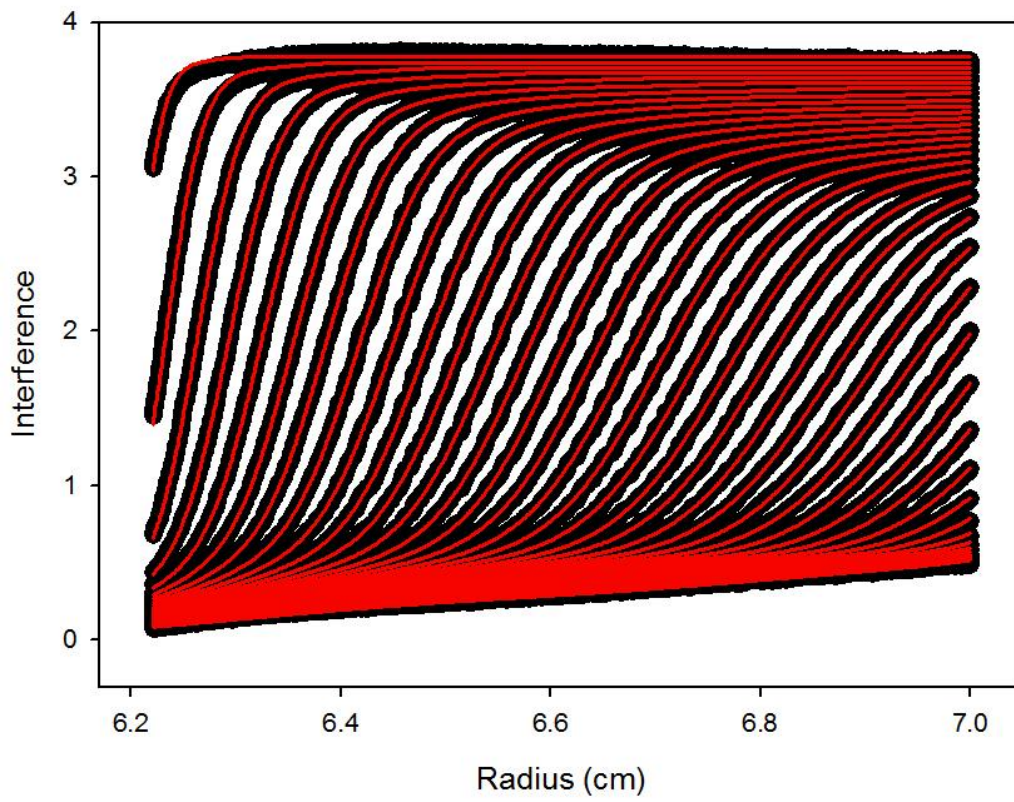
SB338 40K IP1



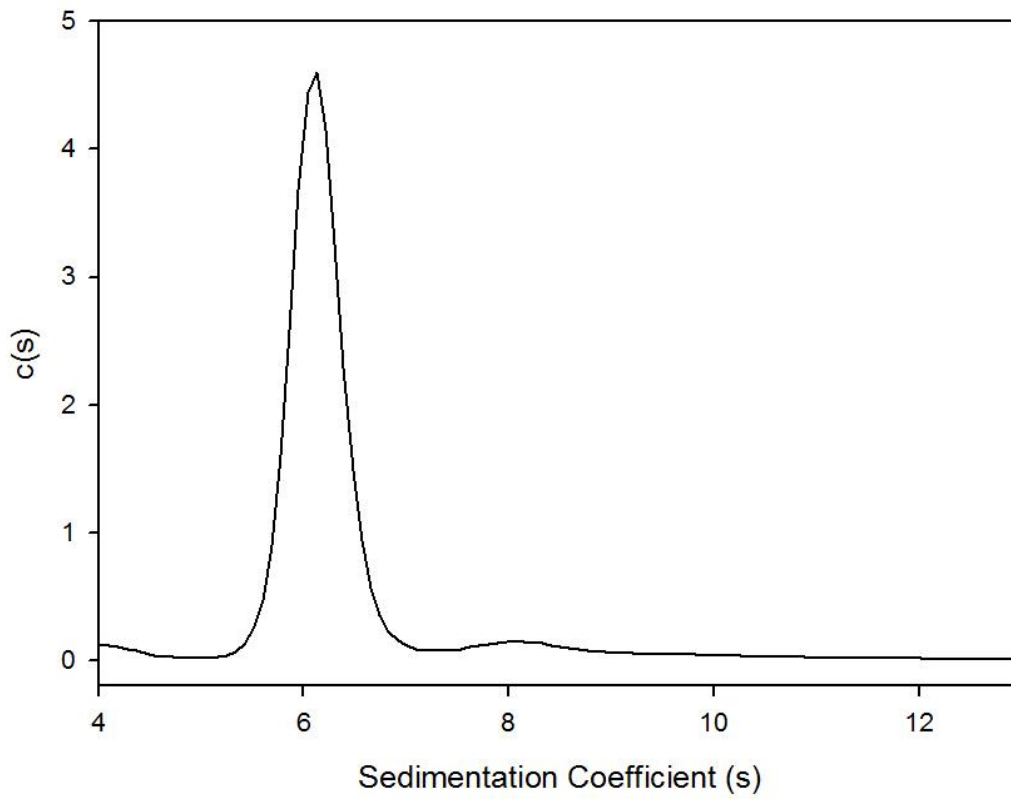
SB338 40K IP1 c(s) distribution



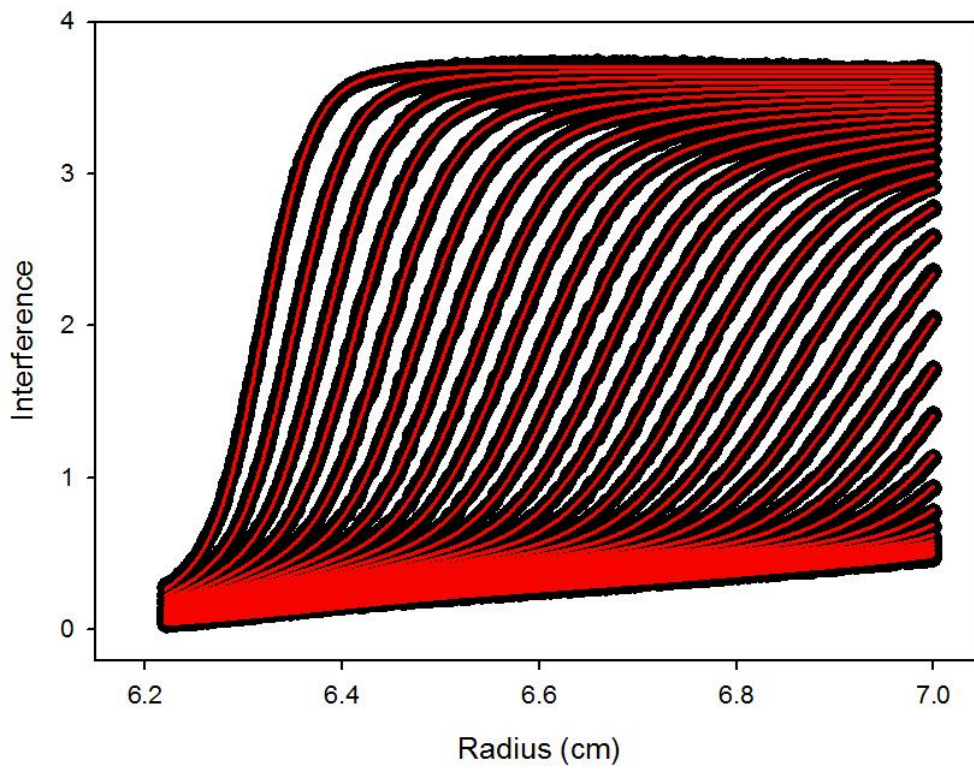
SB338 40K IP2



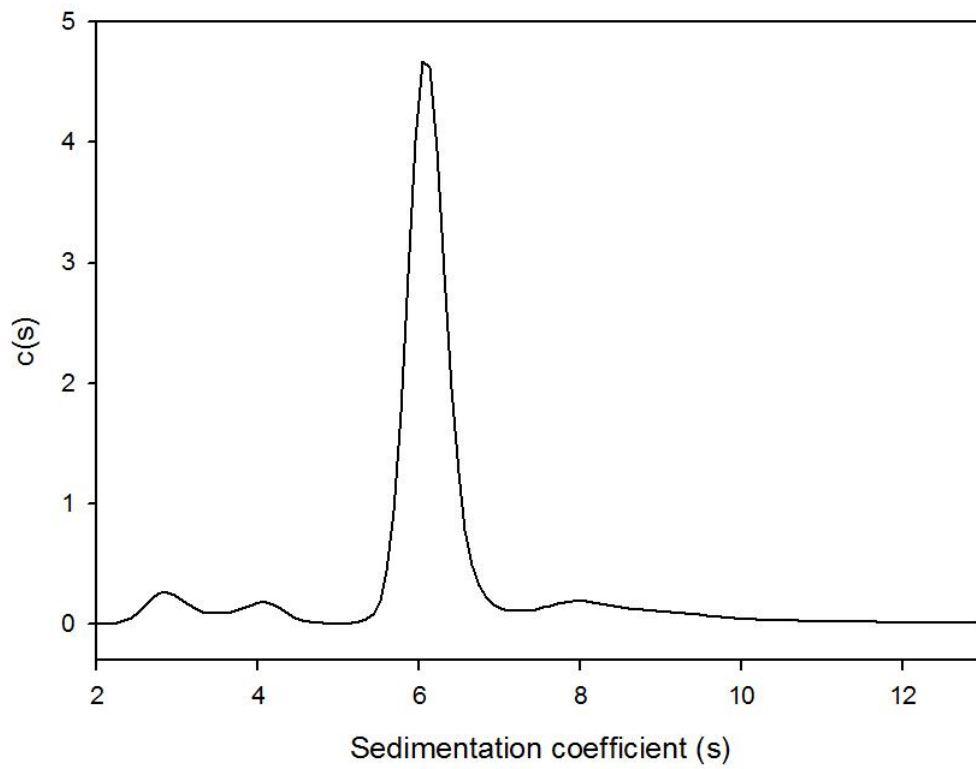
SB338 40K IP2 c(s) distribution



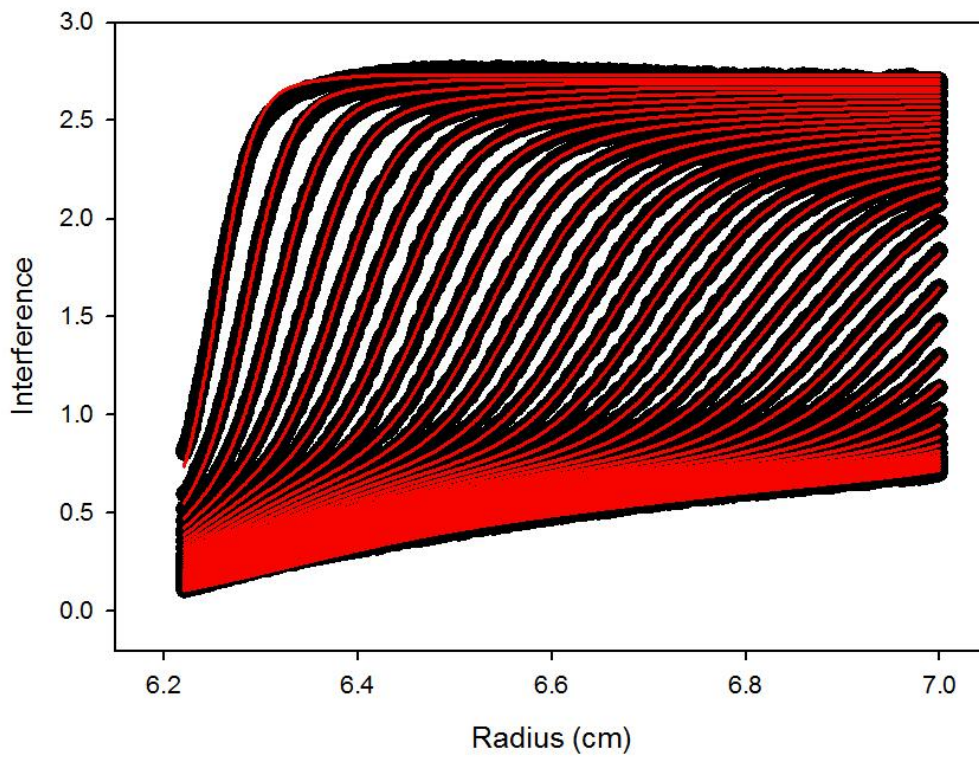
SB338 40K IP3



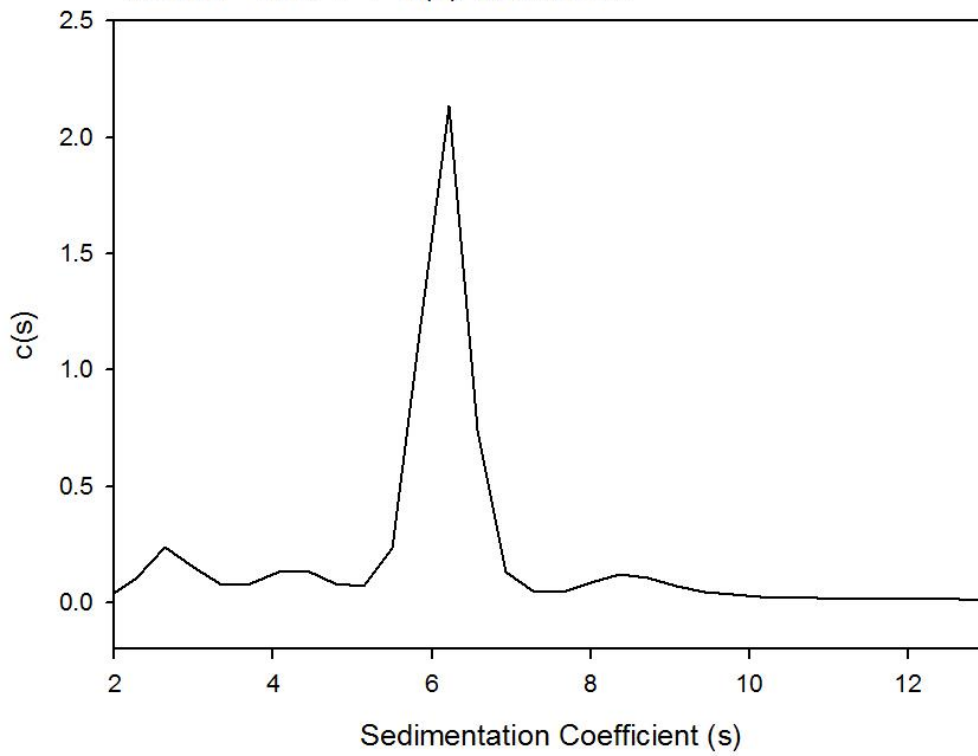
SB338 40K IP3 c(s) distribution



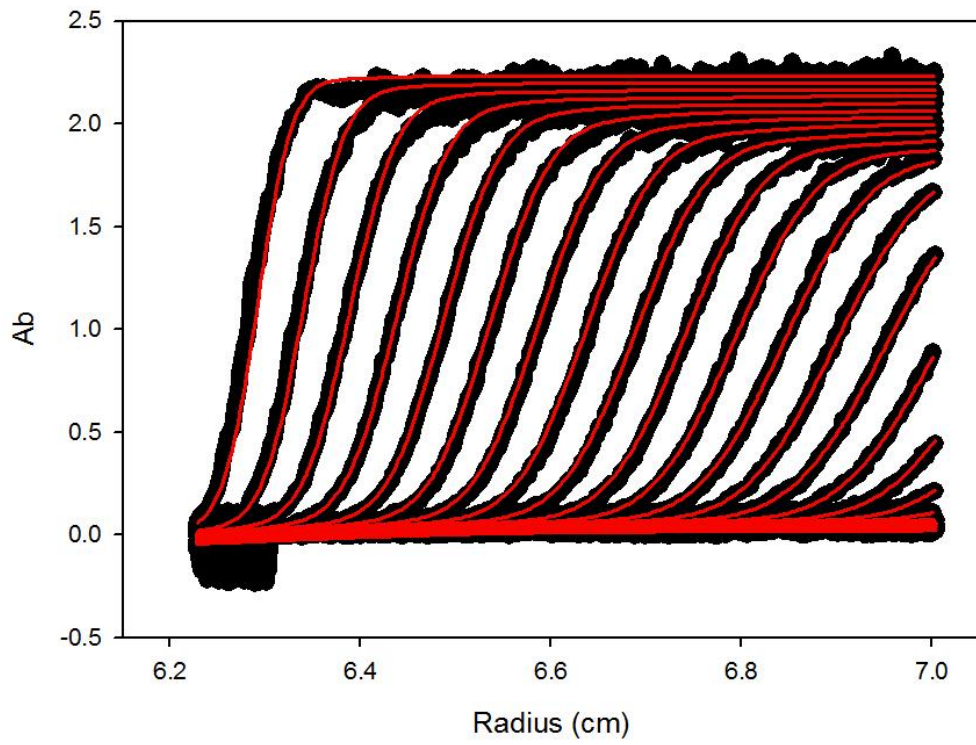
SB338 40K IP1



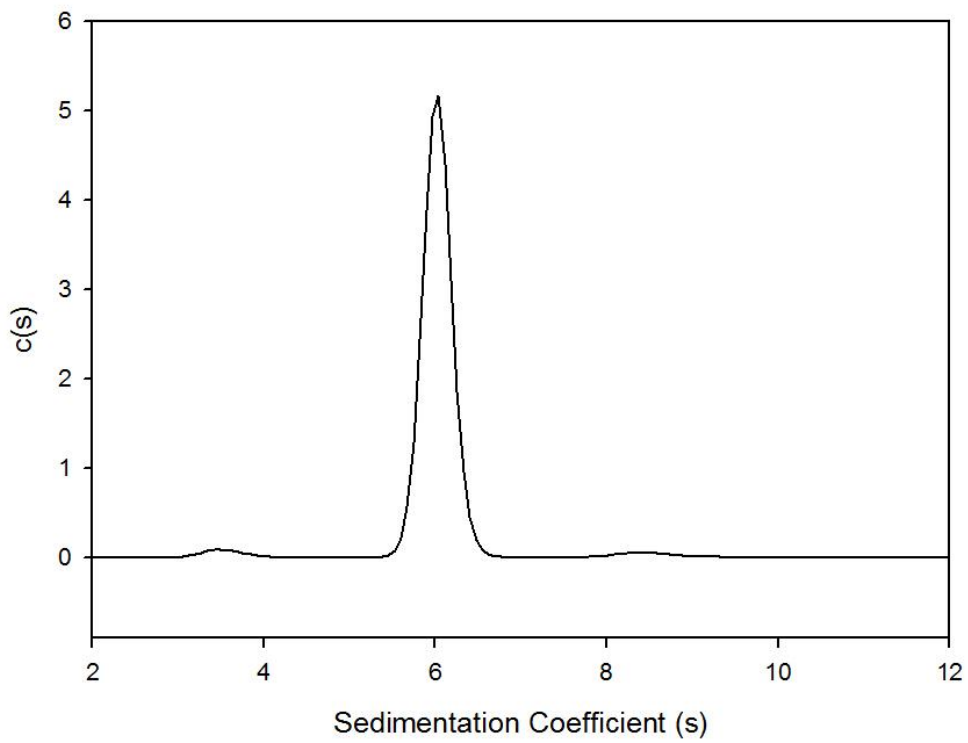
SB338 40K IP1 c(s) distribution



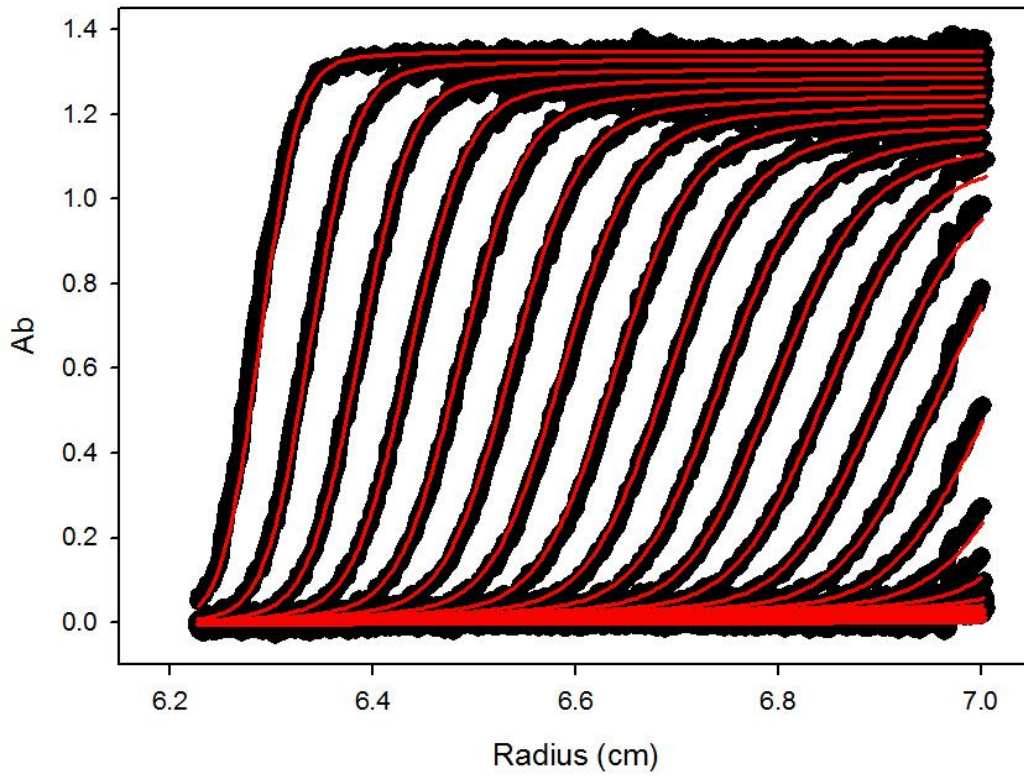
SB338 50K AB1



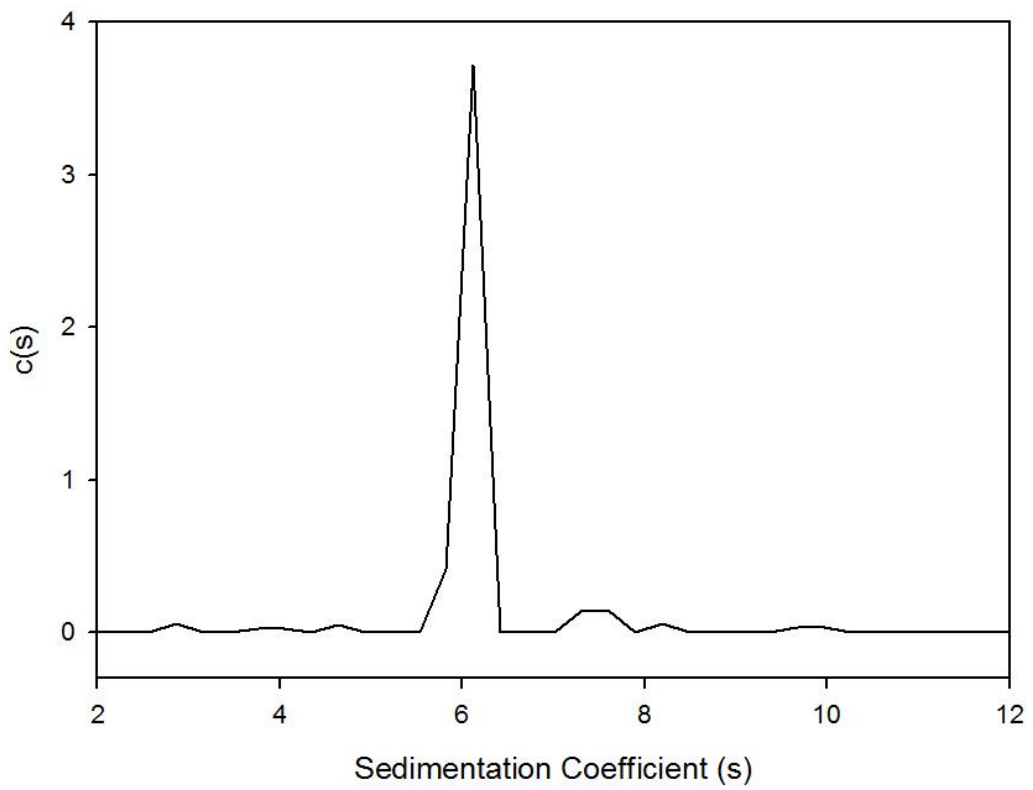
SB338 50K AB1 c(s) distribution



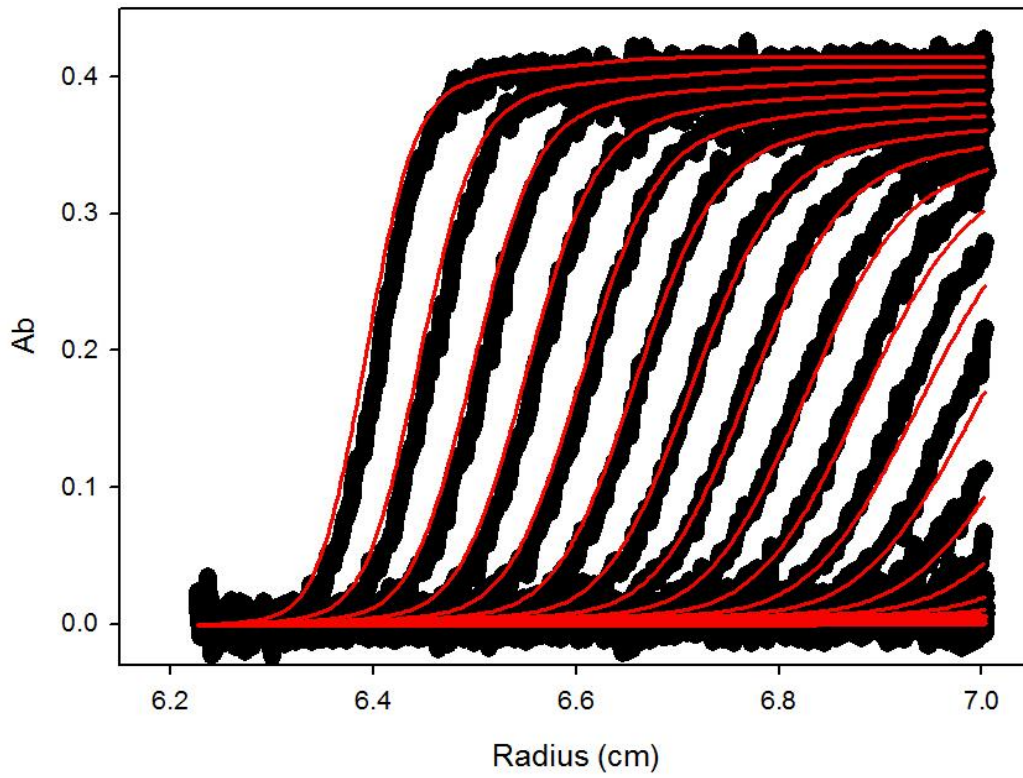
SB338 50K AB2



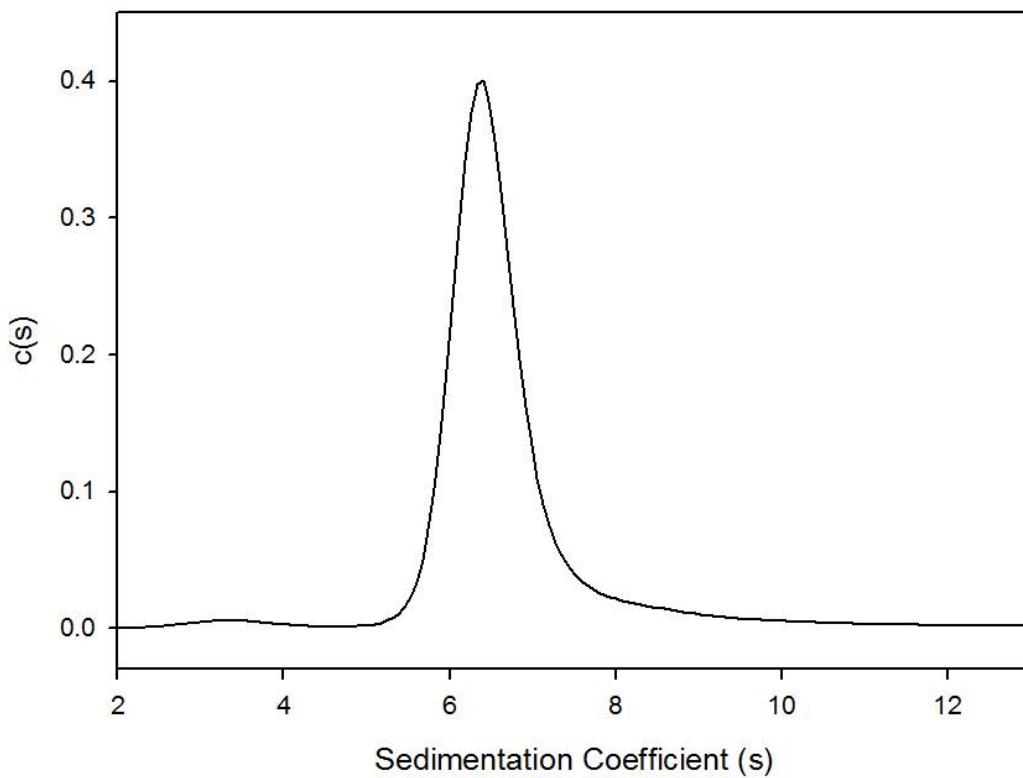
SB338 50K AB2 c(s) distribution



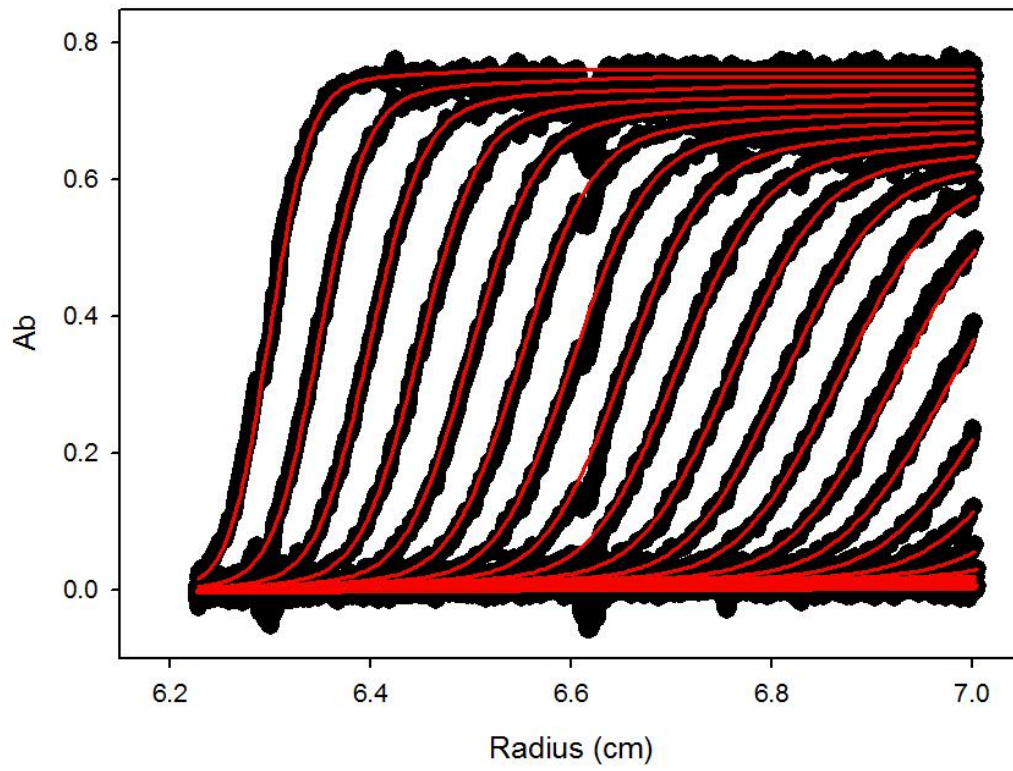
SB338 50K AB3



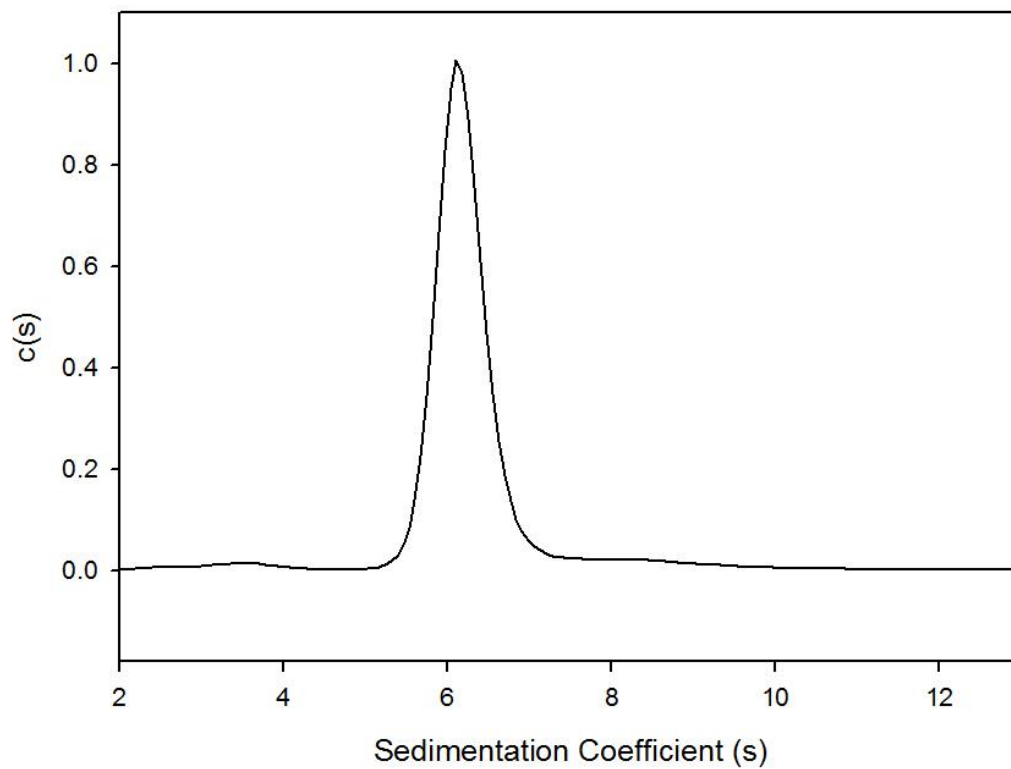
SB338 50K AB3 c(s) distribution



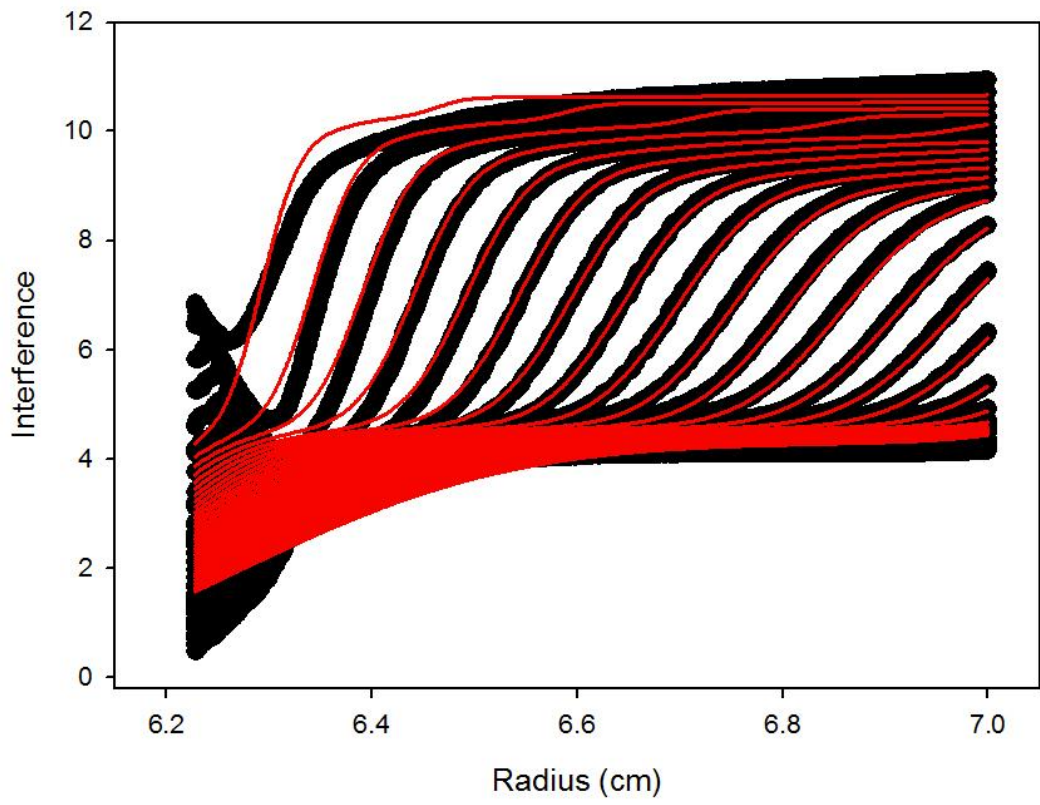
SB338 50K AB4



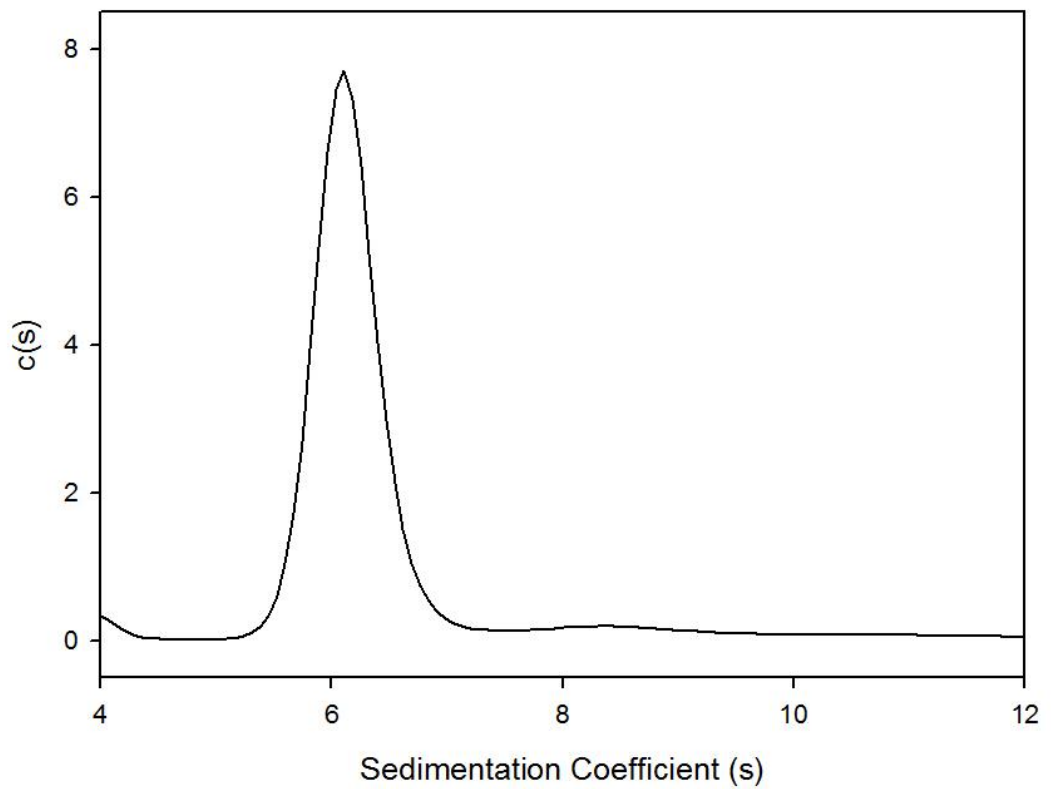
SB338 50K AB4 c(s) distribution



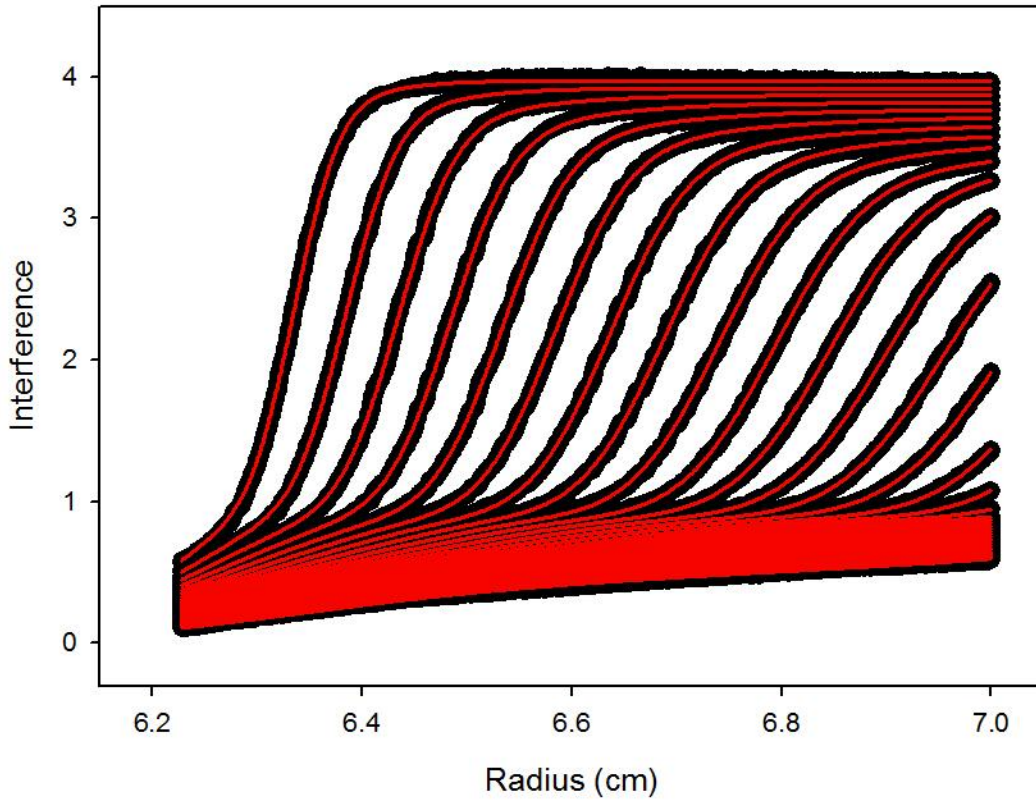
SB338 50K IP1



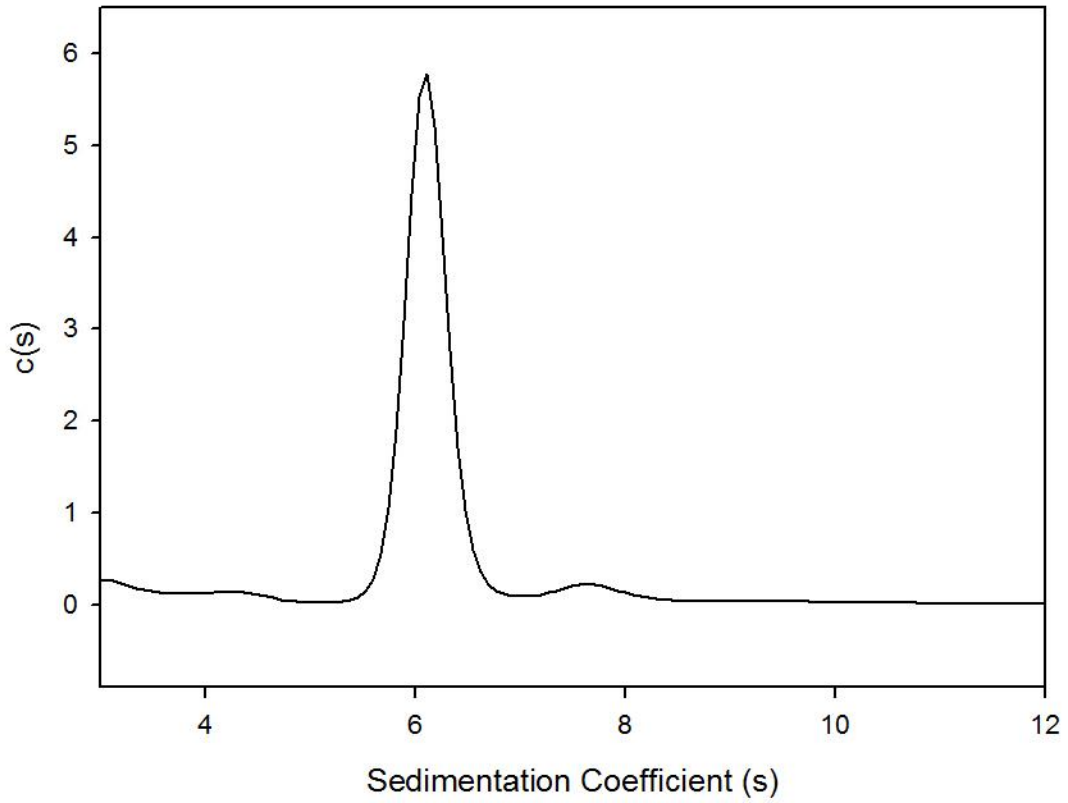
SB338 50K IP1 c(s) distribution



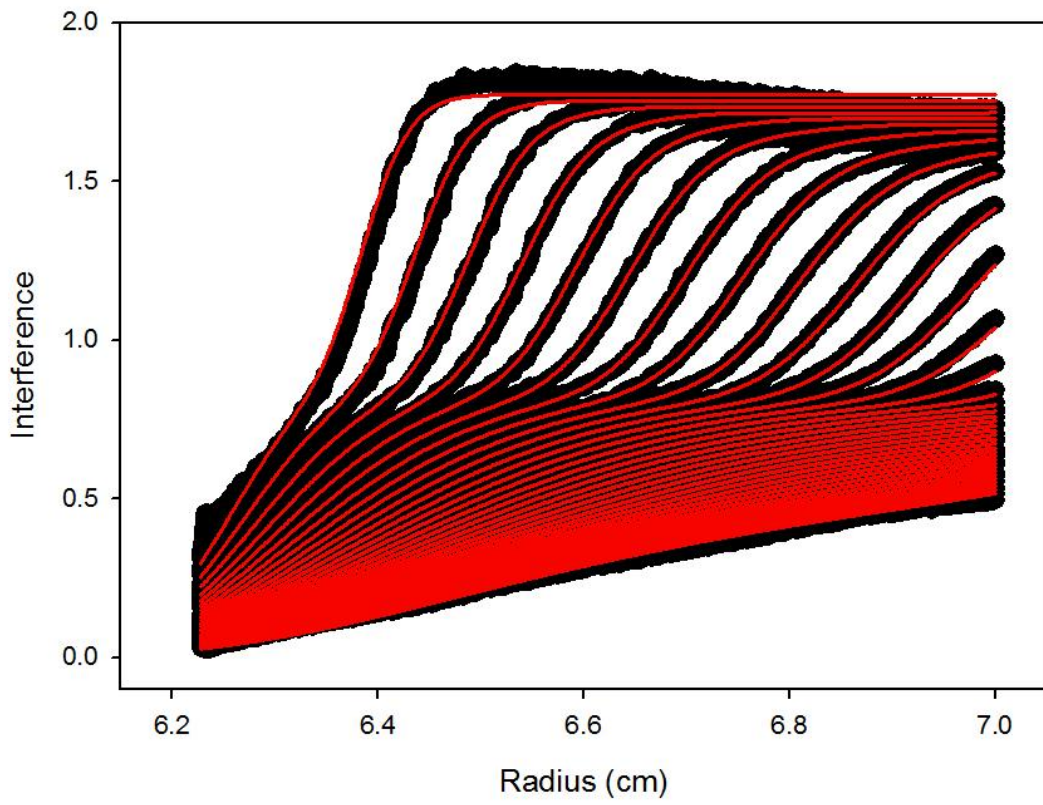
SB338 50K IP2



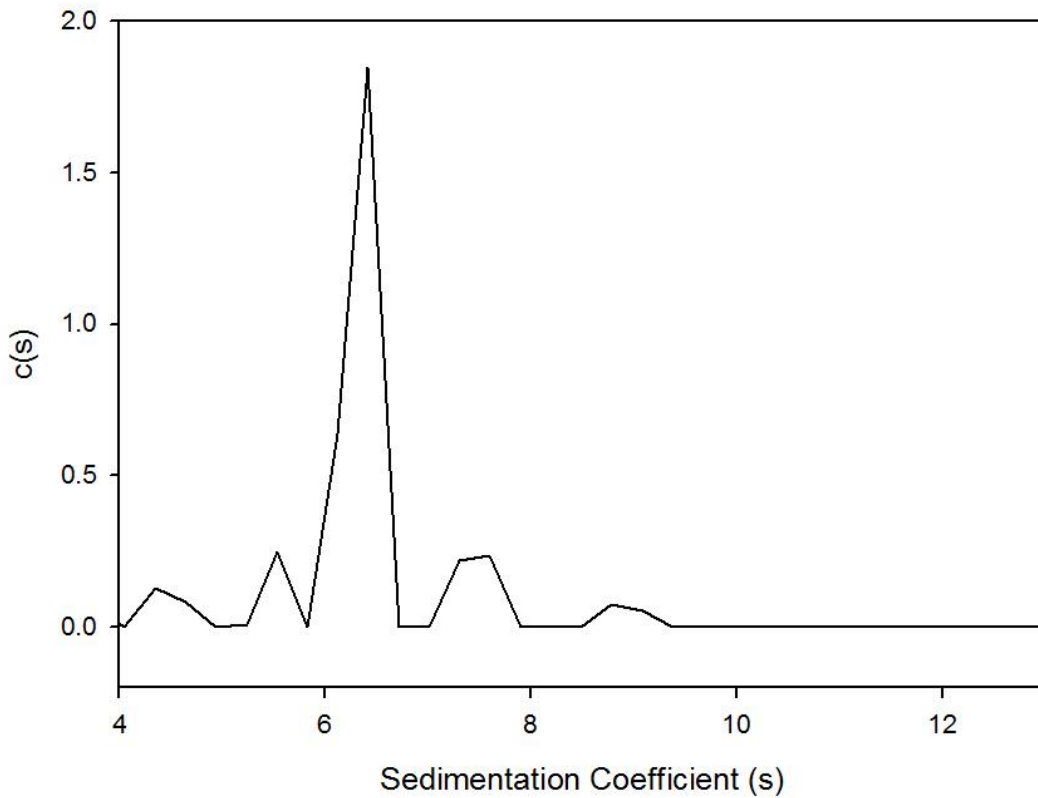
SB338 50K IP2 c(s) distribution



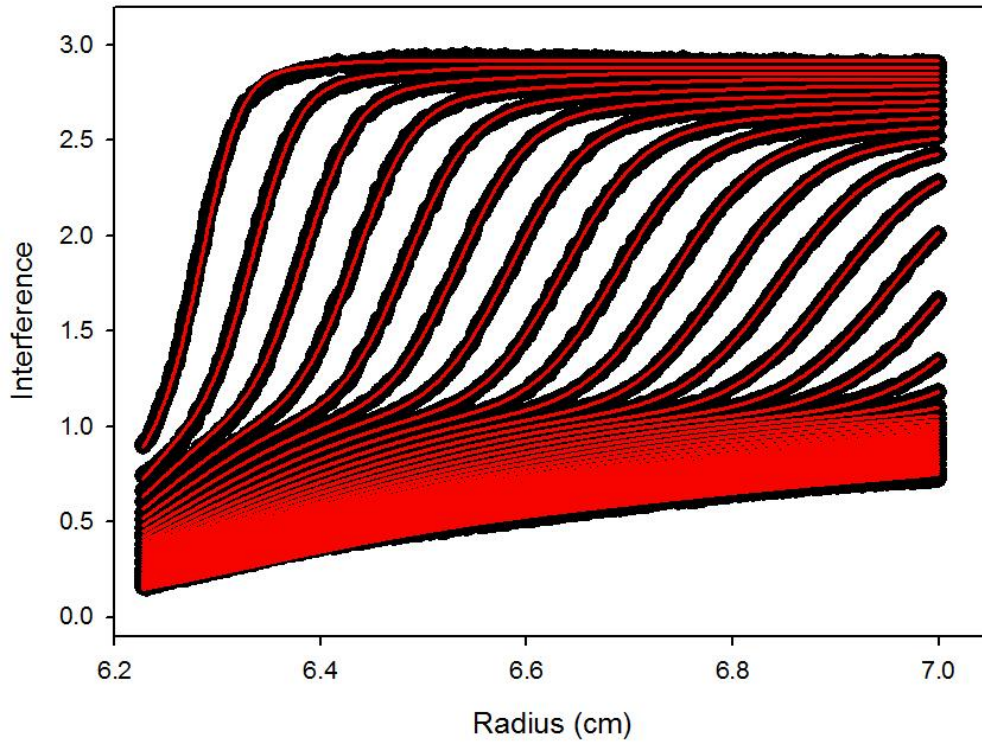
SB338 50K IP3



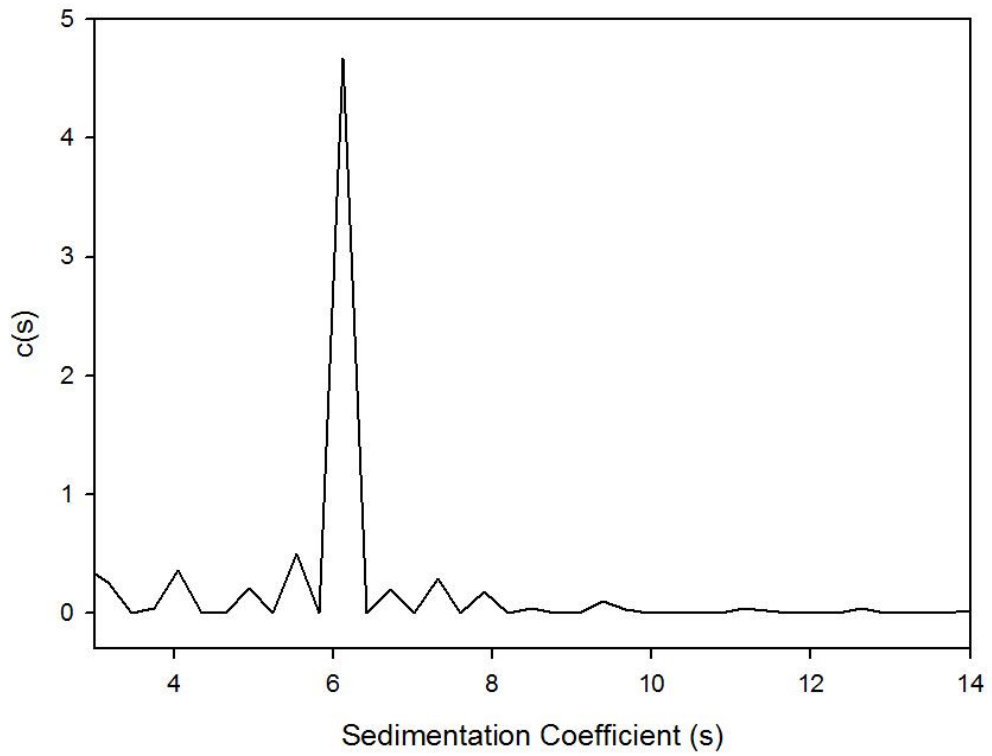
SB338 50K IP3 c(s) distribution



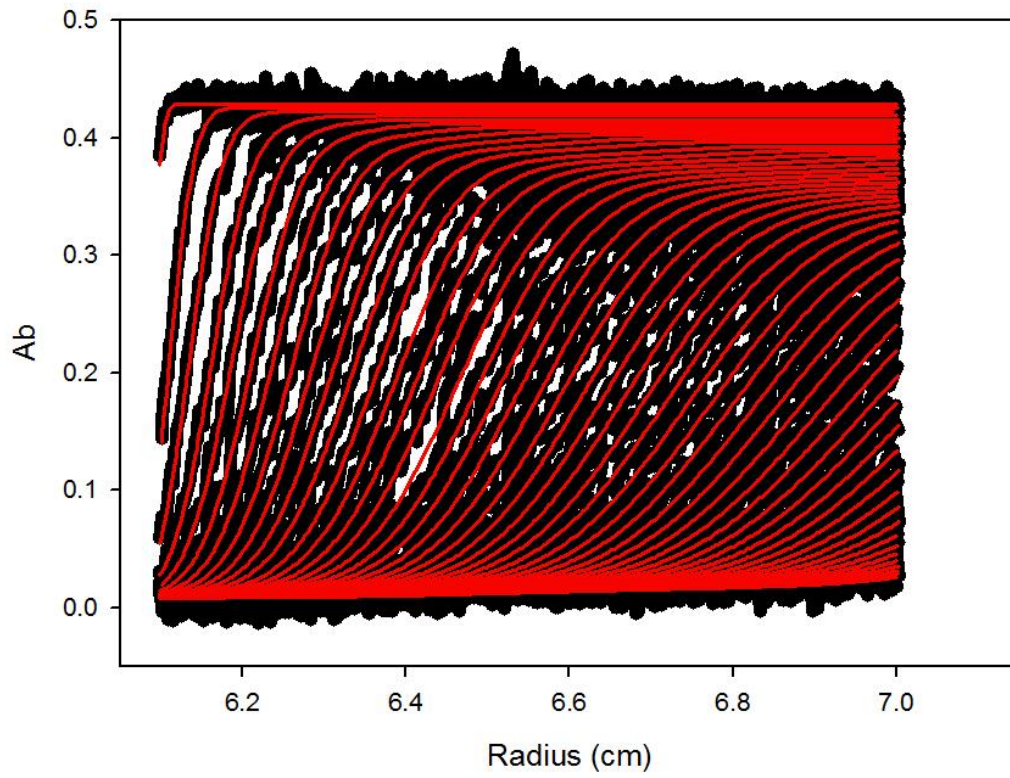
SB338 50K IP4



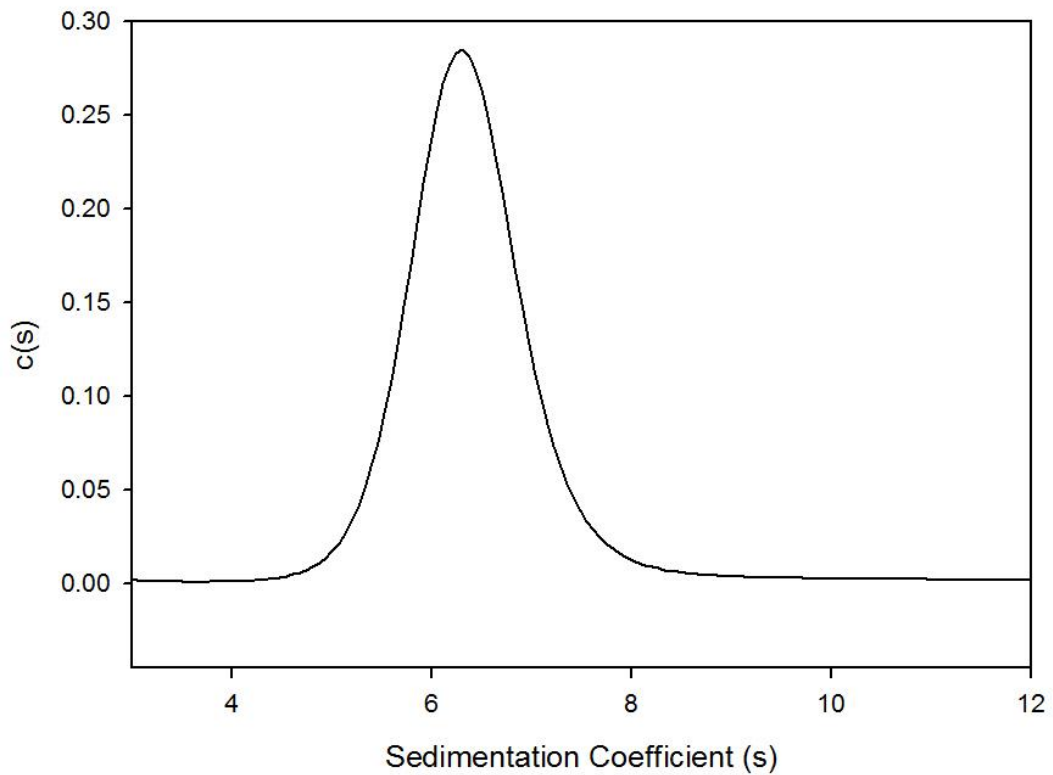
SB338 50K IP4 c(s) distribution



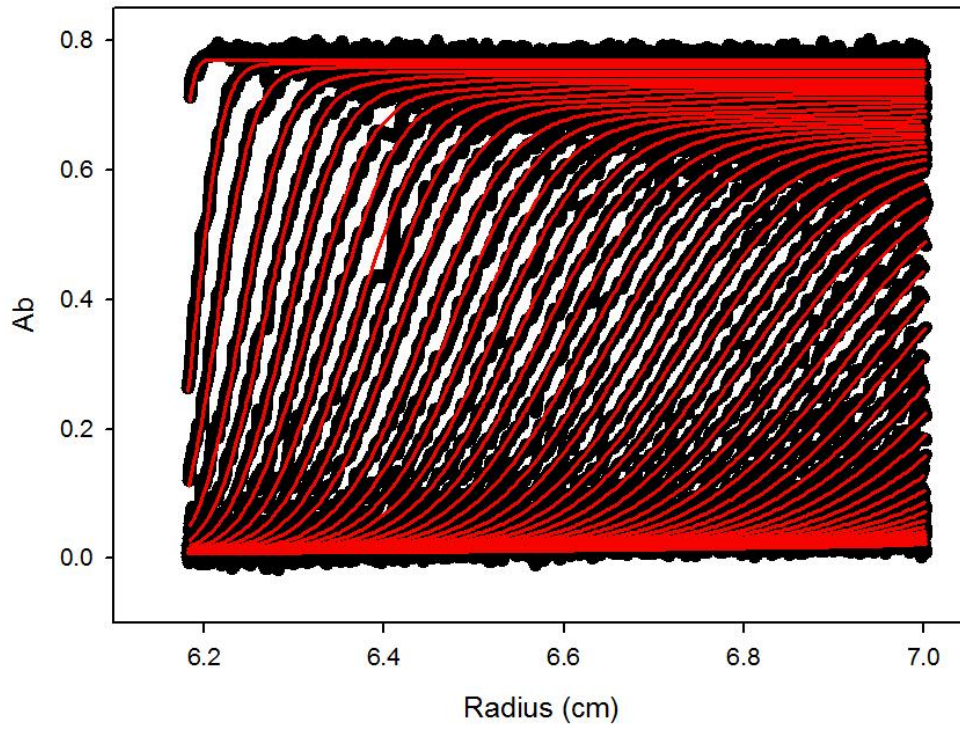
Jk 30K AB2



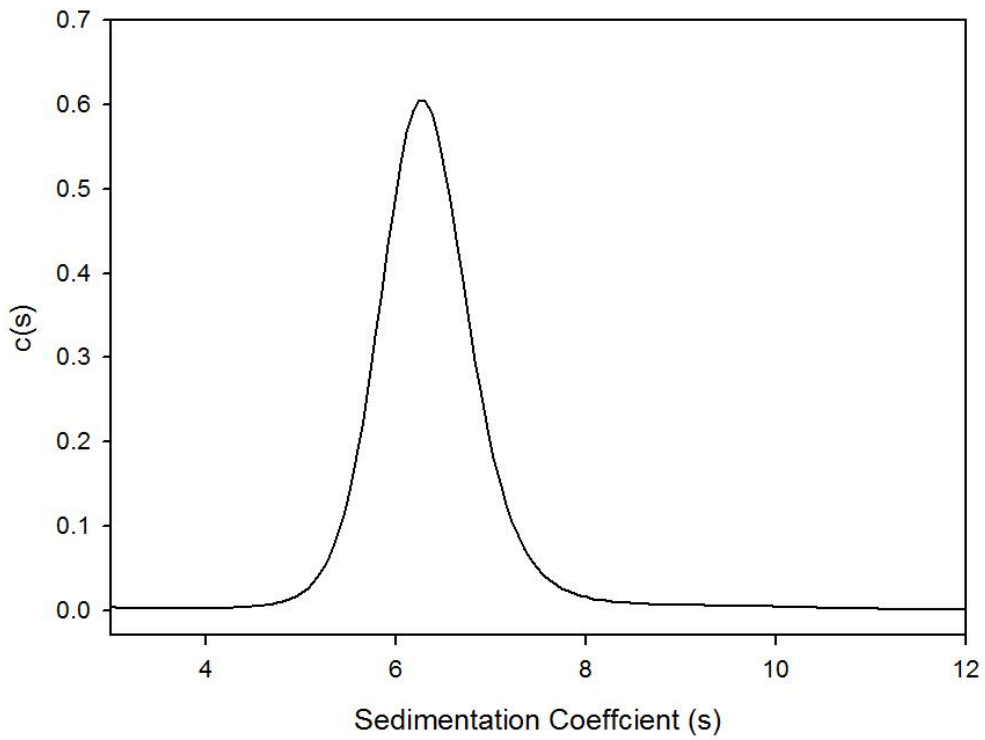
Jk 30K AB2 c(s) distribution



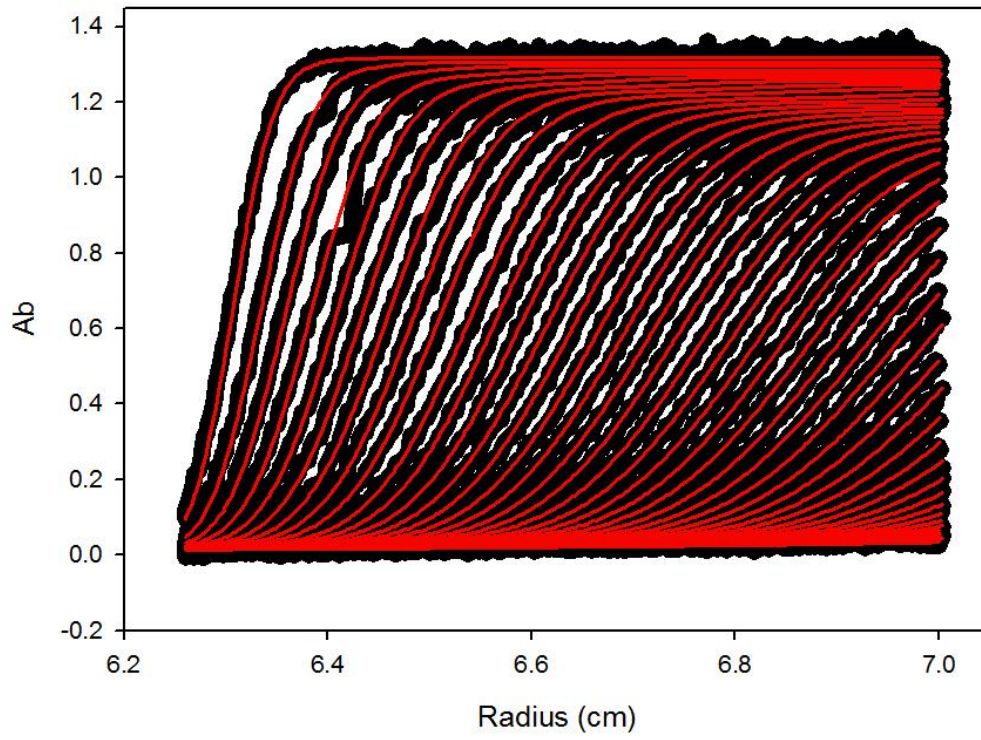
JK 30K AB4



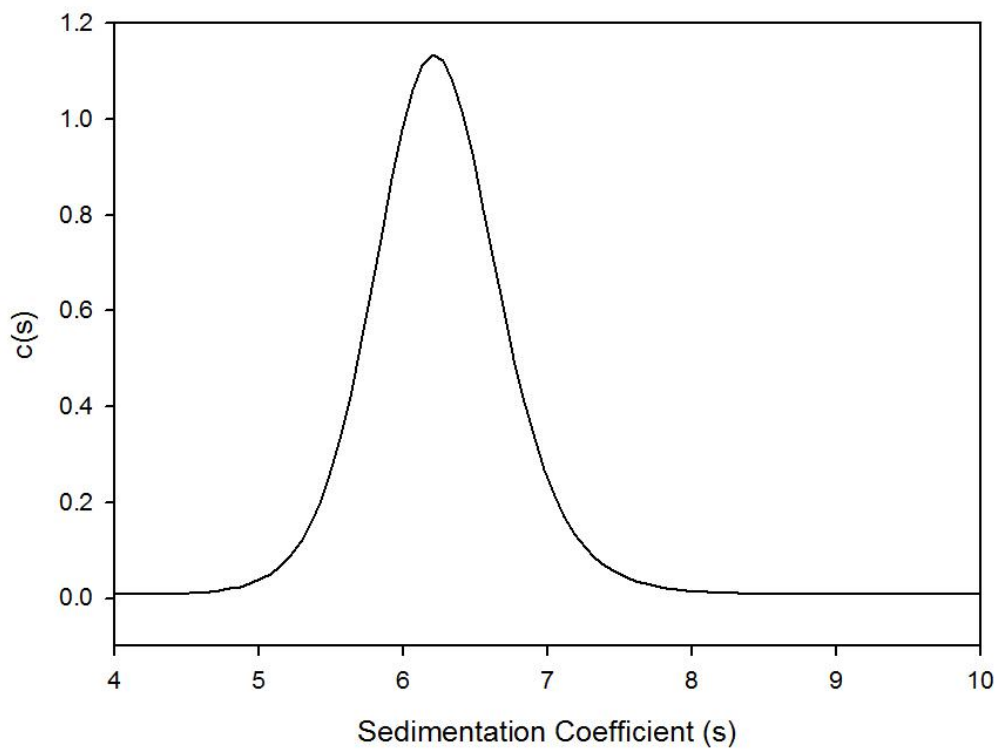
Jk 30K AB4 c(s) distribution



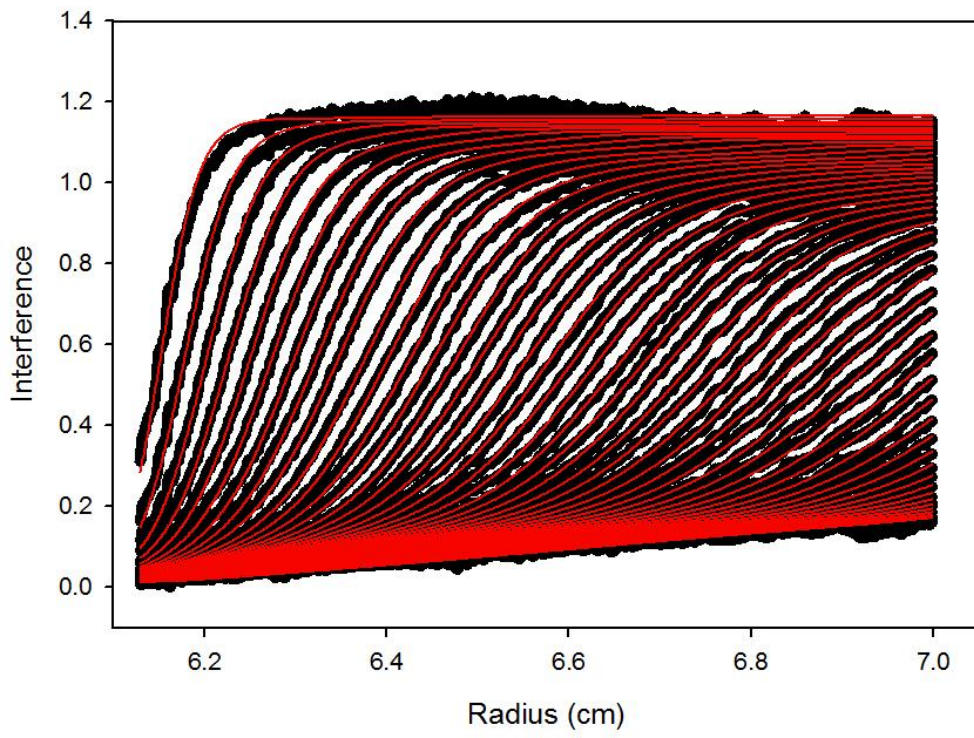
JK 30K AB6



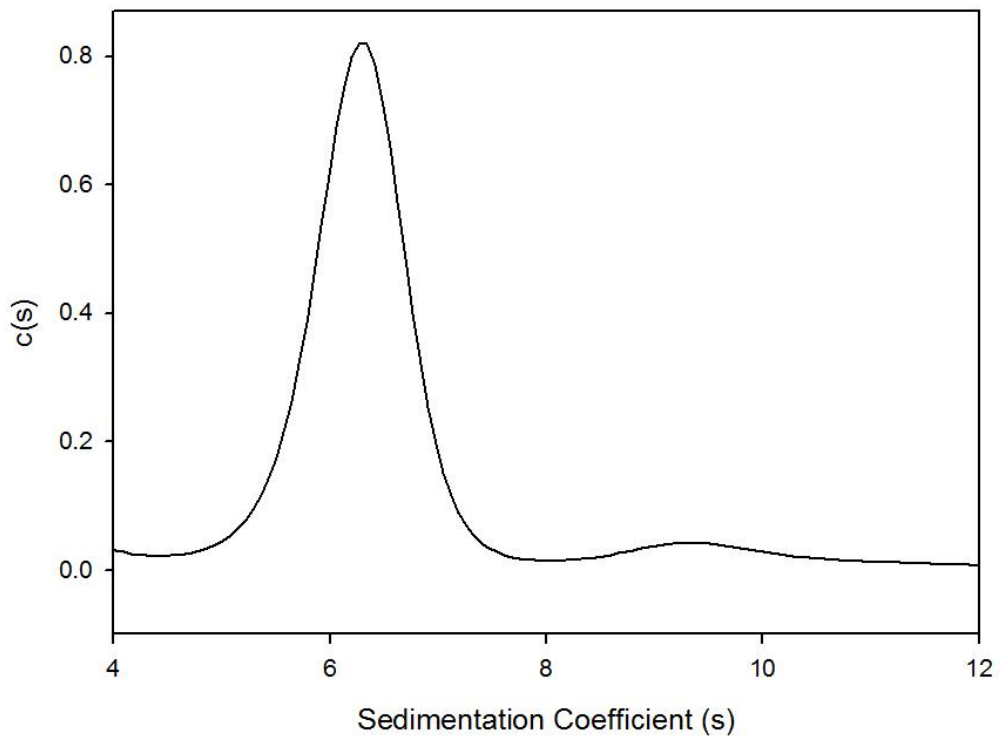
JK 30K AB6 c(s) distribution

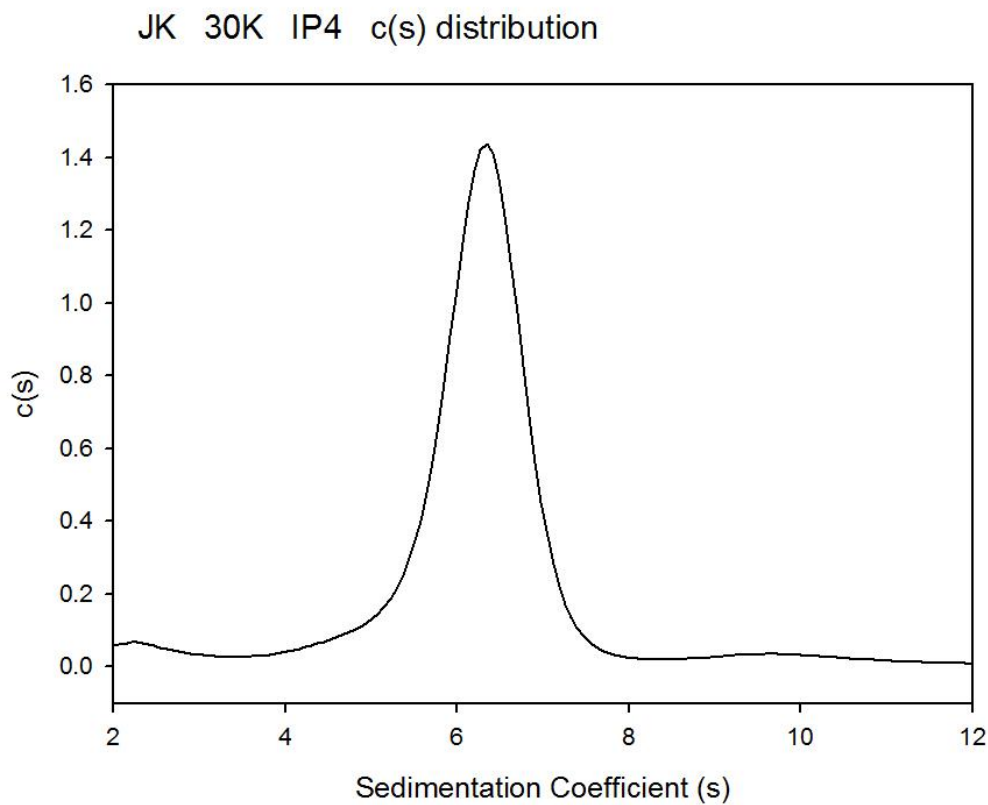
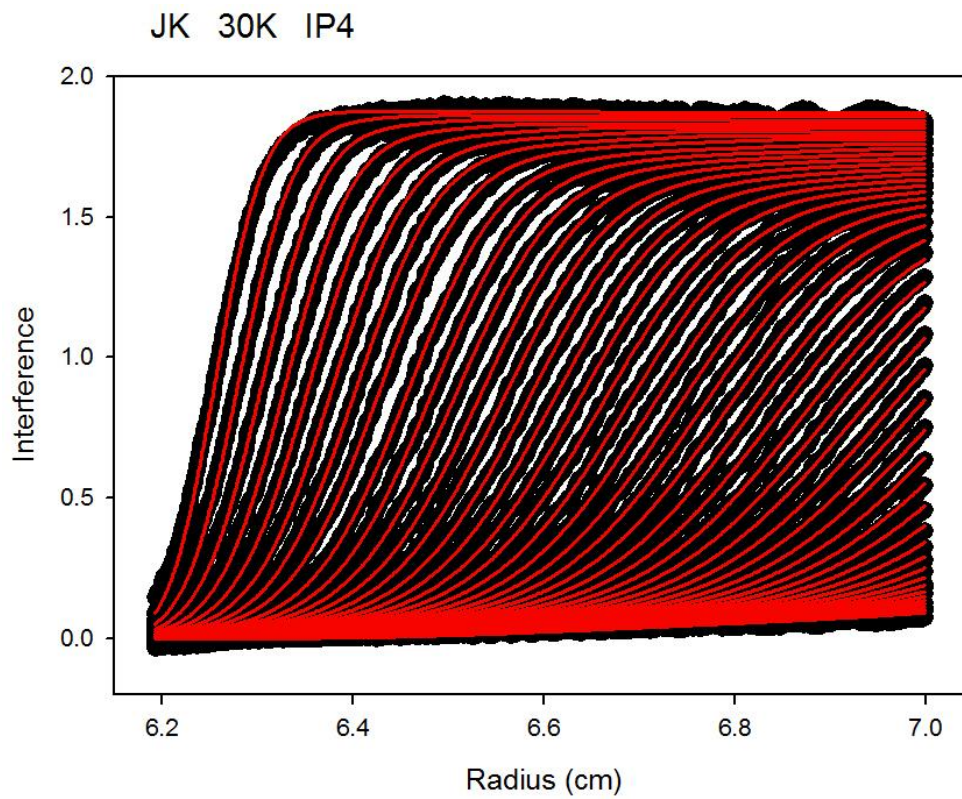


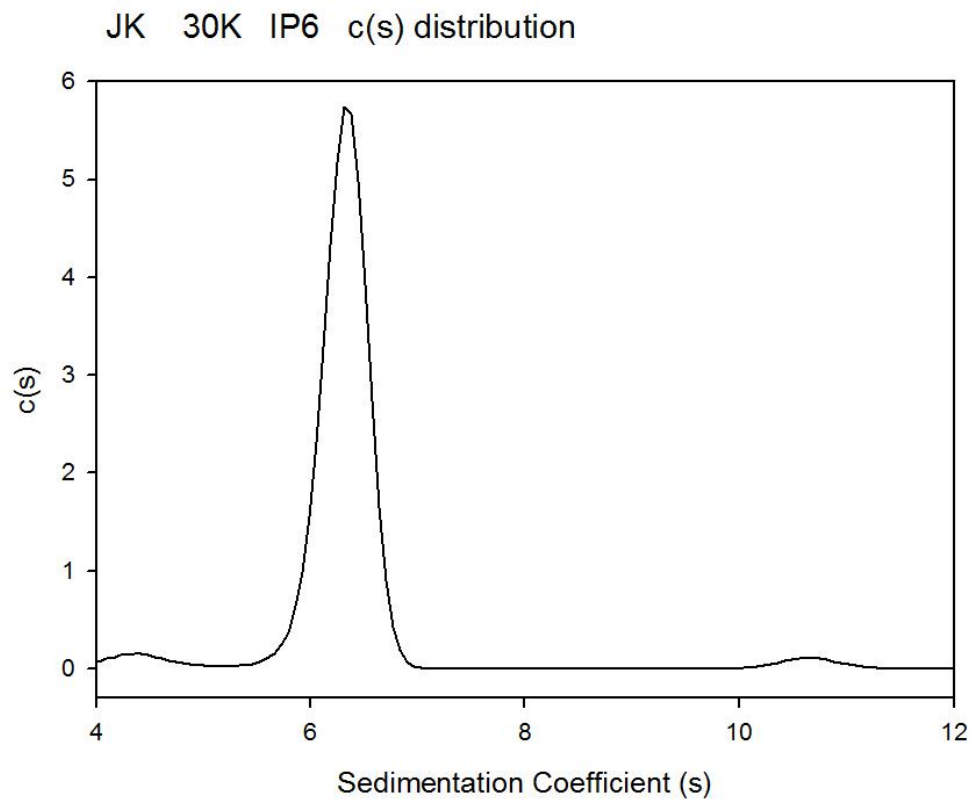
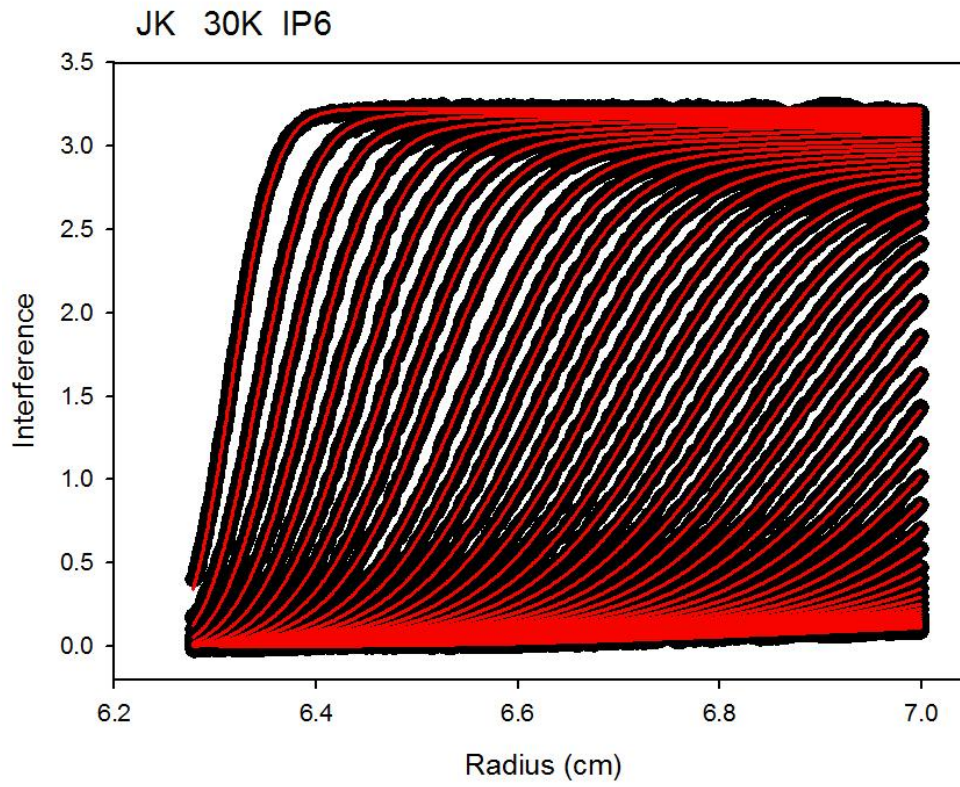
JK 30K IP2



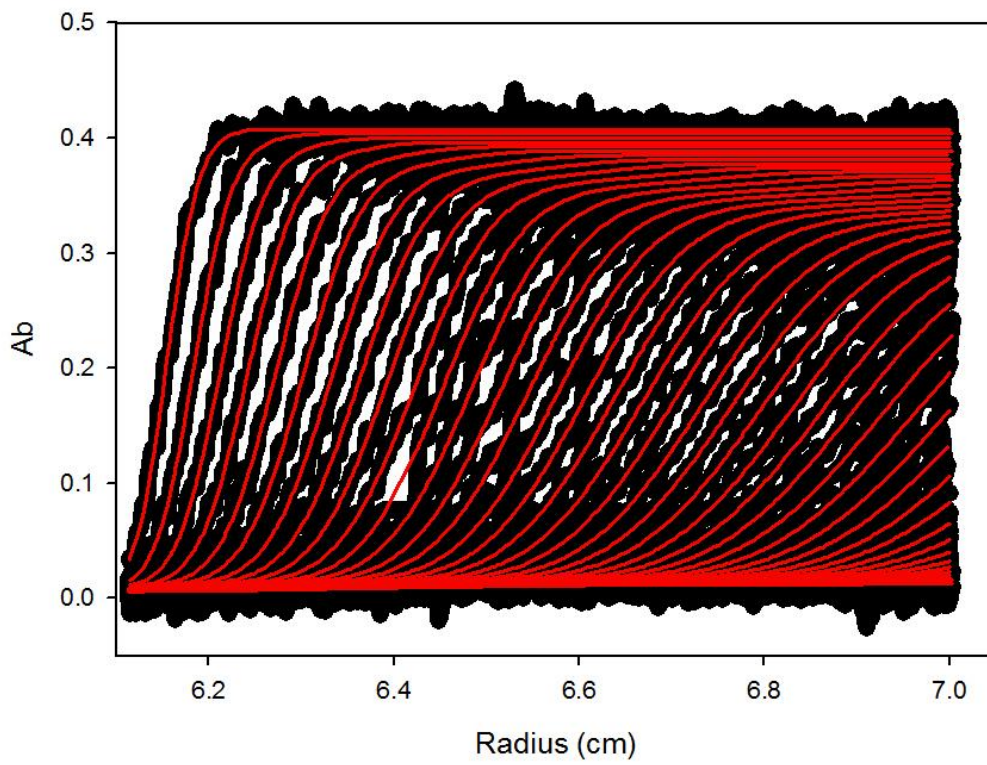
JK 30K IP2 c(s) distribution



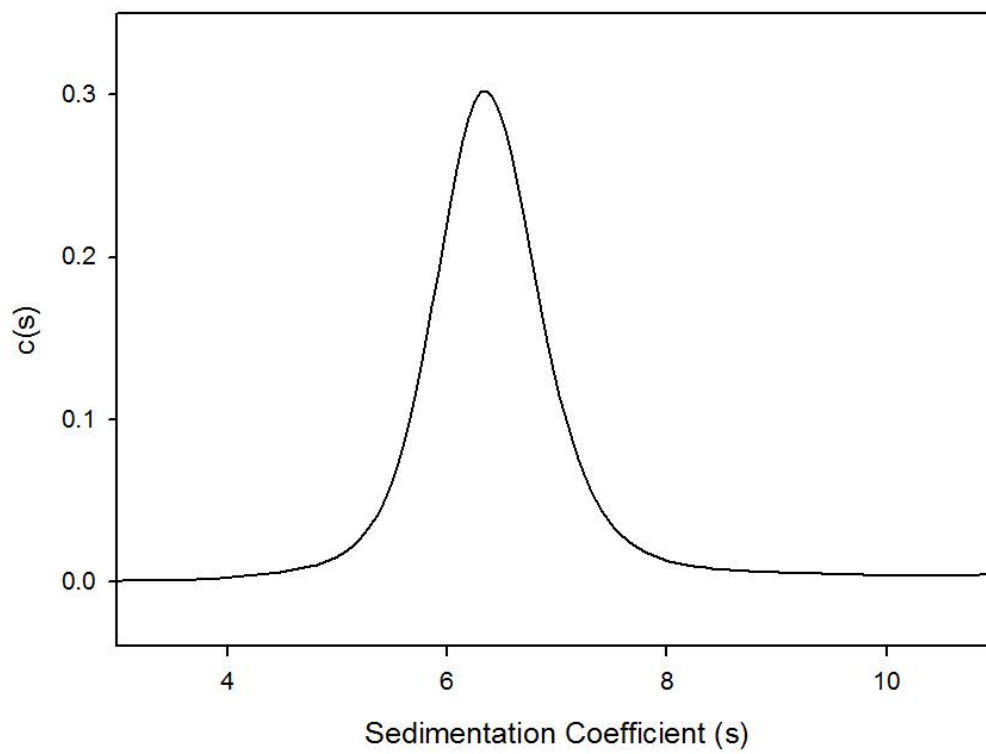




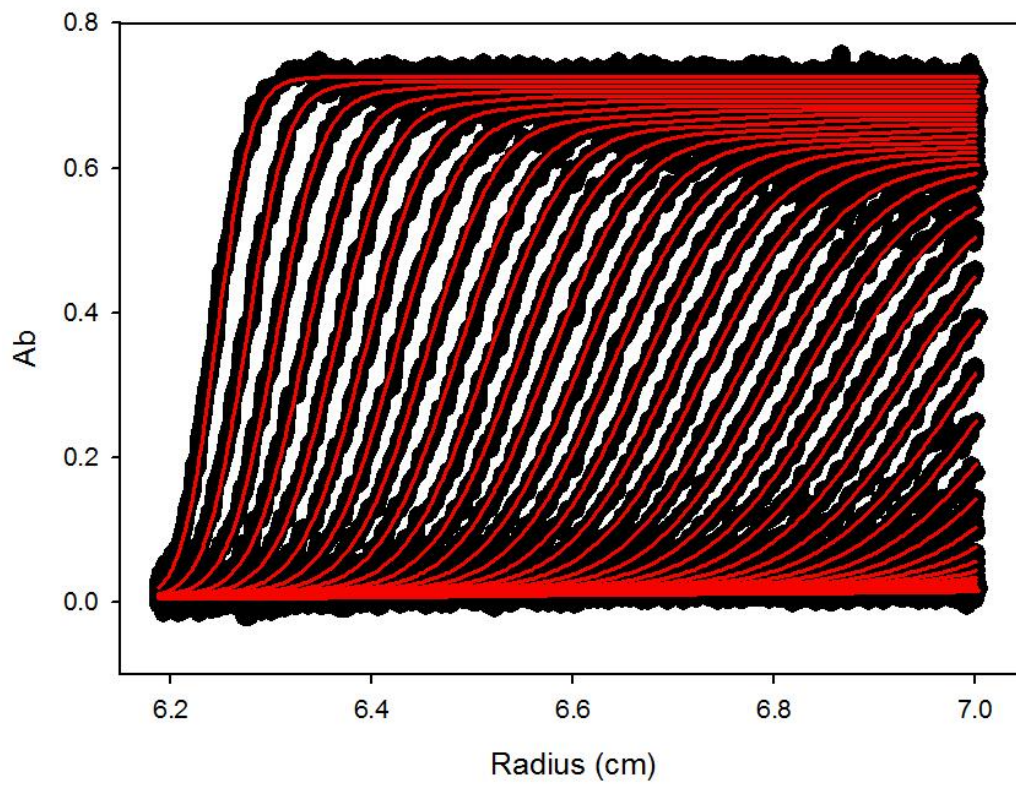
JK 40K AB2



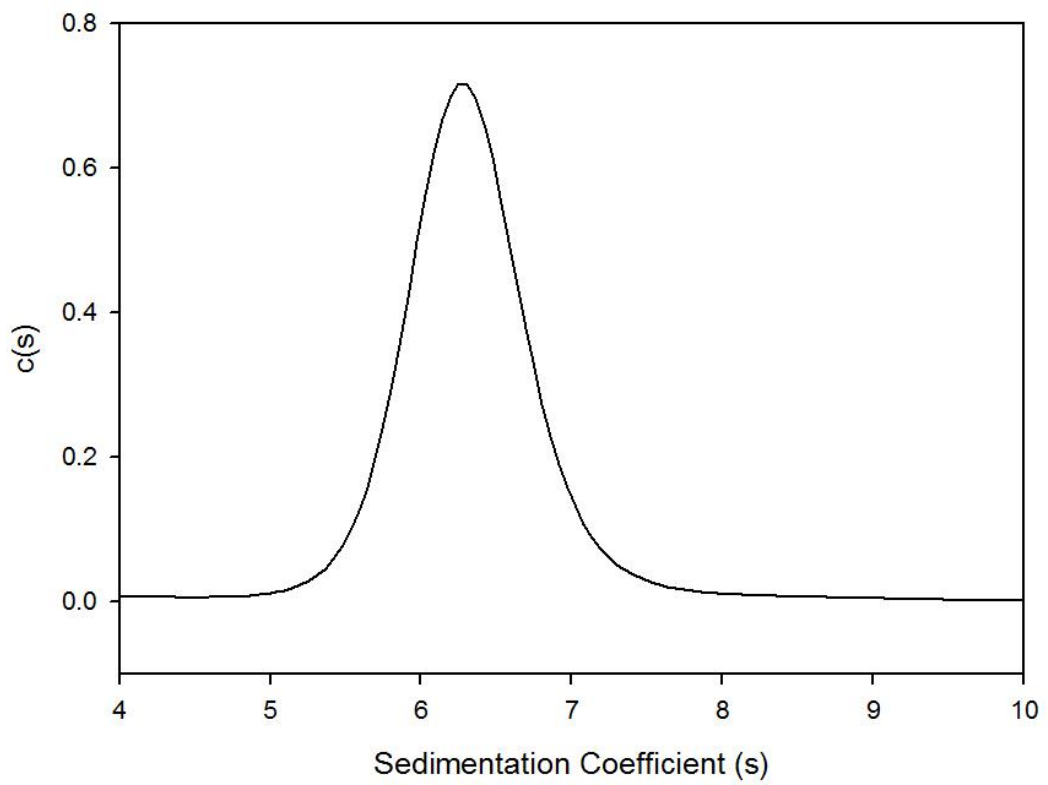
JK 40K AB2 c(s) distribution



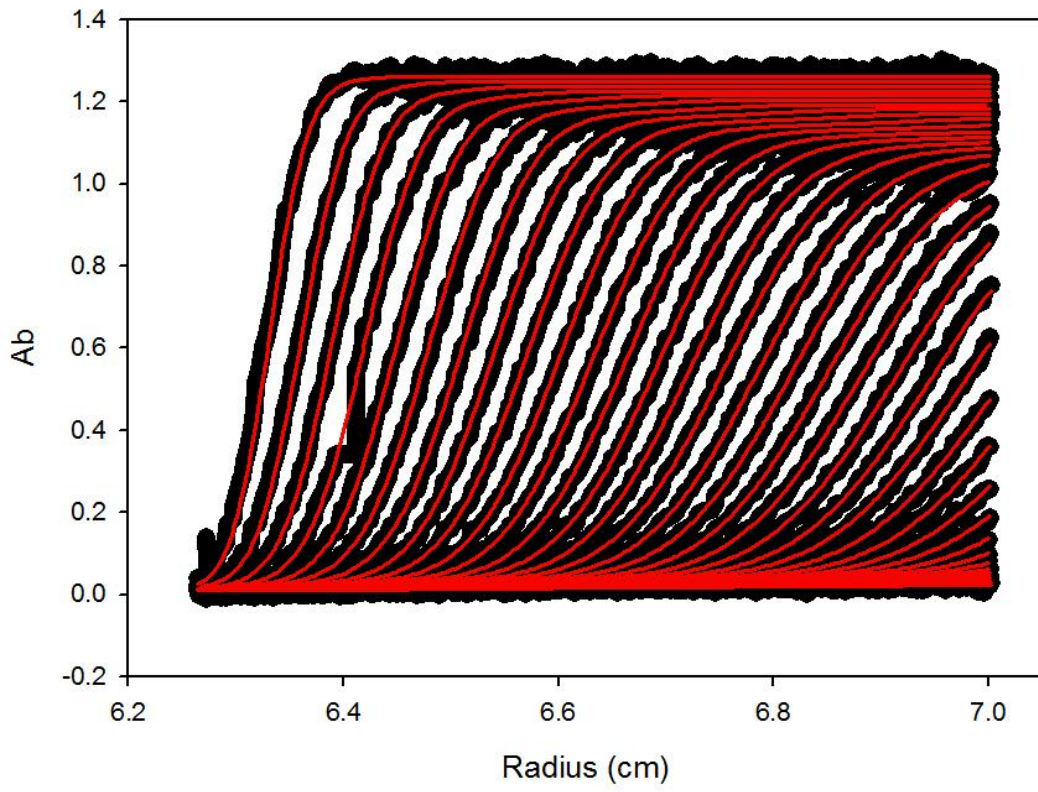
JK 40K AB4



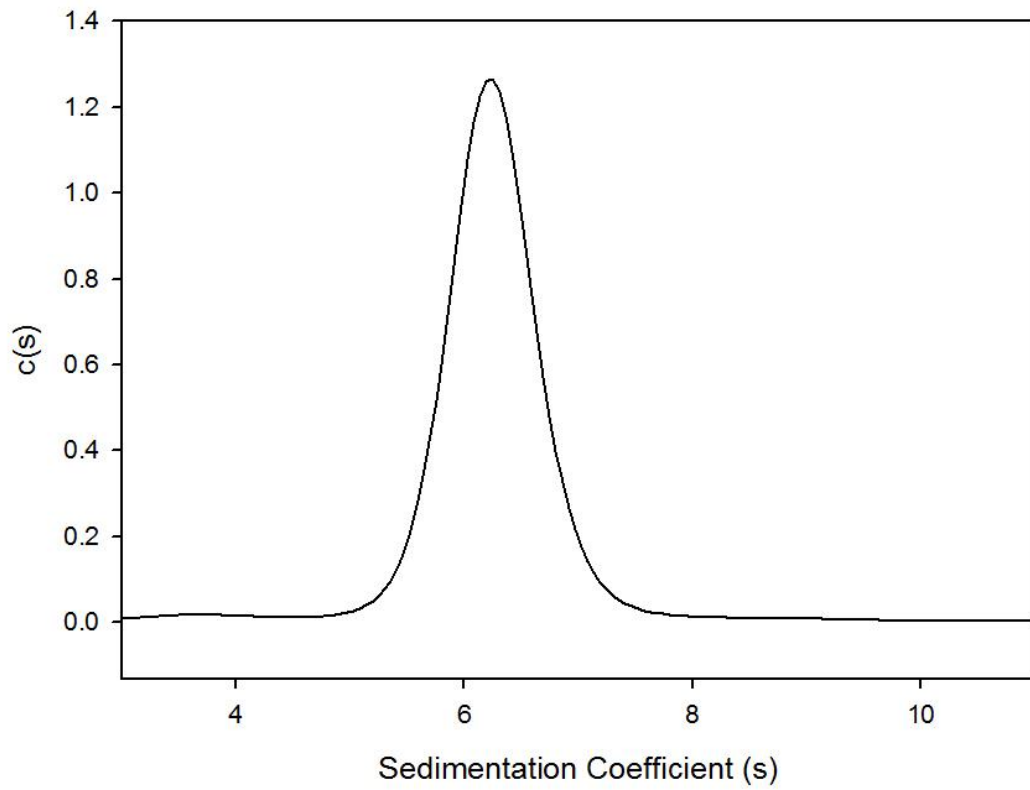
JK 40K AB4 c(s) distribution



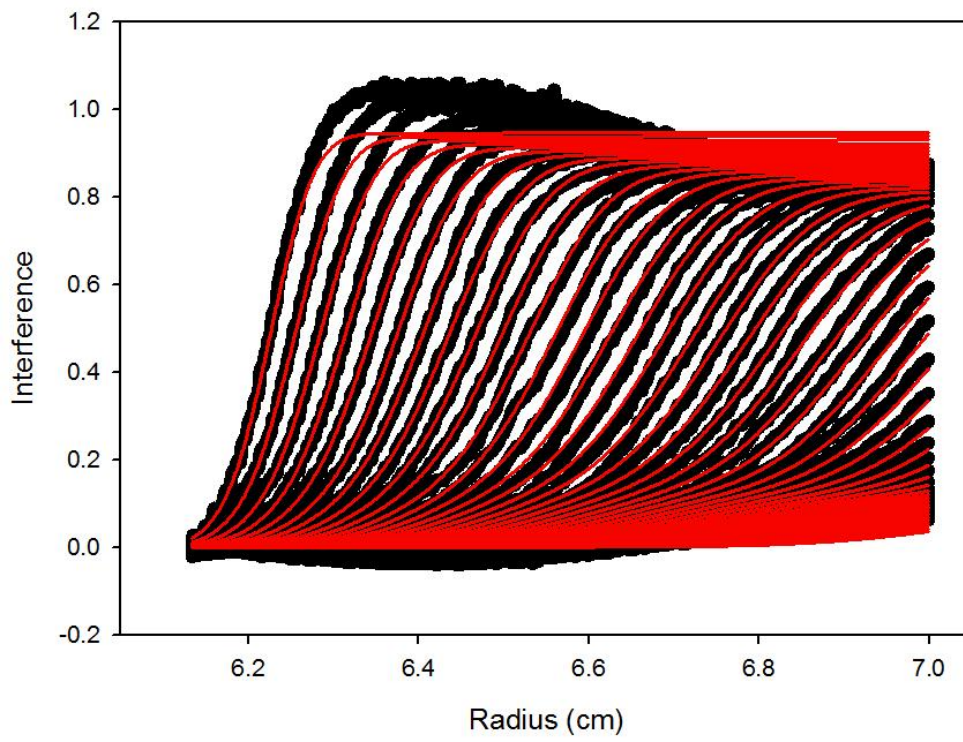
JK 40K AB6



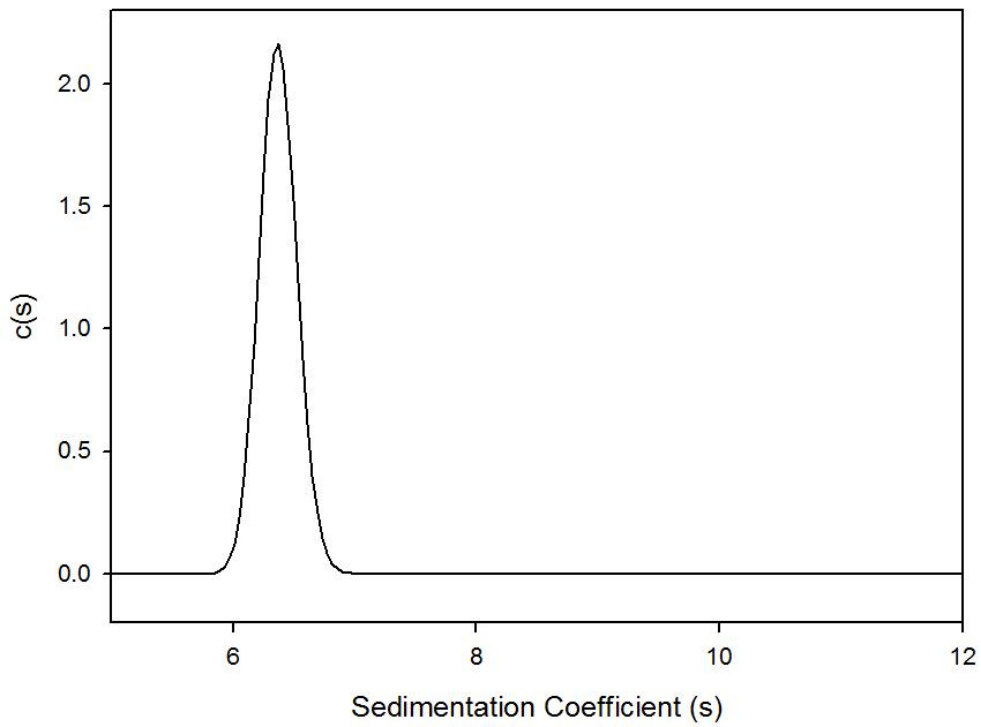
Jk 40K AB6 c(s) distribution



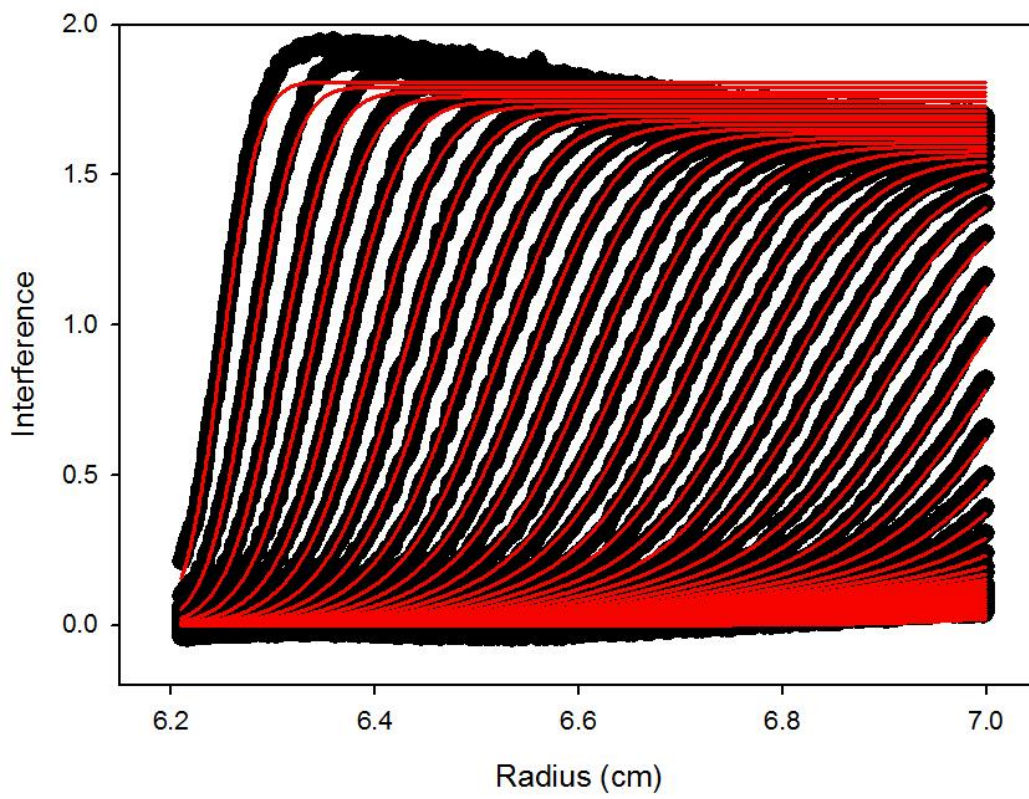
JK 40K IP2



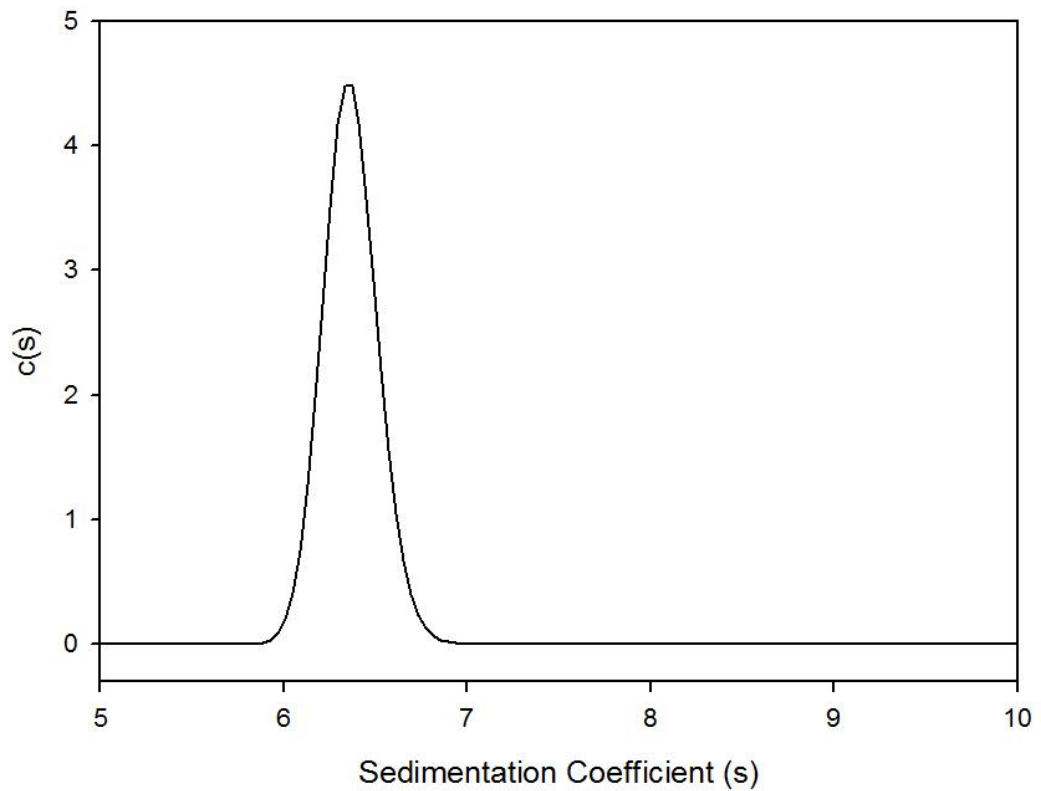
JK 40K IP2 c(s) distribution



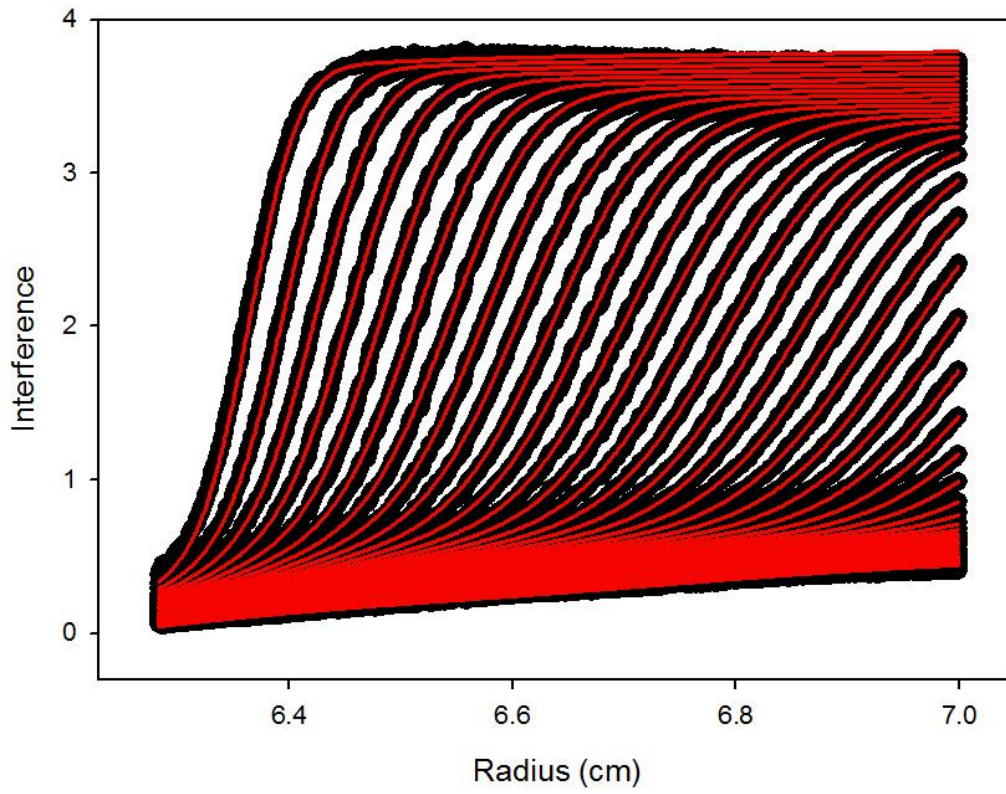
JK 40K IP4



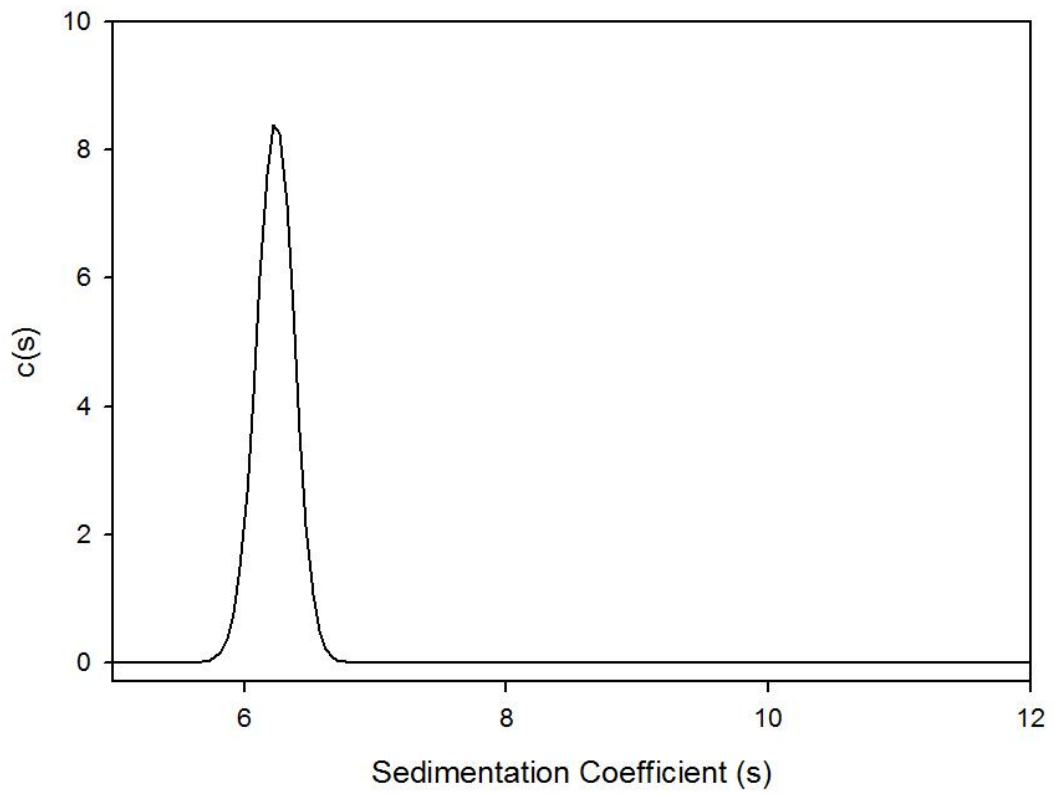
JK 40K IP4 c(s) distribution



JK 40K IP6



JK 40K IP6 c(s) distribution



Appendix III
SAXS Summary Data

RG Q Range: 0.13 - 0.25

IgA Normal Conditions 137mM PBS

Merged files ESRF Dec 2012

File name	Q-range	Point range	RG	Error	QRG	I(0)	Error	Conc (mg/ml)	I(0)/c	Avg I(0)/c	StDev	Avg RG	StDev
sample1_iga_0p25mg_1_merged	0.130->0.250	23->51	5.93	0.02	0.77->1.48	0.006872	0.000057	0.25	0.0275				
sample1_iga_0p25mg_2_merged	0.130->0.250	23->51	6.14	0.02	0.80->1.53	0.006861	0.000058	0.25	0.0274				
sample1_iga_0p25mg_3_merged	0.130->0.250	23->51	5.97	0.02	0.78->1.49	0.00667	0.000065	0.25	0.0267				
sample1_iga_0p25mg_4_merged	0.130->0.250	23->51	6.15	0.02	0.80->1.54	0.006963	0.000079	0.25	0.0279	0.027366	0.000493	6.047500	0.113835
sample1_iga_0p51mg_1_merged	0.130->0.250	23->51	6.09	0.01	0.79->1.52	0.01359	0.000087	0.51	0.0266				
sample1_iga_0p51mg_2_merged	0.130->0.250	23->51	5.93	0.01	0.77->1.48	0.012996	0.000085	0.51	0.0255				
sample1_iga_0p51mg_3_merged	0.130->0.250	23->51	6.08	0.02	0.79->1.52	0.013415	0.0001	0.51	0.0263				
sample1_iga_0p51mg_4_merged	0.130->0.250	23->51	6.19	0.01	0.80->1.55	0.013634	0.000067	0.51	0.0267	0.026292	0.000571	6.072500	0.107199
sample1_iga_0p76mg_1_merged	0.130->0.250	23->51	6.12	0.01	0.80->1.53	0.019949	0.000119	0.76	0.0262				
sample1_iga_0p76mg_2_merged	0.130->0.250	23->51	6.13	0.02	0.80->1.53	0.019781	0.000152	0.76	0.0260				
sample1_iga_0p76mg_3_merged	0.130->0.250	23->51	6.14	0.01	0.80->1.53	0.019918	0.000132	0.76	0.0262	0.026161	0.000118	6.130000	0.010000
sample1_iga_1p02mg_1_merged	0.130->0.250	23->51	6.22	0.01	0.81->1.55	0.026958	0.000127	1.02	0.0264				
sample1_iga_1p02mg_2_merged	0.130->0.250	23->51	6.22	0.01	0.81->1.55	0.026891	0.000146	1.02	0.0264				
sample1_iga_1p02mg_3_merged	0.130->0.250	23->51	6.3	0.01	0.82->1.57	0.027211	0.000157	1.02	0.0267	0.026490	0.000165	6.246667	0.046188
sample2_iga_0p16mg_1_merged	0.130->0.250	23->51	5.85	0.04	0.76->1.46	0.003894	0.000073	0.16	0.0243				
sample2_iga_0p16mg_2_merged	0.130->0.250	23->51	5.69	0.04	0.74->1.42	0.003791	0.00007	0.16	0.0237				
sample2_iga_0p16mg_3_merged	0.130->0.250	23->51	5.8	0.02	0.75->1.45	0.003881	0.000043	0.16	0.0243				
sample2_iga_0p16mg_4_merged	0.130->0.250	22->50	5.58	0.04	0.73->1.40	0.003716	0.000067	0.16	0.0232	0.023878	0.000521	5.730000	0.120277
sample2_iga_0p33mg_1_merged	0.130->0.250	23->51	6.07	0.01	0.79->1.52	0.008493	0.000039	0.33	0.0257				
sample2_iga_0p33mg_2_merged	0.130->0.250	23->51	6	0.02	0.78->1.50	0.008522	0.000073	0.33	0.0258				
sample2_iga_0p33mg_3_merged	0.130->0.250	23->51	6.01	0.01	0.78->1.50	0.008545	0.00006	0.33	0.0259				
sample2_iga_0p33mg_4_merged	0.130->0.250	23->51								0.025818	0.000079	6.026667	0.037859
sample2_iga_0p49mg_1_merged	0.130->0.250	23->51	6.15	0.01	0.80->1.54	0.01447	0.000067	0.49	0.0295306				
sample2_iga_0p49mg_2_merged	0.130->0.250	23->51	6.11	0.01	0.79->1.53	0.014517	0.000089	0.49	0.0296				
sample2_iga_0p49mg_3_merged	0.130->0.250	23->51	6.16	0.02	0.80->1.54	0.014684	0.000109	0.49	0.0300				
sample2_iga_0p49mg_4_merged	0.130->0.250	23->51	6.17	0.02	0.80->1.54	0.014625	0.00012	0.49	0.0298	0.029743	0.000200	6.147500	0.026300
sample2_iga_0p66mg_1_merged	0.130->0.250	23->51	6.18	0.01	0.80->1.54	0.01738	0.000094	0.66	0.0263333				
sample2_iga_0p66mg_2_merged	0.130->0.250	23->51	6.21	0.01	0.81->1.55	0.017566	0.000087	0.66	0.0266152				
sample2_iga_0p66mg_3_merged	0.130->0.250	23->51	6.32	0.01	0.82->1.58	0.017666	0.000105	0.66	0.0267667				
sample2_iga_0p66mg_4_merged	0.130->0.250	23->51	6.47	0.02	0.84->1.62	0.016897	0.000154	0.66	0.0256015	0.026329	0.000517	6.295000	0.131276
sample2_iga_0p99mg_1_merged	0.130->0.250	23->51	6.29	0.01	0.82->1.57	0.026942	0.000142	0.99	0.0272				
sample2_iga_0p99mg_2_merged	0.130->0.250	23->51	6.29	0.01	0.82->1.57	0.026929	0.000153	0.99	0.0272				
sample2_iga_0p99mg_3_merged	0.130->0.250	23->51	6.41	0.01	0.83->1.60	0.027241	0.000191	0.99	0.0275				
sample2_iga_0p99mg_4_merged	0.130->0.250	23->51								0.027310	0.000178	6.330000	0.069282
sample2_iga_1p33mg_1_merged	0.130->0.250	23->51	6.46	0.01	0.84->1.61	0.038288	0.000189	1.33	0.0288				
sample2_iga_1p33mg_2_merged	0.130->0.250	23->51	6.48	0.01	0.84->1.62	0.038652	0.000271	1.33	0.0291				
sample2_iga_1p33mg_3_merged	0.130->0.250	23->51	6.52	0.01	0.85->1.63	0.039071	0.00028	1.33	0.0294				
sample2_iga_1p33mg_4_merged	0.130->0.250	23->51	6.48	0.01	0.84->1.62	0.038625	0.000297	1.33	0.0290	0.029067	0.000241	6.485000	0.025166
sample3_iga_0p12mg_1_merged	0.130->0.250	21->49	5.9	0.04	0.77->1.48	0.002985	0.000058	0.12	0.0249				
sample3_iga_0p12mg_2_merged	0.130->0.250	21->49	5.85	0.04	0.76->1.46	0.00298	0.000059	0.12	0.0248				
sample3_iga_0p12mg_3_merged	0.130->0.250	23->51	5.7	0.05	0.74->1.43	0.002883	0.00006	0.12	0.0240				

sample3_iga_0p12mg_4_merged	0.130->0.250	23->51	5.56	0.04	0.72->1.39	0.002883	0.000056	0.12	0.0240	0.024440	0.000479	5.752500	0.153921
sample3_iga_0p24mg_1_merged													
sample3_iga_0p24mg_2_merged	0.130->0.250	23->51	6.13	0.02	0.80->1.53	0.005817	0.000064	0.24	0.0242				
sample3_iga_0p24mg_3_merged										0.024238	#DIV/0!	6.130000	#DIV/0!
sample3_iga_0p36mg_1_merged	0.130->0.250	23->51	6.01	0.02	0.78->1.50	0.009754	0.000101	0.36	0.0271				
sample3_iga_0p36mg_2_merged	0.130->0.250	23->51	5.98	0.01	0.78->1.50	0.009389	0.000052	0.36	0.0261				
sample3_iga_0p36mg_3_merged	0.130->0.250	23->51	6.2	0.02	0.81->1.55	0.009756	0.000074	0.36	0.0271				
sample3_iga_0p36mg_4_merged	0.130->0.250	23->51	5.95	0.01	0.77->1.49	0.009364	0.000051	0.36	0.0260	0.026572	0.000608	6.035000	0.112694
sample3_iga_0p48mg_1_merged	0.130->0.250	23->51	6.16	0.02	0.80->1.54	0.011603	0.000118	0.48	0.0242				
sample3_iga_0p48mg_2_merged	0.130->0.250	23->51	6.22	0.01	0.81->1.55	0.011822	0.000073	0.48	0.0246				
sample3_iga_0p48mg_3_merged	0.130->0.250	23->51	6.09	0.02	0.79->1.52	0.011813	0.000098	0.48	0.0246				
sample3_iga_0p48mg_4_merged										0.02	0.00	6.16	0.07
sample3_iga_0p72mg_1_merged	0.130->0.250	23->51	6.14	0.01	0.80->1.53	0.020023	0.000126	0.72	0.0278				
sample3_iga_0p72mg_2_merged	0.130->0.250	23->51	6.17	0.01	0.80->1.54	0.019879	0.000126	0.72	0.0276				
sample3_iga_0p72mg_3_merged	0.130->0.250	23->51	6.2	0.01	0.81->1.55	0.020118	0.000138	0.72	0.0279				
sample3_iga_0p72mg_4_merged	0.130->0.250	23->51	6.17	0.01	0.80->1.54	0.020012	0.000099	0.72	0.0278	0.027789	0.000137	6.170000	0.024495
sample3_iga_0p97mg_1_merged	0.130->0.250	23->51	6.26	0.01	0.81->1.56	0.026704	0.000196	0.97	0.0275				
sample3_iga_0p97mg_2_merged	0.130->0.250	23->51	6.32	0.01	0.82->1.58	0.026854	0.000173	0.97	0.0277				
sample3_iga_0p97mg_3_merged	0.130->0.250	23->51	6.31	0.01	0.82->1.58	0.026825	0.000163	0.97	0.0277				
sample3_iga_0p97mg_4_merged	0.130->0.250	23->51	6.3	0.01	0.82->1.57	0.026852	0.000184	0.97	0.0277	0.027638	0.000073	6.297500	0.026300
sample4_iga_0p15mg_1_merged	0.130->0.250	23->51	5.87	0.02	0.76->1.47	0.003634	0.000035	0.15	0.0242				
sample4_iga_0p15mg_2_merged	0.130->0.250	23->51	6.02	0.03	0.78->1.50	0.00344	0.000057	0.15	0.0229				
sample4_iga_0p15mg_3_merged	0.130->0.250	23->51	5.77	0.04	0.75->1.44	0.003397	0.000064	0.15	0.0226				
sample4_iga_0p15mg_4_merged	0.130->0.250	23->51	6.11	0.04	0.79->1.53	0.003561	0.000065	0.15	0.0237	0.023387	0.000727	5.942500	0.151740
sample4_iga_0p31mg_1_merged	0.130->0.250	22->50	5.96	0.02	0.77->1.49	0.008021	0.000075	0.31	0.0259				
sample4_iga_0p31mg_2_merged	0.130->0.250	20->48	6.04	0.02	0.79->1.51	0.008057	0.000082	0.31	0.0260				
sample4_iga_0p31mg_3_merged	0.130->0.250	20->48	5.97	0.02	0.78->1.49	0.008026	0.00007	0.31	0.0259				
sample4_iga_0p31mg_4_merged	0.130->0.250	23->51	7.53	0.04	0.98->1.88	0.010413	0.000269	0.31	0.0336	0.027836	0.003836	6.375000	0.770822
sample4_iga_0p47mg_1_merged	0.130->0.250	23->51	6.06	0.01	0.79->1.51	0.011664	0.00008	0.47	0.0248				
sample4_iga_0p47mg_2_merged	0.130->0.250	22->50	6.17	0.01	0.80->1.54	0.011745	0.000061	0.47	0.0250				
sample4_iga_0p47mg_3_merged	0.130->0.250	22->50	6.06	0.01	0.79->1.51	0.011681	0.000074	0.47	0.0249				
sample4_iga_0p47mg_4_merged	0.130->0.250	23->51	6.09	0.01	0.79->1.52	0.011588	0.000081	0.47	0.0247	0.024829	0.000137	6.095000	0.051962
sample4_iga_0p63mg_1_merged	0.130->0.250	23->51	6.22	0.02	0.81->1.55	0.016211	0.000136	0.63	0.0257				
sample4_iga_0p63mg_2_merged	0.130->0.250	23->51	6.3	0.01	0.82->1.57	0.016771	0.000113	0.63	0.0266				
sample4_iga_0p63mg_3_merged	0.130->0.250	23->51	6.27	0.01	0.82->1.57	0.016855	0.000101	0.63	0.0268				
sample4_iga_0p63mg_4_merged	0.130->0.250	23->51	6.61	0.02	0.86->1.65	0.016382	0.000189	0.63	0.0260	0.026277	0.000489	6.350000	0.176446
sample4_iga_0p94mg_1_merged	0.130->0.250	23->51	6.22	0.01	0.81->1.55	0.023496	0.000108	0.94	0.0250				
sample4_iga_0p94mg_2_merged	0.130->0.250	23->51	6.24	0.01	0.81->1.56	0.024123	0.000141	0.94	0.0257				
sample4_iga_0p94mg_3_merged	0.130->0.250	23->51	6.28	0.01	0.82->1.57	0.024933	0.000145	0.94	0.0265				
sample4_iga_0p94mg_4_merged	0.130->0.250	23->51	6.3	0.01	0.82->1.57	0.02494	0.000185	0.94	0.0265	0.025929	0.000744	6.260000	0.036515
sample4_iga_1p26mg_1_merged	0.130->0.250	23->51	6.33	0.01	0.82->1.58	0.033615	0.000191	1.26	0.0267				
sample4_iga_1p26mg_2_merged	0.130->0.250	23->51	6.35	0.01	0.83->1.59	0.03425	0.000235	1.26	0.0272				
sample4_iga_1p26mg_3_merged	0.130->0.250	23->51	6.42	0.01	0.83->1.60	0.034824	0.000264	1.26	0.0276				
sample4_iga_1p26mg_4_merged	0.130->0.250	23->51	6.44	0.02	0.84->1.61	0.035021	0.000298	1.26	0.0278	0.027323	0.000502	6.385000	0.053229

*Data point omitted, sample error eg. Air bubble

RXS-1 Q Range: 0.28 - 0.51

IgA Normal Conditions 137mM PBS

Merged files ESRF Dec 2012

File name	Q-range	Point range	Rxs1	Error	QRxs	I(0)	Error	Conc (mg/ml)	Avg RXs	StDev
sample1_iga_Op25mg_1_merged	0.280->0.510	57->110	2.41	0.02	0.67->1.23	0.000931	0.000016	0.25		
sample1_iga_Op25mg_2_merged	0.280->0.510	57->110	2.34	0.02	0.65->1.19	0.000901	0.000013	0.25		
sample1_iga_Op25mg_3_merged	0.280->0.510	57->110	2.42	0.02	0.68->1.24	0.000936	0.000013	0.25		
sample1_iga_Op25mg_4_merged	0.280->0.510	57->110	2.52	0.02	0.70->1.28	0.000954	0.000017	0.25	2.422500	0.074106
sample1_iga_Op51mg_1_merged	0.280->0.510	57->110	2.54	0.02	0.71->1.29	0.00188	0.000029	0.51		
sample1_iga_Op51mg_2_merged	0.280->0.510	57->110	2.43	0.02	0.68->1.24	0.001781	0.000027	0.51		
sample1_iga_Op51mg_3_merged	0.280->0.510	57->110	2.54	0.01	0.71->1.29	0.00185	0.000018	0.51		
sample1_iga_Op51mg_4_merged	0.280->0.510	57->110	2.42	0.01	0.68->1.23	0.001771	0.000021	0.51	2.482500	0.066521
sample1_iga_Op76mg_1_merged	0.280->0.510	57->110	2.49	0.01	0.70->1.27	0.002692	0.000027	0.76		
sample1_iga_Op76mg_2_merged	0.280->0.510	57->110	2.47	0.01	0.69->1.26	0.002635	0.000029	0.76		
sample1_iga_Op76mg_3_merged	0.280->0.510	57->110	2.49	0.01	0.70->1.27	0.002644	0.000027	0.76	2.483333	0.011547
sample1_iga_1p02mg_1_merged	0.280->0.510	57->110	2.47	0.02	0.69->1.26	0.003463	0.000046	1.02		
sample1_iga_1p02mg_2_merged	0.280->0.510	57->110	2.48	0.01	0.69->1.26	0.003494	0.000042	1.02		
sample1_iga_1p02mg_3_merged	0.280->0.510	57->110	2.46	0.02	0.69->1.26	0.003484	0.000044	1.02	2.470000	0.010000
sample2_iga_Op16mg_1_merged	0.280->0.510	57->110	2.44	0.03	0.68->1.25	0.000562	0.000012	0.16		
sample2_iga_Op16mg_2_merged	0.280->0.510	57->110	2.57	0.03	0.72->1.31	0.000572	0.000013	0.16		
sample2_iga_Op16mg_3_merged	0.280->0.510	57->110	2.51	0.03	0.70->1.28	0.000574	0.000013	0.16		
sample2_iga_Op16mg_4_merged	0.280->0.510	56->109	2.43	0.03	0.68->1.24	0.000561	0.000014	0.16	2.487500	0.065511
sample2_iga_Op33mg_1_merged	0.280->0.510	57->110	2.51	0.01	0.70->1.28	0.001177	0.000015	0.33		
sample2_iga_Op33mg_2_merged	0.280->0.510	57->110	2.51	0.01	0.70->1.28	0.001207	0.000012	0.33		
sample2_iga_Op33mg_3_merged	0.280->0.510	57->110	2.47	0.02	0.69->1.26	0.001178	0.000019	0.33		
sample2_iga_Op33mg_4_merged	0.280->0.510	57->110	2.47	0.02	0.69->1.26	0.001178	0.000019	0.33	2.496667	0.023094
sample2_iga_Op49mg_1_merged	0.280->0.510	57->110	2.48	0.01	0.69->1.26	0.00194	0.000023	0.49		
sample2_iga_Op49mg_2_merged	0.280->0.510	57->110	2.5	0.01	0.70->1.27	0.00195	0.000015	0.49		
sample2_iga_Op49mg_3_merged	0.280->0.510	57->110	2.5	0.01	0.70->1.28	0.001975	0.00002	0.49		
sample2_iga_Op49mg_4_merged	0.280->0.510	57->110	2.47	0.01	0.69->1.26	0.001931	0.000023	0.49	2.487500	0.015000
sample2_iga_Op66mg_1_merged	0.280->0.510	57->110	2.48	0.02	0.69->1.26	0.002283	0.000029	0.66		
sample2_iga_Op66mg_2_merged	0.280->0.510	57->110	2.52	0.01	0.71->1.29	0.002304	0.00003	0.66		
sample2_iga_Op66mg_3_merged	0.280->0.510	57->110	2.49	0.02	0.70->1.27	0.002235	0.000032	0.66		
sample2_iga_Op66mg_4_merged	0.280->0.510	57->110	2.75	0.01	0.77->1.40	0.002158	0.000023	0.66	2.560000	0.127802
sample2_iga_Op99mg_1_merged	0.280->0.510	57->110	2.49	0.01	0.70->1.27	0.003444	0.000041	0.99		
sample2_iga_Op99mg_2_merged	0.280->0.510	57->110	2.51	0.01	0.70->1.28	0.003442	0.000038	0.99		
sample2_iga_Op99mg_3_merged	0.280->0.510	57->110	2.5	0.02	0.70->1.27	0.003374	0.000048	0.99		
sample2_iga_Op99mg_4_merged	0.280->0.510	57->110	2.49	0.02	0.70->1.27	0.003374	0.000048	0.99	2.500000	0.010000
sample2_iga_1p33mg_1_merged	0.280->0.510	57->110	2.45	0.02	0.68->1.25	0.004659	0.000058	1.33		
sample2_iga_1p33mg_2_merged	0.280->0.510	57->110	2.47	0.01	0.69->1.26	0.00471	0.000053	1.33		
sample2_iga_1p33mg_3_merged	0.280->0.510	57->110	2.5	0.01	0.70->1.28	0.004771	0.000054	1.33		
sample2_iga_1p33mg_4_merged	0.280->0.510	57->110	2.47	0.01	0.69->1.26	0.004679	0.000055	1.33	2.472500	0.020616
sample3_iga_Op12mg_1_merged	0.280->0.510	55->108	2.22	0.04	0.62->1.13	0.000407	0.000013	0.12		
sample3_iga_Op12mg_2_merged	0.280->0.510	55->108	2.55	0.04	0.72->1.30	0.000439	0.000017	0.12		
sample3_iga_Op12mg_3_merged	0.280->0.510	57->110	2.31	0.04	0.65->1.18	0.000399	0.000012	0.12		

sample3_iga_0p12mg_4_merged	0.280->0.510	57->110	2.34	0.03	0.66->1.20	0.000429	0.00001	0.12	2.355000	0.139642
sample3_iga_0p24mg_1_merged										
sample3_iga_0p24mg_2_merged	0.280->0.510	57->110	2.57	0.02	0.72->1.31	0.000819	0.000015	0.24		
sample3_iga_0p24mg_3_merged									2.570000	#DIV/0!
sample3_iga_0p36mg_1_merged	0.280->0.510	57->110	2.4	0.02	0.67->1.22	0.001312	0.00002	0.36		
sample3_iga_0p36mg_2_merged	0.280->0.510	57->110	2.56	0.01	0.72->1.31	0.001345	0.000015	0.36		
sample3_iga_0p36mg_3_merged	0.280->0.510	57->110	2.47	0.01	0.69->1.26	0.001308	0.000014	0.36		
sample3_iga_0p36mg_4_merged	0.280->0.510	57->110	2.51	0.01	0.70->1.28	0.001335	0.000015	0.36	2.485000	0.067577
sample3_iga_0p48mg_1_merged	0.280->0.510	57->110	2.5	0.02	0.70->1.28	0.001547	0.000028	0.48		
sample3_iga_0p48mg_2_merged	0.280->0.510	57->110	2.39	0.01	0.67->1.22	0.001528	0.000016	0.48		
sample3_iga_0p48mg_3_merged	0.280->0.510	57->110	2.47	0.02	0.69->1.26	0.001623	0.000024	0.48		
sample3_iga_0p48mg_4_merged									2.45	0.06
sample3_iga_0p72mg_1_merged	0.280->0.510	57->110	2.47	0.02	0.69->1.26	0.002657	0.000034	0.72		
sample3_iga_0p72mg_2_merged	0.280->0.510	57->110	2.41	0.02	0.67->1.23	0.00259	0.000033	0.72		
sample3_iga_0p72mg_3_merged	0.280->0.510	57->110	2.41	0.02	0.67->1.23	0.002606	0.000032	0.72		
sample3_iga_0p72mg_4_merged	0.280->0.510	57->110	2.46	0.01	0.69->1.26	0.002656	0.000027	0.72	2.437500	0.032016
sample3_iga_0p97mg_1_merged	0.280->0.510	57->110	2.45	0.01	0.69->1.25	0.003454	0.000042	0.97		
sample3_iga_0p97mg_2_merged	0.280->0.510	57->110	2.45	0.01	0.68->1.25	0.003401	0.000038	0.97		
sample3_iga_0p97mg_3_merged	0.280->0.510	57->110	2.46	0.01	0.69->1.25	0.00343	0.00004	0.97		
sample3_iga_0p97mg_4_merged	0.280->0.510	57->110	2.43	0.02	0.68->1.24	0.003397	0.000046	0.97	2.447500	0.012583
sample4_iga_0p15mg_1_merged	0.280->0.510	57->110	2.79	0.02	0.78->1.42	0.000594	0.000013	0.15		
sample4_iga_0p15mg_2_merged	0.280->0.510	57->110	2.5	0.03	0.70->1.27	0.000478	0.000014	0.15		
sample4_iga_0p15mg_3_merged	0.280->0.510	57->110	2.57	0.03	0.72->1.31	0.000507	0.000014	0.15		
sample4_iga_0p15mg_4_merged	0.280->0.510	57->110	2.62	0.03	0.73->1.34	0.000499	0.000012	0.15	2.620000	0.123558
sample4_iga_0p31mg_1_merged	0.280->0.510	56->109	2.41	0.02	0.68->1.23	0.001105	0.000016	0.31		
sample4_iga_0p31mg_2_merged	0.280->0.510	54->107	2.48	0.01	0.70->1.27	0.001133	0.000013	0.31		
sample4_iga_0p31mg_3_merged	0.280->0.510	54->107	2.46	0.02	0.69->1.25	0.001103	0.000018	0.31		
sample4_iga_0p31mg_4_merged	0.280->0.510	57->110	3.08	0.02	0.86->1.57	0.001117	0.000018	0.31	2.607500	0.316373
sample4_iga_0p47mg_1_merged	0.280->0.510	57->110	2.34	0.02	0.66->1.19	0.001513	0.00002	0.47		
sample4_iga_0p47mg_2_merged	0.280->0.510	56->109	2.46	0.02	0.69->1.25	0.001579	0.00002	0.47		
sample4_iga_0p47mg_3_merged	0.280->0.510	56->109	2.47	0.02	0.69->1.26	0.001585	0.000021	0.47		
sample4_iga_0p47mg_4_merged	0.280->0.510	57->110	2.48	0.02	0.69->1.26	0.001574	0.000024	0.47	2.437500	0.065511
sample4_iga_0p63mg_1_merged	0.280->0.510	57->110	2.45	0.02	0.69->1.25	0.002099	0.000032	0.63		
sample4_iga_0p63mg_2_merged	0.280->0.510	57->110	2.49	0.01	0.70->1.27	0.002163	0.000027	0.63		
sample4_iga_0p63mg_3_merged	0.280->0.510	57->110	2.51	0.01	0.70->1.28	0.002192	0.000027	0.63		
sample4_iga_0p63mg_4_merged	0.280->0.510	57->110	2.72	0.01	0.76->1.39	0.002025	0.000026	0.63	2.542500	0.120934
sample4_iga_0p94mg_1_merged	0.280->0.510	57->110	2.45	0.01	0.68->1.25	0.003045	0.000036	0.94		
sample4_iga_0p94mg_2_merged	0.280->0.510	57->110	2.47	0.02	0.69->1.26	0.003125	0.000042	0.94		
sample4_iga_0p94mg_3_merged	0.280->0.510	57->110	2.45	0.01	0.69->1.25	0.003172	0.000038	0.94		
sample4_iga_0p94mg_4_merged	0.280->0.510	57->110	2.46	0.01	0.69->1.25	0.003194	0.000038	0.94	2.457500	0.009574
sample4_iga_1p26mg_1_merged	0.280->0.510	57->110	2.48	0.02	0.70->1.27	0.004277	0.000054	1.26		
sample4_iga_1p26mg_2_merged	0.280->0.510	57->110	2.46	0.01	0.69->1.25	0.004292	0.000046	1.26		
sample4_iga_1p26mg_3_merged	0.280->0.510	57->110	2.47	0.01	0.69->1.26	0.004304	0.000054	1.26		
sample4_iga_1p26mg_4_merged	0.280->0.510	57->110	2.44	0.01	0.68->1.24	0.004277	0.000048	1.26	2.462500	0.017078

*Data point omitted, sample error eg. Air bubble

RXS-2 Q Range: 0.56 - 1.01

IgA Normal Conditions 137mM PBS

Merged files ESRF Dec 2012

File name	Q-range	Point range	RxsZ	Error	QRxs	I(0)	Error	Conc (mg/ml)	Avg Rxs	StDev
sample1_iga_0p25mg_1_merged	0.560->1.010	121->223	1.63	0.02	0.91->1.65	0.000682	0.000028	0.25		
sample1_iga_0p25mg_2_merged	0.560->1.010	121->223	1.63	0.02	0.92->1.65	0.000666	0.000027	0.25		
sample1_iga_0p25mg_3_merged	0.560->1.010	121->223	1.39	0.02	0.78->1.41	0.000543	0.000018	0.25		
sample1_iga_0p25mg_4_merged	0.560->1.010	121->223	1.68	0.02	0.94->1.70	0.000666	0.000029	0.25	1.582500	0.130480
sample1_iga_0p51mg_1_merged	0.560->1.010	121->223	1.51	0.01	0.85->1.53	0.001206	0.000026	0.51		
sample1_iga_0p51mg_2_merged	0.560->1.010	121->223	1.65	0.01	0.92->1.67	0.001313	0.00003	0.51		
sample1_iga_0p51mg_3_merged	0.560->1.010	121->223	1.57	0.01	0.88->1.58	0.001239	0.000034	0.51		
sample1_iga_0p51mg_4_merged	0.560->1.010	121->223	1.5	0.01	0.84->1.52	0.001196	0.000024	0.51	1.557500	0.068981
sample1_iga_0p76mg_1_merged	0.560->1.010	121->223	1.54	0.01	0.86->1.55	0.001808	0.000022	0.76		
sample1_iga_0p76mg_2_merged	0.560->1.010	121->223	1.54	0.01	0.86->1.55	0.001785	0.000029	0.76		
sample1_iga_0p76mg_3_merged	0.560->1.010	121->223	1.62	0.01	0.91->1.64	0.001863	0.000029	0.76	1.566667	0.046188
sample1_iga_1p02mg_1_merged	0.560->1.010	121->223	1.58	0.01	0.89->1.60	0.002466	0.000026	1.02		
sample1_iga_1p02mg_2_merged	0.560->1.010	121->223	1.59	0.01	0.89->1.61	0.002491	0.000029	1.02		
sample1_iga_1p02mg_3_merged	0.560->1.010	121->223	1.56	0.01	0.87->1.57	0.002462	0.000028	1.02	1.576667	0.015275
sample2_iga_0p16mg_1_merged	0.560->1.010	121->223	1.71	0.03	0.96->1.72	0.000399	0.000028	0.16		
sample2_iga_0p16mg_2_merged	0.560->1.010	121->223	1.65	0.03	0.92->1.66	0.00036	0.000021	0.16		
sample2_iga_0p16mg_3_merged	0.560->1.010	121->223	1.65	0.03	0.92->1.67	0.000376	0.000024	0.16		
sample2_iga_0p16mg_4_merged	0.560->1.010	120->222	1.81	0.04	1.02->1.83	0.000451	0.000046	0.16	1.705000	0.075498
sample2_iga_0p33mg_1_merged	0.560->1.010	121->223	1.5	0.01	0.84->1.52	0.000724	0.00002	0.33		
sample2_iga_0p33mg_2_merged	0.560->1.010	121->223	1.54	0.01	0.86->1.56	0.000773	0.00002	0.33		
sample2_iga_0p33mg_3_merged	0.560->1.010	121->223	1.45	0.01	0.81->1.47	0.000717	0.000017	0.33		
sample2_iga_0p33mg_4_merged	0.560->1.010	121->223	1.55	0.01	0.87->1.57	0.001291	0.000022	0.49	1.496667	0.045092
sample2_iga_0p49mg_1_merged	0.560->1.010	121->223	1.55	0.01	0.87->1.57	0.001276	0.000019	0.49		
sample2_iga_0p49mg_2_merged	0.560->1.010	121->223	1.54	0.01	0.86->1.55	0.001285	0.000024	0.49		
sample2_iga_0p49mg_3_merged	0.560->1.010	121->223	1.48	0.01	0.83->1.50	0.001204	0.000024	0.49	1.532500	0.035940
sample2_iga_0p49mg_4_merged	0.560->1.010	121->223	1.56	0.01	0.87->1.57	0.001508	0.000025	0.66		
sample2_iga_0p66mg_1_merged	0.560->1.010	121->223	1.64	0.01	0.92->1.66	0.001632	0.000031	0.66		
sample2_iga_0p66mg_2_merged	0.560->1.010	121->223	1.57	0.01	0.88->1.59	0.001523	0.000022	0.66		
sample2_iga_0p66mg_3_merged	0.560->1.010	121->223	2.11	0.01	1.18->2.14	0.001817	0.000062	0.66	1.720000	0.262425
sample2_iga_0p66mg_4_merged	0.560->1.010	121->223	1.52	0.01	0.85->1.54	0.002241	0.000024	0.99		
sample2_iga_0p99mg_1_merged	0.560->1.010	121->223	1.54	0.01	0.86->1.56	0.0023	0.000025	0.99		
sample2_iga_0p99mg_2_merged	0.560->1.010	121->223	1.56	0.01	0.87->1.57	0.002303	0.000028	0.99		
sample2_iga_0p99mg_3_merged	0.560->1.010	121->223	1.56	0.01	0.87->1.57	0.002303	0.000028	0.99	1.540000	0.020000
sample2_iga_0p99mg_4_merged	0.560->1.010	121->223	1.55	0	0.87->1.57	0.003206	0.000028	1.33		
sample2_iga_1p33mg_1_merged	0.560->1.010	121->223	1.57	0	0.88->1.58	0.00321	0.000029	1.33		
sample2_iga_1p33mg_2_merged	0.560->1.010	121->223	1.56	0	0.87->1.58	0.003226	0.000027	1.33		
sample2_iga_1p33mg_3_merged	0.560->1.010	121->223	1.59	0	0.89->1.60	0.003263	0.000032	1.33	1.567500	0.017078
sample2_iga_1p33mg_4_merged	0.560->1.010	121->223	1.48	0.04	0.83->1.49	0.00028	0.000021	0.12		
sample3_iga_0p12mg_1_merged	0.560->1.010	119->221	1.4	0.03	0.79->1.42	0.000275	0.000017	0.12		
sample3_iga_0p12mg_2_merged	0.560->1.010	119->221	1.65	0.04	0.92->1.66	0.000325	0.00003	0.12		
sample3_iga_0p12mg_3_merged	0.560->1.010	121->223	1.65	0.04	0.92->1.66	0.000325	0.00003	0.12		

sample3_iga_0p12mg_4_merged	0.560->1.010	121->223	2.08	0.03	1.16->2.10	0.000503	0.000047	0.12	1.652500	0.303466	
sample3_iga_0p24mg_1_merged											
sample3_iga_0p24mg_2_merged	0.560->1.010	121->223	1.43	0.02	0.80->1.45	0.000464	0.000019	0.24			
sample3_iga_0p24mg_3_merged									1.430000	#DIV/0!	*
sample3_iga_0p36mg_1_merged	0.560->1.010	121->223	1.5	0.01	0.84->1.51	0.000826	0.000023	0.36			
sample3_iga_0p36mg_2_merged	0.560->1.010	121->223	1.46	0.01	0.82->1.47	0.000799	0.000021	0.36			
sample3_iga_0p36mg_3_merged	0.560->1.010	121->223	1.67	0.02	0.93->1.68	0.000919	0.000035	0.36			
sample3_iga_0p36mg_4_merged	0.560->1.010	121->223	1.53	0.01	0.85->1.54	0.000851	0.000025	0.36	1.540000	0.091287	
sample3_iga_0p48mg_1_merged	0.560->1.010	121->223	1.72	0.01	0.96->1.73	0.001174	0.000035	0.48			
sample3_iga_0p48mg_2_merged	0.560->1.010	121->223	1.63	0.01	0.91->1.64	0.001137	0.000027	0.48			
sample3_iga_0p48mg_3_merged	0.560->1.010	121->223	1.61	0.01	0.90->1.63	0.001114	0.000024	0.48			
sample3_iga_0p48mg_4_merged									1.65	0.06	*
sample3_iga_0p72mg_1_merged	0.560->1.010	121->223	1.59	0.01	0.89->1.60	0.00184	0.000025	0.72			
sample3_iga_0p72mg_2_merged	0.560->1.010	121->223	1.45	0.01	0.81->1.46	0.001679	0.00002	0.72			
sample3_iga_0p72mg_3_merged	0.560->1.010	121->223	1.51	0.01	0.85->1.53	0.001766	0.000022	0.72			
sample3_iga_0p72mg_4_merged	0.560->1.010	121->223	1.6	0.01	0.89->1.61	0.001849	0.000032	0.72	1.537500	0.070887	
sample3_iga_0p97mg_1_merged	0.560->1.010	121->223	1.58	0.01	0.89->1.60	0.002404	0.000032	0.97			
sample3_iga_0p97mg_2_merged	0.560->1.010	121->223	1.54	0.01	0.86->1.56	0.002349	0.000031	0.97			
sample3_iga_0p97mg_3_merged	0.560->1.010	121->223	1.57	0	0.88->1.58	0.002345	0.000023	0.97			
sample3_iga_0p97mg_4_merged	0.560->1.010	121->223	1.59	0	0.89->1.61	0.002356	0.000018	0.97	1.570000	0.021602	
sample4_iga_0p15mg_1_merged	0.560->1.010	121->223	2.31	0.07	1.29->2.33	0.000568	0.000122	0.15			
sample4_iga_0p15mg_2_merged	0.560->1.010	121->223	1.87	0.03	1.05->1.89	0.000447	0.000036	0.15			
sample4_iga_0p15mg_3_merged	0.560->1.010	121->223	1.61	0.04	0.90->1.62	0.000285	0.000025	0.15			
sample4_iga_0p15mg_4_merged	0.560->1.010	121->223	1.99	0.04	1.12->2.01	0.000393	0.000042	0.15	1.945000	0.290459	
sample4_iga_0p31mg_1_merged	0.560->1.010	120->222	1.6	0.01	0.89->1.61	0.000744	0.000023	0.31			
sample4_iga_0p31mg_2_merged	0.560->1.010	118->220	1.51	0.02	0.84->1.52	0.000719	0.000024	0.31			
sample4_iga_0p31mg_3_merged	0.560->1.010	118->220	1.48	0.01	0.83->1.50	0.000701	0.000021	0.31			
sample4_iga_0p31mg_4_merged	0.560->1.010	121->201	3.01	0.07	1.68->3.04	0.001389	0.000342	0.31	1.900000	0.741755	
sample4_iga_0p47mg_1_merged	0.560->1.010	121->223	1.66	0.01	0.93->1.68	0.001185	0.000032	0.47			
sample4_iga_0p47mg_2_merged	0.560->1.010	120->222	1.5	0.01	0.84->1.51	0.00103	0.000028	0.47			
sample4_iga_0p47mg_3_merged	0.560->1.010	120->222	1.48	0.01	0.83->1.49	0.001018	0.000019	0.47			
sample4_iga_0p47mg_4_merged	0.560->1.010	121->223	1.5	0.01	0.84->1.52	0.001054	0.000021	0.47	1.535000	0.083865	
sample4_iga_0p63mg_1_merged	0.560->1.010	121->223	1.61	0.01	0.90->1.63	0.001505	0.000033	0.63			
sample4_iga_0p63mg_2_merged	0.560->1.010	121->223	1.56	0.01	0.87->1.58	0.001413	0.000024	0.63			
sample4_iga_0p63mg_3_merged	0.560->1.010	121->223	1.53	0.01	0.85->1.54	0.001422	0.000026	0.63			
sample4_iga_0p63mg_4_merged	0.560->1.010	121->223	2.29	0.02	1.28->2.32	0.001989	0.00011	0.63	1.747500	0.363169	
sample4_iga_0p94mg_1_merged	0.560->1.010	121->223	1.52	0.01	0.85->1.53	0.002126	0.000026	0.94			
sample4_iga_0p94mg_2_merged	0.560->1.010	121->223	1.54	0.01	0.87->1.56	0.002148	0.000025	0.94			
sample4_iga_0p94mg_3_merged	0.560->1.010	121->223	1.54	0.01	0.86->1.55	0.002189	0.000027	0.94			
sample4_iga_0p94mg_4_merged	0.560->1.010	121->223	1.58	0.01	0.88->1.59	0.00227	0.00003	0.94	1.545000	0.025166	
sample4_iga_1p26mg_1_merged	0.560->1.010	121->223	1.55	0.01	0.87->1.56	0.002962	0.000033	1.26			
sample4_iga_1p26mg_2_merged	0.560->1.010	121->223	1.51	0	0.85->1.53	0.002846	0.000025	1.26			
sample4_iga_1p26mg_3_merged	0.560->1.010	121->223	1.55	0	0.87->1.57	0.002947	0.000026	1.26			
sample4_iga_1p26mg_4_merged	0.560->1.010	121->223	1.54	0	0.86->1.55	0.002912	0.000029	1.26	1.537500	0.018930	

*Data point omitted, sample error eg. Air bubble

Bibliography

Alebiosu, C. O., & Ayodele, O. E. (2005). The global burden of chronic kidney disease and the way forward. *Ethnicity & disease, 15*(3), 418–23. Retrieved from <http://www.ncbi.nlm.nih.gov/pubmed/16108301>

- Allen, A. C., Bailey, E. M., Barratt, J., Buck, K. S., & Feehally, J. (1999). Analysis of IgA1 O-glycans in IgA nephropathy by fluorophore-assisted carbohydrate electrophoresis. *Journal of The American Society Of Nephrology*, *10*(8), 1763–1771. Retrieved from <http://www.ncbi.nlm.nih.gov/pubmed/10446944>
- Almogren, A., & Kerr, M. A. (2008). Irreversible aggregation of the Fc fragment derived from polymeric but not monomeric serum IgA1--implications in IgA-mediated disease. *Molecular Immunology*, *45*(1), 87–94. Retrieved from <http://www.ncbi.nlm.nih.gov/pubmed/17606293>
- Atkin, J. D., Pleass, R. J., Owens, R. J., & Woof, J. M. (1996). Mutagenesis of the human IgA1 heavy chain tailpiece that prevents dimer assembly. *Journal of immunology (Baltimore, Md. : 1950)*, *157*(1), 156–9. Retrieved from <http://www.ncbi.nlm.nih.gov/pubmed/8683109>
- Barratt, J., & Feehally, J. (2005). IgA nephropathy. *Journal of the American Society of Nephrology : JASN*, *16*(7), 2088–97. doi:10.1681/ASN.2005020134
- Barratt, J., & Feehally, J. (2006). Treatment of progressive IgA nephropathy. *Kidney International*.
- Barratt, Jonathan, Smith, A. C., Molyneux, K., & Feehally, J. (2007). Immunopathogenesis of IgAN. *Seminars in immunopathology*, *29*(4), 427–43. doi:10.1007/s00281-007-0089-9
- Beerman, I., Novak, J., Wyatt, R. J., Julian, B. A., & Gharavi, A. G. (2007). The genetics of IgA nephropathy. *Nature clinical practice. Nephrology*, *3*(6), 325–38. doi:10.1038/ncpneph0492
- Boehm, M. K., Woof, J. M., Kerr, M. A., & Perkins, S. J. (1999). The Fab and Fc fragments of IgA1 exhibit a different arrangement from that in IgG: A study by X-ray and neutron solution scattering and homology modelling. *Journal of Molecular Biology*, *286*(5), 1421–1447. Retrieved from <http://discovery.ucl.ac.uk/154642/>
- Bonner, A., Almogren, A., Furtado, P. B., Kerr, M. A., & Perkins, S. J. (2009). The Nonplanar Secretory IgA2 and Near Planar Secretory IgA1 Solution Structures Rationalize Their Different Mucosal Immune Responses. *The Journal of Biological Chemistry*, *284*(8), 5077–5087. Retrieved from <http://discovery.ucl.ac.uk/173377/>
- Bonner, A., Furtado, P. B., Almogren, A., Kerr, M. A., & Perkins, S. J. (2008). Implications of the near-planar solution structure of human myeloma dimeric IgA1 for mucosal immunity and IgA nephropathy. *The Journal of Immunology*, *180*(2), 1008–1018. Retrieved from http://www.ncbi.nlm.nih.gov/entrez/query.fcgi?cmd=Retrieve&db=PubMed&dopt=Citation&list_uids=18178841

- Boyd, J. K., Cheung, C. K., Molyneux, K., Feehally, J., & Barratt, J. (2012). An update on the pathogenesis and treatment of IgA nephropathy. *Kidney international*, *81*(9), 833–43. doi:10.1038/ki.2011.501
- Brandtzaeg, P. (2007). Induction of secretory immunity and memory at mucosal surfaces. *Vaccine*, *25*(30), 5467–84. doi:10.1016/j.vaccine.2006.12.001
- Cattran, D. C., Coppo, R., Cook, H. T., Feehally, J., Roberts, I. S. D., Troyanov, S., Alpers, C. E., et al. (2009). The Oxford classification of IgA nephropathy: rationale, clinicopathological correlations, and classification. *Kidney international*, *76*(5), 534–45. doi:10.1038/ki.2009.243
- Coppo, R., & Amore, A. (2004). Aberrant glycosylation in IgA nephropathy (IgAN). *Kidney international*, *65*(5), 1544–7. doi:10.1111/j.1523-1755.2004.05407.x
- Dourmashkin, R. R., Virella, G., & Parkhouse, R. M. (1971). Electron microscopy of human and mouse myeloma serum IgA. *Journal of molecular biology*, *56*(1), 207–8. Retrieved from <http://www.ncbi.nlm.nih.gov/pubmed/5573763>
- D'Amico, G. (2000). Natural history of idiopathic IgA nephropathy: role of clinical and histological prognostic factors. *American journal of kidney diseases : the official journal of the National Kidney Foundation*, *36*(2), 227–37. doi:10.1053/ajkd.2000.8966
- Feehally, J., & Floege, J. (2010). *CHAPTER 22 - IgA Nephropathy and Henoch-Schönlein Nephritis. Comprehensive Clinical Nephrology* (Fourth Edi., pp. 270–281). Elsevier Inc. doi:10.1016/B978-0-323-05876-6.00022-8
- Frohnert, P. P., Donadio, J. V., Velosa, J. A., Holley, K. E., & Sterioff, S. (1997). The fate of renal transplants in patients with IgA nephropathy. *Clinical Transplantation*, *11*(2), 127–133.
- Furtado, P. B., Whitty, P. W., Robertson, A., Eaton, J. T., Almogren, A., Kerr, M. a, Woof, J. M., et al. (2004). Solution structure determination of monomeric human IgA2 by X-ray and neutron scattering, analytical ultracentrifugation and constrained modelling: a comparison with monomeric human IgA1. *Journal of molecular biology*, *338*(5), 921–41. doi:10.1016/j.jmb.2004.03.007
- Gomes, M. M., Suzuki, H., Brooks, M. T., Tomana, M., Moldoveanu, Z., Mestecky, J., Julian, B. A., et al. (2010). Recognition of galactose-deficient O-glycans in the hinge region of IgA1 by N-acetylgalactosamine-specific snail lectins: a comparative binding study. *Biochemistry*, *49*(27), 5671–82. doi:10.1021/bi9019498
- Harada, T., Hobby, P., Courteau, M., Knight, J. F., & Williams, D. G. (1989). Charge distribution of plasma IgA in IgA nephropathy. *Clinical and experimental immunology*, *77*(2), 211–4. Retrieved from

<http://www.pubmedcentral.nih.gov/articlerender.fcgi?artid=1541975&tool=pmcentrez&rendertype=abstract>

- Heremans, J. F., Heremans, M. T., & Schultze, H. E. (1959). Isolation and description of a few properties of the beta 2A-globulin of human serum. *Clinica chimica acta; international journal of clinical chemistry*, 4(1), 96–102. Retrieved from <http://www.ncbi.nlm.nih.gov/pubmed/13629856>
- Hiki, Y., Odani, H., Takahashi, M., Yasuda, Y., Nishimoto, a, Iwase, H., Shinzato, T., et al. (2001). Mass spectrometry proves under-O-glycosylation of glomerular IgA1 in IgA nephropathy. *Kidney international*, 59(3), 1077–85. doi:10.1046/j.1523-1755.2001.0590031077.x
- Hiki, Y., Tanaka, A., Kokubo, T., Iwase, H., Nishikido, J., Hotta, K., & Kobayashi, Y. (1998). Analyses of IgA1 hinge glycopeptides in IgA nephropathy by matrix-assisted laser desorption/ionization time-of-flight mass spectrometry. *Journal of the American Society of Nephrology : JASN*, 9(4), 577–82. Retrieved from <http://www.ncbi.nlm.nih.gov/pubmed/9555659>
- Ji, S., Liu, M., Chen, J., Yin, L., Sha, G., Chen, H., Liu, Z., et al. (2004). The fate of glomerular mesangial IgA deposition in the donated kidney after allograft transplantation. *Clinical Transplantation*, 18(5), 536–540.
- Johansen, F. E., Braathen, R., & Brandtzaeg, P. (2000). Role of J chain in secretory immunoglobulin formation. *Scandinavian journal of immunology*, 52(3), 240–8. Retrieved from <http://www.ncbi.nlm.nih.gov/pubmed/10972899>
- Kerr, M. A. (1990). The structure and function of human IgA. *Human cell official journal of Human Cell Research Society*, 271(2), 285–296. Retrieved from <http://www.pubmedcentral.nih.gov/articlerender.fcgi?artid=1149552&tool=pmcentrez&rendertype=abstract>
- Lai, K. N. (2006). Pathogenic IgA in IgA nephropathy: still the blind men and the elephant? *Kidney international*, 69(7), 1102–3. doi:10.1038/sj.ki.5000205
- Lai, K. N., Chui, S. H., Lewis, W. H., Poon, A. S., & Lam, C. W. (1994). Charge distribution of IgA-lambda in IgA nephropathy. *Nephron*, 66(1), 38–44. Retrieved from <http://www.ncbi.nlm.nih.gov/pubmed/8107951>
- Lai, K. N., To, W. Y., Li, P. K., & Leung, J. C. (1996). Increased binding of polymeric lambda-IgA to cultured human mesangial cells in IgA nephropathy. *Kidney international*, 49(3), 839–45. Retrieved from <http://www.ncbi.nlm.nih.gov/pubmed/8648928>

- Leung, J. C., Tang, S. C., Lam, M. F., Chan, T. M., & Lai, K. N. (2001). Charge-dependent binding of polymeric IgA1 to human mesangial cells in IgA nephropathy. *Kidney international*, 59(1), 277–85. doi:10.1046/j.1523-1755.2001.00489.x
- Laue, T. M., Shah, B. D., Ridgeway, T. M., and Pelletier, S. L. (1992). Computer-aided interpretation of analytical sedimentation data for proteins. In *Analytical Ultracentrifugation in Biochemistry and Polymer Science* (Harding, S. E., Rowe, A. J. and Horton, J. C., eds) The Royal Society of Chemistry, Cambridge, U.K., 90-125.
- Liu, J., Andya, J. D., & Shire, S. J. (2006). A critical review of analytical ultracentrifugation and field flow fractionation methods for measuring protein aggregation. *The AAPS journal*, 8(3), E580–9. doi:10.1208/aapsj080367
- Liu, Y. S., & Putnam, F. W. (1979). Primary structure of a human IgA1 immunoglobulin. I. Isolation, composition, and amino acid sequence of the chymotryptic peptides. *The Journal of biological chemistry*, 254(8), 2839–49. Retrieved from <http://www.ncbi.nlm.nih.gov/pubmed/107163>
- Mahler, H.-C., Friess, W., Grauschopf, U., & Kiese, S. (2009). Protein aggregation: pathways, induction factors and analysis. *Journal of Pharmaceutical Sciences*, 98(9), 2909–2934. Retrieved from <http://www.ncbi.nlm.nih.gov/pubmed/18823031>
- Mattu, T. S. (1998). The Glycosylation and Structure of Human Serum IgA1, Fab, and Fc Regions and the Role of N-Glycosylation on Fc α Receptor Interactions. *Journal of Biological Chemistry*, 273(4), 2260–2272. doi:10.1074/jbc.273.4.2260
- Mertens, H. D. T., & Svergun, D. I. (2010). Structural characterization of proteins and complexes using small-angle X-ray solution scattering. *Journal of structural biology*, 172(1), 128–141. Retrieved from <http://www.ncbi.nlm.nih.gov/pubmed/20558299>
- Miller, A., Phillips, A., Gor, J., Wallis, R., & Perkins, S. (2012). Near-planar solution structures of mannose-binding lectin oligomers provide insight on activation of lectin pathway of complement. *The Journal of Biological Chemistry*, 287(6), 3930–45. Retrieved from <http://discovery.ucl.ac.uk/1338816/>
- Monteiro, R. C., Hostoffer, R. W., Cooper, M. D., Bonner, J. R., Gartland, G. L., & Kubagawa, H. (1993). Definition of immunoglobulin A receptors on eosinophils and their enhanced expression in allergic individuals. *The Journal of clinical investigation*, 92(4), 1681–5. doi:10.1172/JCI116754
- Munn, E. A., Feinstein, A., & Munro, A. J. (1971). Electron microscope examination of free IgA molecules and of their complexes with antigen. *Nature*, 231(5304), 527–9. Retrieved from <http://www.ncbi.nlm.nih.gov/pubmed/4932999>

- Nan, R., Gor, J., & Perkins, S. J. (2008). Implications of the progressive self-association of wild-type human factor H for complement regulation and disease. *Journal of Molecular Biology*, 375(1), 75–83. Retrieved from <http://discovery.ucl.ac.uk/120720/>
- Neylon, C. (2008). Small angle neutron and X-ray scattering in structural biology: recent examples from the literature. *European biophysics journal : EBJ*, 37(5), 531–41. doi:10.1007/s00249-008-0259-2
- Novak, J., Julian, B. A., Tomana, M., & Mestecky, J. (2008). IgA glycosylation and IgA immune complexes in the pathogenesis of IgA nephropathy. *Seminars in nephrology*, 28(1), 78–87. doi:10.1016/j.semnephrol.2007.10.009
- Novak, J., Moldoveanu, Z., Julian, B. A., Raska, M., Wyatt, R. J., Suzuki, Y., Tomino, Y., et al. (2011). Aberrant glycosylation of IgA1 and anti-glycan antibodies in IgA nephropathy: role of mucosal immune system. *Advances in oto-rhino-laryngology*, 72, 60–3. doi:10.1159/000324607
- Novak, J., Moldoveanu, Z., Renfrow, M. B., Yanagihara, T., Suzuki, H., Raska, M., Hall, S., et al. (2007). IgA nephropathy and Henoch-Schoenlein purpura nephritis: aberrant glycosylation of IgA1, formation of IgA1-containing immune complexes, and activation of mesangial cells. *Contributions to nephrology*, 157, 134–8. doi:10.1159/0000102455
- Oortwijn, B. D., Roos, A., Royle, L., Van Gijlswijk-Janssen, D. J., Faber-Krol, M. C., Eijgenraam, J.-W., Dwek, R. A., et al. (2006). Differential glycosylation of polymeric and monomeric IgA: a possible role in glomerular inflammation in IgA nephropathy. *Journal of the American Society of Nephrology : JASN*, 17(12), 3529–39. doi:10.1681/ASN.2006040388
- Perkins, S J. (1988). Structural studies of proteins by high-flux X-ray and neutron solution scattering. *The Biochemical journal*, 254(2), 313–27. Retrieved from <http://www.pubmedcentral.nih.gov/articlerender.fcgi?artid=1135080&tool=pmcentrez&rendertype=abstract>
- Perkins, S J, Ashton, a W., Boehm, M. K., & Chamberlain, D. (1998). Molecular structures from low angle X-ray and neutron scattering studies. *International journal of biological macromolecules*, 22(1), 1–16. Retrieved from <http://www.ncbi.nlm.nih.gov/pubmed/9513811>
- Perkins, S J, Okemefuna, A. I., Fernando, A. N., Bonner, A., Gilbert, H. E., & Furtado, P. B. (2008). X-ray and neutron scattering data and their constrained molecular modeling. *Methods in cell biology*, 84(07), 375–423. doi:10.1016/S0091-679X(07)84013-1

- Perkins, Stephen J, & Bonner, A. (2008). Structure determinations of human and chimaeric antibodies by solution scattering and constrained molecular modelling. *Biochemical Society transactions*, 36(Pt 1), 37–42. doi:10.1042/BST0360037
- Petoukhov, M. V, & Svergun, D. I. (2006). Joint use of small-angle X-ray and neutron scattering to study biological macromolecules in solution. *European biophysics journal EBJ*, 35(7), 567–576. Retrieved from <http://www.ncbi.nlm.nih.gov/pubmed/16636827>
- Petoukhov, M. V, & Svergun, D. I. (2007). Analysis of X-ray and neutron scattering from biomacromolecular solutions. *Current opinion in structural biology*, 17(5), 562–571. Retrieved from <http://www.ncbi.nlm.nih.gov/pubmed/17714935>
- Plaut, A. G., Wistar, R., & Capra, J. D. (1974). Differential susceptibility of human IgA immunoglobulins to streptococcal IgA protease. *The Journal of clinical investigation*, 54(6), 1295–300. doi:10.1172/JCI107875
- Putnam, C. D., M. Hammel (2007). X-ray solution scattering (SAXS) combined with crystallography and computation: defining accurate macromolecular structures, conformations and assemblies in solution. *Quarterly Reviews of Biophysics*, 40(3): 191-285.
- Ralston, G. (1993). *Introduction to Analytical Ultracentrifugation* (pp. 8–15). Sydney, Australia: Beckman Instruments.
- Richard, J., Atkin, J. D., & Woof, M. (n.d.). Structural Requirements for Assembly of Dimeric IgA Probed, 1–6.
- Sanfilippo, F., Croker, B. P., & Bollinger, R. R. (1982). Fate of four cadaveric donor renal allografts with mesangial IgA deposits. *Transplantation*.
- Schena, F. P., Scivittaro, V., Ranieri, E., Sinico, R., Benuzzi, S., Di Cillo, M., & Aventaggiato, L. (1993). Abnormalities of the IgA immune system in members of unrelated pedigrees from patients with IgA nephropathy. *Clinical and experimental immunology*, 92(1), 139–44. Retrieved from <http://www.pubmedcentral.nih.gov/articlerender.fcgi?artid=1554876&tool=pmcentrez&rendertype=abstract>
- Schuck, P. (2000). Size-distribution analysis of macromolecules by sedimentation velocity ultracentrifugation and lamm equation modeling. *Biophysical journal*, 78(3), 1606–19. doi:10.1016/S0006-3495(00)76713-0
- Suen, K. K., Lewis, W. H., & Lai, K. N. (1997). Analysis of charge distribution of lambda- and kappa-IgA in IgA nephropathy by focused antigen capture immunoassay. *Scandinavian journal of urology and nephrology*, 31(3), 289–93. Retrieved from <http://www.ncbi.nlm.nih.gov/pubmed/9249895>

- Suzuki, H., Suzuki, Y., Yamanaka, T., Hirose, S., Nishimura, H., Toei, J., Horikoshi, S., et al. (2005). Genome-wide scan in a novel IgA nephropathy model identifies a susceptibility locus on murine chromosome 10, in a region syntenic to human IGAN1 on chromosome 6q22-23. *Journal of the American Society of Nephrology : JASN*, *16*(5), 1289–99. doi:10.1681/ASN.2004030219
- Suzuki, K., Honda, K., Tanabe, K., Toma, H., Nihei, H., & Yamaguchi, Y. (2003). Incidence of latent mesangial IgA deposition in renal allograft donors in Japan. *Kidney International*, *63*(6), 2286–2294.
- Svergun, D. I. (1991). GNOM - a Program Package for Small-Angle Scattering Data Processing. *The Journal of Applied Crystallography*, *24*, 537–540.
- Takahashi, K., Hiki, Y., Odani, H., Shimozato, S., Iwase, H., Sugiyama, S., & Usuda, N. (2006). Structural analyses of O-glycan sugar chains on IgA1 hinge region using SELDI-TOFMS with various lectins. *Biochemical and biophysical research communications*, *350*(3), 580–7. doi:10.1016/j.bbrc.2006.09.075
- Tanaka, M., Seki, G., Someya, T., Nagata, M., & Fujita, T. (2011). Aberrantly glycosylated IgA1 as a factor in the pathogenesis of IgA nephropathy. *Clinical & developmental immunology*, *2011*, 470803. doi:10.1155/2011/470803
- Tomino, Y. (2008). IgA nephropathy: lessons from an animal model, the ddY mouse. *Journal of nephrology*, *21*(4), 463–7. Retrieved from <http://www.ncbi.nlm.nih.gov/pubmed/18651534>
- Toraño, A., & Putnam, F. W. (1978). Complete amino acid sequence of the alpha 2 heavy chain of a human IgA2 immunoglobulin of the A2m (2) allotype. *Proceedings of the National Academy of Sciences of the United States of America*, *75*(2), 966–9. Retrieved from <http://www.pubmedcentral.nih.gov/articlerender.fcgi?artid=411380&tool=pmcentrez&rendertype=abstract>
- White, S. L., Cass, A., Atkins, R. C., & Chadban, S. J. (2005). Chronic kidney disease in the general population. *Advances in chronic kidney disease*, *12*(1), 5–13. Retrieved from <http://www.ncbi.nlm.nih.gov/pubmed/15719328>
- Widmer, H., & Jahnke, W. (2004). Protein NMR in biomedical research. *Cellular and molecular life sciences : CMLS*, *61*(5), 580–99. doi:10.1007/s00018-003-3382-3
- Yu, H.-H., Chiang, B.-L., & Yang, Y.-H. (2012). Altered glycosylation of circulatory IgA1 involved in Henoch-Schönlein purpura and IgA nephropathy. *Journal of the Formosan Medical Association*, *111*(3), 121–122. doi:10.1016/j.jfma.2011.04.002